UNIVERSITÉ DE STRASBOURG

ÉCOLE DOCTORALE SCIENCES CHIMIQUES ED222

UMR7042 CNRS-Unistra-UHA,
Laboratoire d'Innovation Moléculaire et Applications (LIMA)

&

U963 Inserm / UPR9022 CNRS-Unistra,
Réponse Immunitaire et Développement chez les Insectes (RIDI)

THÈSE présentée par :

Vrushali KHOBRAGADE

soutenue le : **20 Juillet 2020**

pour obtenir le grade de : **Docteur de l'université de Strasbourg**

Discipline / Spécialité : Chimie Biologique et Thérapeutique / Sciences de la vie, biologie, biochimie

Développement d'outils chimiques et de sondes sélectives basées sur l'activité de la plasmodione pour identifier les cibles de ce nouvel agent antipaludique

THÈSE dirigée par :

Mme DAVIOUD-CHARVET Elisabeth DR CNRS, Université de Strasbourg

Mme BLANDIN Stéphanie, co-Directrice de thèse CR INSERM, université de Strasbourg

RAPPORTEURS :

Mme PEYROTTES Suzanne DR CNRS, Université de Montpellier

Mr DUVAL Romain CR IRD, Université de Paris Descartes

AUTRES MEMBRES DU JURY :

Mme VONTHRON Catherine Professeur des Universités, Université de Strasbourg

Mme PALOQUE Lucie CR CNRS, Université de Toulouse

ACKNOWLEDGEMENT

I take this opportunity to express my sincere and heartfelt gratitude to my Ph.D. thesis supervisor Dr. Elisabeth Davioud-Charvet for believing in my capabilities and encouraging me to understand and link complex concepts in the interdisciplinary field of drug and chemical tools development. I appreciate your constant support throughout broadening my knowledge and professional development. You taught me to be like a sponge and absorb all the knowledge that comes along the way and that there is no evidence or measure of failure or success if you do not even try.

I appreciate Dr. Stéphanie Blandin for generously offering the parasitology platform and extensive help with review. Thanks to Dr. Katharina Ehrhardt for introducing parasites to me. It was a pleasure to share parasites with you Brice. I wish you great success in the future.

I am thankful to Dr. Mourad Elhabiri for sharing his insights on analytical chemistry and introducing me to the colourful world of bioinspired azides.

I am highly indebted to Jean-Marc Strub and Christine Schaeffer for offering me the HPLC-MS platform and sharing their expertise for bringing the momentum in my PhD research.

Bogdan, I appreciate your help in progressing with the project. I enjoyed all our brainstorming and constructive criticism sessions with you. Indeed, it was hard at times, but it was fun working with you. I would also like to thank Leandro, Maxime, Mustapha, Michael, Nathan, and Valerie for entertaining my naïve questions in the organic chemistry and synthesizing the chemistry tools.

I am grateful to Dr. Patrick Bastien and Dr. Catherine Vonthron, the advisory board of my mid-thesis, for encouraging me to embrace the troubleshooting part of science.

I am thankful to Dr. Katja Becker for giving me the opportunity of training in enzyme kinetics at her crossfunctional laboratory full of dynamic experts in Giessen, Germany.

I would like to thank ParaFrap for their financial support and for arranging the interesting meetings for curricular development.

I am grateful to Dr. Suzanne Peyrottes, Dr. Romain Duval, Dr. Catherine Vonthron, Dr. Lucie Paloque, and Christine Schaeffer on the jury panel of my PhD thesis for showing the enthusiasm to understand and examine my research project. I am looking forward to having fruitful discussions with all of you.

My special thanks to Emily, Arghyashree, Layale, Raquel, Nathalie, Bechara and Gaetan for their kind words and warm company. Many thanks to my very special “BIOTechno Grand Est Team” for encompassing the dynamic socio-professional environment for navigating exciting future opportunities. Lastly, I express gratitude towards my dear ParaFrap friends Sheena and Pratima for their unconditional support throughout this roller coaster of Ph.D.

I will not be able to thank enough my parents who always strengthen me by teaching to stand tall and fight hard to find the way through the world of uncertainties. I feel blessed to have my sister Sonal, Sanket, my boyfriend-Pratik and his family’s immense support and love throughout my journey.

I consider my PhD completion as an outcome of my parent’s values, the inspiration for the thirst of knowledge from Dr. Babasaheb Ambedkar and the mentoring lead by Elisabeth.

RESUME DE LA THESE DE DOCTORAT

Introduction

Le paludisme est une maladie mortelle causée par le parasite *Plasmodium falciparum* (*P. falciparum*). Les premiers stades du parasite (anneau précoce et gamétocyte mature) sont impliqués dans la résistance des parasites aux médicaments chez l'homme et de leur transmission aux moustiques anophèles, respectivement. Peu de médicaments ciblent ces deux stades. L'artémisinine (Art) est le médicament antipaludique le plus efficace, mais il est maintenant menacé par l'émergence de la résistance croisée à l'Art et autres médicaments en Asie du Sud-Est (1). Il y a donc un besoin urgent de nouveaux médicaments ou de combinaisons de médicaments puissants qui pourraient cibler les anneaux et les gamétocytes et contourner la résistance à l'Art. La Plasmodione (PD, Fig. 1a), agent antipaludique puissant et peu toxique, est actif sur les anneaux avec une vitesse d'action similaire à celle de l'Art. Il a un faible potentiel d'induction de la résistance chez le parasite et présente une synergie avec plusieurs médicaments antipaludiques, dont l'Art (2, 3). La PD tue les parasites en générant un stress oxydatif, en mimant les effets de déficiences en glucose-phosphate déshydrogénase (G6PD) dans les globules rouges (RBC), connues pour induire une protection naturelle contre de sévères épisodes palustres (4). Cependant, la PD est faiblement efficace à bloquer la transmission *in vitro* (3). Récemment, deux analogues optimisés de la PD ayant une liaison plus faible aux protéines sériques (bMD30), ou des propriétés anti-gamétocytes matures (stade V) élevées in vitro et in vivo (bMD40) ont été identifiés, respectivement. L'objectif est maintenant de valider l'analogue supérieur de PD qui pourrait être utilisé à l'avenir comme médicament antipaludique et bloquant la transmission, et de déchiffrer leur mécanisme d'action pour potentialiser l'effet de la drogue seule ou en combinaison avec d'autres médicaments. Les dérivés de la PD sont des substrats efficaces des glutathion réductases recombinantes humaine (hGR) et de *P. falciparum* (PfGR) *in vitro* (5). Cependant, chez le parasite de rongeur *P. berghei*, la glutathion réductase n'est pas la seule cible principale responsable de la bioactivation ou de l'activité de la PD (Goetz et al. en préparation). En considérant le fait que d'autres oxydoréductases peuvent compenser l'absence de GR, nous supposons qu'il existe de multiples réductases-cibles de PD responsables de la bioactivation de la molécule et/ou de la mort des parasites. Ainsi, le but de mon projet de doctorat a été d'identifier les cibles de la PD et de ses analogues en utilisant une approche « *fish & click* » par marquage covalent des protéines-cibles en utilisant la photochimie et la réaction click, et d'analyse protéomique à l'aide de sondes basées sur l'activité de la PD (PD-ABP) (Fig 1b). Tout au long de ce travail, nous utilisons la définition pour la réaction « click », la réaction décrite en 2001, par Sharpless, Finn et Kolb, un variant de la cycloaddition azide-alcyne de Huisgen catalysée par le cuivre(I) (réaction CuAAC). Pour cela, nous avons d'abord validé la preuve de concept des PD-ABP en caractérisant leur photoréactivité et leur « clickabilité » à l'aide de partenaires-modèles spécifiques, et identifié les meilleures sondes PD-ABP qui seront utilisées, dans le futur proche, chez le parasite pour identifier les cibles de la PD par analyse protéomique. Ces informations essentielles seront d'une grande utilité pour optimiser les propriétés de ces séries de composés, concevoir des produits plus actifs et cibler des dérivés spécifiques.

Selon la littérature, il n'existe que 4 publications (6-9) utilisant des approches « *fish & click* » pour la détection de cibles de molécules actives chez *P. falciparum*. Comme les propriétés physicochimiques des sondes ABP diffèrent selon leurs structures, les conditions de

photoréaction et de réaction click varient également dans chaque cas. Par conséquent, avant d'appliquer la sonde PD-ABP pour identifier les cibles de l'agent par une approche « *fish & click* », mon projet s'est concentré sur les cinq objectifs suivants :

I. Évaluation de la résistance croisée, entre l'artémisinine et la PD et ses deux analogues, de souches de *P. falciparum*

II. Évaluation de l'activité antipaludique des analogues de PD, et des sondes PD-ABP

III. Caractérisation des propriétés photoréactives des sondes PD-ABP à l'aide de partenaires-modèles de protéines

IV. Caractérisation des propriétés de clickabilité des sondes PD-ABP à l'aide de partenaires-modèles azides

V. Preuve de concept de l'approche « *fish & click* » par l'évaluation de l'enchainement des deux réactions, de photoirradiation suivie de la réaction click.

Résultats

Détermination de l'activité antipaludique des analogues de la PD dans un essai modifié de mesure des valeurs d'IC50 avec une exposition au médicament de 72 heures.

Stratégie: Etant donné que les analogues de la PD, bMD30 et bMD40, aux propriétés pharmacocinétiques améliorées ont des propriétés anti-gamétocytes (Goetz et al en préparation), nous avons évalué leur activité antiplasmodiale sur des stades asexués précoces de parasites de 3 souches différentes de *P. falciparum* : la souche Dd2 résistante à la chloroquine, deux isolats de patients cambodgiens atteints de paludisme sensibles (Art-S) ou résistants à l'artémisinine (Art-R).

Méthode :

L'activité antipaludique de la PD, et de ses deux dérivés, bMD030 et bMD040 (tests d'IC_{50} et exposition à 72h avec les molécules) : L'activité antiplasmodiale des analogues de la PD et des médicaments de référence a été évaluée par le test IC_{50} modifié par une exposition de 72 heures des anneaux âgés de 3 heures hautement synchrones, suivie de l'analyse de la survie du parasite en utilisant le fluorophore-rapporteur *SYBRgreen*. Dans le test classique IC_{50}, les anneaux de 2 cultures synchronisées au sorbitol sont traités avec la molécule à tester mais ce protocole a été spécifiquement modifié pour obtenir des anneaux très synchrones au stade précoce. Pour ce faire, les anneaux envahis dans les 3 heures suivant la synchronisation par percolation des schizontes matures et segmentés ont d'abord été fractionnés au sorbitol puis utilisés pour le traitement des molécules.

Résultat et conclusion :

Même si l'IC_{50} de la bMD40 sur les stades asexués des parasites est deux fois supérieure à celle du bMD3O et de la PD (fig. 2a), la bMD40 a été identifiée comme un meilleur analogue de la PD en raison de son activité très puissante contre les stades sexués des parasites - les gamétocytes matures (Goetz et al en préparation). Les valeurs d'IC_{50} de la bMD30 et de la bMD40 ont été utilisées pour déterminer la concentration de molécule à tester pour le test de survie de l'anneau (RSA).

Détermination de la résistance croisée des analogues de la PD avec l'artémisinine par le test de survie des anneaux..

Stratégie: La résistance à l'artémisinine n'est mesurable que par une augmentation de la survie des stades anneaux aux impulsions courtes d'Art à des concentrations élevées (RSA : 6h, 700 nM). Pour tester la résistance croisée entre l'Art et la PD et ses analogues, j'ai établi le protocole de l'essai de survie des anneaux (RSA) dans le laboratoire à l'IBMC en utilisant des souches de parasites Art-S et Art-R cambodgiens.

Méthode : L'efficacité de la PD et de ses dérivés (bMD30 et bMD40) sur le stade précoce des anneaux des souches Art-S et Art-R a été déterminée selon le protocole rapporté (10, 11) en exposant des anneaux âgés de ~3h à des concentrations élevées de drogue (700 nM de DHA comme témoin, 2,5 µM et 5 µM de PD et bMD40, 1µM et 2,5 µM de MB) pendant une période de 6 heures. Après l'élimination de la drogue, on a laissé les parasites se développer pendant 66 heures supplémentaires et la parasitémie a été déterminée par analyse de frottis sanguins microscopiques après coloration au Giemsa.

Résultats et conclusion : Nos premiers résultats suggèrent l'existence d'une résistance croisée entre la PD ou son analogue et l'Art (fig 2c). Nous avons cependant noté une grande variabilité entre les réplicats (à la fois au sein des expériences et entre elles), y compris pour le contrôle bleu de méthylène (MB) et une destruction partielle des parasites Art-S aux concentrations de médicaments choisies. L'analyse FACS est un autre moyen de confirmer la résistance croisée en évitant l'erreur manuelle dans le comptage microscopique des frottis (Amaratunga et al 2013). Afin de contourner la résistance croisée, l'analyse de combinaison des benzylmenadiones avec d'autres agents partenaires a été recommandée pour la suite du travail.

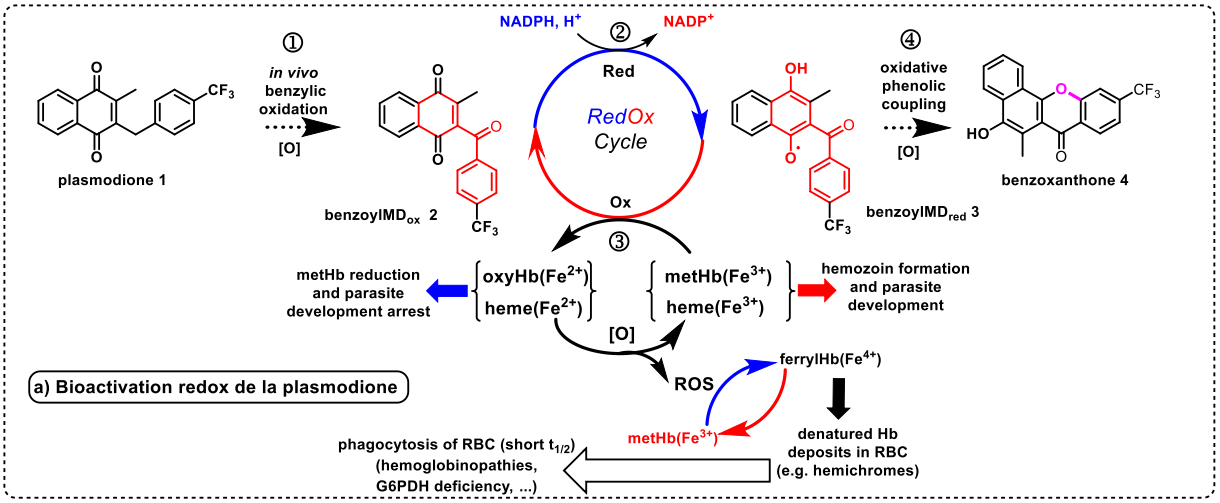
plasmodione 1
in vivo benzylic oxidation
[O]
benzoylMD$_{ox}$ 2
NADPH, H$^+$
NADP$^+$
Red
RedOx Cycle
Ox
benzoylMD$_{red}$ 3
oxidative phenolic coupling
benzoxanthone 4
metHb reduction and parasite development arrest
oxyHb(Fe^{2+})
heme(Fe^{2+})
metHb(Fe^{3+})
heme(Fe^{3+})
hemozoin formation and parasite development
ferrylHb(Fe^{4+})
ROS
metHb(Fe^{3+})
phagocytosis of RBC (short t$_{1/2}$) (hemoglobinopathies, G6PDH deficiency, ...)
denatured Hb deposits in RBC (e.g. hemichromes)
a) Bioactivation redox de la plasmodione

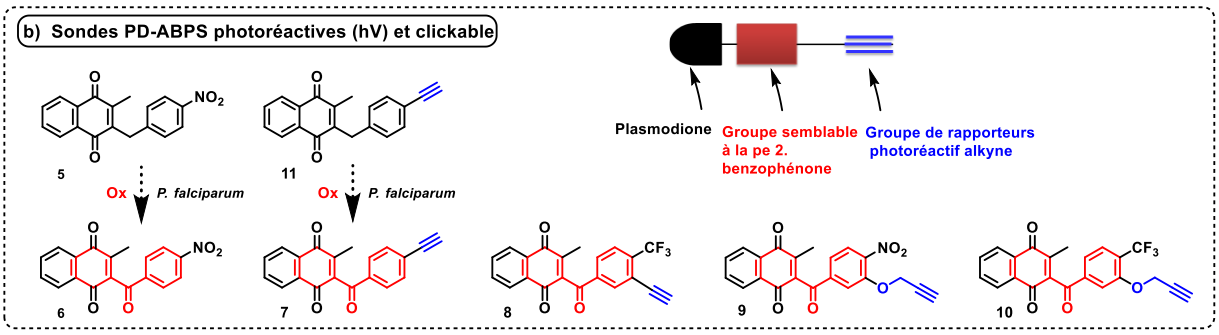
b) Sondes PD-ABPS photoréactives (hV) et clickable
Plasmodione
Groupe semblable à la pe 2. benzophénone
Groupe de rapporteurs photoréactif alkyne
5
11
Ox
P. falciparum
6
7
8
9
10

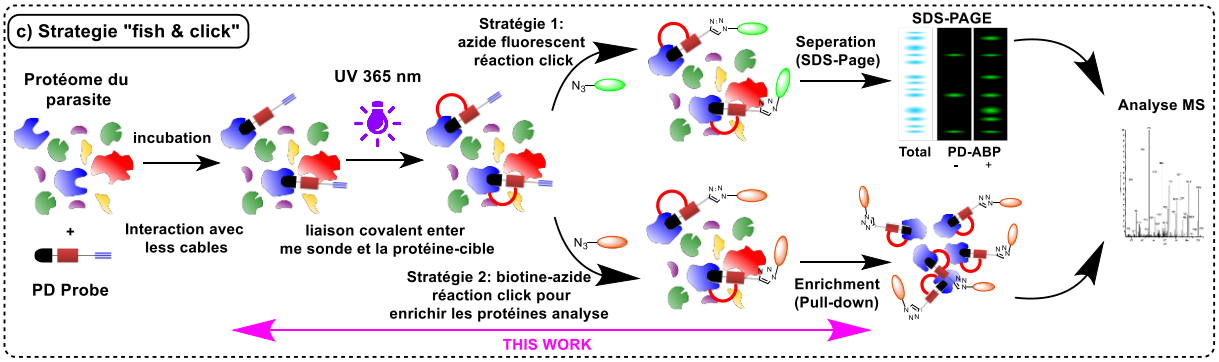
c) Strategie "fish & click"
Protéome du parasite
incubation
Interaction avec less cables
PD Probe
UV 365 nm
liaison covalent enter me sonde et la protéine-cible
Stratégie 1: azide fluorescent réaction click
Stratégie 2: biotine-azide réaction click pour enrichir les protéines analyse
Seperation (SDS-Page)
SDS-PAGE
Total
PD-ABP
Enrichment (Pull-down)
Analyse MS
THIS WORK

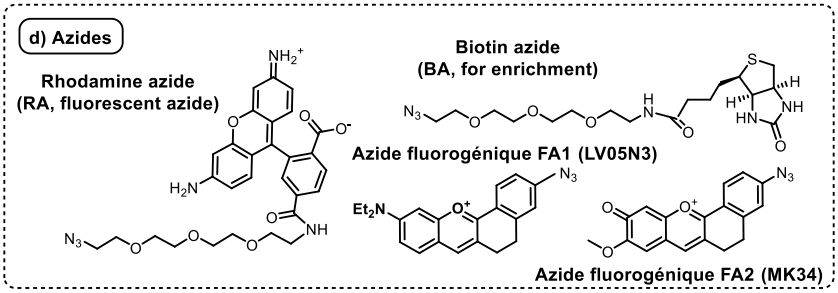
d) Azides
Rhodamine azide (RA, fluorescent azide)
Biotin azide (BA, for enrichment)
Azide fluorogénique FA1 (LV05N3)
Azide fluorogénique FA2 (MK34)

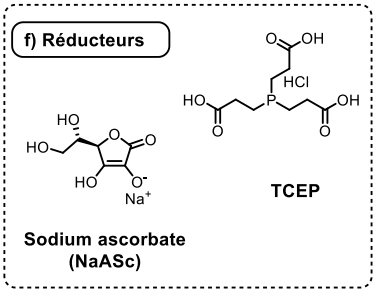
f) Réducteurs
Sodium ascorbate (NaASc)
TCEP

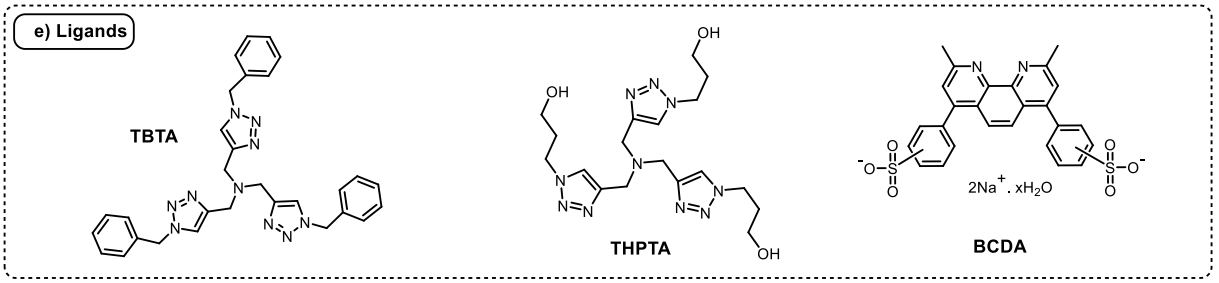
e) Ligands
TBTA
THPTA
BCDA
2Na$^+$. xH$_2$O

Fig. 1. a) Bioactivation de la plasmodione selon une cascade de réactions redox impliquant la 3-benzoylmenadione comme métabolite-clef. **b)** Structure des outils *clickables* des métabolites photoréactifs de plasmodione (PD-ABP) : le squelette des outils PD-ABP est basé sur la structure 3-benzoylmenadione possédant intrinsèquement la structure de la benzophenone photoréactive (hV 365 nm). Les différents groupes électron-attracteurs (-CF_3 or -NO_2) ou conjugables (*p*-alcyne) en position *para* des PD-ABP **8, 7, 9, 10** modulent leurs propriétés photoactivables et leur réactivité dans la chimie click. Le groupe alcyne joue le rôle d'étiquette pour révéler les adduits PD-ABP—protéine, après réaction click avec un azide émettant de la fluorescence. **c)** approche par la chimie « fish & click » : elle fait intervenir une PD réactive sous irradiation UV. En premier lieu, les parasites sont incubés avec les PD-ABP. Sous irradiation UV un lien covalent se produit entre le dérivé PD-ABP et ses cibles potentielles. De plus, une réaction click-rapportrice entre l'alcyne de la sonde et l'azide de la rhodamine fluorescente et/ou l'azide fluorogène (stratégie 1) ou l'azide de la biotine (stratégie 2) permet de révéler l'alkylation réussie de la sonde à la protéine par LC-MS/MS. Puis, une analyse bioinformatique des cibles positives de la PD, à partir des bandes de protéines fluorescentes sur gel SDS PAGE (stratégie 1) ou des protéines enrichies selon la stratégie 2. Les boîtes **d-f** indiquent les réactifs-clés qui ont été étudiés pour la réaction click: **d)** montre les partenaires azides, azide fluorescent et azides fluorogènes, **e)** montre les ligands : l'ATBT insoluble dans l'eau, l'ATBT soluble dans l'eau et le bathosulfonate disodique sont les principaux catalyseurs de la réaction click, **f)** montre les réducteurs : NaASc et TCEP ont été utilisés pour normaliser les meilleures conditions click pour la détection de cibles de PD, même à l'état de traces.

(a)

Activité antipaludique des analogues de plasmodione (PD), exprimée en valeurs d'IC_{50} ± SD[a] (nM), sur les stades asexués et sexués de P. falciparum		
Molécules de reference / PD-analogues	IC_{50} sur les stades asexués, souche Dd2- chloroquine résistante	IC_{50} sur les stades sexués gametocyte mature stade V, souche NF54
Dihydroartemisinine	0.71 ±0,23	ND
Chloroquine	189±12	ND
Bleu de methylene	7±0.3	97
Plasmodione	48±3	>10000
bMD30	42±3	8150
bMD40	92±12	227
3 expériences indépendantes dans l'essai basé sur le SYBRgreen.		

(b)

Activité antipaludique des analogues PD-ABP de plasmodione (PD), exprimée en valeurs d'IC_{50} ± SD[a] (nM), sur les stades aséxués synchrones de la souche de P. falciparum Dd2.					
BenzoylMD	(probe 6) 513	(probe 7) 1806	(probe 8) 2993	(probe 9) 417	(probe 10) >5000
controls	DHA 0.7 ± 0.2	MB 7 ± 0.3	CQ 189 ± 12	PD 48 ± 3	—

(c)

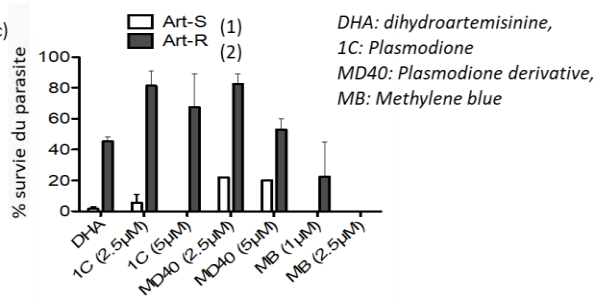

DHA: dihydroartemisinine,
1C: Plasmodione
MD40: Plasmodione derivative,
MB: Methylene blue

Fig. 2. Activité antipaludique de **a)** la plasmodione (PD), des analogues bMD30, bMD40 sur les stades asexués et sexués de *P. falciparum*, **b)** des dérivés PD-ABP, sur les stades anneaux hautement synchronisés de la souche *P. falciparum* Dd2. **c)** Données préliminaires obtenues dans l'essai de survie des anneaux (RSA) de parasites Art-S et Art-R pour mesurer la résistance croisée entre la Plasmodione ou bMD40 et l'artémisinine (Art). Les résultats sont obtenus par comptage microscopique d'anneaux à partir de frottis de sang colorés au Giemsa (nombre d'expériences).

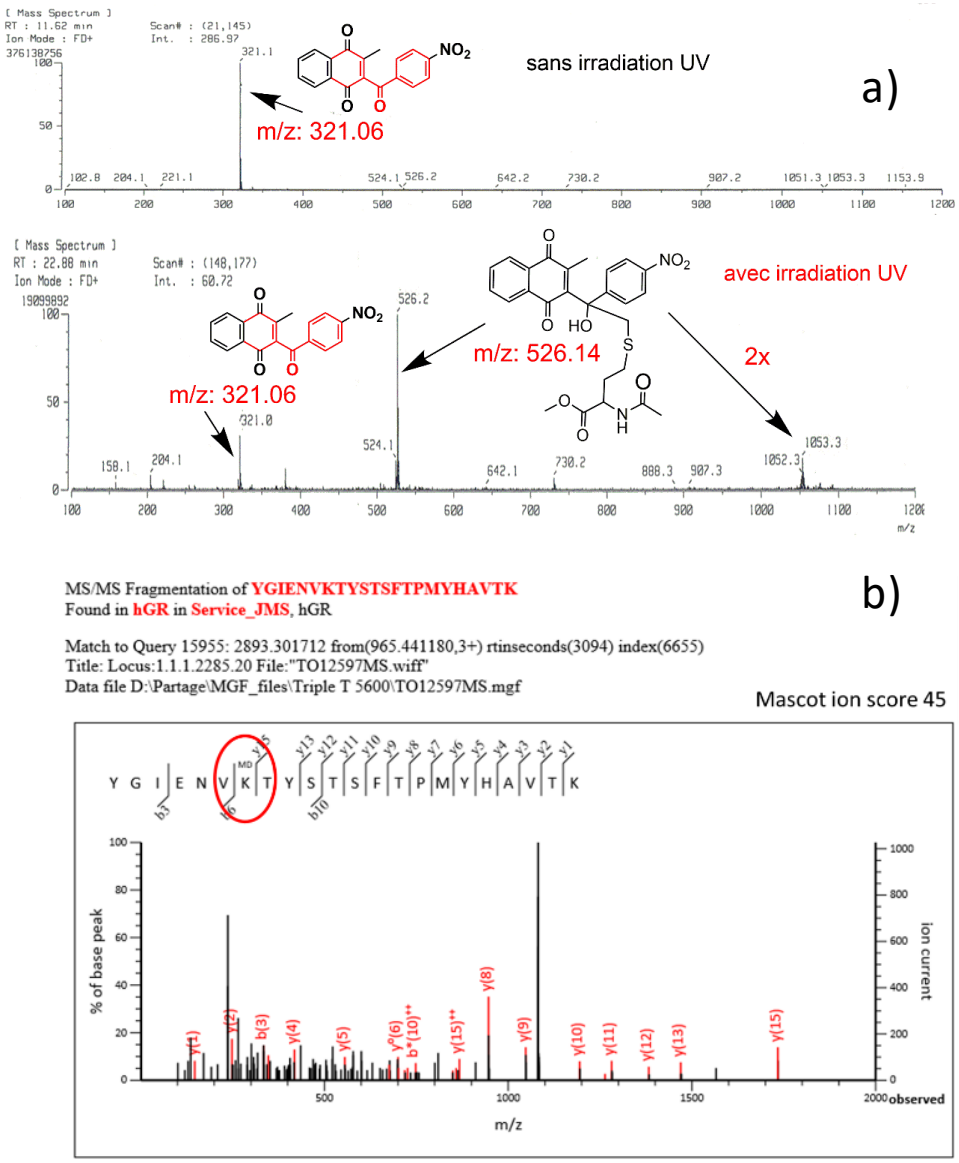

Fig. 3. (a) La spectrométrie de désorption de champ a confirmé la formation de l'adduit **7**-nMet, produit de la réaction photochimique de la sonde 7 avec la nMet, avec le pic *m/z* 526,2. **(b)** Le profil de fragmentation du peptide hGR par analyse Mascot a confirmé la présence de l'adduit du peptide hGR avec la sonde **6** après analyse LC-MS/MS.

Évaluation des propriétés antipaludiques de la PD-ABP (test IC50 modifié, exposition au médicament pendant 72 heures)

Stratégie : La synthèse d'outils chimiques avec un composant photoréactif (hV) et un marqueur "clickable" (alcynes) nous a permis de générer des sondes basées sur l'activité, structurellement proches du métabolite de la PD, afin d'identifier à la fois l'interactome du médicament et les modèles métaboliques pour des études ultérieures sur des parasites vivants *in situ*. Pour cela, nous avons d'abord évalué l'activité antipaludique des PD-ABP (Fig. 2b) afin de trouver la sonde potentielle optimisée.

Méthode : L'activité antipaludique de la PD-ABP a été analysée par l'évaluation de l'IC_{50} sur la souche Dd2 après une exposition aux molécules de 72 h sur des parasites au stade anneau âgé de 3 h.
Résultats et conclusion : Ces expériences nous ont permis de sélectionner des PD-ABP qui conservent une bonne activité antipaludique. Elles indiquent qu'un groupe attracteur d'électrons en position para est essentiel pour l'activité antiparasitaire. La sonde **3** (Fig. 1b) est une benzylMD substituée en *para* par un groupe alcyne (au lieu de CF_3 dans la PD) ; son IC_{50} est comparable à celle de la PD. Comme les sondes benzoylMD (sondes **7, 8 , 9 , 10** Fig. 1b) sont plus polaires et plus planes que les sondes benzylMD (sondes **1**,**3**,**5**), elles ne sont pas aussi facilement internalisées par les parasites que les sondes benzylMD, ce qui explique pourquoi leur IC_{50} est en général 100 fois supérieure à celle des sondes benzylMD. Les sondes benzoylMD photoréactives ont ensuite été utilisées pour la preuve de concept de la chimie « fish & click » à l'aide de partenaires-modèles. Pour les études de faisabilité, nous avons sélectionné la sonde **11** pour l'analyse de l'interactome PD car elle est photoréactive sous irradiation UV (à 350 nm).

Caractérisation de la photoréactivité des sondes PD-ABP en utilisant un dérivé de methionine (nMet) et la GR comme modèles.

L'abondance des protéines exprimées dans les parasites est variable. Les protéines majoritaires peuvent ne pas être les cibles réelles de la PD. Par conséquent, les cibles réelles de la PD produites en traces seraient difficiles à mettre en évidence lors de l'analyse par spectrométrie de masse (MS). Cela peut également conduire à l'obtention de faux positifs, ceci a déjà été observé dans la littérature (6-9). Il est donc très difficile de mettre en place directement dans les parasites des conditions générales de photoréaction et de réaction click avec une PD-ABP. Pour éviter le marquage non spécifique de nos sondes à des protéines non ciblées, nous avons utilisé des systèmes modèles pour standardiser les conditions de photoréaction et de réaction click avant l'utilisation de la PD-ABP sur les parasites. La méthionine modifiée P_TM52 (nMet, c'est-à-dire l'ester méthylique de *N*-acétylméthionine ou N-Ac-Met-OMe, Fig. 3), les glutathion réductases de *P. falciparum* (PfGR) ou humaine (hGR) ont été utilisées comme modèles pour standardiser la photoréaction.

Normalisation des paramètres d'irradiation UV à l'aide de nMet
Stratégie: Les résultats de la réaction modèle ont montré qu'après photoactivation, le nMet peut se lier de manière covalente avec les benzoylMD, fonctionnalisées de préférence par un groupe électroattracteur (par exemple, NO_2) en position *para*. Les résultats de la spectrométrie de masse par désorption de champ ont confirmé la formation du produit alkylé (fig. 3a). Le choix du dérivé de méthionine, i.e. l'acide aminé préféré comme partenaire de photoréaction avec la benzophénone, est basé sur les résultats de G. Ourisson *et al.*, 1989 (12). Nous avons donc utilisé le nMet comme modèle pour évaluer la photoréactivité des benzoylMD spécifiques (fig. 1b) synthétisés dans notre équipe de recherche.
Méthode : Nous avons d'abord analysé le coefficient d'extinction moléculaire au λmax de tous les PD-ABP par spectrophotométrie d'absorption UV-Vis. Comme le maximum d'absorption λmax est d'environ 340 nm pour les sondes **3, 7, 9, 6** et 320 nm pour les sondes **8** et **10**, nous avons donc choisi une longueur d'onde optimale de 360 nm comme source d'excitation lumineuse pour étudier la photoréaction correspondante. La photoréaction du nMet et des sondes a été réalisée en utilisant 2 sources de lumière différentes : 1. un photoréacteur avec

des lampes UV irradiant à 360 nm de 224 W d'intensité lumineuse (total) ; 2. un monochromateur UV de 360 nm et de plus haute intensité à 1000 W. Divers facteurs tels que la longueur d'onde de photo-irradiation, le solvant et la distance de l'échantillon par rapport à la source d'excitation, le temps d'exposition de l'échantillon à la photo-irradiation et la présence ou l'absence d'oxygène ont été modifiés et leur influence a été analysée en détail. Le produit alkylé de manière covalente a été confirmé par CCM, spectrométrie de masse et par analyse RMN.

Résultats : La photoréactivité des sondes dépend du groupe présent en position *para*. Nous avons observé qu'un produit nMet-PD-ABP lié de manière covalente se forme après 20 heures d'irradiation du nMet et des sondes dans un photoréacteur de 224 W, alors qu'il ne fallait que 2 minutes pour que la même réaction se produise lors de l'exposition à une lampe monochromateur UV de 1000 W à haute intensité. Cette photoréaction se produit de préférence avec des groupes électroattracteurs (EWG) (-NO_2 et -CF_3) fonctionnalisés en position *para* avec un rendement d'environ 20 % calculé à partir des données de RMN ^{1}H. Dans certains cas, la PD-ABP a montré une photoréactivité encore meilleure que celle de l'agent photoréactif bien connu qu'est la benzophénone. Sur la base de ces données, nous pouvons conclure que, après une fonctionnalisation appropriée, les benzoylMD sont photoréactives en soi, et sont utiles à la mise en œuvre de notre stratégie « fish & click ».

Les protéines comme modèle de photoréaction

Les conditions de photoréaction précédentes engageant le nMet avaient été réalisées dans les solvants organiques à des concentrations de l'ordre du mM. Nous avons donc utilisé trois peptides -GSH, MSH et P-52C - pour établir les conditions de photoréaction dans des conditions physiologiques et pour caractériser le comportement des adduits dans l'analyse HPLC-MS. Il est attendu que le rendement de la photoréaction devrait augmenter avec les protéines comme partenaires en raison de l'affinité et de la liaison de la sonde à la protéine. Nous avons observé le produit adduit de la sonde **6**-hGR après réaction avec la hGR (5 µM) et la sonde **6** (5 µM) dans un tampon phosphate, et 2% d'acétonitrile, dans des conditions sans oxygène et 8 minutes d'exposition à 360 nm UV (monochromateur 1000W). La figure 3b montre le profil de fragmentation du peptide adduit le mieux identifié (le plus sûr) de la hGR à la sonde **9** . Le fragment peptidique, au niveau du site de clivage de l'acide aminé alkylé (la lysine K399) n'est pas digéré par la trypsine. Le même peptide a été identifié trois fois dans deux échantillons différents, chaque fois avec un haut degré de confiance. De nombreuses modifications sur plusieurs sites d'interaction sonde-protéine sont un peu difficile à détecter avec un intervalle de confiance élevé si l'interaction sonde-protéine est faible. Par conséquent, l'étape suivante a consisté à étiqueter avec une réaction click.

Caractérisation des produits de réaction click des sondes PD-ABP à des fluorophores azotures modèles:

Stratégie : Le développement d'une sonde à haute efficacité de marquage de protéines est particulièrement difficile car les groupes photo-réactifs et rapporteur du marquage peuvent influencer la spécificité de liaison de la sonde à des cibles plus ou moins abondamment exprimées. C'est pourquoi nous avons transposé ici la réaction click qui pourrait ainsi permettre ainsi de révéler une interaction sonde-protéine même mineure. La réaction « click » de cycloaddition biorthogonale 1,3-dipolaire entre un alcyne et un partenaire azide conduit à la formation d'un motif 1,2,3-triazole 1,4-disubstitué. En raison de sa biocompatibilité, la réaction

CuAAC a été fréquemment utilisée pour révéler et permettre l'identification de petites molécules telles que l'ADN, l'ARN, les peptides ou les protéines en chimie médicale, pharmacologie et pour la recherche en science des matériaux (13). Dans notre cas, les PD-ABP (Fig. 1b) présentent des groupements fonctionnels de type alcyne. Le groupe alcyne a été introduit dans différentes positions de la chaîne benzoyle (3' ou 4'). Dans d'autres molécules, l'alcyne a été introduit soit directement sur la benzoylménadione **(8 , 7**), soit en utilisant un espaceur O-CH_2 (**9, 10**). Cette série de PD-APB s'est avérée d'une forte utilité pour évaluer la position et la longueur de l'espaceur nécessaires pour améliorer l'efficacité de formation du 1,2,3-triazole lors de la réaction de type CuAAC. Afin de sélectionner la meilleure sonde PD-ABP pour identifier l'interactome de la PD, nous avons d'abord évalué l'efficacité de la réaction CuAAc de 4 PD-ABP en utilisant différents azotures tels que l'azoture de rhodamine (RA) fluorescent disponible commercialement et des azotures fluorogènes développés au sein de l'équipe (LV05N3 - azoture fluorogène 1 (FA1) et MK34N3 azoture fluorogène 2 (FA2), Fig. 1d). Les azotures fluorogènes, construits autour d'un noyau flavylium bioinspiré contraint, sont peu fluorescents sur forme azoture et devraient émettre fortement après réaction click (17). Les composés LV05N3 et MK34N3 ont été préparés à partir des dérivés aminés correspondants ($NaNO_2$, HNO_3, EtOH) émettant dans le rouge LV05 (λ^{em} = 628 nm/Φ^{abs} = 14% à pH 7,41 et λ^{em} = 626 nm/Φ^{abs} = 73% dans l'éthanol) and MK34 (λ^{em} = 595 nm/Φ^{abs} = 30,9% à pH 7,41 et λ^{em} = 583 nm/Φ^{abs} = 50% dans l'éthanol), respectivement. Les deux azotures fluorogènes, LV05N3 et MK34, ont été étudiés en solution par des moyens spectroscopiques (non présentés dans ce rapport) et préparés pour discriminer la fluorescence des réactifs (fluorescence OFF) par rapport à celle du produit de cycloaddition (fluorescence ON, impossible avec l'azoture de rhodamine fluorescent).

Méthode : Selon la littérature, le complexe de cuivre(I) est essentiel pour la réaction CuAAC. Plus de 10 complexes de cuivre(I) stables ont été décrits jusqu'à présent dans la littérature, et tous ne sont pas cependant disponibles commercialement. De ce fait, l'efficacité de la réaction CuAAc dépendra fortement de la combinaison et des rapports entre précurseur de cuivre(II), chélateur et réducteur pour permettre une conversion efficace du Cu(II) en Cu(I). Les données de la littérature montrent qu'entre 2011 et 2015, pas moins de 4 sources de cuivre(II), 4 ligands, 5 agents réducteurs et environ 10 combinaisons de solvants ont été testés dans des réactions de type CuAAC (14-16). Nous avons donc standardisé notre réaction click CuAAC en utilisant différentes combinaisons de réactifs (alcyne, azoture, la source de cuivre(II), ligand et agent réducteur). À cette fin, nous avons utilisé comme source de cuivre soit le sulfate de cuivre(II) pentahydraté, soit un complexe de Cu(I) avec la 2,9-diméthyl-1,10-phénanthroline ($Cu^{I}(dmp)_2.BF_4$), fourni par l'équipe du Dr Jean Pierre Sauvage. En outre, trois autres ligands tels que la tris(benzyltriazolylméthyl)amine (TBTA), la tris(3-hydroxypropyltriazolylméthyl)amine (THPTA), ou le disulfonate de bathocuproine disodique, ligand aussi fourni par l'équipe du Dr Jean Pierre Sauvage, ont été considérés. Enfin, 2 agents réducteurs, l'ascorbate de sodium (NaAsc) et la tris(2-carboxyéthyl)phosphine (TCEP), ont été testés. D'autres facteurs tels que la composition du solvant, la teneur en oxygène, la température ont été examinés. Les principales combinaisons seront présentées dans la thèse.

Résultats : La meilleure combinaison pour la réaction CuAAC a été obtenue pour les sondes de DP-ABP **8, 7, 9 , 10** et l'azoture de rhodamine (fig. 1) dans des conditions strictes d'absence d'oxygène avec 4 ajouts successifs de complexe de cuivre(I) ($CuSO_4.5H_2O$ 1equiv. + THPTA 1 equiv. + TCEP 1 eq.) de la manière suivante : à T0 -45 minutes de complexe CuI pré-incubé et à T30, T60 et T90, 20 minutes de pré-incubation (Fig. 4d). Les produits de réaction CuAAC ont été ensuite analysés par spectroscopie de fluorescence et par HPLC-MS. Nous avons pu ainsi observer que l'ajout de doses multiples de complexes de Cu(I) dans des conditions

anaérobiques strictes permettait d'augmenter le rendement de la réaction CuAAC et réduire le temps de réaction de 24 heures à 2,5 heures. Selon le rendement de la réaction CuAAC, les efficacités mesurées pour les différentes sondes PD-ABP sont les suivantes: sonde **7**(47,33%) > sonde **9** (25,33%) > sonde **10** (5,67%) > sonde **8** (3,04%).
Les sondes **7** et **9** sont également compatibles pour la réaction CuAAC avec l'azoture FA1 avec une efficacité respective de 58,25% avec la sonde 4 et de 40,02% avec la sonde **6**. Même si la réaction CuAAC avec AF1 a conduit à des rendements de réaction CuAAC supérieurs par rapport à ceux déterminés avec l'azoture RA, une légère réduction d'émission de fluorescence du produit de réaction (RA) est observée, tandis que l'émission de fluorescence (AF1) est significativement diminuée. D'autre part, même la couleur de l'azoture FA1 s'est atténuée après la réaction CuAAC témoignant d'une altération du fluorophore au cours de la réaction. Par conséquent, FA1 n'a pas été retenu dans la suite de nos expériences car il ne permettrait pas de distinguer les protéines sur gel ou de visualiser la cible de PD-ABP in vivo. La réaction CuAAC avec l'azoture de rhodamine RA pourra donc être utilisée pour apporter une preuve de concept de notre approche.

Conclusion générale

Mon projet de recherche a contribué à identifier i) la bMD40 comme meilleur analogue de la PD en validant sa capacité à tuer les stades asexués de différentes souches de parasites sensibles et résistantes à l'Art ; ii) Une résistance croisée existante entre la PD/MD40 et l'artémisinine ; iii) Les 3-benzoylmenadiones **7** et **9** sont les plus efficaces des sondes PD-ABP, avec des propriétés photoréactives et de « cliquabilité » ; iv) Comme l'IC_{50} de la sonde benzylMD **7** – la prodrogue de la sonde 3-benzoylmenadione **7** - est aussi puissante que la PD, nous sommes certains qu'elle peut être utilisée comme un outil chimique efficace pour l'identification de l'interactome de la PD dans l'approche « fish & click ».

References :

1. Dondorp A.M., Nosten F., Yi P., Das D., Phyo A.P., Tarning J., Lwin K.M., Ariey F., Hanpithakpong W., Lee S.J., Ringwald P., Silamut K., Imwong M., Chotivanich K., Lim P., Herdman T., An S.S., Yeung S., Singhasivanon P., White N.J. Artemisinin resistance in Plasmodium falciparum malaria. N Engl J Med 2009, 361, 455–467. https://doi.org/10.1056/NEJMoa0808859
2. Ehrhardt K, Davioud-Charvet E., Ke H., Vaidya A.B., Lanzer M., Deponte M. The antimalarial activities of methylene blue and the 1,4-naphthoquinone 3-[4-(trifluoromethyl)benzyl]-menadione are not due to inhibition of the mitochondrial electron transport chain. Antimicrob Agents Chemother 2013, 57, 2114–2120. https://doi.org/10.1128/AAC.02248-12
3. Ehrhardt K., Deregnaucour C., Goetz A.A., Tzanova T., Gallo V., Arese P., Pradines B., Adjalley S.H., Bagrel D., Blandin S., Lanzer M., Davioud-Charvet E. The redox cycler plasmodione is a fast-acting antimalarial lead compound with pronounced activity against sexual and early asexual blood-stage parasites. Antimicrob Agents Chemother 2016, 60, 5146–5158. https://doi.org/10.1128/AAC.02975-15
4. Bielitza M., Belorgey D., Ehrhardt K., Johann L., Lanfranchi D.A., Gallo V., Schwarzer E., Mohring F., Jortzik E., Williams D.L., Becker K., Arese P., Elhabiri M., Davioud-Charvet E. Antimalarial NADPH-consuming redox-cyclers as superior glucose-6-phosphate dehydrogenase deficiency copycats. Antioxid Redox Signal 2015, 22, 1337–1351. https://doi.org/10.1089/ars.2014.6047
5. Müller T., Johann L., Jannack B., Brückner M., Lanfranchi D.A., Bauer H., Sanchez C., Yardley V., Deregnaucourt C., Schrével J., Lanzer M., Schirmer R.H., Davioud-Charvet, E.

Glutathione reductase-catalyzed cascade of redox reactions to bioactivate potent antimalarial 1,4-naphthoquinones – a new strategy to combat malarial parasites. J Am Chem Soc 2011, 133, 11557–11571. https://doi.org/10.1021/ja201729z
6. Penarete-Vargas D.M., Boisson A., Urbach S., Chantelauze H., Peyrottes S., Fraisse L., Vial H.J. A chemical proteomics approach for the search of pharmacological targets of the antimalarial clinical candidate albitiazolium in Plasmodium falciparum using photocrosslinking and click chemistry. PLoS One 2014, 9, e113918. https://doi.org/10.1371/journal.pone.0113918
7. Ismail H. M., Barton V. E., Panchana M., Charoensutthivarakul S., Biagini G.A., Ward S.A., O'Neill P.M. A click chemistry-based proteomic approach reveals that 1,2,4-trioxolane and artemisinin antimalarials share a common protein alkylation profile. Angew Chem Int Ed Engl 2016, 55, 6401–6405. Corrigendum: 55, 10548. https://doi.org/10.1002/anie.201607032
8. Lubin A.S., Rueda-Zubiaurre A., Matthews H., Baumann H., Fisher F.R., Morales-Sanfrutos J., Hadavizadeh K.S., Nardella F., Tate E.W., Baum J., Scherf A., Fuchter M.J. Development of a photo-cross-linkable diaminoquinazoline inhibitor for target identification in Plasmodium falciparum. ACS Infect Dis 2018, 4, 523–530. https://doi.org/10.1021/acsinfecdis.7b00228
9. Wright M.H., Clough B., Rackham M.D., Rangachari K., Brannigan J.A., Grainger M., Moss D.K., Bottrill A.R., Heal W.P., Broncel M., Serwa R.A., Brady D., Mann D. J., Leatherbarrow R. J., Tewari R., Wilkinson A. J., Holder A.A., Tate, E.W. Validation of N-myristoyltransferase as an antimalarial drug target using an integrated chemical biology approach. Nat Chem 2014, 6, 112–121. https://doi.org/10.1038/nchem.1830
10. Witkowski B., Amaratunga C., Khim N., Sreng S., Chim P., Kim S., Lim P., Mao S., Sopha C., Sam B., Anderson J.M., Duong S., Chuor C.M., Taylor W. R., Suon S., Mercereau-Puijalon O., Fairhurst R.M., Menard D. Novel phenotypic assays for the detection of artemisinin-resistant Plasmodium falciparum malaria in Cambodia: in-vitro and ex-vivo drug-response studies. Lancet Infect Dis 2013, 13, 1043–1049. https://doi.org/10.1016/S1473-3099(13)70252-4
11. Amaratunga C., Neal A.T., Fairhurst R.M. Flow cytometry-based analysis of artemisinin-resistant Plasmodium falciparum in the ring-stage survival assay. Antimicrob Agents Chemother 2014, 58, 4938–4940. https://doi.org/10.1128/AAC.02902-14
12. Deseke E., Nakatani Y., Ourisson G. Intrinsic reactivities of amino acids towards photoalkylation with benzophenone − a study preliminary to photolabelling of the transmembrane protein glycophorin A. Eur J Org Chem 1998, 243–251. https://doi.org/10.1002/(SICI)1099-0690(199802)1998:2<243::AID-EJOC243>3.0.CO;2-I
13. Bozorov K., Zhao J., Aisa H.A. 1,2,3-Triazole-containing hybrids as leads in medicinal chemistry: A recent overview. Bioorg Med Chem 2019, 27, 3511-3531. https://doi.org/10.1016/j.bmc.2019.07.005
14. Presolski S. I., Hong V.P., Finn, M.G. Copper-catalyzed azide–alkyne click chemistry for bioconjugation. Curr Protoc Chem Biol 2011, 3, 153–162. https://doi.org/10.1002/9780470559277.ch110148
15. Presolski S.I., Mamidyala S.K., Manzenrieder F., Finn, M.G. Resin-supported catalysts for CuAAC click reactions in aqueous or organic solvents. ACS Comb Sci 2012, 14, 527–530. https://doi.org/10.1021/co300076k
16. Bevilacqua V., King M., Chaumontet M., Nothisen M., Gabillet S., Buisson D., Puente C., Wagner A., Taran, F. Copper-chelating azides for efficient click conjugation reactions in complex media. Angew Chem Int Ed Engl 2014, 53, 5872–5876. https://doi.org/10.1002/anie.201310671
17. Shieh P., Dien V.T., Beahm B.J., Castellano J.M., Wyss-Coray T., Bertozzi, C.R. CalFluors: A Universal Motif for Fluorogenic Azide Probes across the Visible Spectrum. J Am Chem Soc 2015, 137, 7145–7151. https://doi.org/10.1021/jacs.5b02383
18. Lenstra D. C., Wolf J. J., Mecinovi, J. Catalytic Staudinger Reduction at Room Temperature. J Org Chem 2019, 84, 6536–6545. https://doi.org/10.1021/acs.joc.9b00831

LISTE DES PRESENTATIONS

Poster 1. Khobragade V., Feufack B., Ehrhardt K., E. Nsango S., Morlais I., Blandin S., Vela A., Oury B., Barnabé C., Solano P., Costales J. A., Kaiser M., Brenière F. S., Feng L., Donzel M., Elhabiri M., Davioud-Charvet E. ***Optimization and molecular understanding of redox-active 3-benzylmenadiones: a new chemotype with cross-pathogen activity***. EMBO Workshop "Molecular advances and parasite strategies in host infection, 30.09.2018, Les Embiez, France.

Poster 2. Khobragade V., Cichocki B., Donzel M., Cotos L., Feng L., Khelladi M., Elhabiri M., Blandin S., Davioud-Charvet E. ***. Development of a selective activity-based probe for identifying targets of the antimalarial drug Plasmodione***. EMBL Conference: BioMalPar XV: Biology and Pathology of the Malaria Parasite, 29.05.2019, EMBL Heidelberg, Germany.

SUMMARY

The research team “Bio(IN)organic and Medicinal Chemistry” headed by Dr. Elisabeth Davioud-Charvet has pioneered the chemistry and development of redox-cyclers as potent antiparasitic agents, which belong to the class of *1,4*-naphthoquinones derivatives. These compounds built on the menadione backbone, display oxidant character accepting 1 or 2 electrons from redox cycling mediated by NADH/NADPH dependent oxidoreductases, such as glutathione reductase (GR, E.C. 1.8.1.7) - a key enzyme involved in maintaining the redox homeostasis of *P. falciparum* and its hosting human erythrocytes. In particular, a series of 3-benzylmenadione derivatives with potent antiplasmodial activities, discovered and studied in details, was designed as prodrugs of efficient redox-cyclers, such as the 3-benzylmenadiones formed by benzylic oxidation. Such redox-cyclers act as subversive substrates of the oxidoreductases and the demonstration was supported by enzyme kinetics with both GR of the infected red blood cells selected as reaction models.

The early lead representative was named plasmodione. Its bioactivation was assumed to be expressed through a cascade of redox reactions generating toxic metabolites for the parasite. The cascade was demonstrated to mimic the clearance effects of a parasite living in infected erythrocytes with established glucose-6-phosphate deficiency and increased oxidative stress. The natural genetic mutation is known to protect G6PD deficient carriers from cerebral malaria.

Over past 20 years, the flourishing interest of the research team in the redox medicinal chemistry has led to the development of antiparasitic agents with major achievement related to chemical substitution pattern of 3-benzyl-menadione derivatives with potent antiparasitic activities in vitro and in vivo against *P. falciparum. The most potent derivatives possess* improved pharmacokinetic properties and tolerance even for G6PD deficient individuals. The mode of action and novel therapeutic targets of such compounds in the parasites are studied with an interdisciplinary approach via enzyme kinetics, metabol- and proteo-omics. For a decade, the team work has led to synthesis and development of several reversible and irreversible inhibitors of oxidoreductases (Biot et al., 2004; Krauth-Siegel et al., 2005; Bauer et al., 2006), redox cyclers (Salmon-Chemin et al., 2001; Morin et al., 2008; Müller et al., 2011), dual drugs with Trojan horse effect, metabolites (Bielitza et al., 2015; Feng et al, 2018), ratiometric fluorescent probes sensitive to pH and redox gradients.

The objectives of my PhD thesis were:

i) to evaluate the antimalarial properties and cross-Art resistance properties of PD analogues and PD probes, both in the standard 72h-drug exposure assays and/or in the ring survivalassays (RSA);

ii) to set up all conditions for the click reactions and photoirradiation of selective activity-based PD probes with various partners;

iii) to use selected phototoreactive and clickable PD probes in P. falciparum to identify high-score

The first chapter of my Ph.D. thesis is a vast introduction compiling the reported effects of a large array of antimalarial redox cyclers and ROS-inducing drugs on the metabolically less active ring stage and late-stage gametocyte of *Plasmodium* parasites. These stages are otherwise less susceptible to the currently available antimalarial drugs. Me, my supervisors – Dr. Elisabeth Davioud Charvet and co-supervisor- Dr. Stéphanie Blandin have contributed to writing this part, which soon will be published as a review. For this, I performed extensive literature analysis and a summary of drugs in the table and figure that links the role of drugs to the organelle development and biological processes, mode of action, targets among different redox-active and redox inducing drugs.

Chapter 2 elucidates that the PD analog, bMD40, with improved pharmacokinetics properties showed cross-resistance with asexual stages of Artemisinin resistant *P. falciparum*, thereby opening an intriguing question about the PD drug combinations as a future therapeutic option. For this, I set the cultures of various drug-susceptible and resistant *P. falciparum* parasites in the laboratory, standardized the conditions for modified IC_{50} assay on tightly synchronized 3-hour-old ring stages of parasites, and contributed to establishing the ring survival assay using FACS analysis. I contributed to the technology transfer to another PhD student-Brice Feufack. In addition, I measured all antimalarial activities of the ABPP probes used in Chapter 3.

Chapter 3 covers the design, synthesis, characterization, and functionality aspects involved in the development of ABPP probes derived from the antimalarial drug plasmodione to identify the drug targets. First, I spent 2 months in Prof. Katja Becker's laboratory in Giessen, Germany to learn the purification of His-tagged GR enzyme with criteria for proteomics studies, and to measure enzyme kinetics. Organic chemists- (Ph.D. student Maxime Donzel, master students Alba Zugasti and Joan Guillem, together with the postdoctoral researcher Dr. Leandro Cotos) in our research group, synthesized all probes mentioned in the study. My role was to validate the clickability and photoreactive properties of the 3-benzoylmenadione-based probes for the proof of concept of the 'fish' and click strategy-using modified amino acids as chemical models of peptides and protein. Standardization of the click reaction conditions was an important contribution of my work focused on the reactions of ABPP probes and rhodamine azide in aqueous conditions. This involved standardization of HPLC-MS conditions for the click reaction analysis in collaboration with Jean-Marc Strub and Christine Schaeffer from the Laboratoire de Spectrométrie de Masse BioOrganique (LSMBO) at IPHC, UV-vis spectral analysis, and fluorometric analysis of every reaction. Further, I standardized the photoreaction conditions using modified amino acid as a model using a UV monochromator and analyzed the extinction co-efficient of all the probes. I initiated setting up the photoreaction conditions using protein as a model, they were further adopted and standardized by the postdoctoral researcher Dr. Bogdan Cichocki. In parallel to my work, B. Cichocki also set up conditions for analysis of peptide and proteins crosslinking by LCMS/MS analysis and adapted click reaction conditions in phosphate buffer using biotin azide instead of rhodamine azide to be able to extract and purify the probe crosslinked protein after click reaction. Additionally, the impact of the BCDA as a ligand instead of THPTA in click reaction was exploited in this study.
To sum up, by combining the photoirradiation of the PD-derived ABPP probes and the click reaction with different azides - probe **7** with a 4'-alkyne group and probe **9** with a 4'-nitro - proved to be the most efficient photoreactive and clickable probes. Probe **4** with good antimalarial activity is a promising candidate for identifying drug targets in parasites.

Chapter 4 includes the proof of concept for using fluorogenic chemical tools with the property of emitting bright fluorescence upon click reaction for in vivo imaging as an alternative to commercially available traditional and expensive rhodamine azide. These newly designed derivatives did not show distinguishable emission properties prior and after the triazole formation in click reaction, however, the yield of probe 9-FA1 triazole product of FA1 was better than rhodamine azide. The fluorogenic flavylium azides (FA1 and FA2) were designed by Mourad Elhabiri and synthesized by Mustapha Khelladi with the assistance of the master student Lea Vella. My role was to validate the physicochemical properties of two azides together with Valérie Mazan and Bogdan Cichocki. Further, I standardized the clickability properties of FA1 and FA2 with PD ABPP alkyne partners. This involved extensive UV-Vis spectrophotometry to understand the stability of azides, followed by HPLC-MS, and fluorometric analysis of the click reactions with probe **7** and probe **9**. This study paved the way to develop novel, affordable, water-soluble, and photostable fluorogenic chemical tools for in vivo imaging. Our study has shown that the substitution pattern of FA1 is important for its reactivity and fluorescence emission properties. FA1 is an affordable, water-soluble and (photo)stable chemical tool, whose reactivity in cycloaddition reactions has been found to be improved with respect to that of rhodamine azide. However, the fluorescence of the constrained flavylium chromophore was not reinstated on reaction with alkyne-based probes (i.e., FA1 did not act as a fluorogenic system). On the other hand, we also clearly demonstrated that the reactivity in CuAAC-type reactions also closely depends on the physico-chemical properties of the alkyne partner.

Overall, my multidisciplinary PhD research including chemical biology, organic chemistry and parasitology has been extensive learning of diverse techniques and linking complex biochemical concepts, which eventually led to setting up ground for a broader development and improvements of chemical tools for identifying drug targets. The collaboration and teamwork involved in this research define true research and development in cross-functional departments.

TABLE OF CONTENTS

ABBREVIATIONS

ABPP	Activity based protein profiling
ACN	acetonitrile
ACT	artemisinin-based combination therapies
AQ	amodiquine
Art	Artemisinin
Art-R	Artemisinin-resistant
Art-S	Artemisinin-sensitive
BA	biotin-azide
BCDA	disodium bathocuproine sulfonate
benzylMD/bMDs	benzylmenadione
ACN	acetonitrile
CID-MS	Collision-induced dissociation mass spectrometry
CQ	chloroquine
CuAAC	Cu(I)-catalyzed alkyne-azide click reaction
$CuSO_4.5H_2O$	Copper sulphate pentahyadrate
Dd2	Chloroquine resistant *P. falciparum* strain
DHA	dihydroxyartemisinin
DMF	dimethylformamide
ESI	Electronspray inonization
EWG	electron-withdrawing group
FA1 or LV05N3	Flavylium azide 1
FA2 or MK34N3	Flavylium azide 2
FAD	Flavin adenine dinucleotide
FD-MS	field desorption-mass spectrometry
FQ	ferroquine
FV	food vacuole
G6PD	glucose-6-phosphate dehydrogenase
GR	glutathione reductases
Hb	hemoglobin
hGR	human glutathione reductase
HO•	hydroxyl radicals
IC50	nucleophilic lysine ε-amine
LC-MS	Liquid chromatogrpahy mass spectrometry
λ_{em}	wavelength of emission
λ_{ex}	wavelength of excitation
MB	Methylene blue
metHb	methemoglobin
MoA	modes of action
NaASc or Na2SO4	sodium ascorbate
NaCl	sodium chloride
NAD(P)H	Nicotinamide adenine dinucleotide phosphate
NAG	N-acetyl glucosamine

nMet / N-Ac-Met-OMe/ P_TM52	N-acetyl-methionine methyl ester
$O_2^{\circ-}$	superoxide anion
ON	overnight
P. falciparum	Plasmodium falciparum
PBS	Phosphate-buffered saline
PD	Plasmodione
PD-ABPPs	Plasmodione-activity based profiling probe
PPP	pentose phosphate pathway
pRBCs	parasitized red blood cells
RA	rhodamine azide
RBCs	red blood cells
RSA	Ring Survival Assay
RT	Room tempterature
SD	Standard deviation
SDS	sodium dodecyl sulfate
TBTA	Tris[(1-benzyl-1*H*-1,2,3-triazol-4-yl)methyl]amine
TCEP	(tris(2-carboxyethyl)phosphine)
TFA	trifluoroacetic acid
THPTA	tris-hydroxypropyltriazolylmethylamine
TICT	Twisted Intramolecular Charge Transfer
TMS	trimethylsilane
UV	Ultra violet
G6PD	Glucose-6-phosphate dehydrogenase
GSSG	Glutathione oxidized form or glutathione disulphide
GSH	Glutathione reduced form

List of probes:

MD83: Probe 6

BenzoylMD

AZ47: Probe 7

MD65: Probe 8

MD43: Probe 9

MD134: Probe 10

BenzylMD

JG43: Probe 11

CHAPTER 1 : Rings and gametocyte stages of *Plasmodium* are sensitive to antimalarial generating oxidative stress

The first chapter of my Ph.D. thesis is a vast introduction compiling the reported effects of a large array of antimalarial redox cyclers and ROS-inducing drugs on the metabolically less active ring stage and late-stage gametocyte of *Plasmodium* parasites. These stages are otherwise less susceptible to the currently available antimalarial drugs Me, my supervisors – Dr. Elisabeth Davioud Charvet and co-supervisor- Dr. Stéphanie Blandin have contributed to writing this part, which soon will be published as a review. For this, I performed extensive literature analysis and a summary of drugs in the table and figure that links the role of drugs to the organelle development and biological processes, mode of action, targets among different redox-active and redox inducing drugs.

Keywords: malaria; oxidative stress; reactive oxygen species; transmission.

Abbreviations :

artemisinin, ART ; artemisinin-based combination therapies, ACTs; chloroquine, CQ; dihydroartemisinin, DHA; ferroquine, FQ; glucose-6-phosphate dehydrogenase, G6PD ; glutathione, GSH ; glutathione disulfide, GSSG ; glutathione reductase, GR; hemoglobin-Fe^{II}, Hb ; indolone-*N*-oxides, iNODs ; Malaria Research Agenda initiative, malERA; medicines for malaria venture, MMV ; methemoglobin-Fe^{III}, metHb; methylene blue, MB ; mitochondrial electron transport chain, mETC ; reduced nicotinamide adenine dinucleotide phosphate, NADPH ; primaquine, PQ ; quinine, QN ; reactive oxygen species, ROS ; tafenoquine, TQ; thioredoxin, Trx ; thioredoxin reductase, TrxR ; tricarboxylic acid cycle, TCA.
bMDs: benzylmenadione, FQ: ferroquine,

TABLE OF FIGURES: CHAPTER 1

Introduction

Rings and gametocyte stages of *Plasmodium* are sensitive to antimalarial generating oxidative stress

With 228 million cases and 405 000 deaths in 2018, mostly in the Sub-Saharan Africa, malaria remains one of the most severe infectious diseases that disproportionally affects both the public health and economic welfare of the world's poorest communities (WHO, 2019). The causative agents of malaria belong to six species of protozoan parasites of the genus Plasmodium. Among them, *P. falciparum*, is responsible for most severe forms of the disease, including cerebral malaria and for most deaths. *P. vivax* also represents an important public health challenge as it has a wide geographical distribution and can develop dormant liver stages known as hypnozoites, causing relapses even months after the initial infection.

The life cycle of this haemosporidian apicomplexan parasite is complex and divided between two hosts, a female *Anopheles* mosquito and a vertebrate host, involving both asexual division (merogony) and sexual division (gamogony). The initiation of the asexual life cycle within human host is initiated by the bite of *Anopheles* injecting sporozoite parasite forms into the dermis. Following successful evasion from the host immune system within the dermis, these parasite forms enter liver where they embark upon their 'asymptomatic' pre-erythrocytic stage. Once the sporozoite has invaded a hepatocyte, it converts to an exo-erythrocytic form (EEF) over the subsequent 2–10 days after invasion. These EEFs undergo massive asexual replication during which karyokinesis precedes cytokinesis, called 'schizogony' culminating in the release of up to 40,000 merozoites per hepatocyte into the bloodstream by budding and active egress of parasite-filled vesicles called merosomes. The release of merozoites initiates the 'symptomatic' intraerythrocytic life cycle of the parasite. Merozoites penetrate red blood cells (RBCs) where they undergo rounds of asexual multiplications. Maturation of the parasite in infected erythrocytes (iRBCs) within the next 48h, from the ring to trophozoite and then schizont stages, is characterised by morphological, cellular, and metabolic changes, generating 16 to 32 new merozoites per iRBC. The end of this process is marked by the destructive release of these merozoites into the blood stream, initiated by the active egress of parasites out of the iRBC and their rapid invasion of new RBCs. A small proportion of parasites commit to sexual development and differentiate into male and female gametocytes. The capacity of parasites to produce sexual stages is a complex trait determined by intrinsic genetic and epigenetic factors as well as environmental clues such as depletion of lysophosphatidylcholine, a common component of human serum (Josling & Llinás, 2015). After commitment, it takes up to 10-15 days for the gametocytes to mature through 5 different stages. Immature stages I-IV sequester and are therefore not visible in blood samples. Maturation to stage V renders gametocytes more deformable, allowing them to return into the blood circulation where they can be ingested by mosquitoes upon a blood meal. Gametocytogenesis acts as an essential 'bottleneck' for *P. falciparum* transmission to its mosquito vector and subsequently other humans. These asymptomatic sexual forms are long lived and resistant to most antimalarial drugs and can thus persist for weeks in cured patients after drug treatment. Thus, a successful malaria eradication strategy must involve interruption of disease transmission by blocking gametocytogenesis or further development of the parasite in mosquitoes. Currently the only antimalarial drug that is effective against gametocytes is Primaquine, which treatment is unfortunately incompatible with malaria patients carrying a glucose-6-phosphate dehydrogenase deficiency. Upon ingestion by a female *Anopheles*

mosquito, the drop in temperature and additional environmental changes trigger the differentiation of gametocytes into male and female gametes in the mosquito midgut, followed by their fusion into a zygote that rapidly initiates meiosis without cellular division, and transforms into a motile ookinete over a period of 24 h. The ookinete traverses the mosquito midgut epithelium and encysts to become an oocyst where asexual sporogenic replication occurs over a period of 10-14 days. As a result of this process thousands of sporozoites are produced which traverse to enter into mosquito salivary gland from where they are transmitted to mammalian host over next blood meal (Josling & Llinás, 2015).

The number of malaria cases and deaths has been halved between 2000 and 2015 thanks to the massive use of long-lasting insecticide treated bednets and indoors residual spraying, and of artemisinin-based combination therapies (ACTs) as a very efficient first line treatment of non-severe cases. Still, the fast rise of insecticide resistance in mosquito populations, and the emergence and spread of drug resistance in parasite populations, notably to Artemisinin in South-East Asia (A M Dondorp et al., 2009), jeopardize global progress towards malaria elimination, as illustrated by a plateau in the number of cases and deaths since 2015.

Efforts to develop an efficient malaria vaccine have thus far been hindered by multiple factors, notably parasite antigenic variability, difficulty to produce and distribute specific vaccine forms. Chemotherapy thus remains a major frontline strategy for the control and future elimination of malaria, with the need for drugs with novel chemical entities that exploit new molecular targets while overcoming established drug resistance mechanisms. Ideally, such drugs should quickly kill pathogenic asexual blood stages and in addition, be effective against other relevant developmental stages, in particular transmittable gametocytes and dormant hypnozoites.

The antimalarial drug arsenal is fairly large, with numerous drugs such as Chloroquine (CQ) , Artemisinin (Art), Methylene blue (MB), Primaquine (PQ), Sulfadoxine, Pyrimethamine, Mefloquine, Tetracycline etc. The large majority of them is active against symptomatic and metabolically active *Plasmodium* asexual stages, notably trophozoites and schizonts, but very few target rings and gametocytes while these are key stages to cure and block parasite transmission. Indeed, trophozoites and schizonts sequester in the microvasculature, causing impaired tissue perfusion and endothelial cell activation that are responsible for the most fatal outcomes (K. R. Hughes et al., 2010).

Thus, killing asexual parasites at the ring stage stops parasite development before the appearance of the cyto-adherent stages and limit severe symptoms (Burrows et al., 2013; Wilson et al., 2013). Moreover, blocking gametocytogenesis or the ability of long-lived gametocytes to further develop and infect mosquitoes is essential to limit disease transmission.

Currently very few drugs are able to target rings and/or gametocytes, and most of them display a mode of action based on the perturbation of the parasite redox homeostasis (Fig. 1.1.). This is for instance the case for Artemisinin (Art) and methylene blue (MB) that are active on both young ring stages and gametocytes, and for primaquine (PQ) whose metabolites are especially efficient against gametocytes and hypnozoites. Here we review a selection of redox antimalarial compounds, either currently used as drugs or drug leads, with antiparasitic properties on rings and/or gametocytes. We classified them in 2 groups, the redox-active compounds, and those whose activity is based on the generation of reactive oxygen species (ROS) to highlight common mechanisms of action. Finally, we review some of the specificities of the ring and gametocyte stages that may render these metabolically less-active stages particularly vulnerable to oxidative stress.

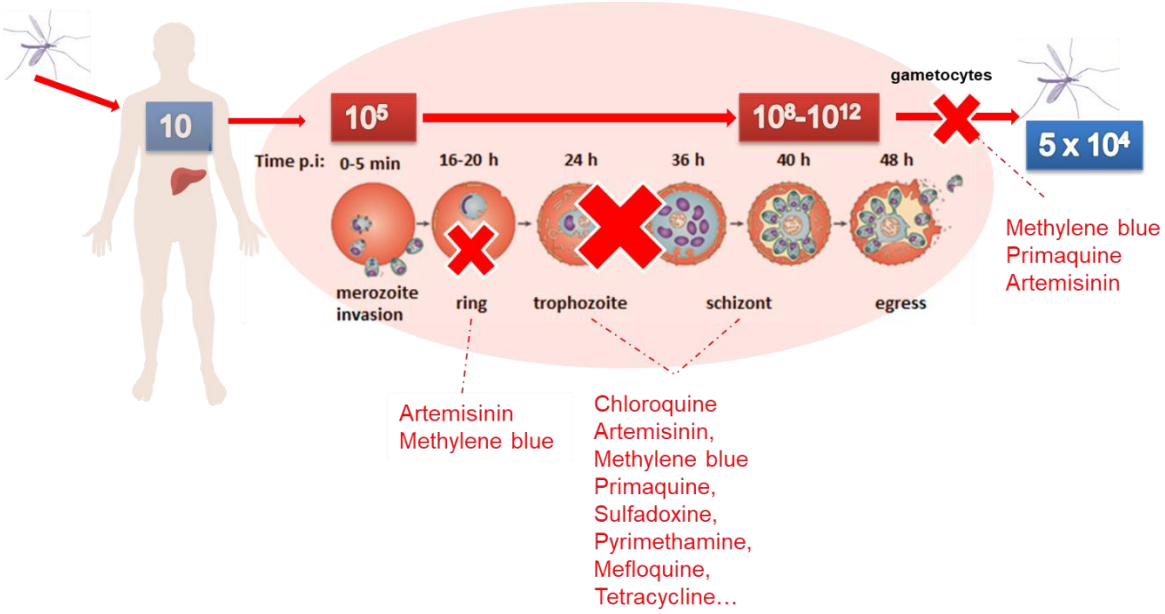

Figure 1.1. Summary of currently available antimalarial drug and their activity on different asexual and sexual stages of P. falciparum parasite

Antimalarial drugs targeting parasite redox homeostasis

A functional redox system is essential for the survival of Plasmodium parasites as they have to cope with high fluxes of reactive oxygen species (ROS) stemming from their own metabolism but also from exogenous sources, e.g. immune reactions (Henrici, Edwards, et al., 2020; Jortzik & Becker, 2012; Mohring et al., 2016).

The natural resistance of G6PD-deficient individuals to severe malaria symptoms further exemplifies the particular susceptibility of intraerythrocytic parasite stages to oxidative stress (Cappellini & Fiorelli, 2008; Luzzatto & Arese, 2018a). Recent studies further point out a particular sensitivity of (mature) gametocytes to redox-active drugs while the antioxidative system of gametocyte stages is only poorly investigated (Coertzen et al., 2018; Siciliano et al., 2017).

Disturbing redox homeostasis in the parasite-host unit has thus become a broadly recognized strategy for the development of new antimalarial drugs (Belorgey et al., 2013; Max Bielitza et al., 2015; Davioud-Charvet & Lanfranchi, 2011; Krauth-Siegel et al., 2005; Nepveu & Turrini, 2013; Pal & Bandyopadhyay, 2012; Yadav et al., 2019).

Destabilization of the redox equilibrium can be achieved in different ways: (I) directly, by agents or their metabolites that act as subversive substrates of parasite oxidoreductase enzymes, as it is the case for redox-cyclers: MB, PQ, tafenoquine, Indolone-N-oxide derivatives (iNODs) and the 3-benzylmenadione Plasmodione (PD), and/or their metabolites, or (II) indirectly by

drugs that generate reactive oxygen species that may overload the parasite antioxidant system: ferroquine, ART or its metabolite dihydroartemisinin (DHA) (Fig 1.2).

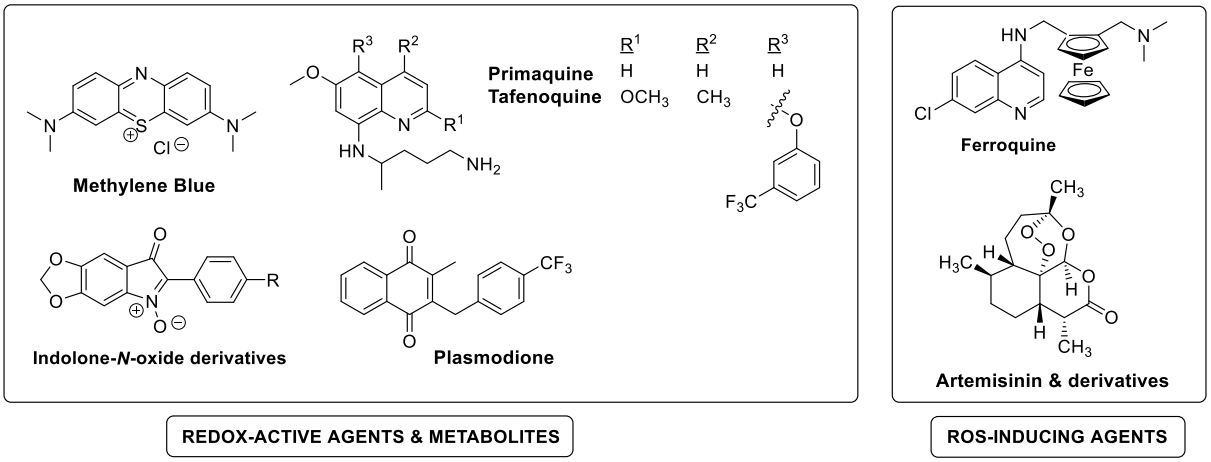

Figure 1.2. Chemical structures of antimalarial redox-active and ROS-inducing agents.

Part 1: Redox-cyclers

Common principles of redox-cycling

The unique feature of redox-cyclers lies in their intrinsic redox potential that allows them to participate in reversible one-electron or two-electron transfer reactions and therefore in a continuous reduction-oxidation cycle. Redox-cyclers do not act as simple inhibitors, they are substrates of oxidoreductase enzymes that belong to multiple intracellular redox systems in eukaryotic cells (e.g. mitochondrial electron transport chain, glutathione and thioredoxin systems…). After enzymatic reduction, the reduced drug/metabolite can be readily reoxidized by molecular oxygen or alternative oxidants, thus regenerating the initial drug that can continue its redox cycling. Under physiological conditions, the overall reaction leads to a NAD(P)H-dependent transfer of electrons from oxidoreductases to intracellular key oxidants, for instance the hemoglobin-associated or free heme (FeIII) species that is present in large quantities in infected erythrocytes, and is accompanied by the formation of reactive oxygen species (ROS) (Fig. 1.3) (M Bielitza et al., 2015; Blank et al., 2012; Tobias Müller et al., 2011; Sidorov et al., 2015)

Redox-cyclers are also designated as subversive substrates because they divert the physiological antioxidant activity of oxidoreductases into a pro-oxidative activity, resulting in depletion of the intracellular reductant NAD(P)H stock and in the generation of considerable amounts of oxidized thiols and ROS.

Conversion from prodrug to drug

Common to all antimalarial redox-cyclers, the initial drug is considered to be a prodrug that is intracellularly converted into an active metabolite, thereby changing its redox potential and generating the subversive substrate. In the case of MB and bMDs, conversion of the prodrug is considered to occur within the Plasmodium-infected erythrocyte upon interaction with a

flavoenzyme in addition to a hemoprotein (hemoglobin, flavohemoprotein…) under a ferryl species. Interestingly, antimalarial MB, bMDs and indolone-N-oxides (iNOD) are thought to be first metabolized by a reductase in iRBCs B (Buchholz et al, 2008; Ibrahim et al, 2011). Instead, PQ needs to be converted to hydroxylated metabolites by the cytochrome P450 NADPH:oxidoreductase and cytochrome P450 CYP2D6 in the liver before it can enter into a redox-cycle that mediates its antiparasitic activities (Fig. 1.3) (Camarda et al., 2019; Vásquez-Vivar & Augusto, 1994)

Enzymatic catalyst

Numerous NAD(P)H-dependent oxidoreductases would be potential candidates to drive the continuous reduction of redox-cyclers. Despite clear phenotypic differences in parasites exposed to MB and bMDs that likely illustrate differences in their specific mode of action (K Ehrhardt et al., 2013), some similarities have been reported. Metabolites of both compounds are subversive substrates of various recombinantly produced NADPH-dependent oxidoreductases in vitro, including hGR and PfGR for MB and bMDs, and PfTrxR for MB ((Blank et al., 2012; Buchholz, Schirmer, et al., 2008; Färber et al., 1998). In the case of MB, its reduction by GR or other oxidoreductases generates a reduced colorless leucomethylene blue form. Of note, the glutathione reductase (GR, EC 1.8.1.7) is part of the parasite antioxidative system and is moreover highly abundant in human erythrocytes. In yeast, the NADH dehydrogenase Nde1 of the mitochondrial electron transport chain is the main target of the lead bMD Plasmodione, with several additional oxidoreductases as minor targets (Mounkoro et al., 2019). Taken together, these observations strongly suggest that MB and bMDs are likely to be able to cycle with different oxidoreductases within the iRBC, possibly depending on their concentration, localization and on parasitic stages. Importantly and in contrast to inhibitors, the target oxidoreductases do not need to be essential enzymes and should in contrast stay active to mediate the antiparasitic activity of redox cyclers. In the case of PQ, redox-cycling takes place in presence of the cytochrome P450 NADPH:oxidoreductase in the liver and bone marrow but not directly in the iRBC, with concomitant generation of large amounts of H2O2.

Antiparasitic redox-cycling

Parasite death resulting from the redox cycling of the drug metabolites with oxidoreductases occurs through different means. In the case of MB and bMDs, the reduction of the hemoglobin-catabolites methemoglobin and hematin is catalysed by the reduced redox-cyclers, recycling methemoglobin into oxyhemoglobin that is not digestible by parasites, thus resulting in their developmental arrest (Atamna et al., 1996; M Bielitza et al., 2015; Blank et al., 2012; Johann, 2012; T Müller et al., 2011)

Of note, the reductant methemoglobin is only present in large quantities in infected erythrocytes, possibly contributing to the specific activity of redox-cyclers on iRBCs. Furthermore, cycling pumps electron from the NAD(P)H stocks, which is likely detrimental to parasite survival. In addition, the continuous redox-cycling of MB, bMDs and iNODs also generates high levels of ROS creating a highly oxidative / chemically reactive environment within the parasite and its host cell and generating additional drug metabolites that may contribute to the global overall antimalarial activities. To illustrate this in the case of the bMD plasmodione (PD), an oxidative phenolic coupling might generate a benzoxanthone derivative

from the reduced redox-cycling PD metabolite (reduced benzoylmenadione, PDOred), which has been shown to interact with □-hematin as potently as CQ in vitro, and thus suspected to be a strong inhibitor of hemozoin formation in parasitized cells. PDOred also revealed an iron (III) chelation site, which was antagonized by deferoxamine (DFO) in PD-DFO combinations in PfDd2 assays (M Bielitza et al., 2015) Moreover, a set of putative PD metabolites was synthesized and many of them were shown to inhibit the blood stages of P. falciparum infected RBCs in vitro with IC50 values around 100 nM (Feng et al., 2018). In the case of PQ, cycling of the hydroxylated metabolites with cytochrome P450 NADPH:oxidoreductase generates high levels of H2O2 locally in organs where otherwise difficult to kill stages are localized, i.e. pre-erythrocytic stages and hypnozoites in hepatocytes, and gametocytes that sequester in the bone marrow. Of note, due to their potential to target multiple oxidoreductases and to their pleitropic effects, redox-cyclers retain their full antimalarial capacity on all tested drug resistant parasites (please also see paragraph below on resistance).

Methylene Blue – a renewed historical weapon

Methylene blue (MB, Fig. 1.1) is not only the first characterized redox-cycler but was once the first synthetic drug used for the treatment of malaria, discovered at the end of the 19th century by Guttmann and Ehrlich (Guttmann & Ehrlich, 1891). Because of its slow in vivo efficacy when used alone in humans (Blank et al., 2012; Schirmer et al., 2003). MB was replaced by more effective or rapidly acting drugs, such as chloroquine (CQ), but regained attention with the appearance and spread of parasite resistance to those massively used drugs, and also thanks to its transmission blocking properties. It is also cheap and usually well tolerated with limited side effects.

MB is a blue dye that belongs to the family of phenothiazines. Owing its redox-cycling properties in the presence of methemoglobin (FeIII) (described above), MB is clinically applied for the treatment of methemoglobinemia, which can also occur during severe forms of malaria (Schirmer et al., 2011). It has been extensively researched for medicinal applications, e.g. in cancer therapy, as an inhibitor of Tau protein aggregation (Schirmer et al., 2011) (Table 1). Interestingly, MB's activity against *P. falciparum* blood stages is unaffected by the parasite's acquired resistance to most other antimalarial drugs although no data has yet been published on potential cross resistance with Art (Table 1). Several MB-based drug combinations are currently in clinical trials (Coulibaly et al., 2015; Lu et al., 2018; Meissner et al., 2005, 2006; Zoungrana et al., 2008). Of particular interest for drug application is MB activity against all stages of gametocytes that was explored in vitro (S H Adjalley et al., 2011; Akoachere et al., 2005; Coertzen et al., 2018; Siciliano et al., 2017) and further confirmed in field studies (Coulibaly et al., 2009).

3-Benzylmenadiones – G6PD-deficiency copycats

The lead benzylmenadione (bMD) plasmodione (PD, Fig. 1.1) is a 2-methyl-1,4-naphthoquinone (menadione) derivative, substituted at the C-3 of the quinone moiety by a para-trifluoromethyl-benzyl chain. It has been identified among a whole series of 3-benzylmenadiones with high antimalarial potencies (T Müller et al., 2011; Rodo et al., 2016). Upon drug treatment of Plasmodium-infected erythrocytes, continuous redox-cycling ultimately leads to over-oxidation of hemoglobin-bound iron, thus forming ferrylhemoglobin (FeV) and leading to the denaturation of hemoglobin to hemichromes that bind to the erythrocyte membrane (M Bielitza et al., 2015). Hemichromes are biomarkers of senescent erythrocytes in vivo and trigger active removal of those cells from the circulation by macrophagic phagocytosis, notably in the spleen (Ayi et al., 2004; Reeder, 2010) The rapid phagocytic

removal of Plasmodium-infected G6PD-deficient erythrocytes is responsible for the natural protective mechanism of those patients, based on accelerated / increased oxidative stress and hemichrome deposition in ring-stage infected erythrocytes. Hence, for the first time, low-molecular weight molecules were shown to mimic the effects of a genetic deficiency that protects from severe malaria. Strikingly, hemolysis and increased deposition of hemichrome were not observed on non-infected erythrocytes from WT and G6PD-deficient patients, indicating that bMDs can be considered safe for application on G6PD-deficient individuals (M Bielitza et al., 2015).

Indolone-N-oxides

Indolone-N-oxide derivatives (iNODs, Fig 1.1) contain a redox pharmacophore that enables reversible oxidation-reduction reactions, a prerequisite for their activity as redox-cyclers (Nepveu et al., 2010; Tahar et al., 2011). Intracellular bioactivation of iNODs was proposed to be thiol- and/or enzyme-dependent and leads to the formation of a reduced metabolite, the dihydro-iNOD, which could be isolated from uninfected and P. falciparum-infected erythrocytes (Ibrahim et al., 2011). The subsequent cascade of iNODs redox reactions has not been fully explored so far but the current understanding is discussed in a review (Nepveu & Turrini, 2013). Ultimately, drug activity was shown to cause a strong destabilization of the cell membrane in P. falciparum-infected erythrocytes, which might stem from a direct activation of redox signalling pathways by iNODs-generated radicals (Nepveu & Turrini, 2013; Pantaleo et al., 2012). A stable erythrocyte membrane is considered vital for parasite maturation, a hypothesis that is supported by observations with erythrocytes that naturally present unstable membranes or mutations in critical structural proteins (Pantaleo et al., 2012). The role of the quinone reductase 2 has been recently discussed to account for the antimalarial properties of indolone-type derivatives (Cassagnes et al., 2017).

Primaquine

Primaquine (PQ, Fig. 1.1) is an 8-aminoquinoline developed in the 1940's that displays antimalarial activity against multiple parasite stages (M. J. Delves et al., 2012; Dembele et al., 2011; Plouffe et al., 2016). It has major clinical history against P. vivax and P. ovale relapses as it targets hypnozoites. PQ has also an immense clinical value as a transmission-blocking agent through its sterilizing activity against mature P. falciparum gametocytes. Currently PQ is the only marketed drug targeting these two overlooked parasite stages. Last, PQ is also active on Plasmodium hepatic schizonts. PQ is toxic in G6PD / met-hemoglobine reductase (MetHbR)-deficient patients treated during fourteen days for hypnozoites radical cure (WHO working group, 1989; Cohen et al, 1968), provoking erythrocyte-related, severe side effects in these people due to deficiency of these erythrocyte enzymes controlling oxidative stress. However, a growing number of evidence indicate that PQ is non-toxic under the single low dose of PQ used for the sterilizarion of P. falciparum gametocytes (Dicko et al., 2018). Although PQ is currently underused (Recht et al., 2018), it is under intense clinical validation for widespread use in combination with ACTs, and it has great potential to reduce malaria transmission and contain ART resistance (Landier et al., 2018).

Despite this unique position among antimalarial drugs, the suggested biological mechanisms of action of the extensively metabolized PQ remained largely hypothetical in Plasmodium until recently. This was in part due to different results obtained in in vitro and in vivo systems, to the various Plasmodium species studied *(P. falciparum, P. vivax, P. cynomolgi, P. berghei)* as well as the diverse stages examined (hepatic hypnozoites and

schizonts, blood trophozoites and schizonts, blood gametocytes) and to the very large number of metabolites produced upon PQ treatment in vivo.

PQ itself is moderately active in vitro (IC_{50} = 1-25 mM) on *Plasmodium* sp. asexual blood stages and gametocytes (Sophie H. Adjalley et al., 2011b; M. Delves et al., 2012; Vennerstrom et al., 1999). In a model of mouse malaria, similar levels of prophylactic activity against blood stage *P. berghei* infection were obtained in a CYP2D6 knocked-out (KO) mice strain compared to the wild type controls (Milner et al., 2016). Regarding liver stages, PQ clinical efficacy to cure *P. vivax* hypnozoites is diminished in humans exhibiting a deficiency in CYP2D6 activity (J. W. Bennett et al., 2013). Similarly, PQ has no activity against liver stages in *P. berghei*-infected CYP 2D22-KO mice (CYP2D6 ortholog) but full prophylactic activity in h-CYP2D6 knocked-in animals (Potter et al., 2015; Pybus et al., 2013). These results suggest that different PQ metabolites are active on the different parasite stages. In vivo, PQ undergoes an important Phase I metabolization in the liver, consisting in a combination of oxidative and deaminating transformations mediated by P450 cytochromes and monoamine oxydases, respectively (Marcsisin et al., 2016). Following a major metabolisation in vivo by hepatic monoamine oxidase (85-90 % metabolisation), PQ is rapidly turned into carboxy-PQ (CPQ), which shows poor in vitro activity (IC50 = 50-100 mM) against Plasmodium liver and blood asexual stages and gametocytes (Bates et al., 1990; Kim et al., 2004; Peters et al., 1984). A low proportion (10-15 %) of PQ is metabolized with ca. 30 metabolites generated principally by the host CYP2D6 cytochrome, other CYPS such as C19 and 3A4 corresponding to minor contributors (J. W. Bennett et al., 2013; Marcsisin et al., 2016; Milner et al., 2016). The yielded metabolites show an impressive chemodiversity. Importantly, CYP2D6-mediated 5-hydroxylation is pivotal as it yields presumably hyperactive metabolites (Vásquez-Vivar & Augusto, 1994).

6-demethylation is another major pathway leading to hybrid catechol-quinolamine systems when coupled to 5-hydroxylation, with again formation of ortho-quinone upon CYP2D6 and/or air oxidation. Some of these compounds are highly active *in vitro* (IC_{50} = 50-500 nM) on Plasmodium replicating liver stages (Bates et al., 1990) which correlates with the fact that CYP2D6 metabolization is mandatory for PQ liver-stage activity (J. W. Bennett et al., 2013; Pybus et al., 2013).

With respect to inhibitory mechanisms and biological targets, CYP2D6-originating metabolites are likely to exert both antimalarial and toxic mechanisms. Camarda et al recently demonstrated that oxidation of hydroxylated metabolites, generates 1,4-quinone-imine forms that are in turn reduced by cytochrome P450 reductase, thus leading to H2O2 accumulation. In red blood cells, oxidation of hydroxylated metabolites is likely to occur through electron-transfer reactions in complex with O2-bound hemoglobin species, thereby leading to the formation of methemoglobin and reactive oxygen species (Davioud-Charvet & Lanfranchi, 2011). While this is desirable in iRBCs, the elevation of methemoglobin levels in non-infected erythrocytes is an undesirable side effect of this drug that causes hemolytic anemia in patients with G6PD deficiency. Hydrogen peroxide accumulation likely leads to protein oxidation, damage to Fe-S cluster proteins or to the generation of superoxide and hydroxyl radicals at the sites where it is produced, including in the liver where hepatic stages and hypnozoites are located, and in the bone marrow where gametocytes sequester, providing a clear model for the mode of action of the potent hydroxylated PQ metabolites (Camarda et al., 2019). This model is further corroborated by studies performed in yeast showing that yeast sensitivity to PQ is markedly increased in strains that lack the key components of the antioxidant defense, Sod1 and Sod2, the cytoplasmic and mitochondrial superoxide dismutases respectively (Lalève et al., 2016). Other putative mechanisms include covalent modification of target by electrophilic quinone and quinone-imine species, disruption of iron-containing proteins (e. g.,

Fe-S clusters, aconitase) by metal-chelating catechol or 8-aminoquinoline species (the last mechanism being potentially at play with native PQ), as well as non-covalent, chelate-independent inhibition of targets. These mechanisms remain partially characterized (Ganesan et al., 2012; Magwere et al., 1997; Vásquez-Vivar & Augusto, 1994), mostly due to the difficulty of obtaining and studying these often unstable metabolites and to account for their synergic effects in parasitized cells. The existence of a physiologically protonated basic group in the side-chain of various antimalarial quinolines is of paramount importance in their ability to bind electrostatically to their parasite interactome (Bellanca et al., 2014; Reiling & Rohrbach, 2015; Wong et al., 2017) , and is crucial for the antiplasmodial and gametocytocidal activities of these drugs (Bates et al., 1990; Portela et al., 1999; Vale et al., 2009).

Recent progress in our understanding of PQ mode of action will be instrumental in the rational re-design of PQ analogues towards enhanced antimalarial activity that could be independent of the CYP2D6 status of the host and that could possibly be decoupled from its haemotoxicity in G6PD- and metHbR-deficient patients.

Tafenoquine

Tafenoquine (TQ, Table 1) is an 8-aminoquinoline analogous to PQ, which is being co-developed by the Walter Reed Army Institute of Research and GlaxoSmithKline and is currently in phase III of clinical development. Designed for the radical cure and causal prophylaxis of *P. vivax* malaria, early investigations showed that TQ exhibits schizontocidal activity against blood stage parasites in both *P. vivax* and *P. falciparum* and is also a potent transmission-blocking agent (Obaldia et al., 1997; Ponsa et al., 2003; Ramharter et al., 2002; Vennerstrom et al., 1999). One major improvement of TQ relatively to PQ for the radical cure of *P. vivax* malaria is its long half-life and the potential for more convenient dosing, compared to the currently recommended 14-day PQ regimen.

In vitro studies on *P. falciparum* field isolates and reference strains indicate a slightly greater activity of TQ on asexual replicative stages compared to PQ (M. J. Delves et al., 2012; Vennerstrom et al., 1999). *In vivo* data also indicate a higher efficacy in prophylactic activity of TQ treatment over PQ in mice infected with *P. berghei* sporozoites, and it inhibits sporogonic development in *Anopheles Dirus*, making it a good candidate for transmission-blocking studies (Q. Li et al., 2014; Ponsa et al., 2003). Gametocytocidal activity of tafenoquine has been reported in rodent models but has not yet been thoroughly investigated in humans. A recent study assessed the efficacy of a TQ treatment once daily for 3 days compared to CQ plus PQ once daily for 3 and 14 days, respectively, in *P. vivax* infected patients. A slower clearance rate of parasite, gametocyte and fever was reported in the TQ cohort compared to the CQ+PQ one (Fukuda et al., 2017). Like for most 8-aminoquinolines, the mechanism of action of TQ remains to be fully elucidated. Akin to CQ but unlike PQ, the biological activity of TQ against the asexual erythrocytic stages is reportedly due to its capacity to impair hemozoin formation by inhibiting hematin polymerization (Vennerstrom et al., 1999). However, against the liver and sexual stages of the parasite the postulated mechanisms of action are linked, as with other 8-aminoquinolines, to the redox cycling properties of TQ's metabolites, and generation of hydrogen peroxide and hydroxyl radicals through spontaneous oxidation of metabolites (Ebstie et al., 2016).

In a study designed to assess the safety of tafenoquine use, subjects treated with TQ exhibited higher levels of methemoglobin compared to PQ, however no signs of methemoglobinemia-related clinical symptoms have been reported with treatment concentrations under 600mg/kg (Fukuda et al., 2017). However, as for PQ, TQ increases hemolysis in G6PD deficient patients at high doses (Rueangweerayut et al., 2017).

Part 2: Pro-oxidative agents

We have seen that redox cyclers not only pump electrons from cellular reductants, but also generate large amounts of ROS that may explain, largely, or at least in part, their antiparasitic activity. This is in common with other drugs such as Ferroquine and Artemisinin that are not substrates of cellular oxidoreductases, but also generate large amounts of ROS that may ultimately lead to an overload of oxidative stress in the parasite, causing important intracellular damage and inhibiting further development.

Artemisinin and derivatives

Qinghaosu/artemisinin-is a prodrug carrying a 15-carbon sesquiterpene lactone with an endoperoxide group. Dihydroartemisinin, an Art metabolite is the most efficient and fast-acting antimalarial drug since its discovery in 1971 by Youyou Tu (N. J. White, 2008) . Art kills young ring stages circulating into the host bloodstream and prevents further parasite maturation in replicating stages -trophozoite and schizont- which adhere to endothelial cells, blood cells, and platelets, and sequester in blood vessels to escape the clearance of infected RBCs in the spleen, thus leading to severe complications (White et al, 2008, 2011; Endour et al 2015). To avoid the emergence of resistances and parasite recrudescence after Art monotherapy (Barnes et al., 2008; Nicholas J. White, 2004) , therapies combining Art and at least one additional antimalarial drug with a longer half-life and alternative mechanism of action are currently the treatments of choice for uncomplicated malaria. This approach is called Artemisinin Combination Therapy (ACT) and is usually prescribed for a maximum of 3 days (WHO). In this case, the short time of treatment increases patient compliance and reduces the risk of resistant parasites with limited exposure to Art during the therapy. Once Art is eliminated from the body, the associated long-lasting partner drug can exert its activity and kill remaining parasites (Yang et al 2016).

SPECIES AND STAGE SPECIFICITY. Art rapidly and efficiently kills *P. falciparum* asexual stages in vitro, with IC50 of ~0.6–1.1 nmol/L for the asynchronous or mixed intra-erythrocytic stage. It is most potent against ring stages with IC50 of ~0.3 nmol/L, compared to trophozoite and schizont stages (IC50 ~5.0 nmol/L) (S. R. Krungkrai & Yuthavong, 1987). Art also kills young sexual stages of parasites i.e. gametocyte stages I to III, but is not considered active against stage IV-V gametocytes (Sophie H. Adjalley et al., 2011a). It also lacks activity on the pre-erythrocytic stages developing in liver cells. The lack of Art activity on both late gametocytes and liver stages is likely explained by the lack of haemoglobin at these stages while it is required for Art bioactivation (see below). Art can contribute to reduce parasite transmission “directly” by eliminating young gametocyte stages, and indirectly by reducing the population of asexual parasites that are responsible for the development of gametocytes (J. Krungkrai et al., 1999; Hay et al, 2010). However, its contribution is limited as Art treatment per se does not reduce gametocyte burden and transmission to mosquitoes (Ouologuem et al., 2018; Djimbe, Parasite 2016) and may even facilitate transmission of ArtR parasites [Witmer, BioRxiv 2020]. Art can kill asexual stages of *P.vivax* as well. Clinical trials of ACT treatment for *P. malariae*, *P. ovale* and *P. knowlesi* are limited with inadequate data however the ACT is as efficient as chloroquine for non-falciparum malaria (Visser et al., 2014).

MODE OF ACTION. Within 1-2 hours after Art oral or parenteral administration, the active metabolite dihydroartemisinin (DHA) is observed at concentrations of ~10–30 µmol/L (~2.4–4.0 mg/kg body weight). Art accumulates in the parasite membranes and cytosol and is activated upon reduction of the endoperoxide group by FeII-heme that is released upon hemoglobin digestion (Klonis et al., 2011; Robert et al., 2005a). This generates radical species that react with nucleophiles in proteins, lipids and hemes, generating reactive oxygen species, mitochondrial membrane depolarization, and leading to massive cellular damages (Cui & Su, 2009; S. R. Meshnick et al., 1996; Jigang Wang et al., 2015). In mitochondria, Art generates ROS by activating the electron transport chain (W. Li et al., 2005; Juan Wang et al., 2010) and by inhibiting the cytochrome C oxidase complex responsible for the transfer of mitochondrial oxygen (J. Krungkrai et al., 1999; Murphy, 2009). In addition to this, Art further damages the parasite proteasome function, thus leading to overall ER stress (Bridgeford et al 2018). Art also interferes with proteins associated with the removal of toxic haem/detoxification of haem and inhibits haem polymerization (Meunier & Robert, 2010; Robert et al., 2005b).

RESISTANCE. Due to its pleiotropic activity on multiple cellular targets, no resistance identified in a target gene. However, prolonged clearance of parasites upon Art treatment was reported in South East Asia in the late 2000s (E. A. Ashley et al., 2014; A M Dondorp et al., 2009; Noedl et al., 2008) and Art resistant parasite lines were selected upon exposure to escalating Art doses (Rocamora et al., 2018; Benoit Witkowski et al., 2010), allowing the community to investigate the molecular and cellular bases of Art resistance. Art resistant parasites are characterized by a prolonged ring phase, that is also the stage at which resistance is displayed, other intraerythrocytic stages (trophozoites and schizonts) remaining sensitive to Art (Rocamora et al., 2018; Benoit Witkowski et al., 2010). The main Art resistance mechanism relies on a decreased hemoglobin uptake at the ring stage and is linked to mutations in genes involved in hemoglobin endocytosis and digestion, such as AP-2u, UBP1, falcipain, coronin and most commonly, in the Kelch protein K13 that was identified in the laboratory selected F32-Art5 resistant strain and that remains the main resistance marker in South East Asia (Ariey et al., 2014; E. A. Ashley et al., 2014; Birnbaum et al., 2020; Demas et al., 2018; Henrici, Edwards, et al., 2020; Henrici, van Schalkwyk, et al., 2020; Henriques et al., 2013, 2014, 2015; T. Yang et al., 2019). K13 mutations have been postulated to mediate increased parasite post-stress defense mechanisms by improving clearance/removal of Art induced damaged proteins by the proteasome and by delaying apoptotic/cell death pathways (Dogovski et al., 2015; Mbengue et al., 2015). Finally, a decreased cytotoxic stress, possibly due to the upregulation of redox proteins and of the unfolded protein response, has been detected in laboratory selected Art-resistant lines as well as in parasite isolates from patients presenting a delayed parasite clearance post Art treatment (Mok et al., 2015; Rocamora et al., 2018). Importantly, this resistance mechanism appears unlinked to mutations in proteins involved in hemoglobin uptake and digestion (including K13), and may favor the appearance - or alleviate the fitness cost - of Art resistance mutations in the K13 gene (Rocamora et al., 2018; L. Zhu et al., 2018).

QUIESCENCE. Interestingly, both Art alone or Art with any of drugs such as quinolines (amodiaquine, mefloquine, chloroquine, quinine) or pyrimethamine induce temporary quiescence in all treated parasites, with a larger fraction of them becoming quiescent in Art resistant parasites such as in the F32-ART5 (Benoit Witkowski et al., 2010) or in Cambodian clinical isolates with Kelch 13 mutation associated with the delayed clearance (Benoit Witkowski et al., 2010, 2013). After drug removal, the parasite “wakes up” and resumes development (Ménard et al., 2015; Benoit Witkowski et al., 2010). Noteworthy, metabolism and

DNA replication get arrested at ring-stage in dormant parasites, but they have an active mitochondrial electron transport chain and are therefore sensitive to atovaquone, a compound blocking complex III of the mitochondrial electron transport chain (Peatey et al., 2015). Still, atovaquone resistance is quickly acquired by parasites, which therefore hinders its use (Kessl et al., 2007). They also retain several apicoplast functions such as fatty acid synthesis that could be targeted to kill quiescent parasites (Duvalsaint & Kyle, 2018). Finally, wake and kill strategies relying on compounds such as epigenetic modifiers that wake dormant parasites (Nardella et al., 2020). associated with antimalarial drugs, may also prove interesting to circumvent resistance linked to the ability of parasites to enter dormancy to avoid drug effect.

In conclusion, it is likely that mutations affecting hemoglobin uptake and digestion will also confer resistance to other drugs requiring hemoglobin for their bioactivation or for their mode of action. Still, these mutations come with a fitness cost that should prevent them from leading to full resistance at all parasite stages.

Ferroquine

Ferroquine (FQ, Table 1) is a hybrid redox-active-chloroquine derivative, which had been designed in the 1990‘s (Biot et al., 1997): its structure combine in the same skeleton both the lysosomotropic properties of the 4-aminoquinoline moiety present in the widely used antimalarial drug in the first half of 20th century chloroquine (CQ), and the ferrocene moiety. As CQ, ferroquine acts as inhibitor of hemozoin formation (Biot et al., 2009; Dubar et al., 2011). In addition, its unique ferrocene core allows reversible one-electron redox reactions under oxidizing conditions such as those present in the digestive vacuole, i.e. oxidation of ferrocene (Fe^{2+}) to ferricinium (Fe^{3+}). Owing to this reaction, FQ generates lethal hydroxyl radicals that contribute considerably to its antiparasitic activity (Chavain et al., 2009). A plethora of FQ analogues and derivatives, and many other classes of compounds have been developed since, and studied to overcome drug resistance because of the significant loss of CQ efficacy in resistant parasite strains worldwide ((Wani et al., 2015b, 2015a). Interestingly, certain hybrid FQ-1,4-napthoquinones are more effective to catalyze the Fenton reaction (Chavain et al., 2009). However, thus far, no other FQ derivative had been found superior to FQ in terms of antimalarial activity both in vitro and in vivo. Chloroquine resistance is caused by multiple mutations in the Plasmodium falciparum CQ resistance transporter (PfCRT) that result in an increased efflux of CQ from the acidic digestive vacuole to the cytosol of the parasite. Using synchrotron based X-ray imaging, direct fluorescence measurements of the unlabelled CQ and FQ showed that resistant parasites treated by FQ were unable to extrude FQ from the food vacuole and they accumulated a sulfur-containing compound, assigned to be glutathione, in their digestive vacuole(Dubar et al., 2012). Although the precise biological targets that FQ affects are not entirely known, recent studies revealed that FQ and derivatives displayed anti-tumour activities and FQ has potential application as an adjuvant to existing anticancer therapy through inhibition of autophagic-lysosomal function (Kondratskyi et al., 2017; Tóth et al., 2010). FQ is developed by Sanofi since 2012, currently in clinical trials, as the drug combination OZ439 (Artefenomel)/FQ (Ferroquine) to determine whether a single dose combination of OZ439 (Artefenomel)/FQ (Ferroquine) is an efficacious treatment for uncomplicated Plasmodium falciparum malaria in adults and children.

Part 3: Issues linked to redox active antimalarial drugs

G6PD deficiency and hemoglobino-pathies: natural protections from severe forms of malaria

Several genetic mutations of human erythrocytes are known for protecting carriers from the severe, life-threatening forms of malaria. Glucose-6-phosphate dehydrogenase (G6PD) deficiency (Luzzatto & Arese, 2018b) and hemoglobinopathies, e.g. thalassemia and sickle cell disease, are important examples of such genetic polymorphisms. The similar geographic distribution of these genetic traits and past or present malaria infections support the so-called malaria protection hypothesis, which claims that co-evolution of humans and *P. falciparum* shaped the human genome in these regions (Cappellini & Fiorelli, 2008; Cyrklaff et al., 2011, 2012)

The most widespread genetic defect of human erythrocytes is G6PD deficiency, which also represents the most common human enzyme defect (reviewed in Cappellini & Fiorelli, 2008) G6PD is the first enzyme of the pentose phosphate pathway and the main producer of NADPH (nicotinamide adenine dinucleotide phosphate) in erythrocytes. Affected individuals are generally asymptomatic but more susceptible to oxidative insults in forms of oxidant drugs, chemicals or food components that may induce acute hemolytic anemia. Hemoglobinopathies result from unpaired globin chains in α- or β-thalassemia or from structurally altered β-globin in sickle-cell hemoglobin (HbS), hemoglobin C (HbC) or hemoglobin E (HbE) (Cyrklaff et al., 2012; Taylor et al., 2013). Heterozygous carriers are generally asymptomatic but may suffer from mild anemia.

The molecular mechanism(s) that protects affected individuals from the severe symptoms of malaria are complex and still not fully understood. Interestingly, in all cases, erythrocytes were shown to be more susceptible to oxidative stress, marked by a higher tendency of hemoglobin to oxidize and denature, caused either by structurally unstable mutant hemoglobin or decreased antioxidant capacity of the host cell (Ayi et al., 2004; Cyrklaff et al., 2012; Reeder, 2010). In support of this hypothesis, enhanced binding of hemichrome (i.e. denatured hemoglobin) to the erythrocyte membrane and enhanced phagocytosis of infected cells were observed for G6PD-deficient erythrocytes (Luzzatto & Arese, 2018b), heterozygous sickle cells (HbAS) and heterozygous thalassaemic cells (β-thalassemia and HbH) (Ayi et al., 2004) (Cappadoro 1998,). Furthermore, denatured and oxidized hemoglobin species were identified as candidates for preventing host actin re-organization in *P. falciparum*-infected homozygous HbCC and heterozygous HbSC erythrocytes (Cyrklaff et al., 2012). Remodeling of the host actin cytoskeleton was shown to be important to establish the parasite's protein trafficking system and their inhibition might contribute to the protection against severe malaria infections (Cyrklaff et al., 2011, 2012). These protective mechanisms against severe malaria generate oxidative stress in iRBC and parasite developmental arrest in ring stages

Hemolytic risk in G6PD-deficient individuals treated by drugs/nutrients inducing oxidative stress

While high doses of primaquine produce hemolytic anemia in individuals with glucose-6-phosphate deficiency (G6PD) and thus cannot be used in classical 14 days treatments that are required to eradicate hypnozoites, PQ retains its transmission blocking properties when used in a single low-dose, a treatment that is well tolerated, even in G6PD-deficient patients

(Bancone et al., 2018). This can be compared to the absence of hemolysis in G6PD-deficient subjects after ingestion of faba beans with low concentrations of the b-glucosides vicine and convicine whose metabolites generate irreversible oxidative stress in these subjects (Gallo et al., 2018) Importantly, other redox cyclers such as MB and bMDs do not present any increase of hemolysis in g6pd-deficient RBCs, instead bMDs even phenocopies the protection acquired through G6PD-deficiency leading to enhanced hemichrome deposition (Bielitza et al, 2015 and above, paragraph on bMDs). Underlying the extreme sensitivity of malaria parasites to oxidative stress, an increase ROS production in the liver mediated by a transient high-fat diet perturbs the establishment of the hepatic stages of the murine malaria parasite *P. berghei* that is then unable to cause severe malaria (Zuzarte-Luís et al., 2017).

Potential for drug resistance to redox active compounds

Molecules with multiple drug targets or with a pleiotropic mode of action are considered to be less prone to select for resistance (Ding et al., 2012). This is the case for redox-cyclers, such as bMDs and the closely related MB, which interfere with a complex and tightly regulated redox network in the host/parasite unit (Katharina Ehrhardt et al., 2016; Nepveu & Turrini, 2013; Schirmer et al., 2003). Similarly, the lack of a specific parasite target or motif for ROS producing compounds such as Art or FQ and redox cyclers also makes it impossible for parasites to develop point mutations that control the susceptibility of these multiple targets to the drugs.

Still, Art-resistance has emerged and spread in South-East Asia, revealing the pivotal role of mutations in the Kelch protein K13 in mediating resistance (Ariey et al., 2014; B Witkowski et al., 2013). Multiple hypotheses have been proposed to explain K13 role and how mutations may affect it, until very compelling data were published earlier this year (Birnbaum et al., 2020). K13 is actually required for the endocytosis of hemoglobin from the host cell in ring stages, and parasites with mutated or inactivated K13 display reduced hemoglobin endocytosis. This is also true for other proteins located in the K13 compartment, such as UBP1 and AP2u whose mutations had previously been associated with Art-resistance. Thus, reduced endocytosis at the ring stage that seems especially sensitive to oxidative stress, results in reduced uptake of hemoglobin that is necessary for Art activation, and possibly reduced endocytosis of Art or its metabolites themselves. Worryingly, this mechanism of resistance is likely to be shared with numerous other drugs that require efficient endocytosis to be up-taken by the parasite in large enough quantities, or that require hemoglobin to mediate their antiparasitic activity as the models for bMDs and MB modes of action predict.

Of note, PQ antiparasitic activity is mediated by the ability of its hydroxylated metabolites to cycle with the host cytochrome P450 reductase, thus locally generating oxidative stress that kills parasites developing in this environment. In this case, K13 mutations are expected to have little to no effect on PQ activity, although Art-R parasites seem to also have an enhanced ability to enter into quiescence (Paloque et al., 2016), which may protect them from external insults.

Part 4: Why metabolically less active rings and gametocyte stages are especially sensitive to antimalarials generating oxidative stress?

Plasmodium parasites are extremely versatile during their development, living mostly intracellularly in the human host while they develop extracellularly in mosquitoes, and even within one host, they are able to invade different cells and differentiate in different forms with specific functions. This versatility is supported by major changes in their metabolism that may in part explain why some stages are more sensitive to drugs generating oxidative stress. In addition, *Plasmodium* parasites are highly adapted to cope with the oxidative stress arising from its own metabolism of haemoglobin, generating reactive oxygen species, and releasing of toxic heme species.

Of note, despite the fact that ring stages are metabolically less active, and that they display underdeveloped organelles, notably mitochondria, apicoplast, digestive vacuole and cytostome, as compared to trophozoites and schizonts, they are more sensitive to redox cyclers and ROS inducers (Fig. 1.4). This may be explained by a less efficient antioxidant system, at a stage where it is not strongly required as there is very limited haemoglobin digestion. For instance, superoxide dismutases (SODs) and thioredoxin peroxidases (TPXs) that are key enzymes to detoxify intracellular ROS, are expressed at much lower levels in rings compared to later stages (Otto et al., 2010).

In contrast to asexual stages that carry out glutamine dependent glycolysis, gametocytes rely on glucose-dependent tricarboxylic acid cycle (TCA) to produce energy (Zhang et al, 1992), which can be correlated with the presence of more developed and electron dense cristae mitochondria in gametocytes (Wu, 2002)in contrast to smaller acristae mitochondria in asexual parasite stages where the mitochondrial electron transport chain is mostly associated with the regeneration of ubiquinone for pyrimidine biosynthesis (Klonis et al., 2011) (Berman et al, 1997,. This is associated with a higher expression of SODs and TPXs in gametocytes. The susceptibility of gametocytes to redox active drugs might thus have different grounds from that of asexual stages. Of note, early gametocyte stages are metabolically active, with active glycolysis, haemoglobin digestion and protein synthesis, while later stages shut down these biological processes and become quiescent (Buchholz et al., 2011; Coulibaly et al., 2015). While young gametocytes are susceptible to most drugs targeting young rings, intermediate and mature stages become increasingly resistant to drugs, including Art, MB and bMDs (Sophie H. Adjalley et al., 2011b; M. Delves et al., 2012; Katharina Ehrhardt et al., 2016), probably reflecting the decreasing endocytosis/ metabolic activity of the later stages. This is not the case for PQ in vivo, which is coherent with a host-dependent and parasite-independent generation of ROS for this drug.

Common principles of redox-cycling

The unique feature of redox-cyclers lies in their intrinsic redox potential that allows them to participate in reversible one-electron or two-electron transfer reactions and therefore in a continuous reduction-oxidation cycle. Redox-cyclers do not act as simple inhibitors, they are substrates of oxidoreductase enzymes that belong to multiple intracellular redox systems in eukaryotic cells (e.g. mitochondrial electron transport chain, glutathione and thioredoxin

systems). After enzymatic reduction, the reduced drug/metabolite can be readily reoxidized by molecular oxygen or alternative oxidants, thus regenerating the initial drug that can continue its redox cycling. Under physiological conditions, the overall reaction leads to a NAD(P)H-dependent transfer of electrons from oxidoreductases to intracellular key oxidants, for instance the hemoglobin-associated or free heme (FeIII) species that is present in large quantities in infected erythrocytes, and is accompanied by the formation of reactive oxygen species (ROS) (Fig. 1.3.) (Max Bielitza et al., 2015; Blank et al., 2012; Johann, 2012; Tobias Müller et al., 2011; Sidorov et al., 2015)

Redox-cyclers are also designated as subversive substrates because they divert the physiological antioxidant activity of oxidoreductases into a pro-oxidative activity, resulting in depletion of the intracellular reductant NAD(P)H stock and in the generation of considerable amounts of oxidized thiols and ROS.

Conversion from prodrug to drug

Common to all antimalarial redox-cyclers, the initial drug is considered to be a prodrug that is intracellularly converted into an active metabolite, thereby changing its redox potential and generating the subversive substrate. In the case of MB and bMDs, conversion of the prodrug is considered to occur within the Plasmodium-infected erythrocyte upon interaction with a flavoenzyme in addition to a hemoprotein (hemoglobin, flavohemoprotein…) under a ferryl species. Interestingly, antimalarial MB, bMDs and indolone-N-oxides (iNOD) are thought to be first metabolized by a reductase in iRBCs ((Buchholz, Comini, et al., 2008; Buchholz, Schirmer, et al., 2008; Ibrahim et al., 2011). Instead, PQ needs to be converted to hydroxylated metabolites by the cytochrome P450 NADPH:oxidoreductase and cytochrome P450 CYP2D6 in the liver before it can enter into a redox-cycle that mediates its antiparasitic activities (Fig. 1.3) (Camarda et al., 2019; Vásquez-Vivar & Augusto, 1994)

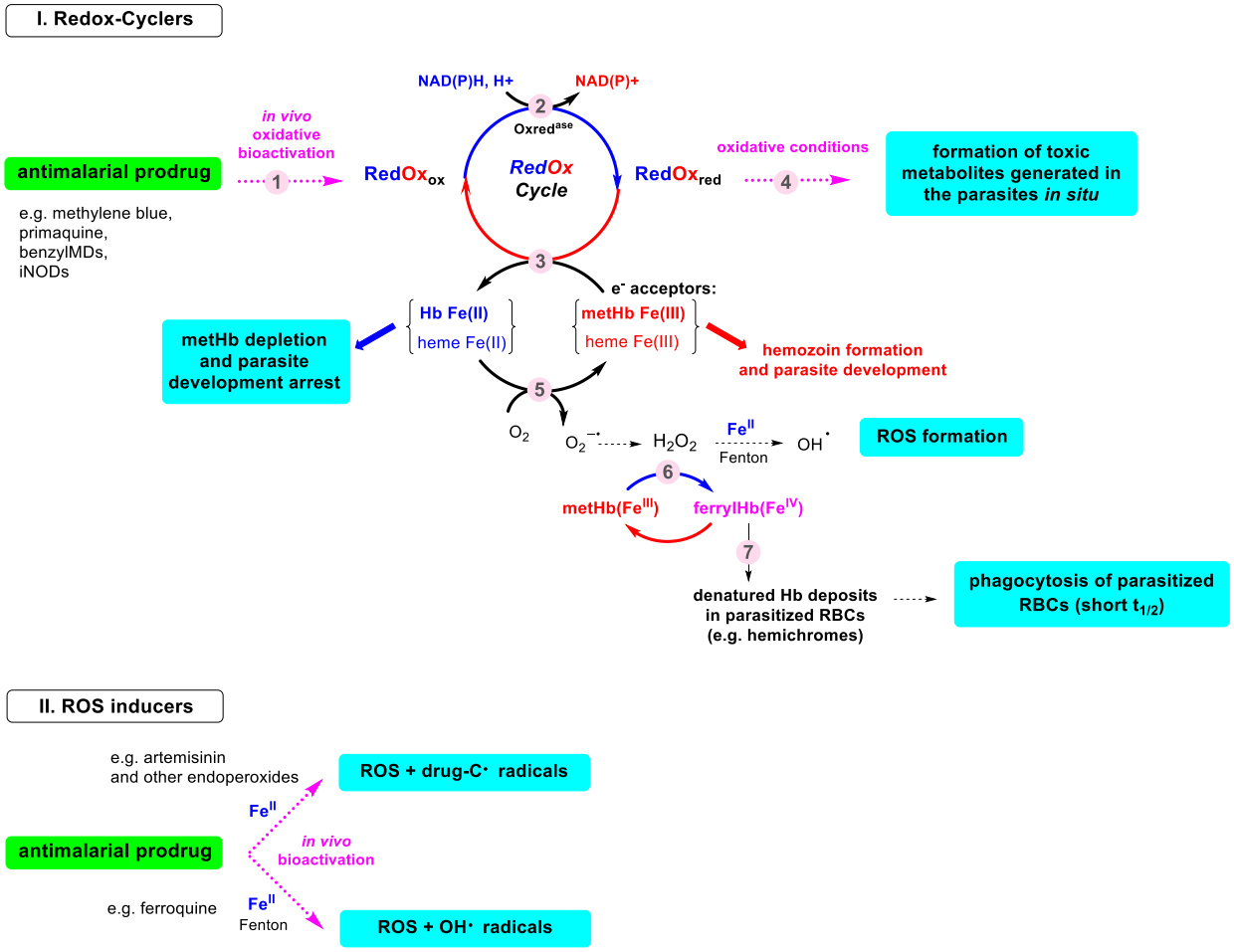

Figure 1.3. Two modes of action of antimalarial prodrugs based on oxidative stress generation: I. Redox-Cyclers, II. ROS Inducers. In the first type, a cascade of redox reactions accounting for the antimalarial activity was proposed to take place, first (step 1) by an oxidative bioactivation of the agent *in vivo* with the formation of a key redox-active principle in its oxidized state ($RedOx_{ox}$). Then, the oxidized metabolite is reduced by a NAD(P)H-dependent oxidoreductase (step 2) in *Plasmodium* parasites, generating the reduced state of the redox-active principle ($RedOx_{red}$), which transfers one electron to a key oxidant (protein) biomolecule (step 3). In the trophozoites stages, key oxidant biomolecules may represent the major nutrient of the malarial parasite, the hemoglobin-associated or free heme Fe^{III} species in infected erythrocytes, that promote parasite development and hemozoin formation, respectively. The reduction-oxidation cycle regenerates the oxidized redox-active principle that can be reduced again in a new cycle, at the expense of NAD(P)H. The continuous redox-cycle occurring in a compartment with oxidative conditions, e.g. the food vacuole, generates other metabolites *in situ* (by Fenton, oxidative coupling reactions, …) that might be toxic for the parasite (step 4). The shift of the Fe^{III}/Fe^{II} balance is lethal for the parasite because only metHb is a substrate for the parasitic proteases while Hb is indigestible. As observed earlier, the microscopic images of *P. falciparum* 3D7 strain ring-parasitized RBCs, treated at 50 nM by distinct $RedOx_{ox}$ (MB, or plasmodione) for 24 h, showed altered morphologies and pycnotic parasites. In the presence of traces of oxygen and of the efficient redox-cycler $RedOx_{ox}$, the redox cycle based on NADPH-dependent methaemoglobin reduction leads to the continuous formation of reactive oxygen species (ROS), ferrylhemoglobin (ferrylHb), and subsequent membrane-bound

hemichrome elevation. This latter hemoglobin catabolite is known to be a biomarker of RBC senescence, and enhances phagocytosis of drug-treated ring-parasitized RBCs (Bielita et al., 2015). Structure-activity relationships evidenced that both drug metabolites and hemoglobin catabolites contribute to potentiate drug effects and inhibition of parasite development. Disruption of redox homeostasis by the lead redox-cyclers was specifically induced in *P. falciparum* parasitized RBCs and not in non-infected cells, and visualized by changes in the glutathione redox potential of living parasite cytosols. The lead antimalarial redox-active prodrugs (MB, plasmodione) were shown to act by mimicking the behaviour of a *falciparum* parasite developing inside a G6PD-deficient RBC giving rise to malaria protection, and exerting specific additive effects inhibitory to parasite development, without harm for non infected G6PD-sufficient or -deficient RBCs.

In the second type, ROS inducers are represented by two chemotypes : artemisinin and endoperoxides, and ferroquine, which is in Phase 2b as a drug combination with a trioxolane partner artefenomel (OZ439).

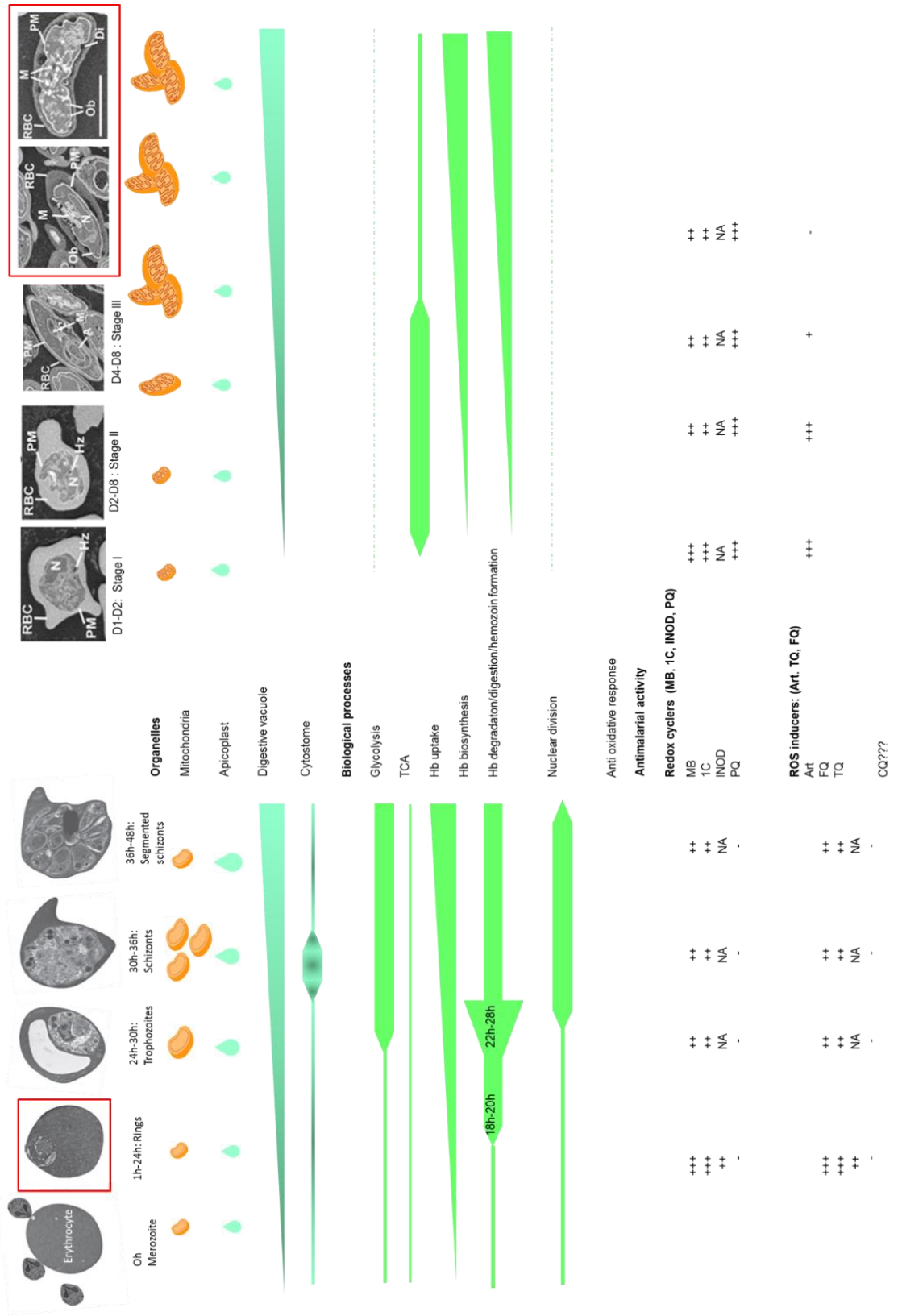

Figure. 1.4. Summary figure depicting relation between organelle development, biological processes and anti-oxidative response of redox cyclers (MB, 1c/PD, INOD, PQ) and ROS inducers (Art, FQ, TQ) in different stages of asexual parasite and sexual parasite stages.

Table 1. Characteristics of antimalarial redox active and ROS inducing compounds.

Methylene blue: tricyclic thiazine dye (Redox active compound), dibenzyl analogue of paraquat, pro-oxidant with potential for one-electron reduction . Redox cycler dependent on NADPH for its reduction				
Target parasite stages	**Mode of action: Active metabolites & molecular targets**	**Genetic resistance/ Effect in G6PD-deficient patients**	**Advantages**	**Drawbacks**
• All asexual stages • Very young rings are especially sensitive (Katharina Ehrhardt et al., 2013) • Gametocytocidal against early & mature gametocytes in vitro • IC50 gametocyte stage V IC50 90nM) (Katharina Ehrhardt et al., 2016) • o activity on liver stages (Bosson-Vanga et al., 2018) • ecreases the number of oocyst & viable mature gametocytes (Sophie H. Adjalley et al., 2011b)	• Following oral administration MB is absorbed from the gastrointestinal tract and partly monodemethylated to azure B. It reaches maximal plasma concentrations within 2 hours with a 20h plasma half-life (Walter-Sack et al., 2009). • MB exhibits pro-oxidant properties, possibly by inhibiting GR in both cytoplasm and apicoplast (Akoachere et al., 2005; Atamna et al., 1996; Färber et al., 1998; Kehr et al., 2010; Schirmer et al., 2003) • In vitro, MB or metabolites can enter a redox cycle with NADPH-dependent GR and metHb. It is reduced by GR, and can then reduce metHb (Fe^{3+}) into oxyHb (Fe^{2+}), a form that is not digestible by parasites (Belorgey et al., 2013; Blank et al., 2012; Tobias Müller et al., 2011) • MB also inhibits hemozoin formation by preventing polymerization of haem (Atamna et al., 1996; Blank et al., 2012)	• No genetic resistant mutant identified. • Cytotoxicity against G6PD deficient individuals at high dose (Akoachere et al., 2005; Ghatak et al., 2013) • Not harmful for G6PD-deficient populations at therapeutic doses (Tobias Müller et al., 2011)	• Cheap, pleiotropic with thus a low potential for resistance, good pharmakokinetics, low toxicity (Schirmer et al 2003, Suwanarusk et al, 2015, Wainwright et al 2005) MB has substantial antimalarial activity against all types of malaria (Lu et al, 2018) • In preclinical studies MB acts synergistically with artemisinin & block transmission Can be used in combination therapy with artesunate-amodiaquine for falciparum malaria in children active on drug resistant parasites, notably CQ^R $quinolones^R$ (Akoachere et al., 2005) • Can prevent methemoglobinemia Dose dependent and limited clinical relevance for adverse effects in G6PD Deficient patients. (O. Müller et al., 2013)	• Green/blue coloration of urine and eye white • MB at low concentration is a strong inhibitor of monoamine oxidase A and therefore, should not be given together with serotonin reuptake inhibitor(Ramsay et al., 2007) • Main adverse effects in African clinical studies. Mild urogenital symptoms and gastrointestinal symptoms due to MB bitterness (Lu et al., 2018). • High intravenous doses were related to severe gastrointestinal symptoms (Schirmer et al., 2011)

Artemisinin- sesquiterpene lactone with an endoperoxide bridge
Active antimalarial metabolite: dihydroartemisinin, hemisynthetic form with better pharmacokinetics properties

Target parasite stages	Mode of action: Active metabolites & molecular targets	Genetic resistance/ Effect in G6PD-deficient patients	Advantages	Drawbacks
• Active on all asexual stages including very young rings (Bates et al., 1990; Terkuile et al., 1993) • Active on immature gametocyte stages (I-III), with IC50 12-120 nM (Sophie H. Adjalley et al., 2011a; Buchholz et al., 2011; Kumar & Zheng, 1990) low activity on mature gametocytes (Sophie H. Adjalley et al., 2011a)	• Art is a prodrug whose 1,2,4-trioxane core including an endoperoxide bridge is essential for its antimalarial activity (Steven R. Meshnick, 2002) • Art accumulates in parasite cytosol and membranes. It is activated when the endoperoxide bridge reacts with reduced iron (FeII)-heme released during hemoglobin digestion (Klonis et al., 2011). This generates radical species that react with nucleophiles in proteins, lipids, nucleic acids and hemes, generating ROS, depolarization of both mitochondrial an cytoplasmic membranes and leading to massive cellular damages (Jigang Wang et al., 2015). • Heme alkylation inhibits hemozoin formation • Activated Art also reduces parasite proteasome activity (Bridgford et al., 2018) adding to production of active metabolites by cleavage of peroxide bond in artemisinin consequently increasing ROS (Rudrapal & Chetia, 2016). • Limited activity on late stage gametocytes (Sophie H. Adjalley et al., 2011a) and on parasite transmission to mosquitoes at physiological doses (M. J. Delves et al., 2013; Ruecker et al., 2014; Vanaerschot et al., 2017) • Art treatment does not reduce gametocyte burden and transmission to mosquitoes	• No genetic resistance involving a target protein as expected from Art mode of action. • Resistance and delayed clearance caused by: reduced hemoglobin uptake at the ring stage linked to mutations in K13, AP-2u, UBP1, falcipain and coronin (E. A. Ashley et al., 2014; Birnbaum et al., 2020; Demas et al., 2018; Henrici, van Schalkwyk, et al., 2020; Henriques et al., 2013, 2014; T. Yang et al., 2019) decreased cytotoxic stress, possibly through upregulated unfolded protein response (Mok et al., 2015), but most likely linked to decreased oxidative damage in these mutants; and induction of dormancy (Benoit Witkowski et al., 2010), a mechanism unlinked to K13 mutations and probably similar to bacterial persistence (Wellems et al., 2020). • Causes hemolytic anemia in G6PD-deficient patients of parasite (Francis et al., 2013)	• Fast parasite killer, fast parasite clearance (N. J. White, 2008) • Kill parasites at ring stage, thus preventing formation of adherent trophozoites that are responsible for severe symptoms (Teuscher et al., 2010) • Short in vivo half-life that reduces long exposure to decreasing drug concentrations and resistance selection (Aweeka & German, 2008; Klonis et al., 2011; Vanaerschot et al., 2017) • Active against quinolines, and antifolates resistant parasites (Arjen M. Dondorp et al., 2010) • Potent activity against drug resistant parasites, notably chloroquine & sulphadoxine–pyrimethamine (SP) resistant strains in vivo & in vitro (N. J. White, 2008)	• Art has low solubility in oil & water (Butler & Wu, 1992; Klayman, 1985), which is not the case for several synthetic analogues (Rudrapal & Chetia, 2016) • Artemisinin resistance with delayed parasite clearance in patients in South East Asia (Chanaki Amaratunga et al., 2012; A M Dondorp et al., 2009) • Induces dormancy that may favor generation of resistant parasites to ACT partner drug (Wellems et al., 2020). Causes hemolytic anemia in G6PD-deficient patients

	(Djimde et al., 2016; Ouologuem et al., 2018) and may facilitate transmission of ArtR parasites [Witmer, BioRxiv 2020].			• Causes hemolytic anemia in G6PD-deficient patients neurotoxicity (Brewer, 1998)

Plamodione: 2-methyl-1,4-naphthoquinone (Redox active compound) (Katharina Ehrhardt et al., 2013)

Target parasite stages	Mode of action: Active metabolites & molecular targets	Genetic resistance/ Effect in G6PD-deficient patients/	Advantages	Drawbacks
• active on all asexual stages, with higher efficiency on young rings • Active on young gametocytes induces pycnotic dead parasites (Katharina Ehrhardt et al., 2013, 2016)	• Bioactivation via a cascade of redox reactions is required to generate active metabolites (Elhabiri et al., 2015; Feng et al., 2018; Tobias Müller et al., 2011) • In vitro, benzoylmenadione metabolite can cycle with flavoenzymes and metHb. In vivo, this would lead to oxidative stress • and deplete parasites from NAD(P)H and metHb, the digestible form of Hb, thus leading to parasite death (Belorgey et al., 2013; M Bielitza et al., 2015; Blank et al., 2012; Lanfranchi et al., 2012; Tobias Müller et al., 2011) • PD increases hemichrome deposition on infected RBCs,a marker for cell removal in the spleen (M Bielitza et al., 2015) • PD metabolites can also inhibit hemozoin formation (Katharina Ehrhardt et al., 2013, 2016) • Respiratory growth in yeast also inhibited by PD, most likely via redox cycling of PD metabolites with NADH dehydrogenases (Mounkoro et al., 2019)	• No stable genetic resistance reported after exposing parasites to high or escalating doses of PD. Recrudescent parasites have a similar sensitivity to PD as non-treated parental strain (classical drug assay, 72h exposure) (Katharina Ehrhardt et al., 2016). • Not cytotoxic for G6PD deficient populations at therapeutic dose (M Bielitza et al., 2015)	• Cheap to produce with a broad chemical space for drug optimization (Elhabiri et al., 2015; Lanfranchi et al., 2012) • fast parasite killer (similar to Art) and Kill parasites at ring stage, thus preventing formation of adherent trophozoites that are responsible for severe symptoms(Katharina Ehrhardt et al., 2016) • No cross resistance with 3D7, D6, 845, VoII, L1, PA, Bres, FCR3, W2, K2, K14, FCM29 (Ehrhardt et al., 2016) • Synergistic with artemisinin & quinine (Katharina Ehrhardt et al., 2016), and with nicotinamide (M Bielitza et al., 2015) • Can prevent malarial anemia and methemoglobinemia. Not cytotoxic for G6PD deficient populations at therapeutic dose (M Bielitza et al., 2015) • Pleotropic effect (Sidorov et al., 2016)	• High lipophilicity, low solubility

Indolone-N-oxide (Redox active compound): conjugation of nitrone moiety (C=N+-O-) and phenolic group undergo oxidation-reduction reactions their reduction leads to loss of antimalarial activity

Target parasite stages	Mode of action: Active metabolites & molecular targets	Genetic resistance/ Effect in G6PD-deficient patients or Clinical applications other than malaria	Advantages	Drawbacks
• Inhibit parasite development at ring stage specifically (IC50 <100nM) (Tahar et al., 2011) • Gets reduced and produces stable radical intermediates in vivo • INOD-1 treatment facilitates hyperactive phosphorylation of band 3 at tyrosine, which is correlated with blebbing of erythrocyte membrane & vesiculation just as in case of G6PD deficient RBCs which resist parasite falciparum habitation and prevent malaria (Nepveu et al., 2010). • Induces overall oxidative stress in addition to parasite invasion mediated stress via denaturation of hemoglobin, decreasing levels of reduced form of glutathione, and peroxidation of	• Syk kinase and/or (potential target to activate for favoring phosphorylation of band 3) • Tyrosine phosphatases of band 3 of host erythrocytes (to inhibit for favoring the phosphorylation of band 3) (Nepveu et al., 2010)	• Antifungal Antibacterial Antileishmanial (HOOPER et al., 1965; Ibrahim et al., 2012)	• IC50 48.6 nM for both CQ sensitive & CQ resistant strains (similar to MB) • According to metabolic studies within mouse liver microsomes best antiplasmodial activity by intraperitoneal (ip) route of administration. • More potent than artemisinin on chloroquine sensitive and CQ and pyrimethamine-resistant (K1) strains (Nepveu et al., 2010)	• 1 min half life, so lowest activity by the oral route of administration related to extensive degradation of compound via first-pass effect (Nepveu et al., 2010)

membrane lipids consequently leading to vesiculation. & destabilization of membrane of ring stage infected erythrocytes (Ferru et al., 2011; Pantaleo et al., 2009, 2011, 2015) • Activity independent of polymerization/bio crystallization of nontoxic heme (Nepveu et al., 2010)				

Primaquine: 8-aminoquinoline, anti-hypnozoite activity due to methoxy group at position 6 & amino sidechain at 8 position of aromatic quinolone core (Redox inducer), exoerythrocytic drug, active metabolite: quinone-imine (5 hydroxy-primaquine) with physiologically protonated basic group in their side-chain (Bates et al., 1990; Portela et al., 1999; Vale et al., 2009)

Target parasite stages	Mode of action: Active metabolites & molecular targets	Genetic resistance/ Effect in G6PD-deficient patients	Advantages	Drawbacks
• tissue schizontocide (Baird et al 2004) • Mature gametocytes (stage-V) (Pybus et al., 2012) • Hypnozoites of Plasmodium vivax and Plasmodium ovale (Krotoski et al., 1980; Pybus et al., 2012) • multiple parasite stages (M. Delves et al., 2012; M. J. Delves et al., 2012; Dembele et al., 2011; Plouffe et al., 2016)	• Primaquine metabolized by CYP 2D6 to form oxidized or phenolic metabolites (A. Bennett et al., 2013; Ganesan et al., 2012; Magwere et al., 1997; Vásquez-Vivar & Augusto, 1994) • PQ mode of action involves 2 steps. In the first step, through the CPR / CYP2D6 • metabolic complex, PQ gets converted into hydroxylated metabolites (OH-PQm), which in the second step gets oxidized to quinonimines (O = PQm) by simultaneous of the generation of H2O2. These coupling reactions involve NADPH donating the 2 electrons to CPR/CYP2D6 while the quinonimines accept electrons from	• Several CYP2D6 polymorphisms associated with loss of PQ activity (A. Bennett et al., 2013; Peters et al., 1984; Pybus et al., 2012) • In G6PD-deficient patients, high doses regimen over several days lead to life threating hemolysis & anemia (Cohen et al., 1968; Vásquez-Vivar & Augusto, 1994)	• Only FDA licensed therapy to treat relapsing strains of malaria (Graves et al., 2015). • As per clinical studies single low dose (0.25 mg base/kg) can block falciparum malaria transmission with very low risk of hemolytic toxicity (Mok et al., 2015) • Primaquine together with artemisinin-based combination therapies lead to high cure rates and substantially reduced gametocyte carriage. • Low doses of primaquine together with a combination of	• rapidly metabolized (14 highly reactive drug metabolites) • half-life of six hour (Klayman, 1985) • anemia, intravascular hemolysis with dark urine, and mild jaundice, renal failure, hemoglobinemia

• swelling and thickening of mitochondrial cristae (A. Bennett et al., 2013; Peters et al., 1984)	FAD/FAMN cofactors. However, the reduction potential of quinonimines is low thereby promoting formations and accumulation of H2O2 at metabolite site bone marrow and liver. Thus, the parasites die because of increased cytotoxicity by H2O2 (Camarda et al., 2019).	• Can cause methemoglobinemia, leading to lipid and membrane protein oxidation events that disrupt the integrity of the cell (Pantaleo et al., 2009, 2011, 2015)	artemisinin and piperaquine eliminate all stages of parasites from human carriers thereby decreasing the incidences of malaria in western Cambodia (Song et al., 2010). • A single dose of PQ lowers the transmission of malaria from the asymptomatic population (Okebe et al., 2016)	(Elizabeth A. Ashley et al., 2014; Clayman et al., 1952; Hockwald et al., 1952) • toxic in met-hemoglobine reductase (MetHbR)-deficient patients (Cohen et al., 1968; Vásquez-Vivar & Augusto, 1994)

Acknowledgements The authors thank xx and yy for editorial contribution and helpful discussion.

Compliance with Ethical Standards

Conflict of Interest The authors received no financial support in the writing of this manuscript.

Human and Animal Rights and Informed Consent This article does not contain any studies with human or animal subjects performed by any of the authors.

CHAPTER 2: Cross resistance of PD derivatives with artemisinin

This chapter elucidates that the PD analogue, bMD40, with improved pharmacokinetics properties showed cross-resistance with asexual stages of Artemisinin resistant *P. falciparum*, thereby opening an intriguing question about the PD drug combinations as a future therapeutic option. For this, I set the cultures of various drug-susceptible and resistant *P. falciparum* parasites in the laboratory, standardized the conditions for modified IC_{50} assay on tightly synchronized 3-hour-old ring stages of parasites, and contributed to establishing the ring survival assay using FACS analysis. I contributed to the technology transfer to another PhD student-Brice Feufack. In addition, I measured all antimalarial activities of the ABPP probes used in Chapter 3.

TABLE OF FIGURES

Introduction

Malaria is a fatal disease caused by the parasite *Plasmodium falciparum (P. falciparum).* Early ring and mature gametocyte stages of the parasite are responsible for multiplication of the disease in humans and its transmission to *Anopheles* mosquitoes. Very few drugs target these two stages. Artemisinin (Art) is the most efficient antimalarial drug but it is now threatened by emergence of Art resistance in South East Asia, India (A M Dondorp et al., 2009; Karbwang & Na-Bangchang, 2020; WHO, 2019). There is therefore an urgent need for new potent drugs or drug combinations that could target rings and gametocytes and bypass Art resistance. Plasmodione (PD, Fig. 2.1), is a potent 3-benzylmenadione (benzylMD) drug candidate, toxicologically safe and active on rings with killing speed similar to Art. It has low potential to induce drug resistance and displays synergy with several antimalarial drugs including Art (Ehrhardt et al., 2013; Ehrhardt et al., 2016). PD kills parasites by generating oxidative stress in parasitized red blood cells (pRBCs), mimicking the effects of glucose phosphate dehydrogenase (G6PD) deficient RBCs, which confers to carriers natural protection from severe malaria (M Bielitza et al., 2015). The interest of our research group is to decipher the mechanism of action of PD and analogues. PD has been proposed to be bioactivated through a cascade of redox reactions generating the key metabolite 3-benzoylmenadione (benzoylMD I,), which is – under its oxidized form – an efficient substrate of both human and *P. falciparum* glutathione reductases (GR) of pRBCs (T Müller et al., 2011). Under its reduced form, the hydronaphthoquinone species transfers one electron to methemoglobin (Fe^{3+}) (metHb), thus entering into a continuous redox cycle. This scenario is relevant since both proteins, human GR and metHb - a major protein of pRBC, actively contribute to hemoglobin (Hb) digestion. However, PD was observed to be the most active against *P. falciparum* young rings and gametocytes (Goetz et al in preparation)- the stages in which Hb digestion takes place at significantly low rate. Because other oxidoreductases can theoretically provide electrons to benzoylMD I, and notably in parasite stages distinct from trophozoites, such as rings and gametocytes; we assume that there are multiple PD targets causing drug bioactivation and parasite killing. PD is active on rings with a speed of action as fast as that of Art. However, the precise targets and mechanism of action and PD drug targets are not yet known. We addressed this question via click and fish strategy. Our lab is also interested in understanding if PD and its analogues bMD30 and bMD40 that present better bioavailability, could represent novel drug leads to circumvent Art resistance. The effect of PD on lab-adapted patient isolates with various Art resistances had been preliminary studied by Katharina Ehrhardt during her stay at Institut Pasteur in Cambodia in 2014. Her results indicated cross resistance between PD and artemisinin. Based on these data, in the beginning of my PhD, I contributed to establish the Ring Survival Assay (RSA) in the laboratory to characterise the activity of PD and its analogue bMD40 on the most Art sensitive (Art-S, IPC5188) and resistant (Art-R, IPC5202) strains. Further steps of this project, including the development of a RSA FACS protocol to test drug combinations that could alleviate resistance, and further characterisation of bMD activity on gametocyte and transmission, have been taken over by another PhD researcher. Here, the preliminary data for cross-resistance of PD and its analogue bMD40 is presented as well as the antimalarial properties of PD and its analogues, with some additional observations I have made while trying to optimise parasite culture conditions to obtain asexual and sexual stages.

(A)

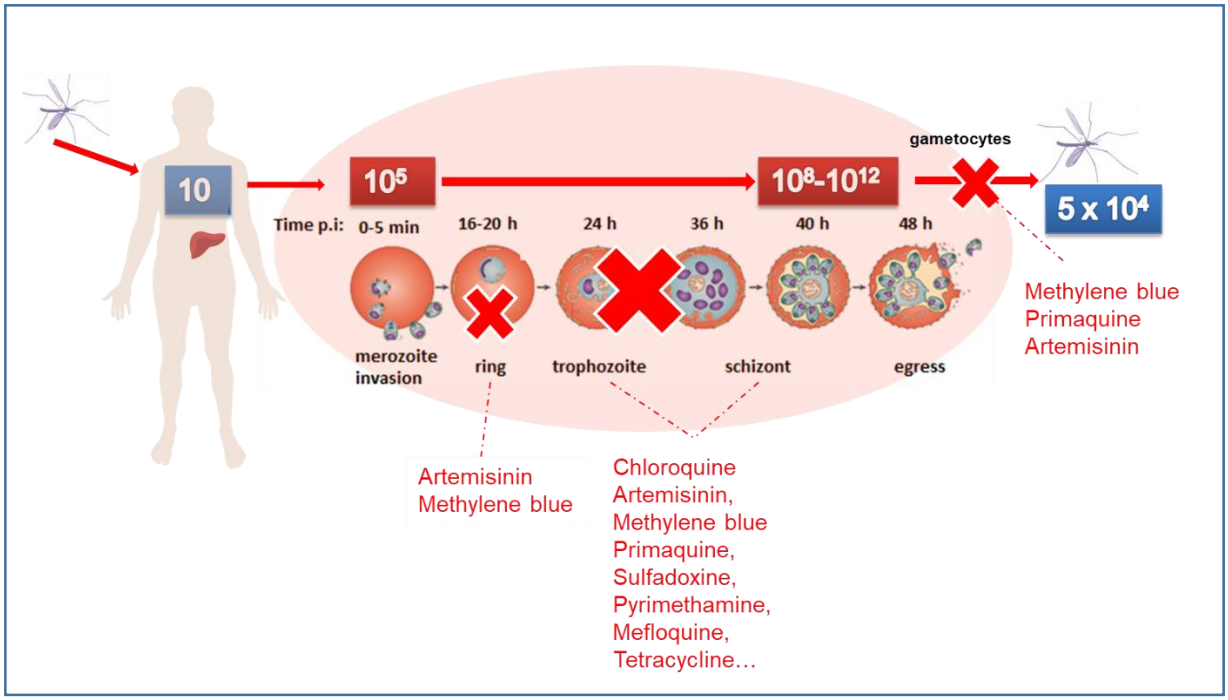

(B)

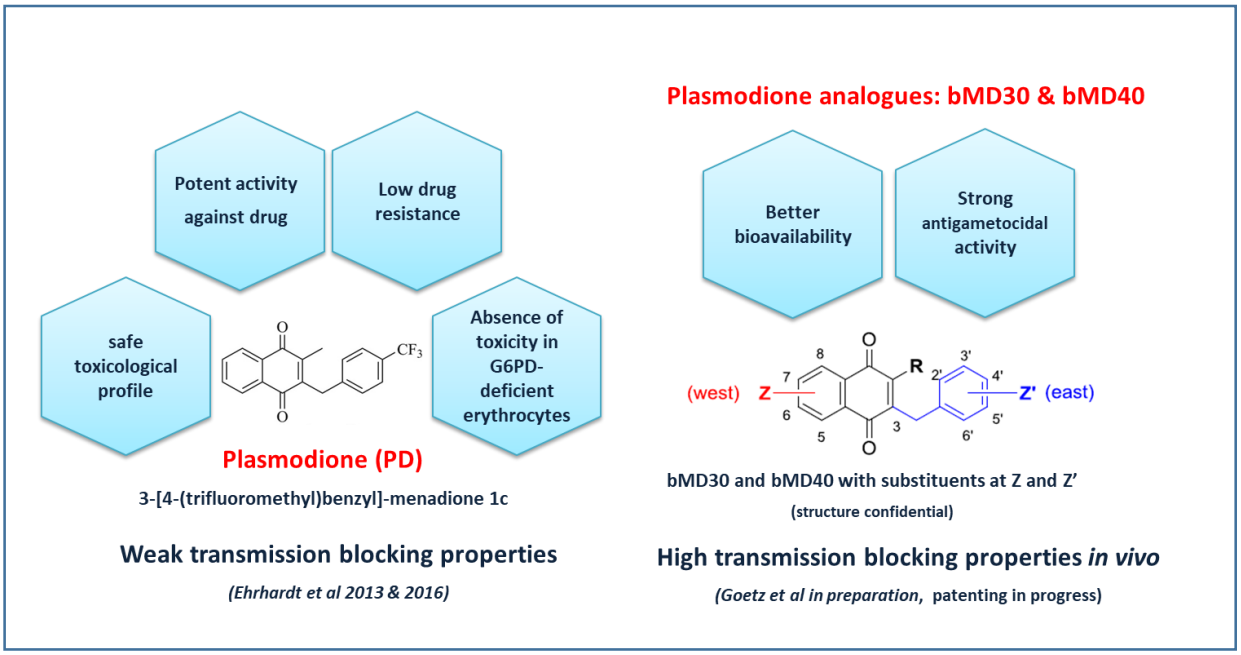

Figure 2. 1 (A) Summary of currently available antimalarial drug and their activity on different asexual and sexual stages of *P. falciparum* parasite. (B) Properties of Plasmodione and its analogues bMD30 and bMD40 (Structures are confidential).

Results

Antimalarial activity (nM) of PD-analogues on sexual and asexual stages of *P. falciparum*

PD-analogues bMD30 and bMD40 have improved pharmacokinetic properties compared to PD. We evaluated their antiplasmodial activity on asexual stages of the *P. falciparum* chloroquine-resistant strain Dd2 and on sexual stages of the NF54 line expressing a GFP-Luciferase fusion under the control of a gametocyte specific gene *pfs16* (S H Adjalley et al., 2011) (Table 1). Our data show that the PD analogue, bMD30 is as efficient as Plasmodione to kill parasites while the bMD40 concentration that kills half of the parasites is twice as high as that of PD and bMD30. Still, bMD40 is the only benzylmenadione that is active on all gametocyte stages with IC50s in the nM range, and a potent activity on stage V gametocytes, with an IC_{50} in similar to MB (Goetz et al in preparation), making it a very attractive new lead.

Table.1. Antimalarial activity (nM) of PD-analogues on sexual and asexual stages of *P. falciparum*

Drugs/PD/ PD-analogues	IC50 on asexual stages of Dd2- chloroquine resistant strain	IC50 on sexual stages (young gametocyte stage I-II) of NF54 strain (Goetz et al in preparation)*	IC50 on sexual stages (mid gametocyte stage III-IV) of NF54 strain (Goetz et al in preparation)*	IC50 on sexual stages (mature gametocyte stage V) of NF54 strain (Goetz et al in preparation)*
Dihydroartemisinin	0.71 ± 0.23	ND	ND	ND
Chloroquine	189 ± 12	ND	ND	ND
Methylene blue	7 ± 0.3	24 ± 12	59 ± 21	97 ± 18
Plasmodione	48 ± 3	31 ± 29	~ 5 000	~ 10 000
bMD30	42 ± 3	30 ± 29	~ 3 800	~ 8 000
bMD40	92 ± 12	4 ± 4	83 ± 20	228 ± 58

One of my goals was also to confirm, in my hands, the results obtained by a former PhD student of the laboratory on the gametocytocidal properties of 3-bMDs, and notably bMD40. For this, I used the protocol described in Adjalley et al., 2011. Although I managed to obtain stage V gametocytes, their numbers were too low to be able to perform a survival experiment (Gametocytemia: Day 2: 1.3%, Day 4: 0.9%, Day 6: 0.6%, Day 8: 0.1%, Day 11: 0.1%). These results are currently being repeated. Still the laboratory recently demonstrated that bMDs do not only block transmission of murine malaria parasites to *Anopheles* mosquitoes, but that this is also true for *P. falciparum* upon pre-incubation of stage V gametocytes with the compounds, thus providing further evidence of the transmission blocking potential of bMDs.

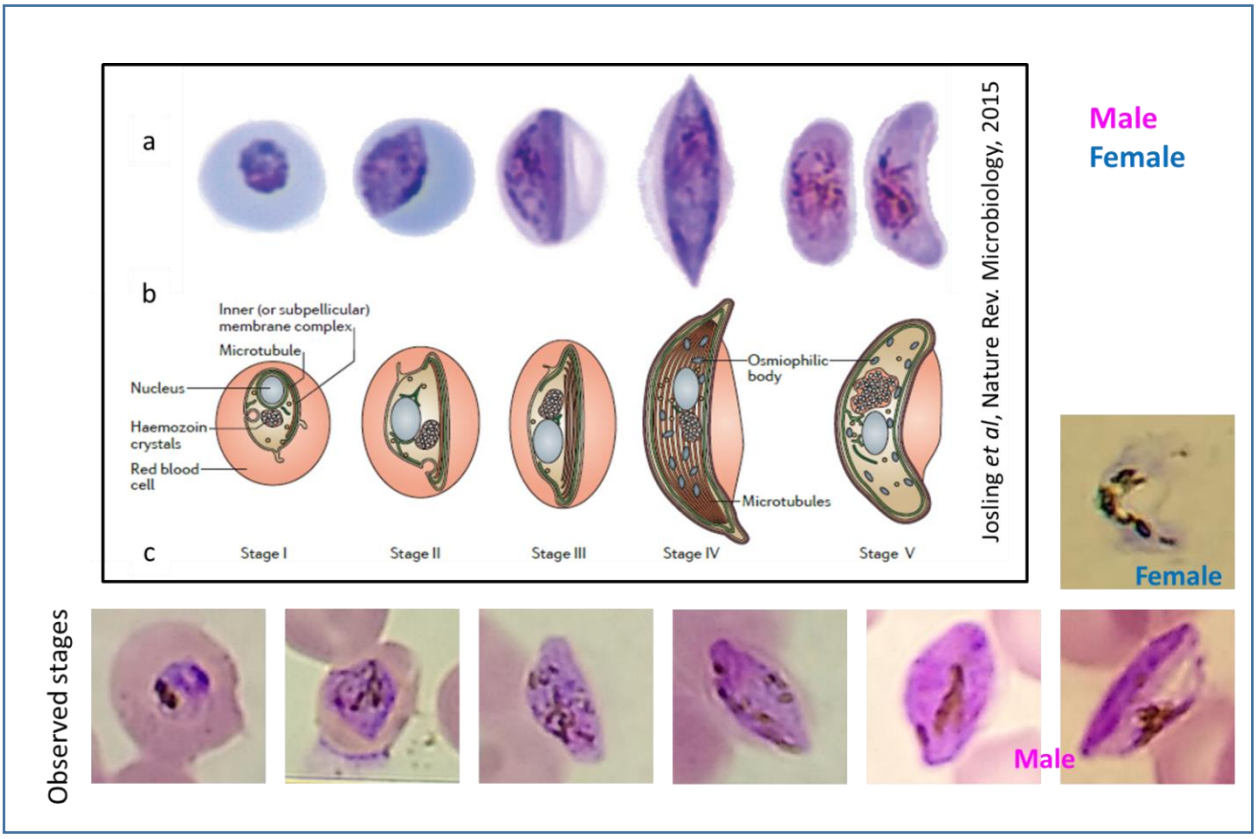

Figure 2. 2 Gametocyte induction of 3D7 strain of P. falciparum. Morphologically distinct sexual stages of *P. falciparum* develop over 10-12 days. Stage I being similar in appearance to the asexual trophozoite stage, it is indistinguishable. Stage II onwards gametocytes begin to elongate with microtubules and bear D shape, further elongated stage III have rounded ends, and stage IV have pointed ends. The characteristic crescent shape of gametocytes is achieved at stage V. After Giemsa staining the stage V females stain blue while male stain pink. Males are thicker while females are more elongated and curved. *Observed gametocytemia: Day 2: 1.3%, Day 4: 0.9%, Day 6: 0.6%, Day 8: 0.1%, Day 11: 0.1% .*

Growth of 3D7 is affected by the nutrient source

Parasites are usually cultured in medium complemented with human serum that is variable from one batch to the other and may thus lead to variations in growth rate and IC50s. To test whether we could replace the human serum with a synthetic supplement (albumax), we measured the growth of the lab-adapted strain 3D7 (Chloroquine sensitive) in medium supplemented with human serum and albumax. The 3D7 strain grow most efficiently (higher multiplication rate = dynamic range in Fig 2.3) in medium complemented with human serum compared to albumax, irrespective of whether the culture was mixed or synchronized. Still, 3D7 parasites grow well in medium with albumax, and can be cultured in medium supplemented by a mix of human serum and Albumax (HS/A, data not shown). Of note, the thawing and culture of Art-R and Art-S parasites is also more efficient in medium supplemented by HS/A in our hands (data not shown). For this reason, we now use medium supplemented by both human serum and Albumax as our regular culture medium in the lab except for specific applications (e.g. gametocytogenesis).

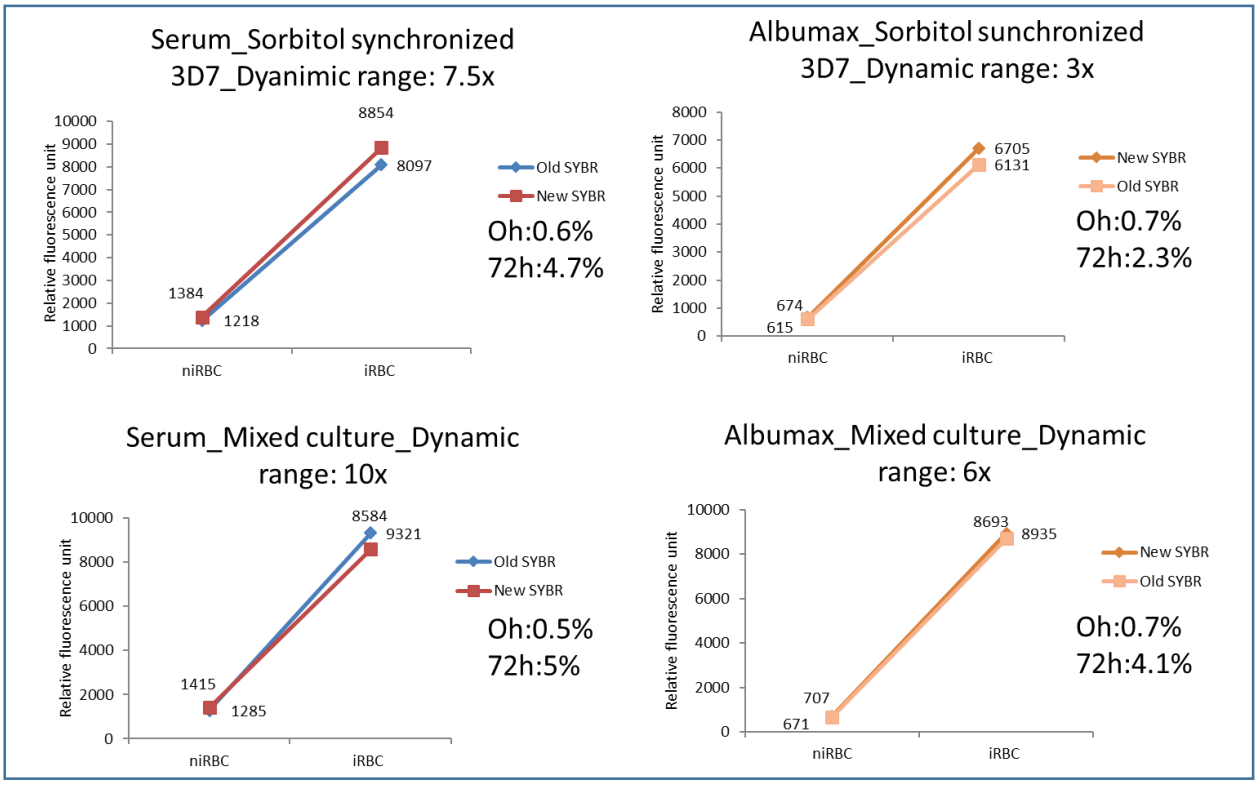

Figure 2. 3. Evaluation of growth conditions of 3D7 chloroquine sensitive strain of parasites after 72 hours in response to distinct nutrient sources such as 10% human serum and lipid rich BSA i.e. 10% albumax *(Gibco Cat. ≠11021-045)* instead of serum**.**

PD and its analogue bMD40 show cross-resistance with Artemisinin

To confirm cross-resistance of bMDs with Art, we developed the “classical” RSA test in the laboratory based on the protocol published by Witkowski et al., 2013, where young rings (0-3h) are exposed for 6h to the compound and allowed to recover and resume their development for 66h. Parasitemia and parasite status (live/dead) are then determined on a Giemsa smear. Our first results confirmed the existence of cross-resistance of PD and bMD40 with Art (fig 2.4). Still we noticed a high variability between replicates (both within and between experiments), including for the MB control, and, unexpectedly, a partial killing of Art-S parasites at the chosen drug concentrations. Importantly, results are strongly dependent on multiple technical and human factors, such as smear quality, ability to distinguish live and dead ring stages, experience of person observing slides, number of counted fields and parasites. To circumvent these issues and also increase the throughput of this test, we reasoned that the FACS protocol developed by Amaratunga et al., 2014 would be a better alternative. Another PhD student took up this challenge and adapted the published protocol to our laboratory settings. He further analysed PD/MD40 cross-resistance and explored drug combinations to bypass it.

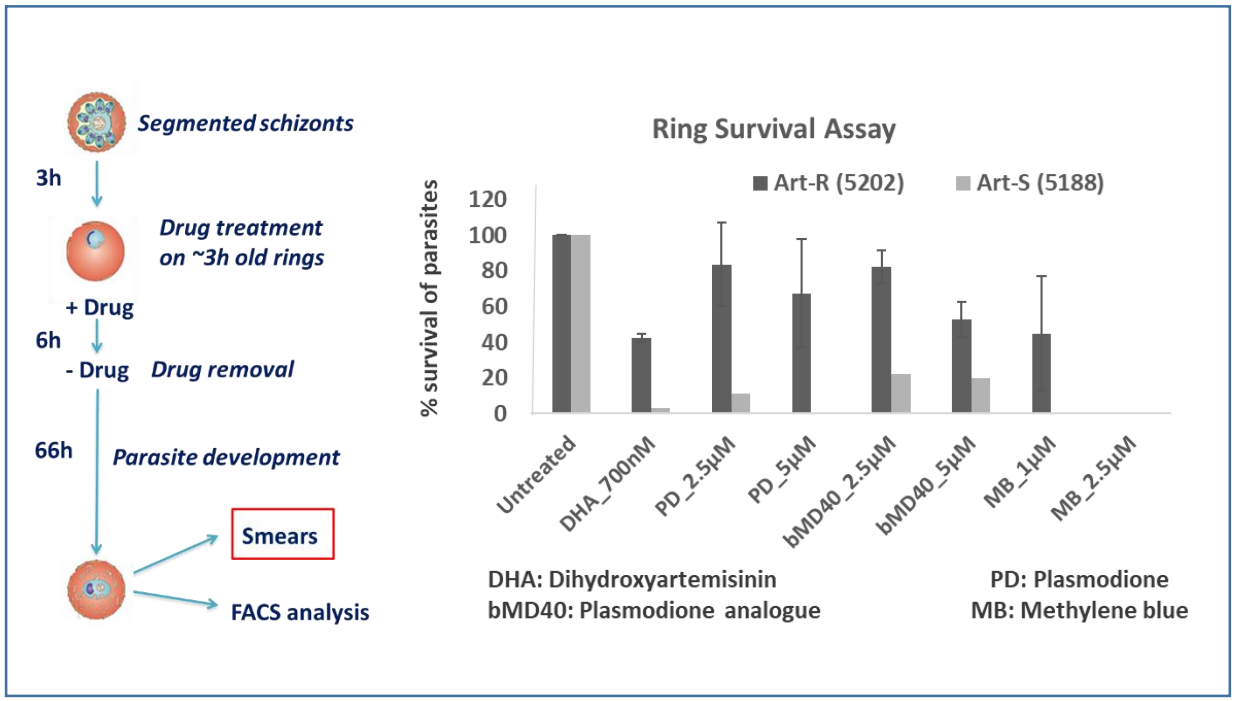

Figure 2. 4. Preliminary data of RSA to evaluate cross resistance of Plasmodione and bMD40 with Art. Early rings of Art-R (IPC5202, n=2) and Art-S (IPC5188, n=1) parasite strains were exposed to PD and bMD40 (2.5 µM and 5 µM), MB (1µM and 2.5 µM) and DHA (700 nM) as a control. Results as per counting of ring stages from microscopic analysis of Giemsa stained blood smears.

Conclusion

In conclusion, PD and its two analogues bMD30 and bMD40 display potent activity on asexual stages as well as young gametocytes, but bMD40 only kills late stage gametocytes. In the future, we would like to test a new analogue combining bMD30 and bMD40 modifications on the 3-bMD scaffold to assess whether we could further improve the antimalarial properties of this series.

Methods

Parasite strains and Culture conditions

Parasites strains used for these experiments are the following: WT 3D7 obtained from the Malaria Research and Reagent Resource center (MR4, BEI resources, USA), chloroquine-resistant Dd2 obtained from MR4 and Prof. Lanzer's laboratory (Heidelberg University, Germany), NF54 expressing the GFP-Luciferase under the control of the Pfs16 gene obtained from Prof. Fidock's laboratory (Columbia University, New York, USA), and the Cambodian artemisinin resistant IPC5202 and susceptible IPC5188 strains obtained from MR4.

Intraerythrocytic stages of *P. falciparum* were cultured according to standard protocols with slight modifications (Trager & Jensen, 1976). Parasites were maintained in a culture flask 75cm^2 with hematocrit 3.3-3.7 % at 37°C, humid atmosphere, 5% O2, 5% CO2 and 90% N2

in a complete medium consisting of RPMI 1640 (Life Technologies Inc.) supplemented with 11 mM glucose, 27.5 mM, NaHCO3, 10µg/ml gentamycin, type A pure erythrocytes and 8-10% heat-inactivated human serum for 3D7 Chloroquine sensitive and DD2 Chloroquine resistant strains. For artemisinin-resistant (IPC5202) and artemisin-sensitive (IPC5188) strains, instead of 10% human serum, a combination of 5% human serum and 5% Lipid rich BSA i.e. (*albumax II, Gibco Cat. ≠11021-045)* was used along with ca ¼ of "conditioned" medium to maintain the growth factors that help the parasite to multiply well in culture. Over the week, the parasitemia was maintained between 1-3% by checking the cultures daily and splitting them accordingly. Parasitemia and culture conditions were monitored by Giemsa staining of 100% methanol fixed blood smears.

Note 1. For Art R and Art S: if P < 1%, replacing 1/2 of the CM by fresh CM was sufficient to allow parasites to multiply to higher densities.

Note 2. Art-R and Art-S strains should not be splitted too low or maintained at too high parasitemia. For optimal growth, parasitemia should be maintained between 0.5% - 6%. When parasites are stressed, they start producing gametocytes or pyknotic stages. Before the weekend, parasitemia is reduced to 0.5% and volume of medium can be increased to 25-30 ml but always with ¼ of conditioned medium.

Note. 3. In case of planning RSA the next day, the culture medium was changed twice a day for a culture with high parasitemia with mostly trophozoite stages.

IC_{50} assay of PD and its analogues bMD30, bMD40 with SYBR Green

Antimalarial activity is represented by IC_{50}, i.e. the concentration of compound at which half of the parasites are killed. The antimalarial activity of PD and its derivatives (bMD30 and bMD40) was evaluated on 0-3 h old rings of the Dd2 (chloroquine-resistant) strain of *P. falciparum*. Our IC_{50} protocol is a combination of the ring survival assay (Ariey et al., 2014; B Witkowski et al., 2013) and the IC_{50} assay based on SYBR green staining of parasite DNA (Beez et al., 2011; Smilkstein et al., 2004). For this, 0-3h old rings (0.5% starting parasitemia and 3% haematocrit) were prepared as for the RSA and exposed to 1/3 serial dilutions of PD, bMD30 and bMD40, methylene blue (MB) and Choloroquine (CQ) for 72h in microtiter plates. Each compound was tested in duplicates in at least three independent biological experiments. Parasite replication was assessed by fluorescent SYBR® green staining of parasitic DNA (Smilkstein et al., 2004) as previously described (Beez et al., 2011). Briefly, after 72 hours of incubation with the drugs, parasites were frozen at -80°C overnight. Parasites were then thawed and their DNA was stained with the fluorescent SYBR green assay. Fluorescence intensity was determined on a Promega plate reader at 591nm wavelength. In addition, untreated iRBCs at T0 and T72 were observed on a Giemsa stained blood smear analysis to follow the pattern of growth and multiplication factor of parasites over time. IC_{50} values were calculated using Prism 6 (GraphPad, log(inhibitor) vs. normalized response – Variable slope).

Ring survival assay

The efficiency of PD and its derivative bMD40 for killing early ring stage of Art-S and Art-R strains was determined according to the reported protocol (Witkowski et al., 2013). For this, mature schizonts of highly synchronous parasite cultures were separated using 60% percoll gradient and the mature segmented schizonts were incubated for 3 hours to allow reinvasion. Remaining trophozoites and schizonts were then killed using 5% sorbitol. The 0-3h old rings (0.5% parasitemia, 2% haematocrit) were exposed to high drug concentrations (700 nM DHA as a control, 2.5 µM and 5 µM PD and bMD40, 1µM and 2.5 µM MB) for a period of 6 hours. After 6h, the drug was removed and parasites were allowed to grow for another 66 hours. Finally, parasitemia and parasite viability were determined at 72h on Giemsa stained blood smears. The parasitemia and viability of untreated iRBCs at T0 and T72 was also determined to follow the pattern of growth and multiplication factor of parasites over time.

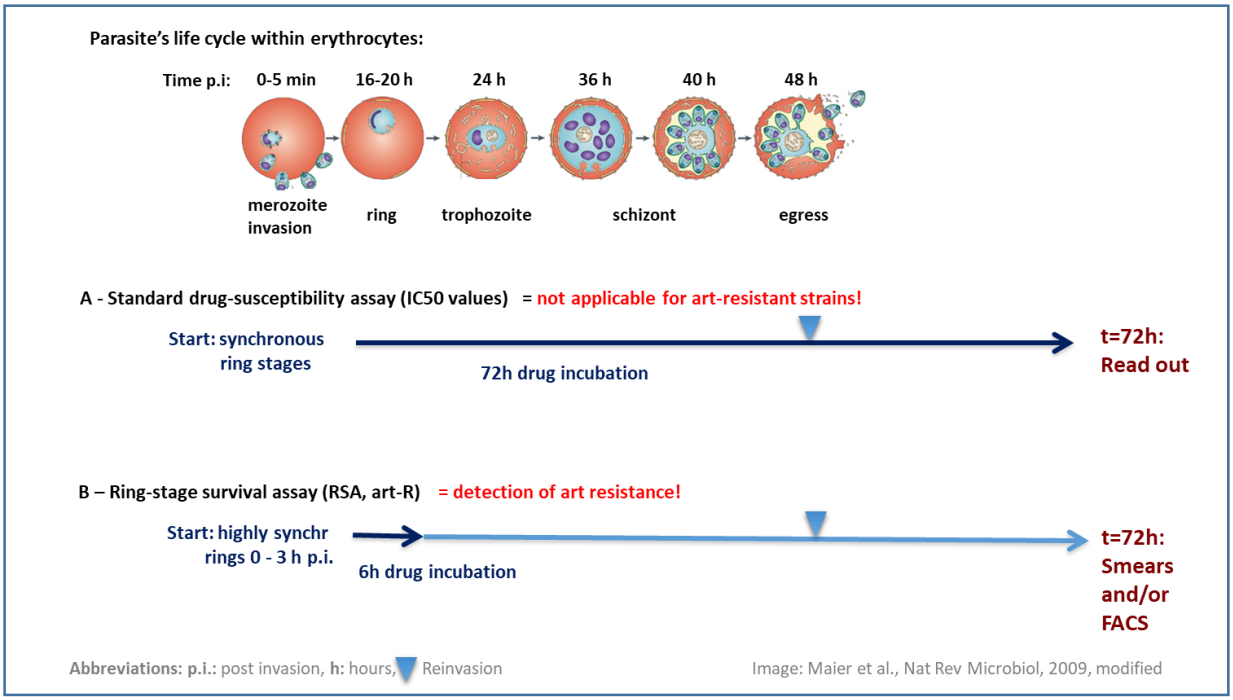

Figure 2. 5 Experimental approach to test Plamsodione cross-resistance with Artimisinin. Distinction between standard drug-susceptibility assay (A) and Ring Survival Assay (B).

Gametocyte induction

The gametocyte induction was done as per protocol described in Adjalley et al., 2011 based on nutrient deprivation and high parasitemia. 3D7 parasites with 10-13.5% parasitemia of ring stages were synchronized tightly with 5% sorbitol over 2-3 growth cycles and maintained in 10cm Petri dishes with ~2.5% haematocrit. On day -3, the cultures (trophozoite stages) were diluted four-fold. On the following day (Day -2), gametocytogenesis was induced by feeding the ring stages in cultures with a mixture of conditioned and fresh media (1:1). The next day, cultures were diluted four-fold and cultures were kept untouched for another day (Day: 0) when the commitment to gametocytogeesis is expected. The next day cultures were supplemented with N-acetyl glucosamine (NAG; Sigma-Aldrich) at a final concentration of 50mM to get rid of mature asexual stages like schizonts upon rupturing. The NAG treatment was continued for next 2-3 cycles to eliminate all asexual forms, and methanol fixed blood smears stained with Giemsa were observed to follow gametocyte development and gametocytemia until day 12.

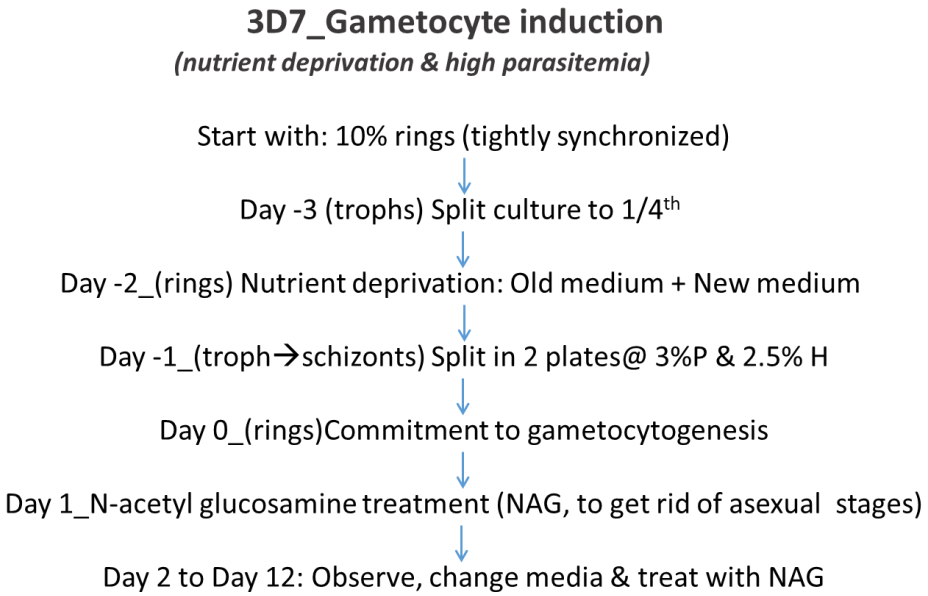

Figure 2. 6 Flowchart explaining different stages of gametocyte induction via nutrient deprivation ad high parasitemia as explained in (Adjalley et al., 2011).

CHAPTER 3: Development of selective activity-based protein profiling probes derived from the antimalarial drug Plasmodione

This chapter covers the design, synthesis, characterization, and functionality aspects involved in the development of ABPP probes derived from the antimalarial drug plasmodione to identify the drug targets. First, I spent 2 months in Prof. Katja Becker's laboratory in Giessen, Germany to learn the purification of His-tagged GR enzyme with criteria for proteomics studies, and to measure enzyme kinetics. Organic chemists- (Ph.D. student Maxime Donzel, master students Alba Zugasti and Joan Guillem, together with the postdoctoral researcher Dr. Leandro Cotos) in our research group synthesized all probes mentioned in the study. My role was to validate the clickability and photoreactive properties of the 3-benzoylmenadione-based probes for the proof of concept of the 'fish' and click strategy using modified amino acids as chemical models of peptides and protein. Standardization of the click reaction conditions was an important contribution of my work focused on the reactions of ABPP probes and rhodamine azide in aqueous conditions. This involved standardization of HPLC-MS conditions for the click reaction analysis in collaboration with Jean-Marc Strub and Christine Schaeffer from the Laboratoire de Spectrométrie de Masse BioOrganique (LSMBO) at IPHC, UV-vis spectral analysis, and fluorometric analysis of every reaction. Further, I standardized the photoreaction conditions using modified amino acid as a model using a UV monochromator and analyzed the extinction co-efficient of all the probes. I initiated setting up the photoreaction conditions using protein as a model; they were further adopted and standardized by the postdoctoral researcher Dr. Bogdan Cichocki. In parallel to my work, B. Cichocki also set up conditions for analysis of peptide and proteins crosslinking by LCMS/MS analysis and adapted click reaction conditions in phosphate buffer using biotin azide instead of rhodamine azide to be able to extract and purify the probe crosslinked protein after click reaction. Additionally, the impact of the BCDA as a ligand instead of THPTA in click reaction was exploited in this study.

To sum up, by combining the photoirradiation of the PD-derived ABPP probes and the click reaction with different azides - probe **7** with a 4'-alkyne group and probe **9** with a 4'-nitro - proved to be the most efficient photoreactive and clickable probes. Probe **4** with good antimalarial activity is a promising candidate for identifying drug targets in parasites.

TABLE OF FIGURES: CHAPTER 3

Development of selective activity-based protein profiling probes derived from the antimalarial drug Plasmodione

Vrushali Khobragade,[1,]# Bogdan Cichocki,[1,]# Maxime Donzel,[1] Leandro Cotos,[1] Joan Guillem Mayans,[1] Alba Zugasti,[1] Stephanie Blandin,[2] Christine Schaeffer,[3] Jean-Marc Strub,[3] Mourad Elhabiri,[1] Elisabeth Davioud-Charvet[1]

# Both authors contributed equally.

1 UMR7042 Université de Strasbourg–CNRS–UHA, Laboratoire d'Innovation Moléculaire et Applications (LIMA), Team Bio(IN)organic and Medicinal Chemistry, European School of Chemistry, Polymers and Materials (ECPM), 25 Rue Becquerel, Strasbourg 67087, France.

2 Université de Strasbourg–CNRS–INSERM UPR9022/U963, Mosquito Immune Responses (MIR), F-67000, Strasbourg, France

3 Université de Strasbourg–CNRS UMR7178, Laboratoire de Spectrométrie de Masse BioOrganique (LSMBO), IPHC, 25 Rue Becquerel, 67087 Strasbourg, France

Abstract:

Malaria is a fatal disease caused by the parasite *Plasmodium falciparum*. Artemisinin (Art) is the most effective antimalarial drug, but it is threatened by the emergence of resistance to Art in Southeast Asia. There is therefore an urgent need for new agents or artemisinin combinations that can target rings and gametocytes, which are parasitic stages involved in Art resistance and malaria transmission to mosquitoes, respectively. Plasmodione (PD) is active on rings with a speed of action as fast as that of Art. However, the precise targets of the PD are not yet known. Therefore, the design of chemical tools, designed as PD-activity-based protein profiling (PD-ABPP) probes, is essential to identify the PD interactome and to elucidate the mode of action involved in the antimalarial action of PD. This research is oriented towards a 'fish & click' strategy with photoreactive and clickable probes to identify potential targets of PD derivatives in parasites. To this end, we deeply characterized the functionality of PD-ABPP probes for photoreactivity, clickability and antimalarial activities as criteria to recognize the best PD-ABPP probes to be used in parasites. The electron-withdrawing group of the PD derivatives proved to be an important factor for the photoreactivity of PD-ABPPs as compared to the benzophenone. Probe **7** with an alkyne group or probe **9** with $–NO_2$ in *para* position of the benzoyl chain were the most efficient photoreactive and clickable probes. Finally, the antimalarial activity of probe **11**, which is the parent 3-benzylmenadione prodrug of one of the two most efficient PD-ABPP probe **7**, displayed antimalarial effects as potent as those shown by PD. In the future, this work will allow the detailed study of the interactome of this new early lead antimalarial drug called plasmodione with an innovative mode of action.

Keywords: antimalarial – benzophenone – 3-benzyl(o)menadione – click - photoaffinity labeling

Introduction

Besides numerous genetic approaches to decipher drug modes of action (MoA), chemical strategies for functional proteomics have been developed in the recent years with the activity-based protein profiling (ABPP) being one of the most specific (Galmozzi et al., 2014). This indirect, unbiased and alternative methodology for identifying drug / drug metabolites interactors in diverse organisms has successfully detected protein partners of miscellaneous biomolecules such as lipids, nucleic acids, amino acids, glycoproteins, or polysaccharides and even post translational modification (see the pioneer work from Cravatt BF et al. with the first reports about HDAC inhibitors from Salisbury CM et al., 2007 and 2008; Whitby LR et al., 2017). ABPP allows monitoring and dissecting a drug interactome from complex proteomes in their native forms. This is achieved by the design and synthesis of small drug-activity based probes that can react with the protein targets. The selective separation of the drug-protein adducts from the whole proteome is made possible by the Cu(I)-catalyzed alkyne-azide click reaction (CuAAC), also known as the seminal Huisgen reaction adapted for biological chemistry and proteomics purposes (Rostovtsev et al., 2002; Lewis, L. G. et al.,2002). The ABPP probe consists of three general functional chemical elements: (1) a recognition group – drug/metabolite that has affinity to specific proteins defined as interactome; (2) a reactive group – either electrophilic or photoreactive that favors crosslinking or covalent binding of the probe to the target; (3) a reporter group/tag (like alkynes or azides) enabling to react with a partner in the click reaction (like azides or alkynes) functionalized by either a fluorophore for visualization of the drug-protein adducts or a chromatography affinity tag for enrichment and identification of the adduct (Parker & Pratt, 2020). An important advantage in ABPP field is the enlargement of the pool of chemical probes that trap representatives of various enzyme classes with complex catalytic activities that covers the proteome as broadly as possible. In the case of the flavin-dependent oxidoreductase family, the design of clickable ABPP probes was limited to the cytochrome P450 (Wright A. T. et al., 2009), 2-oxoglutarate oxygenases (Rotili D et al., 2011), amine oxidases (Krysiak JM et al., 2012; Burke AA et al., 2018).

Since several years, we have an interest in NAD(P)H-dependent flavoenzymes from the malarial parasites that have been proposed as one of the possible targets of an antimalarial early lead agent, the 3-[4-(trifluoromethyl)benzyl]-menadione, called plasmodione (PD, Fig. 3.1). The initial studies have focused on the chemical reactivity of this 1,4-naphthoquinone, and of its key putative metabolites, the 3-benzoylmenadiones, which were shown to act as effective subversive substrates of recombinant glutathione reductases (GR) from human and *P. falciparum in vitro*. Human GR is a homodimeric NADPH-dependent FAD-containing enzyme (GR; EC 1.8.1.7) that belongs to the family of NADPH-dependent oxidoreductases possibly involved in PD bioactivation in parasitized red blood cells (pRBCs) (Müller et al. 2011). The homodimeric flavoenzyme catalyses the reduction of glutathione disulfide (GSSG): $NADPH + H^+ + GSSG \rightleftharpoons NADP^+ + 2GSH$ (eq. 1). Human GR, in concert with the glucose-6-phosphate dehydrogenase (G6PD) in the pentose phosphate pathway (PPP) protects red blood cells (RBCs) from oxidative stress by constantly generating a flow of reductants. According to the previous GR inactivation studies, the suicide-substrates such as the fluoromethylmenadione derivative, namely fluoroM_5 not only inhibits the GR activity but

also itself gets reduced by the enzyme at the NADPH-reduced flavin, which is present in trace amount (less than 2%), but is in equilibrium with the major two-electron reduced species EH_2 in the catalytic cycle.(Bauer et al., 2006). The major form EH2 that has a reoxidized flavin and an active dithiol in the active site is responsible for GSSG reduction.

Despite structural similarities, plasmodione is not a drug analogue of the antimalarial drug atovaquone, which targets the bc1 complex of the mitochondrial electron transfer chain. Transgenic parasites rendered resistant to atovaquone by expressing the yeast dihydroorotate dehydrogenase displayed non-changed sensitivity towards PD (Ehrhardt et al., 2013). Furthermore, recent studies in yeast identified Nde2, a NADPH-dehydrogenase type II of the mitochondrial respiratory chain, as a main target of PD, with GR and two other oxidoreductases (Mcr1 and Lpd1) being minor targets (Mounkoro et al., 2019). Two major proteins present in pRBCs, GR and methemoglobin, could account for the PD bioactivation pathway in the asexual stages, i.e. the trophozoites, where hemoglobin digestion takes place. However, because other oxidoreductases can compensate for the low level of GR activity in parasite stages distinct from trophozoites, such as rings and gametocytes; we assume that there are multiple flavoenzyme targets that can cause PD bioactivation and parasite killing. These models support that PD activates via redox cycling, PD targets are flavoenzymes and PD is a pleotropic agent, but there are still some limitations because 1. the comparing: between extracellular studies of yeast-can not mimic intracellular parasite metabolism and targets. 2. homology between *P. falciparum* & *P. berghei* is 70%, so this difference between two species suggest different metabolic targets. 3. It is not possible to make PD resistant parasites since the parasite starts regrowing upon removal of drug pressure (Ehrhardt et al 2016) 4. Knockout of GR for it being essential gene in *P. falciparum* is not possible (Goetz et al unpublished data). Therefore, we need an unbiased approach to identify PD targets in the parasites for which in my PhD, we used Click and Fish approach.

According to the literature, several studies have been conducted using “fish and click” approaches with drug-ABPP probes for the detection of drug targets in *P. falciparum* (Penarete-Vargas et al., 2014; Wright et al., 2014; Wang & Li, 2016; Ismail et al., 2016; Lubin et al., 2018). Three of them (Wang et al., 2015; Ismail et al., 2016; Jourdan J. et al., 2019) exploited a non-photochemical reaction to generate the drug-protein adducts. The endoperoxide-based drugs were bioactivated by ferrous iron (Fe^{2+}) to form the carbon-centered radicals effective to alkylate interacting parasitic proteins. Such a proteomics approach with chemically reactive probes that alkylated nucleophilic proteins non-specifically within cells open possibilities of false positives in which alkylation events not directly linked to parasite killing (of the relevant stages) should be considered (Wang & Li, 2016). Indeed, detection of false positive targets were reported by previous researchers (Ismail et al., 2016; Lubin et al., 2018; Penarete-Vargas et al., 2014; Wright et al., 2014; Jourdan J. et al., 2019).

Additionally, we anticipate that abundance of proteins expressed in parasites during drug treatment is variable and depends on different stages of parasitaemia. While trophozoites stages can be enriched by using magnetic beads, it is not the case of rings and gametocytes, which require highly synchronized cultures albeit with quite high dilution with non pRBCs. In practice, asexual and sexual stages of malarial parasites in pRBCs are cultivated in vitro with 2-10% parasitaemia usually. Thus, during any ABPP study, actual drug

targets expressed in traces would be difficult to distinguish from unspecific labelled but abundantly expressed proteins recovered in the HPLC MS/MS analysis. Indeed, linking drug effects from complex reactions to killing processes/targets in parasites is one of the hardest steps when studying the MoA of any antimalarial agent.

For this reason, we considered it is essential to study in depth new chemical probe models and define standardized conditions for their use, before target validation in parasites. Therefore, the focus of the present study was the design of relevant and specific PD-ABPP probes to establish a proof-of-concept with an isolated protein model before approaching the identification of the parasite targets of the antimalarial drug PD and its analogues in the parasites. In this chapter, we describe the synthesis of five new specific PD-ABPPs along with inhibition, photolabeling experiments, click reactions, and antimalarial activitiy studies.

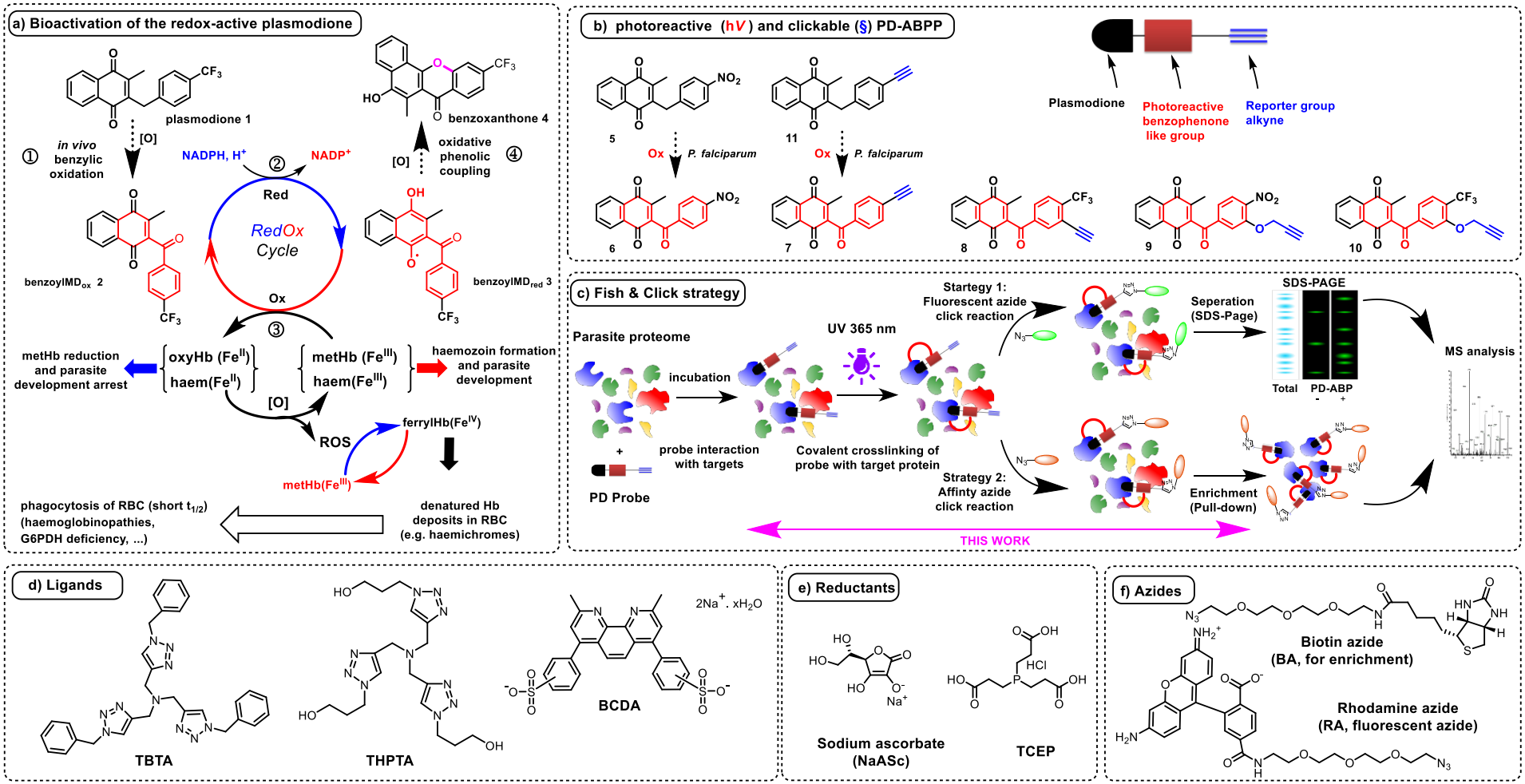

Figure 3. 1 Bioactivation of Plasmodione

a) Bioactivation of Plasmodione: upon internalization in the parasite, plasmodione (**1**) is proposed to generate the drug metabolite (**2**) by benzylic oxidation (step ①), the 3-benzoylmenadione (benzoylMD), which, under its oxidized form, possesses a photoreactive benzophenone-like moiety (indicated in red). This metabolite is further reduced (step ②) and, under its reduced form (**3**) takes part in oxidoreductase-mediated redox-cycling (step ③) leading to ROS inducing parasite death. In addition, the generation of a third metabolite, namely the benzo[*c*]xanthen-7-one (benzoxanthone) derivative **4**, has been envisioned as one possible metabolite generated through an oxidative phenolic coupling reaction from the 1e-reduced benzoylMD **3** radical (step ④). Since glutathione reductase is one of the oxidoreductase involved in the redox cycling, in *P. falciparum* we used it as a protein model to analyse both photoreactivity and clickability of the Plasmodione-activity based probe (PD-ABPP). **b) Plasmodione-activity based probes (PD-ABPP)**: The scaffold of the PD-ABPP probes **7**-**11** is a photoreactive 3-benzoylmenadione, functionalized by different electron-withdrawing groups in *para* position (-CF_3 or -NO_2 or -alkyne) affecting their photoreactivity. 3-Benzylmenadiones (such as plasmodione, **5**, **11**) are not photoreactive *per se* while the probes **6**-**11** in the the benzoylMD series are photoreactive. The reporter group of PD-ABPP probes is a terminal alkyne group, which can react with an azide upon click reaction. **c)** The **fish & click chemistry-based approach** is aimed at identifying drug activity-based protein profiling. First, parasites are incubated with a PD-ABPP probe. Upon UV irradiation covalent crosslinking of PD-ABP to its potential targets is expected to occur. Further, a reporter click reaction between the probe-derived alkyne and the fluorescent rhodamine azide (strategy 1) or biotin azide (strategy 2) reveals successful crosslinking of probe to proteins, which can be analyzed by SDS PAGE and/or LC-MS/MS followed by bioinformatics. **d)** Ligands used in this study: water insoluble-TBTA, water soluble-THPTA and disodium bathocuproine sulfonate (BCDA) stabilize Cu(I) catalyst in the click reaction. **e)** Reductants, NaASc or TCEP, were used in the click reaction for standardizing the detection of PD targets expressed even in traces. **f)** Azide partners used in this study: the fluorescent rhodamine azide and the biotin-PEG_3-azide.

Results and discussion

Design of 3-benzoylmenadiones as photoreactive probes

Our unique strategy for designing the PD-ABPP is leveraged from the postulated MoA of PD (T Müller et al., 2011). PD is a 3-benzylmenadione that is anticipated to act as a prodrug generating *in situ* a key metabolite, the 3-benzoylmenadione **2**, upon PD bioactivation (i.e., benzylic oxidation, Fig 3.1a). This metabolite **2** enters a NADPH-dependent oxidoreductase-promoted redox cycling producing a continuous flux of oxidative stress and toxic metabolites, including the reduced 3-benzoylmenadione **3** (i.e., via 1 or 2-electrons transfer) and the toxic benzoxanthone **4**, and along with haemoglobin catabolites identified as membrane-enriched hemichromes. The latter are known to act as biomarkers of RBC aging that trigger early phagocytosis by macrophage. Therefore, the 3-benzoylmenadione-mediated bioactivation pathway results in the specific removal and clearance of the parasitized RBCs (Bielitza et al., 2015). Interestingly, the PD-derived metabolite **2** possess in its structure the 2-benzoyl-1,4-naphthaledione group that could behave as a 2-benzonaphthone precursor (Oelgemöller et al., 2002). Therefore, we assumed that the PD-derived benzoylmenadione might have the potential intrinsic photoreactive benzophenone-like structure *per se* and thus permit the spontaneous covalent capture of targets upon photoirradiation. We designed photoreactive probes mimicking the translation of a chemically inert prodrug (PD) to its active metabolite – a 3-benzoylmenadione species generated through metabolism in the pRBC – interacting to its biological site/target before it is photoirradiated into alkylating species. Such probes might show high spatiotemporal control of targeted enzyme recognition/alkylation and drastically lower non-specific binding. Noteworthy, no additional bulky photoreactive group was introduced into the PD metabolite structure. Furthermore, the newly designed ABPP probes **7**-**11** were functionalized in the benz(o)yl chain, by a reporter alkyne group known to bring minimal structural perturbation.

First, by comparing the inhibition and the kinetic parameters shown by five menadione derivatives tested as GR inhibitors and subversive substrates (Table 1), the 3-benzoylmenadiones displayed the most efficient inhibition capabilities of both GR-catalyzed GSSG reduction and redox-cycling activities with the parasitic GR, respectively. As previously reported, this agrees with the higher oxidant character of 3-benzoylmenadiones *versus* 3-benzylmenadiones or menadione (Elhabiri et al, 2015; Sidorov et al., 2016).

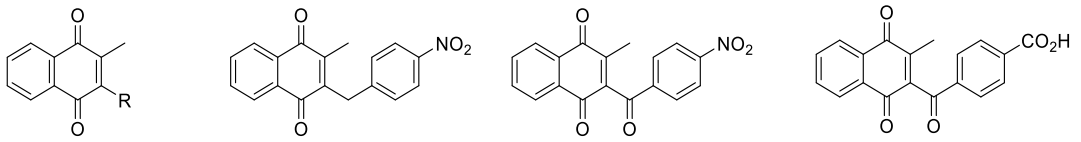

menadione (R = H)
M_5 (R = $(CH_2)_5$-COOH

5 (P_TM37)

6 (P_TM40)

12 (P_TM22)

Scheme 1A. Menadione and its hexanoic acid derivative M_5, the 3-benzylmenadione **5** substituted by a 4'-nitro group (**5**, P_TM37, **1g** from Müller et al. 2011), and the 3-benzoylmenadiones substituted either by a 4'-nitro (**6**, P_TM40) or a 4'-carboxylic group (**12**, P_TM22 from Müller et al., 2011) .

Compound	**IC_{50} (µM)**[a]		**K_M (µM)**	**k_{cat} (s^{-1})**	**k_{cat} / K_M (mM^{-1} s^{-1})**
	***Pf*GR**	**hGR**	**in *Pf*GR assay**		
menadione	42.0	27.5	0.082	0.16	1.95
M_5[b]	4.5	3.2	0.109	0.103	0.95
5 (P_TM37)[c,d]	nd	nd	nd	nd	nd
6 (P_TM40)[c,d]	0.8	0.4	0.018	0.14	7.78
12 (P_TM22)[c,d]	1.1	0.7	1.325	1.86	1.40

[a] in the presence of 100 µM NADPH and 1 mM GSSG; [b] Values from ref. Biot et al., 2004; [c] Compounds **5**, **6** and **12** were previously reported under product codes 1g, 3g, 3f, respectively, in ref. Müller et al, 2011; [d] Values from ref. Müller et al, 2011. Re-precipitation of the compound **5** (P_TM37=BJ323) in the cuvette above 10 µM prevented IC_{50} and kinetic parameters determination.

Table 1. Glutathione reductase inhibition parameters expressed as IC_{50} values and *Plasmodium falciparum* glutathione reductase-catalyzed naphthoquinone reduction for menadione derivatives as compared to menadione.

Benzophenone is a widely used as a photoaffinity labeling reagent in biochemistry and cell imaging (Dormán & Prestwich, 1994; Dormán et al., 2016). The substitution pattern of benzophenone is known to affect the photoreactivity significantly. Upon photo-irradiation at 350 nm (*i.e.,* absorption of benzophenone) that promotes the formation of the nπ* triplet state, a ketyl diradical is generated (Scheme 1). This ketyl diradical is indeed key in the progress of several procedures as coupling, disproportionation, and hydrogen transfer reactions (Dormán et al., 2016). Once formed, this diradicaloid triplet state displaying an electrophilic electron-deficient oxygen n-orbital is prone to interact with weak C-H π bonds, promoting a hydrogen(H)-abstraction to complete its half-filled n-orbital (Scheme 1). It should be noted that benzophenones with electron withdrawing groups promote more efficiently this process owing to their low-lying nπ* triplet states that allow fast H-abstraction. This push-pull effect (termed captodative effect) leads to an increased stability of the radicals – solvent-dependent – when each aromatic ring on either side of the carbonyl group of the benzophenone scaffold is substituted by very strong polarizable donor and acceptor substituents (Viehe et al., 1985; Peterson and Winter, 2019). By contrast, electron-donating groups and/or electron delocalization within aromatic or conjugated systems cause a partial shift of the electron transition from nπ* to ππ* making the latter triplet state much less reactive with respect to H-abstraction. This was exemplified with the *p*-cyano-substituted benzophenone *versus p*-unsubstituted benzophenone in photocleavage of DNA (Nakatani, K. et al., 1998). The nπ* state is related to an overlap between the n C=O and the C-H □ orbitals. With respect to the ππ* state, the electrons of the π and π* orbitals are delocalized over the carbonyl and the

aromatic rings making a rapid attack by C=O on the C-H unlikely. Consequently, electron-withdrawing groups *in para* of the benzophenone might increase the efficiency of H-abstraction.

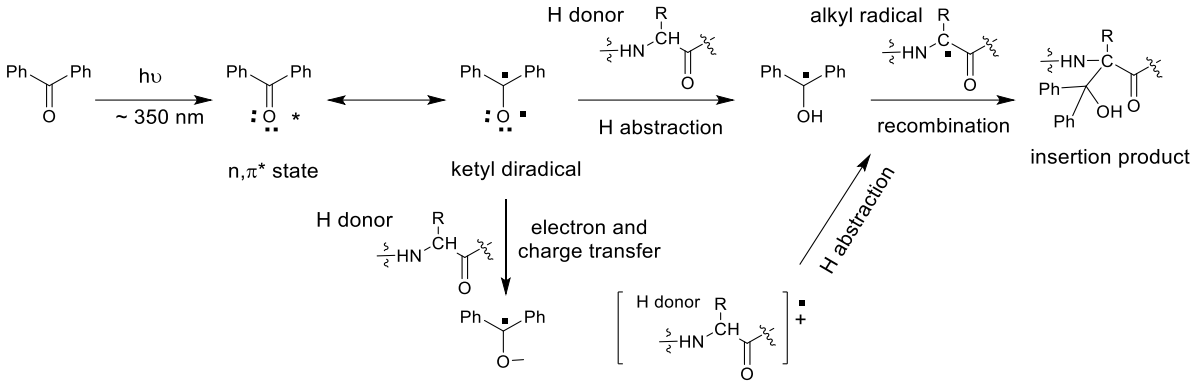

Scheme 1. Reactions of benzophenone upon irradiation.

To validate the hypothesis of the intrinsic photoreactivity properties attributed to the benzophenone-like structure, we studied five menadione derivatives in *P. falciparum* GR inhibition studies, and photochemical reactions (Scheme 1A.) – menadione and its hexanoic acid derivative M_5 from Biot et al., 2004, the 3-benzylmenadione **5** substituted by a 4'-nitro group (**5**, P_TM37, **1g** from Müller et al. 2011), and the 3-benzoylmenadiones substituted either by a 4'-nitro (**6**, P_TM40) or a 4'-carboxylic group (**12**, P_TM22 from Müller et al., 2011) – tested as both human and *P. falciparum* GR inhibitors and subversive substrates of *P. falciparum* GR. We first compared the photoreactivity of the 3-benz(o)ylmenadione **5**-**6** pair (P_TM37 and P_TM40) (Fig. 3.2) in comparison with benzophenone (Fig. S3.2) to evaluate whether the keto group of the benzoyl chain is essential for photoreaction. This was evaluated using *N*-acetyl-methionine methyl ester (*N*-Ac-Met-OMe = P_TM52, shortened as nMet) as a model of protein partner using the following conditions: 4 °C, overnight (17h), UV irradiation with a Rayonet photochemical reactor containing 16 lamps, total 224W of intensity at 350 nm. The regioselectivity of the formation of the insertion product was not studied here because previous studies demonstrated that methionine, the most photoreactive amino acid among the 20 amino acids found in proteins, and its *N*-Ac-Met-OMe derivative are predominantly alkylated at the side-chain in α-position to the sulphur, i.e. at the CH_3 group as well as at the CH_2 group (Deseke et al., 1998; Wittelsberger et al., 2006). The products of photoreaction were analyzed by field desorption-mass spectrometry (FD-MS). As observed in Fig. 3.2, the insertion product of the 3-benzoylmenadione derivative **6** (P_TM40) and nMet displayed a mass peak at *m/z* 526.14. Under the same photoirradiation conditions, the photoreactive benzophenone generated the insertion product with nMet upon photoirradiation as attested by the presence of mass peaks at *m/z* = 387.2 (M^+), and 369.2 (M^+-H_2O) (Fig. S3.1). No insertion product was observed for the 3-benzylmenadione derivative **5** (P-TM37) (Fig.S3.1) demonstrating that the 3-benzoyl chain is essential for the photoreactivity of the benzoylmenadione derivative P_TM40. Interestingly, because probe **6** (P_TM40) is photochemically reactive *per se,* a pre-reduction step in the presence of the NADPH/GR is not essential to form the insertion product through the prior generation of the 3-benzoyl-dihydronaphthoquinone, likely because the latter was generated by photoreduction upon photoirradiation (Oelgemöller et al., 2002, Mitchell et al., 2013). It is the first time that the photoreactivity of 3-benzoylmenadiones is demonstrated in ABPP applications.

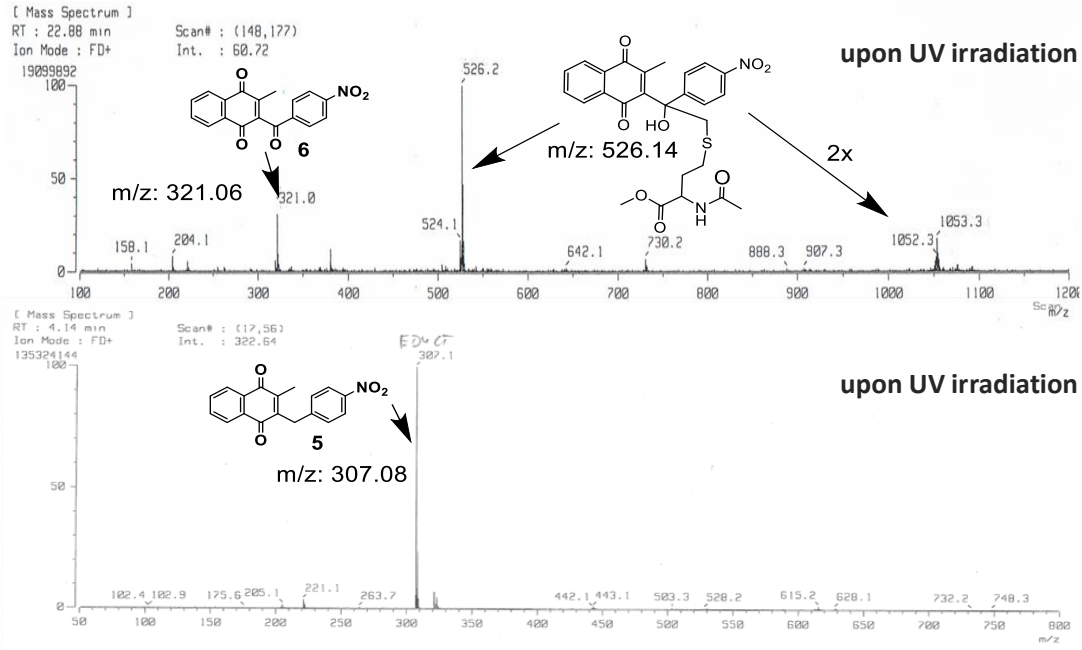

Figure 3. 2 Mass spectrometric analysis of photochemical reaction mixtures

Field-desorption mass spectrometry analyses of the photochemical reaction mixtures of (panel A) the 3-benzoylmenadione 6 (P_TM40) or (panel B) the 3-benzylmenadione **5** (P_TM37) derivatives, in the presence of the diprotected methionine nMet (P_TM52).

As far as the 3-benzoylmenadione is concerned, we were unable to observe by FD-MS under the same experimental conditions the insertion product of **12** (P_TM22) with the carboxylic acid function in *para*- to the benzoyl ring (Fig. S3.1), in contrast to the reaction with the *p*-nitro-benzoyl derivative **6** (P_TM40). This result might be explained by the fact that, under aqueous solution, the carboxylate is not an electron-withdrawing group (EWG) but rather donor or even neutral (Hansch C. et al., 1991); some photochemical decarboxylations were also reported (Cosa G., 2004). Thus, the promising kinetic and photochemical properties of probe **6** (P_TM40) convinced us to design the new PD-ABPP probes **7**-**11** (Fig. 3.1b) functionalized by different EWGs in *para* position of the benz(o)yl chain and by an additional reporter group, i.e. an alkyne function, which is prone to be reactive with fluorescent or biotin azides in the click reaction. Noteworthy is that the *p*-alkyne group can be considered both as the reporter group for the CuAAC reaction, but also an EWG to favor the formation of an insertion product upon photoirradiation (Bizier NP et al., 2013; Chen et al., 2010).

Synthesis of clickable 3-benz(o)ylmenadiones as PD-ABPP probes

Each of the 3-benzoylmenadiones alkyne derivatives 7, 8, 9, and 10 was synthetized using as a key step, the Friedel & Crafts acylation, recently described by our team (Cotos et al., 2020).

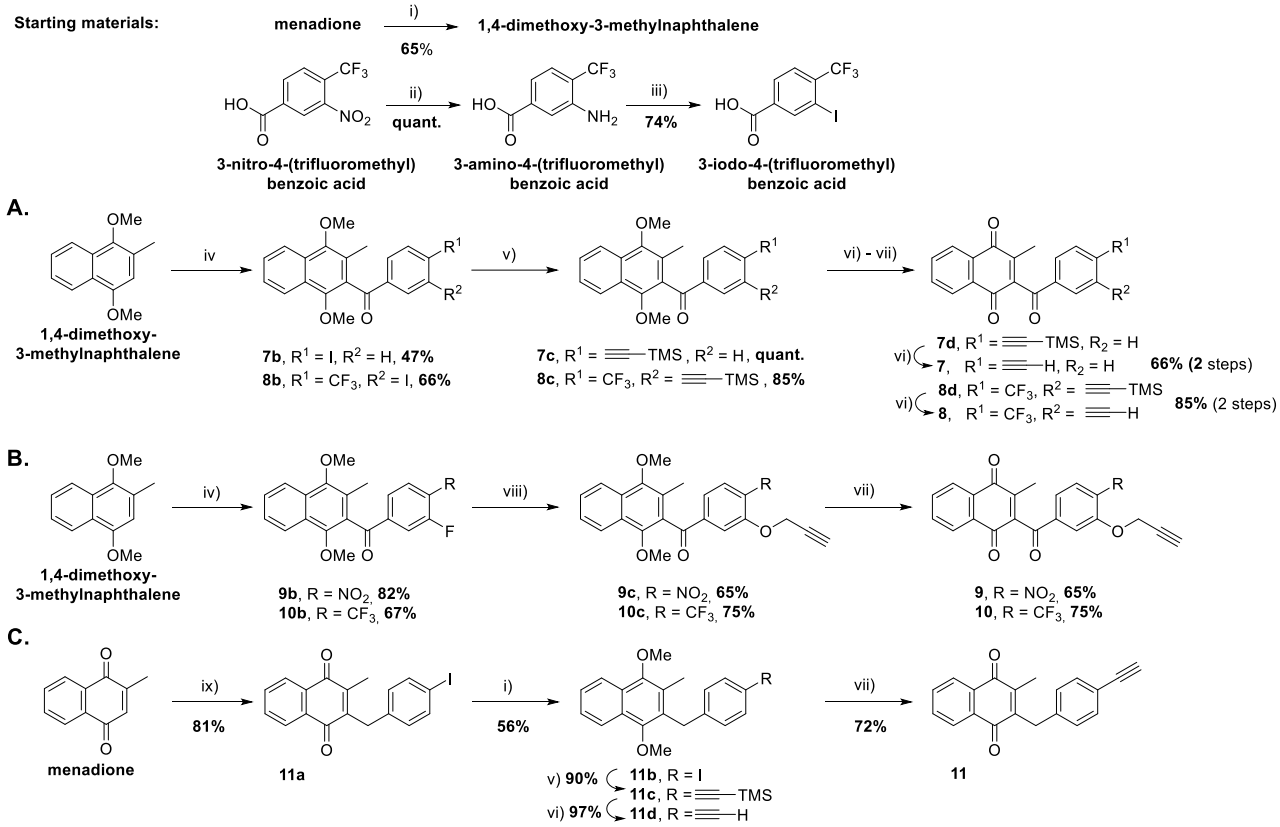

Reaction conditions:
i) 1. $SnCl_2$, cc HCl, EtOH, rt, 2 h, 2. Me_2SO_4, acetone, KOH, MeOH, 60ºC, 4h ; ii) 10% Pd/C, EtOH, rt, overnight ; iii) 1. $NaNO_2$, HCl, 0°C, 1h, 2. KI, I_2, rt, 1h and then refux, overnight ; iv) **A.** 4-iodobenzoic acid, 3-iodo-4-(trifluoromethyl)benzoic acid **B.** 4-nitro-3-fluorobenzoic acid, 3-fluoro-4-(trifluoromethyl)benzoic acid, TfOH/TFAA ; v) CuI, $Pd(PPh_3)_2Cl_2$, NEt_3, rt, 16h, HC≡C-TMS; vi) TBAF, THF, ret, 1.5 h ; vii) CAN, H_2O/MeCN ; viii) K_2CO_3, DMF, propargylic alcohol ; ix) 4-iodophenylacetic acid, $AgNO_3$, $Na_2S_2O_8$, MeCN/H_2O, reflux, 4h.

Scheme 2. Synthesis of the 3-benzoylmenadiones **7**, **8**, **9**, and **10** (paths **A**. & **B**.) through the Friedel-Crafts reaction variant (Cotos et al, 2020) and of the 3-benzylmenadione **11** (path **C**.) through the Kochi-Anderson reaction (Kochi and Anderson, 1965).

Using the electron-rich 1,4-dimethoxy-2-methylnaphthalene (i.e., as aromatic nucleophile) and readily synthetic available benzoic acids (i.e., as acylating agent) as starting materials, this reaction variant allowed us to prepare the corresponding 2-benzoyl-1,4-dimethoxynaphthalenes intermediates (**7b**-**10b**) in mild conditions, as key intermediates, to achieve in a few additional steps the desired chemicals probes, described in paths A and B (Scheme 2). The four benzoyl-1,4-dimethoxy-2-methylnaphthalenes **7b**-**10b** were obtained with 47%, 66%, 82% and 67% yield, respectively. Noteworthy is to mention that without the Friedel-Craft reaction variant the 3-benzoylmenadiones functionalized by an alkyne group could not have been produced easily (i.e., see the different synthetic pathways discussed in Cotos et al., 2020). A Sonogashira pallado-catalyzed coupling allowed the trimethylsilane (TMS)-protected alkyne insertion, starting from the iodinated aromatic compounds **7b**-**8b**, to obtain efficiently intermediates **7c**-**8c**. These were successively deprotected in **7d**-**8d**, first with TBAF, and then by CAN to afford both desired alkynated 3-benzoylmenadiones **7**-**8** upon

oxidative demethylation. For the synthesis of alkynes **9c** and **10c**, propargyl alcohol was first submitted to a nucleophilic aromatic substitution reaction on the electron-poor fluorinated aromatic intermediates **9b** and **10b**, leading to the targeted quinones **9** and **10** after oxidative deprotection with CAN.

3-Benzylmenadione **11** was synthesized from menadione through the Kochi-Anderson reaction (Kochi and Anderson, 1965) according to path C in a 5-step route (Scheme 2). 3-Benzylmenadione **11a** (80%) was produced by benzyl radical addition from 4-iodophenylacetic acid and menadione. Benzyl radical was generated from 4-iodophenylacetic acid, by radical decarboxylative process in the presence of silver salts catalysis and stoichiometric amounts of the oxidant $Na_2S_2O_8$. Owing to the incompatibility of the methyl group of **11a** in basic medium, it was not possible to introduce the alkyne moiety directly on the quinone by palladium cross coupling reaction (Sonogashira reaction). Consequently, the benzylmenadione **11a** was first reduced with $SnCl_2$ in acid medium to the corresponding 2-(4-iodobenzyl)-3-methylnaphthalene-1,4-diol intermediate, which without further purification, was quickly protected to the 2-(4-iodobenzyl)-1,4-dimethoxy-3-methylnaphthalene intermediate **11b** (56%) by methylation using dimethylsulfate. Then, this iodo derivative **11b** was submitted to the pallado-cross coupling reaction, using ethynyl(trimethyl)silane in excess. This reaction successfully promoted the formation of the TMS-protected alkyne **11c** in excellent yield (90%). The TMS group was removed from **11c** by TBAF to obtain the free terminal alkyne **11d** (97%), and the 1,4-quinone moiety was recovered by oxidative demethylation following addition of cerium ammonium nitrate in acetonitrile/ water mixture to obtain in good yields (66%) the targeted 3-benzyl-[4'-alkynyl]-menadione **11**.

Characterization of the ABPP properties of PD-based probes

Standardization of UV crosslinking parameters using PD-ABPP and nMet as protein model

Photoreactivity of the PD-ABPP probes was evaluated under the same photoreaction conditions used for the model reaction between nMet and probe **6** (P_TM40) discussed above. By contrast with the former reaction, PD-ABPP and nMet were irradiated for 2 minutes in a high-intensity 1000W UV monochromator. We observed that among the five PD-ABPP the photoreaction preferably occurred with probes **6**, **7** and **9** bearing strong EWG (-NO_2 and alkyne) in *para*-position in accordance with yields for starting probe consumption and photo-generated product calculated from the ^{1}H NMR spectra (Table 2, Fig S3.2 to Fig. S3.4). For probes **8**, **10**, and benzophenone, the ^{1}H NMR data did not allow to calculate the yields of probe consumption or of formed products because signals were either too small or mixed with other signals. Additionally, we determined the spectrophotometric characteristics (ε_{max} and λ_{max}) of all the PD-ABPP probes, probe **6** (P-TM40) and benzophenone (Fig. S3.5). Based on these data, we can conclude that, upon judicious functionalization, benzoylmenadione probes can be photoreactive *per se* and be used to covalently trap probes-bound targets in an ABPP approach.

Table 2. Photoirradiation of *N*-acetyl methionine acid methyl ester (nMet) and probes **6**, **7**, or **9** in acetonitrile[a].

Probe[b]	**δ (ppm) / signal shape** for each probe and photogenerated product from ^{1}H NMR spectra	**Residual probe (%)**	**Formed products**
6	8.07 (dd) / 8.04 (dd)	69	31
7	7.60 (dd) / 7.38 (dd)	75	25
9	7.51 (dd) / 7.40 (dd)	61	39

[a] Reactant concentrations: 20 mM of probe (1 , 32.1 mg, 0.1 mmol), and 100 mM of nMet (5 equiv., 102.6 mg, 0.5 mmol), were dissolved in 100% acetonitrile (Reaction vol. 200 µl) under strict deoxygenated conditions using argon vacuum cycles. The mixture was exposed to 1000W hv monochromator from Alexander Specht's laboratory at Illkirch, Strasbourg for 2 mins, at room temperature. Calculated yields of residual probe and coupling products formed based on 1H-NMR spectra of crude reaction mixtures. [b] Structures of the probes are given in Figure 1 of this chapter.

Characterization of clickability property of PD probes using azide models

To further demonstrate the feasibility of PD probes for protein target identification we validated the click reaction properties of PD-ABPPs. The click reaction is crucial for the analysis of complex proteomes as it allows to attach a pulldown-tag to the adducts. Subsequent adduct enrichment through the pulldown-tag affinity enhances correct peptide identification during MS analysis.

In this study, the PD-ABPPs (Fig. 3.1b) display different groups such as -alkyne, -CF_3, or -NO_2. The alkyne group was functionalized at different positions of the benz(o)yl ring. In addition, the alkyne group was either directly inserted to the phenyl ring of the benz(o)yl chain or via an O-CH_2 linker. This series of PD-ABPP was of crucial importance to assess the position and length of the linker necessary to lead to improved reactivity and efficiency for 1,2,3-triazole formation. To select the best probe for identifying the PD interactome, we first evaluated the clickability of different PD-ABPPs using distinct azides. The commercially available fluorescent rhodamine azide (RA) was used to develop reaction conditions with high yield of the product while the biotin-PEG3-azide (BA) was employed to enrich proteins by streptavidin-biotin affinity through a prior ligation of the probe with biotin by the click reaction.

Standardization of click reaction using rhodamine azide

First, we revisited the conditions of this click reaction and assessed the importance of each of the partners in this reaction. The stability of Cu(I) complex was first investigated in the presence of two different reductants, sodium ascorbate (NaASc) and tris(2-carboxyethyl)phosphine (TCEP), with or without the water-soluble ligand, tris-hydroxypropyltriazolylmethylamine (THPTA). We observed that TCEP induces significantly higher yields of Cu(I)-ligand complex formation than NaASc in the presence of THPTA (Fig. S3.7). The formation of the Cu(I) complex is optimal for a 1:1:1 stoichiometric mixture of $CuSO_4$:THPTA:TCEP while the use of excess of TCEP results in a precipitation reaction that increases over time (Fig. S3.7). On the other hand, it has been previously reported that NaASc-based click reaction produced high yield of the click product in excess of NaASc (H. Li et al., 2013; S. Li et al., 2017; Miguel-Ávila et al., 2018). However, we observed that NaASc-dependent click reactions were always associated with the precipitation even at 100 µM concentration of the reductant in the presence of either TBTA or THPTA ligand (data not shown). We thus decided to perform the click reactions with TCEP as a reductant rather with NaASc.

Considering the high sensibility of the cuprous complex to oxidation, we used strict oxygen-free conditions for the click reactions. Further, the yield of the reaction was optimized by using several sequential additions of the pre-formed Cu(I) complex (i.e., pre-incubation reaction) at different time intervals, i.e. by dispensing successive doses of the pre-formed Cu(I) complex (i.e., from $CuSO_4$: THPTA: TCEP in 1:1:1 ratio). The Cu(I) complex pre-formation allowed us to avoid side reactions resulting from pre-incubation between the substrates and products with reductant, i.e. we observed that the commonly reported Staudinger reaction (Saxon & Bertozzi, 2000) occurs within less than a minute between rhodamine azide and TCEP at above 100 µM TCEP. Especially at 500 µM and 1 mM TCEP, the side reactions could be prominently observed by recording absorption spectra as well as HPLC-MS analysis (Fig. S3.10).

Next, we added 8.33% of DMF to the Cu(I)-ligand forming reaction, considering that organic solvent might influence the rate of triazole formation as previously reported (Stanislav I. Presolski et al., 2010). Surprisingly, we found that omitting DMF in the pre-incubation reaction and adding it to the reaction instead led to sharp decrease (4x) in reaction efficiency (Fig. 3.5A). The positive effect on the click reaction efficiency of DMF when preincubated with Cu(II)/reductant/ligand mixtures can be explained by the coordination properties of organic solvents for copper ions that can compete to some extent with the ligands. Solvent might lead to dissociation of the cuprous ligand species and/or Cu_2O formation (Presolski et al., 2010). This would give a boost in product formation in the beginning of the reaction when the preincubated Cu(I) complex is added to the reaction. Unless specified otherwise the final concentration of organic solvent in reaction varied from 6.8 % to 7.2 % DMF.

We observed with probes **7** or **9**, that only one addition of the pre-formed Cu(I) complex did not lead to more than 5% yield when the reaction was carried out overnight under aerobic or anaerobic conditions (Fig. 3.3a). When the CuAAC reaction was carried out overnight, the four sequential additions of the pre-formed Cu(I) complex led to eight fold-higher yield than the reaction with only one addition (Fig. 3.3b). This demonstrates that several additions of the pre-formed Cu(I) complex significantly increase the yield of CuAAC reaction over time in aqueous conditions. However, the RA consumption does not increase proportionately over time, because RA was found to be unstable in the CuAAC reaction and thus some part of it or the product is precipitated. In contrast, RA alone or mixed with only alkyne is stable overnight (Fig. S3.11).

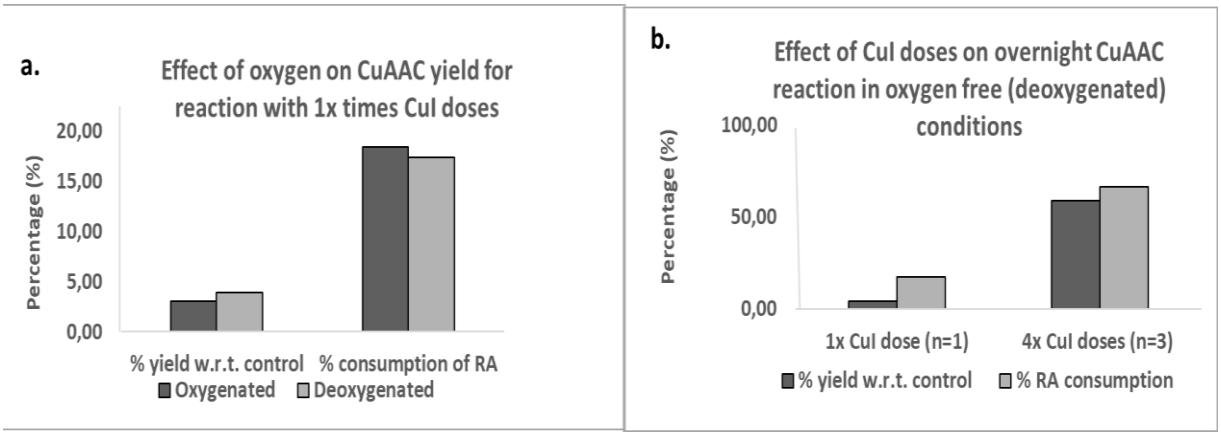

Figure 3. 3 Comparison of the percentage yield of CuAAC reaction in oxygen and oxygen-free (deoxygenated) conditions.Comparison of the percentage yield of CuAAC reaction in oxygen and oxygen-free (deoxygenated) conditions in an overnight reaction of probe **7** and RA with

an addition of one CuI dose of $CuSO_4.5H_2O$ 2.5 equiv. + THPTA 2.5 equiv. + 2.5 equiv. TCEP (n=1). (b) Percentage yield after overnight reaction between probe **7** and RA with addition of one dose or 4 doses of 20 min.-pre-incubated Cu(I) complex. % Yield of reaction was determined using HPLC-MS analysis as described in Fig. S.3.16.

According to the yield of the optimized click reaction (overnight, sequential addition of the pre-incubated cuprous complex, Fig. 3.4a), the sequence of probe efficiency was determined as: Probe **7** with –*p*-alkyne (47.3% yield) > probe **9** with –*p*-NO_2 (25.3% yield) > probe **10** with –*p*-CF_3 (5.7% yield) > probe **8** with –*p*-CF_3 (3.0% yield). This suggest that several factors influence the click reaction such as the solubility of the probes and the reagents as well as the length of the spacer between the benzoyl moiety and the terminal alkyne. To investigate in depth, the structural parameters, we compared the click reaction efficiency of probes **8** and **10**. It appears that the directly functionalized alkyne on the aryl ring either influences the solubility of the probe, offers a limited solvent-exposed accessibility or induces a steric hindrance to react. For instance, solubility of probe **8** is very low, and consequently led to lower levels of both soluble click products and RA (total fluorescence of rhodamine after reaction is reduced) because RA precipitated with probe **8** in the reaction mixture (Fig. S3.12). Noteworthy is that, for all the PD-ABPPs the yield of click product and RA consumption increased after an overnight reaction (Fig. 3.4b) suggesting a slow reaction kinetics. Finally, this reaction time was applied to all subsequent CuAAC unless mentioned otherwise. Especially, these PD-ABPP and RA reactions were used as standards for determining the yields of the CuAAC reactions by HPLC-MS analysis (Fig. S3.16 to S3.25) and for setting up the click reaction conditions with biotin azide or RA (Fig. S3.29).

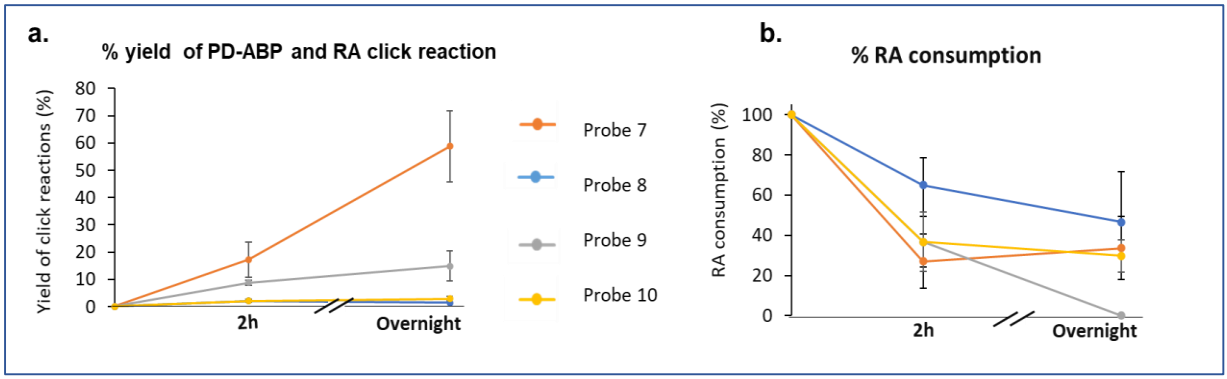

Figure. 3. 4 Standardization of click reaction using rhodamine azide in aqueous conditions for click chemistry.

(CuAAC) was performed between clickable activity-based PD probes **8**, **7**, **9**, **10** and rhodamine azide under strict oxygen-free conditions with 4 doses of pre-formed Cu(I) complex, prepared from $CuSO_4.5H_2O$ 1 equiv. + THPTA 1 equiv. + TCEP 1 equiv. in the following manner – at T0 to T45 minutes pre-incubated Cu(I) complex was added and at T30, T60 and T90 was 20 minutes pre-incubated. Reaction time 2 h. All reactions were performed in 6.8% DMF in aqueous conditions. By the end of reaction time i.e. at 2h or overnight reaction, the CuAAC product was analyzed by fluorimetry and HPLC-MS. For 2 h reaction n=3 for each probe. For 24 h reaction n= 3x for probe **7**, 2x for probe **8**, 2x for probe **9**, 3x for probe **10**.

Standardization of click reaction using rhodamine azide in phosphate buffer

After establishing the initial experimental conditions and working concentrations of reagents in the click reaction, we sought to translate them to conditions used in probe photoactivation. This would allow us to perform the click reaction subsequently to photo-crosslinking. We chose probe **7** that showed the highest reaction yields in aqueous conditions (Fig.3.4), for further reaction optimization. Surprisingly, the replacement of water by PBS buffer (45 mM) completely quenched the triazole adduct formation of probe **7** with RA (Fig.3.5B). Phosphate and Cu(I) ions are known to form insoluble Cu(I) phosphate salts which could lead to catalyst depletion in the reaction medium. To counteract the copper sequestering effects by PBS, Presolski et al. suggested to increase the THPTA levels (up to 5x equivalent of $CuSO_4$) up to 100 mM PBS solutions (Hong et al., 2009; Presolski et al., 2011). However, we found that increasing the ligand concentration alone (from one equivalant to two equivalants of $CuSO_4$:TCEP) slightly improve the reaction yields in PBS buffer (Fig. 3.5C). By contrast, this had a negative impact on the CuAAC reaction efficiency in aqueous conditions (Fig. 3.5C). Consequently, lowering PBS concentration in reaction did increase click reaction yields but diminished the positive effect of THPTA on reaction (Fig. 3.5C).

We anticipated that the formed Cu(I) species can be protected from phosphate by increasing the amount of Cu(II). Cu(II) ions similarly like Cu(I) also form insoluble salts with phosphate ions and thus might, when in excess, sacrifice themselves instead of Cu(I) to interact with the PBS ions. However, as Cu(II) ions are also known to interact with ligands like THPTA, we hypothesized that with increase of $CuSO_4$ amounts we had to increase simultaneously ligand concentrations to not deplete it by Cu(II) species (Elliott, 2014; Z. Zhu et al., 2017). Indeed, increase to 5:5:1 equiv. of $CuSO_4$: THPTA: TCEP led to increase of the overnight reaction yields from 0% to 9.9 % (Fig. 3.5C). In addition to this experimental improvement, the dilution by four times of the PBS concentration (from 47 mM to 12 mM) led to an additional four times increase in yield (42.7 % yield) of the CuAAC product. Surprisingly, the same conditions applied to an unbuffered aqueous reaction resulted in a more three times decrease in efficiency of the triazole formation (14 % yield). These contradicting results obtained between buffered (PBS) and unbuffered (water) conditions are most likely the result of formation of less reactive Cu(I)-THPTA complexes (Neumann et al., 2020; Presolski et al., 2010). Increase of THPTA amount can indeed help to overcome the negative effect of PBS buffer by protecting the Cu(I) species from phosphate ions. However, we suspect that this in parallel leads to formation of the stalling complexes. Thus, in pure water, of the two factors only the stalling effect can take place and the reaction is inhibited. This assumption is supported by the observation that when PBS concentrations were lowered the positive effect of THPTA in the reaction diminished (Fig. 3.5C).

Of note, the reaction performed with 5:5:1 equiv. of $CuSO_4$: THPTA: TCEP (Fig. 3.5C) does not require anymore the four times addition of Cu(I) pre-mixture to reach a maximum efficiency (42.7 % yield) as the was performed with TCEP in stock in water:DMF 75:25 instead of the PBS:DMF 75:25 which inhibits Cu(I) forming the reaction (Fig. 3.5A) . Similarly, just removal of phosphate ions from the TCEP stock solution allowed to reach comparable yields of reaction in aqueous conditions with or without sequential addition of the preformed Cu(I) complex (Fig. 3.3b with 4 times addition of 1:1:1 $CuSO_4$: THPTA: TCEP in PBS:DMF versus 3.5a with 5:5:1 $CuSO_4$: THPTA: TCEP in water:DMF). Thus, it clearly appears that even minor amounts of phosphate ions can have negative impact on the CuAAC reaction if not properly balanced.

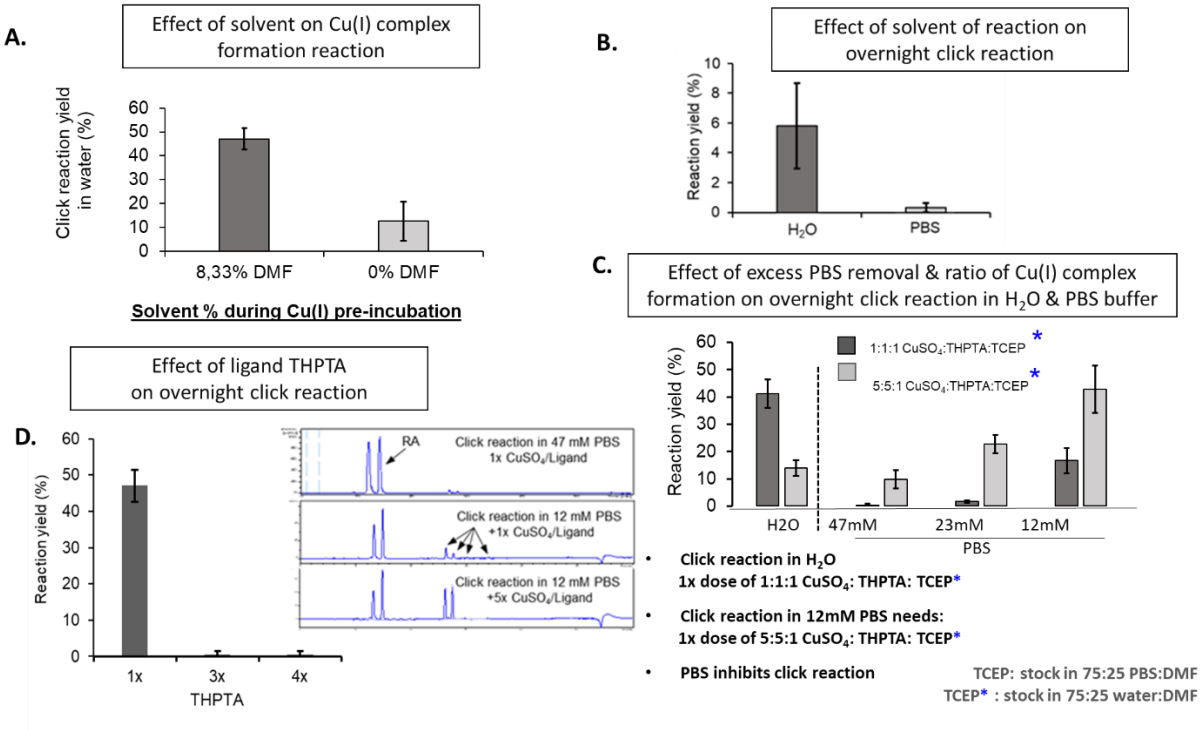

Figure 3. 5 Solvent concentration in Cu(I) complex pre-mix and phosphate buffer affect the click reaction efficiency.

A) Rhodamine azide was reacted overnight with probe **7**. Pre-incubation of pre-formed Cu(I)-ligand complex containing either 8.33% DMF or no organic solvent was added once to the click reaction mixture after 40 min incubation. The pre-formed Cu(I)-ligand complex solution contained 132 µM TCEP and 132 µM of both $CuSO_4$ and THPTA. B) Two hours cycloaddition reaction of RA with probe **7** in H_2O or in PBS buffer. Pre incubated copper-ligand-reductant mix (33 µM $CuSO_4$ + 33 µM THPTA + 33 µM TCEP) was added four times to reaction: first after 40 minutes incubation and 3x after 20 minutes incubation. Increase in THPTA ratio alone does not significantly enhance probe **7** cycloaddition in phosphate buffer but reduction in phosphate concentration does. (C and D) 24 µM RA was click reacted with 24 µM probe **7** in oxygen free conditions in H_2O (C and D) or 47 mM, 24 mM and 12 mM phosphate buffer (D). Cu(I)-ligand preincubation mix was added once after 40 min incubation. Copper-ligand-reductnat preincubation mix – 132 µM $CuSO_4$, with either 1x, 2x, 3x or 4x ratio THPTA and 132 µM TCEP. After 2h or overnight (ON) the reaction was subjected to HPLC-MS analysis. Total area of rhodamine absorption at 507 nm of peaks corresponding to the product mass was measured and normalised to 24 µM RA unreacted control. In A) B) C) and D) reactions were analyzed by HPLC-MS. Total area of rhodamine absorption at 507nm (as in C) of peaks corresponding to the product mass was measured and normalized to 24 µM RA unreacted control. N=3 independent experiments Error bars represent ± SD.

Surprisingly, we found that although the effect of phosphate on the click reaction is noted in literature not much attention has been given to the differences in CuAAC reaction between phosphate buffered and unbuffered solutions and the resulting influence on reagent

stoichiometry (Miguel-Ávila et al., 2018; Presolski et al., 2011). This can be partially explained by the generally used high amounts of reductant (mM concentration) in reported CuAAC reactions, which could compensate for Cu(I) loss by constant generation of catalyst (Christen et al., 2012; Y. Yang et al., 2013; Z. Zhu et al., 2017). We thus conclude that phosphate ions can inhibit the CuAAC reaction and that this problem can be overcome by lowering the phosphate buffer concentration and increasing copper/ligand ratio with respect to TCEP. Under these newly designed experimental conditions, we demonstrate that probe **7** can be clicked with an efficiency as high as in water without increasing concentrations of the reductant.

Standardization of click reaction with water-soluble ligand-bathocuproine disulfonic acid (BCDA)

Since increasing THPTA concentrations in a CuAAC reaction in PBS did not extend its reaction efficiency, we decided to test another ligand with a high affinity for Cu(I) that is closely related to the commercially available sulfonated bathophenanthroline analogue, namely the bathocuproin disulfonic acid (BCDA) (Fig. 3.1.). BCDA is a bidentate chelator displaying two nitrogen coordinating atoms. To fulfill the stereochemical preferences of Cu(I) (tetrahedral geometry), one or two BCDA can firmly bind Cu(I) leading to successive formation monocuprous mono- and bischelate. In contrast to ligands used in biorthogonal reactions, BCDA thus constitutes a powerful chelator of Cu(I) and is anticipated to offer a protecting shell for the metal catalyst from interfering surrounding molecules (Christen et al., 2012; Hong et al., 2008; Lewis et al., 2004; Suzuki et al., 2010). We first checked that NaAsc is not an efficient reductant with the Cu(II)-BCDA complex similarly to what was observed with the THPTA ligand, and we thus decided to work with TCEP (Fig. 3.6). In aqueous conditions, addition of BCDA to the reaction decreased the reaction yields slightly when compared to THPTA with worst result observed upon 2x excess of BCDA over reductant (Fig 3.6). This can be explained by the high stability of the Cu(I) bischelate that prevents access of Cu(I), which catalyzes the CuAAC reaction. Interestingly, when the reaction was carried out in phosphate buffer with the already tailored conditions (method section), addition of 0.5 and 1 equivalent of BCDA with respect to TCEP increased significantly the reaction yields with respect to those measured with THPTA (up to 52% compared to 17% for THPTA) (Fig.3.6). This indicates that the phosphate ions, by competing with the BCDA ligand, destabilize the Cu(I) complex to such an extent that this copper complex, although still sufficiently stable, is able to function efficiently in the click reaction (Berg & Straub, 2013; Christen et al., 2012; Smith et al., 1985; Suzuki et al., 2010). BCDA thus displays opposing effects in CuAAC reactions conducted in aqueous and phosphate buffer similarly to what was observed for THPTA (Fig. 3.6). With BCDA and contrary to what was observed with THPTA, the overall yields of the CuAAC reaction are however much higher in PBS buffer, confirming that in the absence of phosphate ions, the stability of the Cu(I) complex (predominantly Cu(I) bischelate) is such that it prevents the click reaction. However, in the presence of such competing phosphate ions and/or by stabilsation of a more basic pH than in pure water, the formation of Cu(I) monochelate is then favored, thus significantly increasing the yields of the CuAAC reaction (Lewis et al., 2004; Presolski et al., 2010).

Interestingly, when in PBS the BCDA to TCEP ratios were increased five (or ten) times (proportionally with five times increase of the $CuSO_4$ concentrations), they inhibited the reaction nearly completely (Fig 3.6). These lower yields of reaction observed when using excess of BCDA to reductant again suggest that BCDA easily forms very stable complexes

with Cu(I). Interestingly, it stands in contrast to the behavior of THPTA which only inhibited the reaction when in excess to copper and thus underlines that BCDA exhibits a different relationship to Cu(II) and Cu(I) than THPTA does, probably due to higher affinity of BCDA to Cu(I) than to Cu(II).

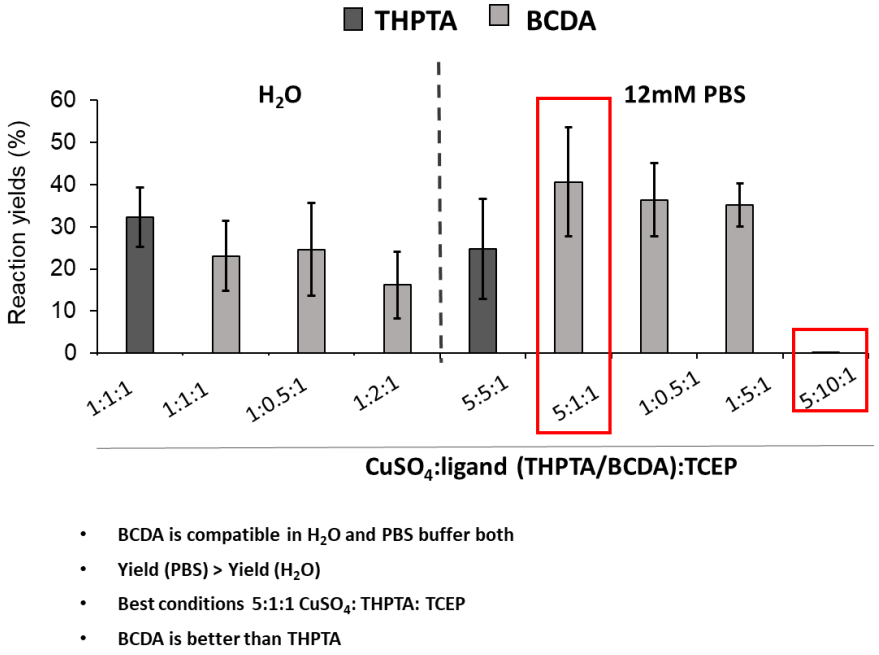

Figure 3. 6 Efficacy of BCDA as a ligand for click reaction: BCDA is a more efficient ligand for click reaction in phosphate buffer than THPTA. Rhodamine azide was reacted overnight (ON) with probe 7. Copper-ligand preincubation mix, containing either THPTA or BCDA in the indicated copper:ligand ratios, was added once after 40 min incubation. One equivalant corresponds to 132 µM TCEP. Reactions were analysed by HPLC-MS. Yield was determined by measuring the aborbtion of rhodamine at 507nm for product and substrate. Total area of rhodamine absorption at 507nm of peaks corresponding to the product mass was measured and normalized to 24 µM RA unreacted control. Figure represents priliminary results. Error bars represent ± SD.

We conclude that BCDA is fully compatible with our click reaction conditions in PBS buffer and water. The yield of reaction is better in buffer with the best conditions are 5:1:1 of $CuSO_4$:BCDA:TCEP in PBS buffer. Excess ligand at 5:10:1 of $CuSO_4$:BCDA:TCEP, the reaction is inhibited in buffer (Fig. 3.6). Furthermore, it supports the observation that BCDA is preferred over THPTA in oxygen-free conditions (Hong et al., 2008). We found that the fast formation of Cu(I) by a strong reductant combined with protection by a powerful ligand allows to perform efficient CuAAC reactions, with the benefit of scaling down the amount of reductant used and accordingly the amount of obtained unspecific reduction side products. We would also like to underline that although many factors important for the optimization of the CuAAC have been found since its initial discovery in 2003, the interplay between these factors (e.g., solvent, salts, counteranions, Cu(I) ligands, reagent ratios, pH) remained more elusive albeit it is essential for reaction success as demonstrated by our findings (Scheme S1).

Using Peptide as a model for photoreaction

Based on nMet-PD-ABPP crosslinking data, we choose probes **7** and **9** to further explore the crosslinking ability of the ABPPs towards a peptide model. Additionally, this allowed us to determine the peptide adduct behavior during HPLC-MS analysis, which is necessary for proteomic analysis. GSH was chosen as a model peptide due to its commercial availability, simple structure, and high solubility in water. To assess the photo-activation of ABPPs in more physiological conditions, crosslinking with GSH was performed in a water:organic solvent mixture (H_2O:ACN, 1:1, v/v). These conditions were different from those used for the crosslinking conditions with nMet where pure ACN solvent was used. However, we observed that the probe solubility is significantly limited in aqueous ACN solutions (Fig. S3.26). The observed solubility properties of the probes followed the order of magnitude: probe **10** < probe **8** = probe **7** < probe **9**. Since probe **9** was the most water-soluble ABPP probe, we thus used it as a binding partner for GSH. We found that although reagent concentrations were lowered (from mM to µM), we were still able to identify a significant fraction of GSH/GSSG-probe adducts after photoirradiation (Fig. 3.7A and B).

The structures of the C-H insertions products formed between probe **9** and GSH, through the experted pathway of photoalkylation by benzophenone (Scheme 1), are shown in Scheme 3 (pathway 1). All regioisomers displayed the same *m/z*: 683.16 Da. Noteworthy is the fact that a S-H insertion could be formed in principle, but it should be reversible. According to the studies with benzophenone and amino acids (Deseke at al., 1998), the C-H insertion product at the glycine of GSH by probe **9** upon photoirradiation might be the major adduct in this reaction.

Furthermore, the positive ESI-MS spectrum of the GSH adducts with probe **9** also displayed peaks of insertion products with m/z: 681.16 Da, suggesting loss of atoms following molecular rearrangement of the adducts (pathway 2). Positive ESI-MS and subsequent MS/MS analyses of the most prominent product (681.16 Da, RT = 33.5 min) revealed that this adduct is apparently monodeprotonated according to the initially expected photo-alkylation of the peptide (Scheme 4, pathway 1). However, fragmentation of this adduct revealed no further abbreviation from predicted peptide fragmentation patterns (Fig. 3.7C).

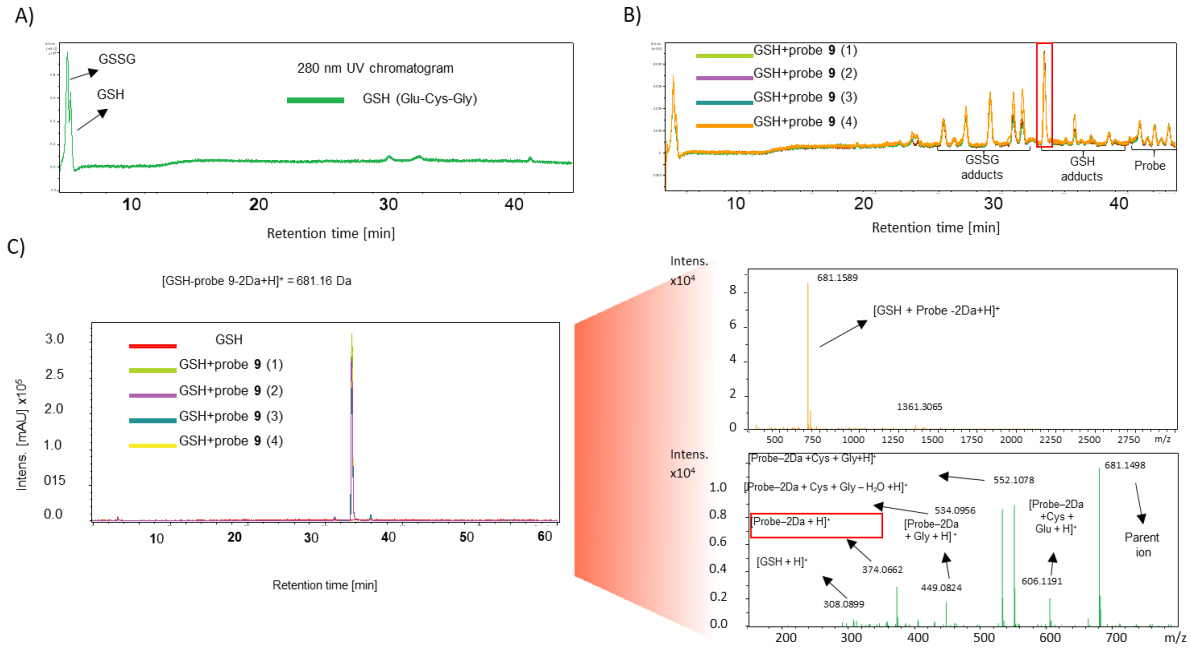

Figure 3. 7 Probe **9** forms photoadducts with GSH in aqueous ACN conditions. A) The absorption spectra at 280 nm after HPLC analysis of reaction mixture containing GSH (3mM) without ABPP upon 8 min UV irradiation. Glutathione disulfide (GSSG, RT = 4 min) is formed in the reaction by oxidation of GSH (RT = 4.25). B) The absorption spectra at 280 nm after HPLC analysis of reaction mixture of Probe 9 (600 µM) and 3 mM GSH upon UV irradiation for 8 min (n=4). Multiple peaks corresponding to different GSH and GSSG adducts (different crosslinking site, GSH and GSSG fragments, double crosslinking) are visible in the 280 nm light absorption spectra. Peak corresponding to mass of photo-crosslinked adduct of full GSH and probe 9 is highlighted in red box (RT = 33.5 min). C) Fragmentation pattern of the selected peak in (B) spectrum showing adduct *m/z* at 681.16 Da. In red box deprotonated probe 9 fragment of adduct.

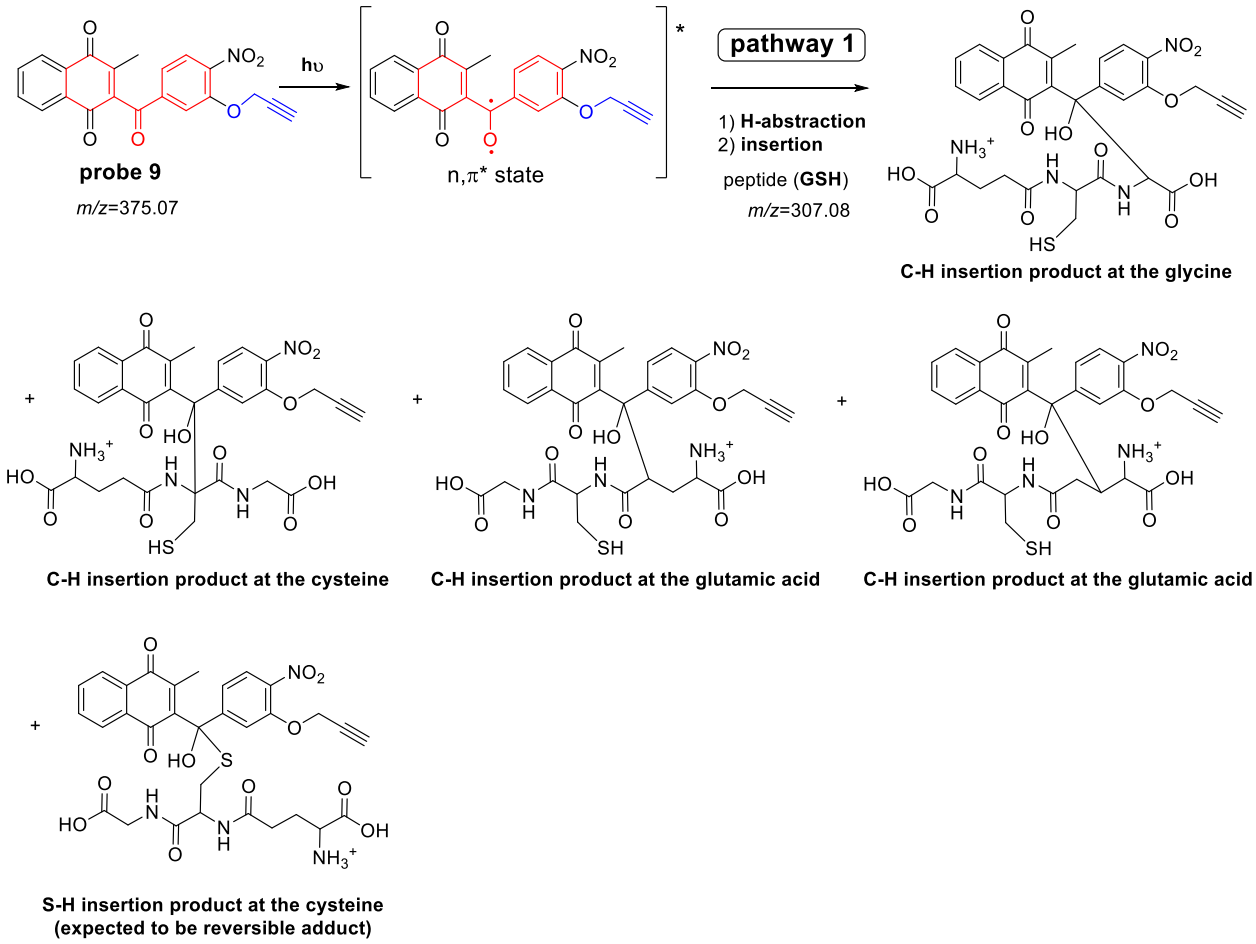

Scheme 3. Formation of expected C-H (and S-H) insertion products with calculated *m/z* = 683.17 $[M+H]^+$ formed between probe **9** and glutathione upon photoirradiation, according to the expected pathway 1.

A more rational explanation for the apparent deprotonation of the observed probe **9**-GSH adduct could stem from the second pathway (Scheme 4) upon photoirradiation of probe **9** in the presence of GSH. After photoreduction, an intramolecular process, much faster because entropically favoured, leads to the benzoxanthone formation. Several studies have indeed shown the photoreduction of quinones and subsequent intramolecular cyclization of a phenoxy radical (Marquardt et al., 1992; Belin et al., 2001; Porhun & Rakhimov, 2011; Ando & Suzuki, 2018) which effectively occurred in the presence of an H-donor. In these experiments, it is important to note that GSH can act both as a reductant and a H-donor. Radical phenolate in position C-2 of the diradicaloid reduced intermediate promotes the oxidative phenolic coupling. The methyl group in *ortho* to the free phenolate radical of the resulting benzoxanthone possesses a very labile –H, which releases owing the favoured energetically structure benzoxanthone-derived enone. Noteworthy is to highlight that the initial photoirradiation of probe **6** (P_TM40) with nMet did show an additional mass peak (m/z = 524.1, upper spectrum), albeit with lower intensity, in the FD-MS spectrum (Fig. 3.2), attesting the expression of two pathways occurring in the photochemical reaction.

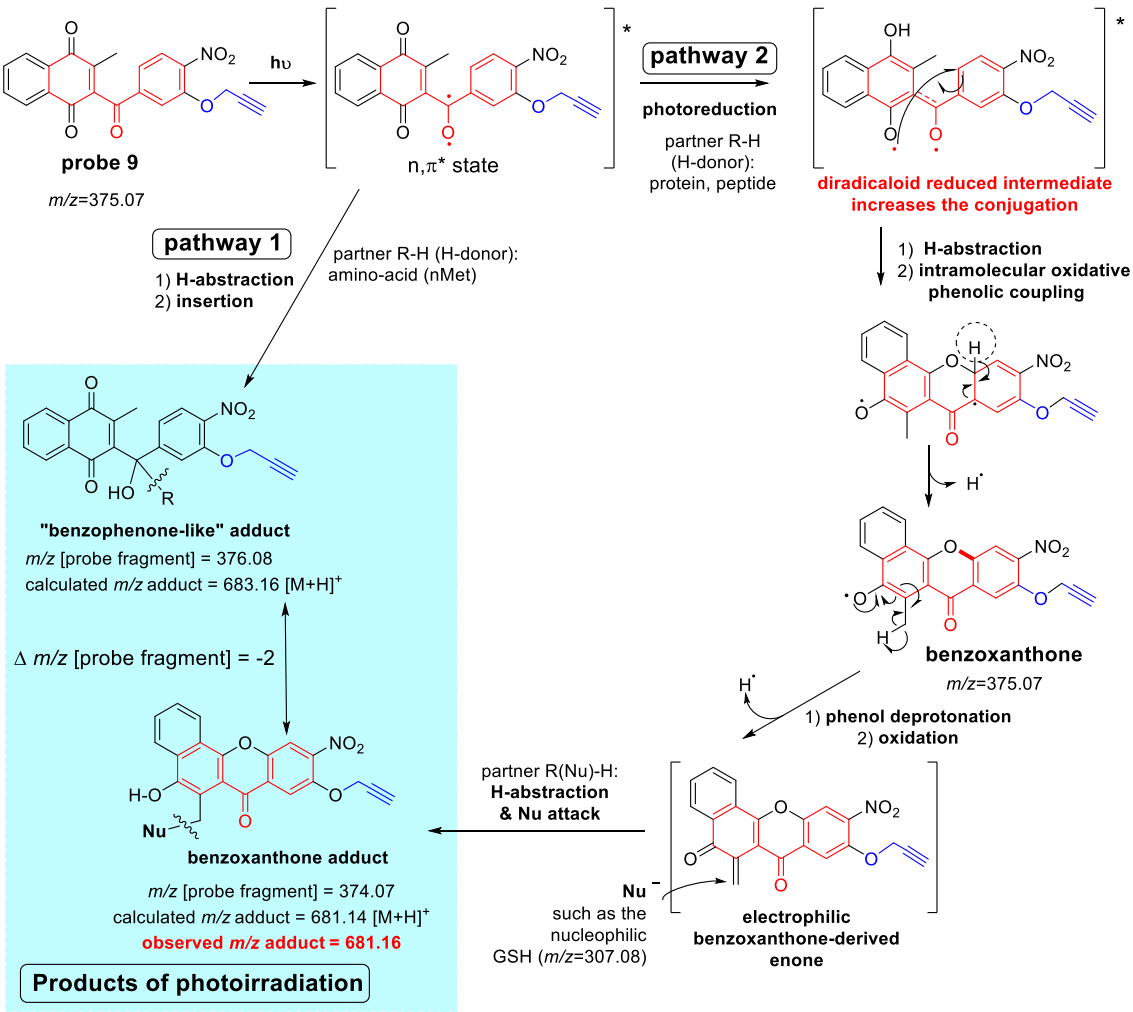

Scheme 4: Chemical analysis of the insertion products upon photoirradiation of the ABPP probe **9** (MD043) with glutathione (GSH) by mass spectrometry. Two pathways of photoreactivity of the benzoylmenadione and insertion products with nucleophilic partners were observed.

With this, we demonstrated that probe **9** can efficiently crosslink to a peptide and the corresponding peptide-ABPP adducts can be detected in standard MS/MS analysis, which is employed during proteomics. Importantly, peptide crosslinking was not possible to be achieved in lower concentrations of GSH and probe (lower than hundreds of µM), which are used during the inhibition assays, confirming that the probe does not display strong affinity towards amino acids which could enforce later unspecific binding to proteins. Additionally, MS analysis of the adducts led to the observation that the probe is able to crosslink to all three amino acids (Q,C,G) of GSH proving that the probe alkylates other amino acids than methionine similarly like benzophenone (Deseke at al., 1998; Wittelsberger et al., 2006). Some of the adduct isomers co-elute on HPLC as visible on the MS/MS spectra (Fig. 3.7B and C).

Therefore, two labelling pathways could occur in the photoirradiation experiments involving probe **9** and GSH, as depicted in the scheme 4. In agreement, the detected mass of the probe from the fragmentation of the GSH adduct was found to be 2 Da less than the observed mass of the initial reagent, indicating the transformation of the ABPP probe to a benz[*c*]-xanthen-7-one (benzoxanthone) (Fig. 3.7C).

Using Glutathione Reductase as a model for photoreaction

After confirming the photo crosslinking ability of PD-ABPPs with nMet and peptides, we sought to test the ability of probes to interact with protein targets. We first used hGR as protein model with the probe **6** analogue (i.e., probe **9** (MD043)) because our protein-centric approach of enzymatic assay proved that probe **6** (P_TM40) with NO_2 electron-withdrawing group in *para*-position to the benzoyl moiety possesses high inhibitory potency and substrate efficiency towards GR (Table 1). Therefore, we used hGR to standardize ABPP conditions and prove that the most effective ABPP probe can crosslink to the protein.

To understand the exact site in GR structure where the probe interacts and to evaluate the interest of the probe for ABPP, we studied the crosslinking pattern of PD-ABPP with human GR upon photoactivation. We tested the crosslinking reaction in similar physiological conditions in which the key PD metabolite, the 3-benzoylmenadione **2**, is known to inhibit the enzymes function. GR activity assays with PD and analogues are typically performed in pM concentrations of protein and µM concentrations of probe (according to methods described in section 3.5) As lowering the concentration will weaken the interactions between crosslinking reagents and so the efficiency of the crosslinking process, we have tested if hGR retained its affinity to probe **9** at concentrations used in GR assays. As shown probe **9** still inhibited 8 mU GR at a concentration of 5 µM. After using this probe concentration in a crosslinking reaction with hGR (5 µM) in PBS buffer at final 2% ACN concentration, we were able to confirm the probe **9**–hGR adduct formation by MS/MS analysis. Identification by fragmentation pattern of the crosslinked peptide to probe **9** adducts revealed one peptide to be identified with high confidence (2893.23 Da = Y393-K416 + M - 19 Da; dehydration is common for benzophenone adducts) (Fig. 3.8A). This protein fragment has been identified as an adduct several times during our MS/MS analysis confirming that the analogue **9** can be used as a photoreactive ABPP probe to bind to target proteins. However, the crosslinking position (K399) does not reside in known binding pockets of hGR (Fig. 3.8B). In contrast, it is localized in the interface domain, known to mediate the dimerization of the protein. This domain is crucial for the activity of GR as the enzyme is not active in monomer state. With this respect, 41 amino acids of both subunits participate to line the GSSG binding site in human GR (Salmon-Chemin et al., 2001). Additionally, in the interface domain, at the 2-fold symmetry axis of the homodimeric protein, a

cavity is present, which was reported to bind numerous GR inhibitors, such as of 2-methyl-1,4-NQ (menadione) (Karplus et al., 1989), 3,7-diamino-2,8-dimethyl-5-phenylphenazinium chloride (safranin) (Karplus et al., 1989) , 6-hydroxy-3-oxo-3H-xanthene9-propionic acid (Savvides et al., 1996), a series of 10-arylisoalloxazines, (Schönleben-Janas et al., 1996) and S-(2,4-dinitrophenyl)glutathione (Krauth-Siegel et al., 1998). This cavity does not have any direct connection with the NADPH or FAD binding sites. It is rather linked to the external surface of the protein and to the GSSG binding site, respectively, by two pairs of short channels (Salmon-Chemin et al., 2001). The channel pair openings, which are located in the catalytic center, emerge at the bottom of the V-shaped catalytic crevices in close proximity to the redox-active disulfide bridges (Salmon-Chemin et al., 2001). Noteworthy, in total 41 amino acids of both subunits participate to line the GSSG binding site in human GR (Salmon-Chemin et al., 2001). It was suggested that compounds docked in the cavity could either led to structural changes disturbing the dimer stability leading to decrease of enzyme activity or interfere with the redox potential of the flavin.

A)

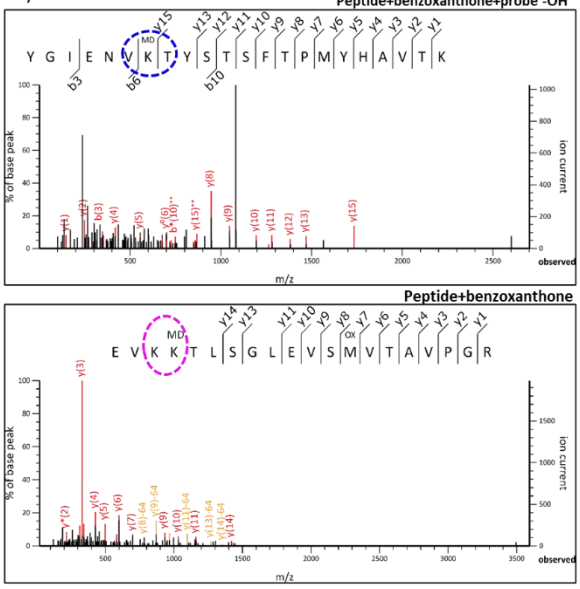

AA position	Mascot ion Score	Expect (p)	RT (s)	Modification position	Mass
392-413	45	0.0011	3094	**K399**	2893.2975
255-275	70	1e -007	3749	**K258 or 257**	2471.2082

B)

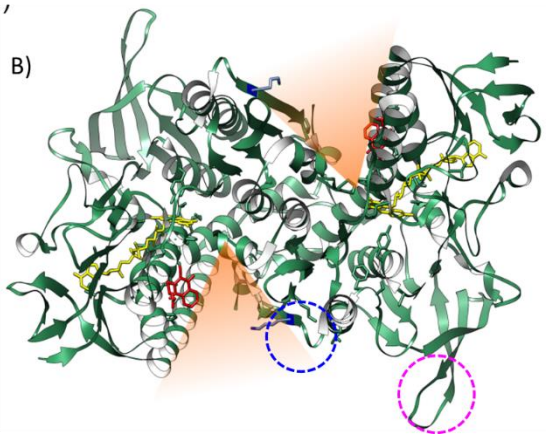

Figure 3. 8 Probe **9** crosslinks to hGR at position K399 and K258 or 257 A) MS/MS fragmentation pattern for the peptide identified with the highest confidence by MASCOT analysis of the photoreaction of hGR (5µM) with probe 9 (5µM) for 8 min at 365 nm UV (1000W monochromator). The reaction mixture was separated on a SDS-Page gel, the protein band cut out, trypsin digested and analysed by HPLC-MS/MS. Search parameters: Peptide Tol: 20 ppm, MS/MS Tol. 7 ppm, 3 miscleavage sites allowed. Red circle indicates identified crosslinking sight. B) Position of K399 (blue) and FAD (yellow) has been marked on the previously reported hGR dimer structure crosslinked to menadione analogue (red). The substrate binding cleft leading to the catalytic disulfide bridge is visible between K399 and menadione core (red). Pink colour indicate position of K258 or 257.

Interestingly, the amino acids of the channel opening (405-**FT**PMYH-412) are present in the identified peptide where K399 was alkylated by the ABPP probe **9**, however separated by a distance of 19 Å from the identified crosslink site or from the active Cys in the GSSG binding site. Lys residues with their intrinsically nucleophilic ε-amine are important amino acids in proteins. Beyond cysteines, lysines represent a source for covalent probe development, and

several studies have started to identify the Lys ligandability map of the human proteome (Hacker et al., 2017).

This could suggest that K399 plays a crucial role in ABPP probe **9** binding to human GR. Another alternative is that the found probe-hGR interaction site does not represent the initial probe binding site but a secondary drug interaction site following mobility through the channels or from the active GSSG binding site to the cavity at the 2-fold symmetry axis of the homodimeric protein. This last hypothesis could be supported by the fact that the suicide-substrate fluoroM5 was found to be bound to the most exposed Cys of the active site in the human GR crystal structure (Bauer et al., 2006). Furthermore, one cannot rule out the possibility that only one of the many crosslink sites on the peptide was identified. The regioselectivity of the ABPP crosslinking to bind to multiple possible positions on a peptide can lead to formation of multiple adducts. If the adducts co-elute during HPLC (as demonstrated for GSH adducts in 2.4.) it could diminish the correct identification of the relevant crosslink site on the peptide during MS analysis.

In the 1st hypothesis (*i.e.,* K399 play a crucial role in ABPP probe **9** binding in human GR), we cannot rule out the fact that the photoirradiation of 1,4-naphthoquinones can promote many other reactions, such as reduction-oxidation as recently reported (Ando & Suzuki, 2018). With the 3-benzoylmenadiones we previously reported that their 1e-reduction can generate the benzoxanthone **4** upon oxidative phenolic coupling (Bielitza et al., 2015). This phenol, upon deprotonation and oxidation, might generate the electrophilic enone species. We can hypothesize that, upon photoirradiation, a sequence of reduction-oxidation of the ABPP probe would generate the highly electrophilic benzoxanthone-derived enone, which could be attacked by the intrinsically nucleophilic lysine ε-amine (K399) (Scheme 4). The generation of the benzoxanthone **4** was recently evidenced in electrochemical measurements upon several cycles of 1e-reduction (Cotos et al., 2020). In this context, the reactivity of a diverse set of lysine-directed electrophilic fragments has been the focus of ABPP strategies (Hacker et al., 2017). It is well documented that lysines are found at many functional sites, including enzyme active sites, at protein–protein interaction sites, and sites for post-translational regulation of protein structure and function through epigenetic events.

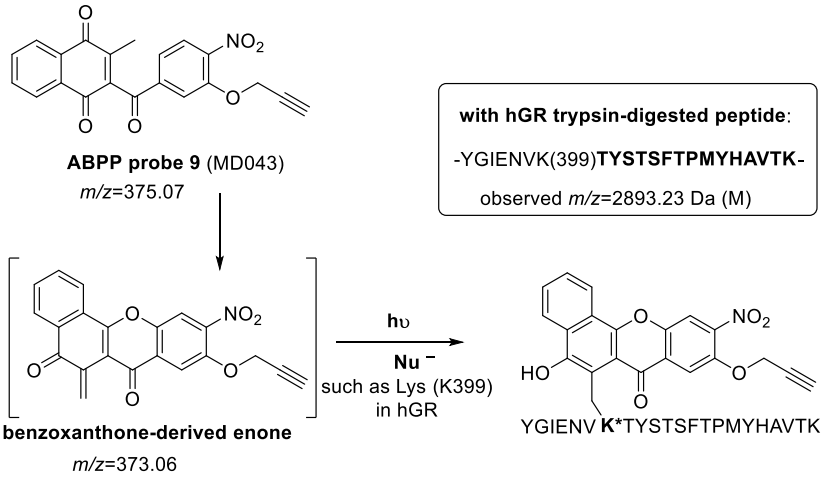

Scheme 5: Chemical analysis of the trypsin digest product upon photoirradiation of the ABPP probe 9 (MD043) with human glutathione reductase by mass spectrometry.

Using the Click reaction with biotin-azide

In order to test if the click reaction conditions with our ABPPs are suitable and efficient for tagging proteins after crosslinking and subsequent enrichment, we thus performed click reactions in the presence of protein and denaturing agent. The CuAAC reaction of probe **7** (6 µM) with RA (6 µM) was performed with addition of hGR, urea and SDS in phosphate buffer. The reaction was scaled down to concentrations similar to the ones applied during crosslinking of ABPPs. Free thiol groups of cysteines like the one in the hGR catalytic centers are known to bind Cu(I) potentially inhibiting the reaction (Hong et al., 2009; S. Li et al., 2017). However, presence of hGR did not change the click reaction yields indicating that the Cu(I) species are properly protected by the ligand. Similarly, addition of chaotropic agent as well as lowering the concentration of reagents did not lead to significant loss of reaction efficiency (Fig. S3.29). Next, we analyzed the click reaction of probe **7** with biotin-azide (BA), which is used to enrich tagged adducts by interaction with streptavidin. Compared to RA, BA is water-soluble and allowed us to lower the concentration of organic solvent in the reaction medium from 7.2% to 4.4 % and substitute DMF to ACN, which is the co-solvent of ABPPs during photo-irradiation (Fig. S3.29). Of note, BA is a poor UV and visible chromophore thus allowing a selective photoexcitation and quantification of the probe. The reaction efficiencies of BA were quantified thanks to the probe absorbance values at 280 nm (*i.e.,* a relative quantification was done due to the unknown values of the ε_{max} of the reaction products). Despite differences in solvent composition, the Cu(I) cycloaddition of BA had a similar pattern in triazole formation efficiency as RA (Fig. S3.29). Thus, we conclude that our optimized click conditions allow for efficient labelling of alkynes with the biotin tag.

The plasmodione-derived benzoxanthone is a strong electrophile with relevant meaning for the antimalarial plasmodione

The benzoxanthone has already been proposed to be a key metabolite of plasmodione (Bielitza et al., 2015; Feng et al., 2018). It might be generated through the redox-cycling, including the 1,4-naphthoquinone reduction, benzylic oxidation, 1,4-naphthoquinone reduction and oxidative phenolic coupling. In the photo-irradiation experiments, the benzoxanthone is proposed to be likely generated in the presence of a H-donor, like GSH or the hGR used as the protein model.

In agreement with our reported study on binding titrations of benzoxanthone and Fe(III), and CID-MS experiments based on a reported methodology (Muñoz-Durango et al., 2012), we clearly showed that the benzoxanthone strongly interacted with hematin (Bielitza et al., 2015). In particular, two intense benzoxanthone **4**/heme adducts at *m/z* = 960.2 ([heme+**4**]$^+$) and *m/z* = 975.3 (formally [Heme+**4**-H+O]$^+$) were clearly detected (Fig. 3.9). The first **4**/heme adduct at *m/z* = 960.2 corresponds to a π-π complex. This feature is assessed by the weak dissociation voltage DV_{50} (150 V) and the absence of a residual complex at high fragmentor voltage. In addition, the π-stacking in the **4/**hematin complex might be strengthened by additional interactions such as hydrogen bonding between the propionate of the heme side chain(Xu Kelly et al., 2001) and the phenol in **4** and Fe^{III} axial coordination of the benzoxanthone carbonyl unit (Fig. 3.9, species A). It is noteworthy that benzoxanthone **4** can be oxidized (E_{pa} = -50 mV and -208 mV) through its phenolic moiety and might undergo an exchange of electron(s) with the tightly bound Fe^{III} heme. The intramolecular **4**→Fe^{III} heme 1e- transfer is favored by hydrogen bonding (Xu Kelly et al.,2001) and generates a carbon radical at the

benzoxanthone core (Fig. 3.9, species B). The Fe^{II} heme concomitantly formed from species B binds O_2, and the resulting species C (Fig. 3.9) might be attacked by the nucleophilic □-keto carbon radical (Bunte et al., 2004) of the tightly bound benzoxanthone, ultimately leading to hematin *meso*-alkylation by the benzoxanthone **4**, as suggested by the ESI-MS experiments (second adduct at *m/z* 975.3) (Meunier et al., 2004). Interestingly, the DV_{50} value of this second **4**/heme adduct is markedly increased (+32 V), and a significant amount of the complex is observed at high fragmentor voltage therefore indicative of a very stable heme adduct (~5% for **4** and ~7 % for the antimalarial drug amodiquine (**AQ)** used as reference). The structural signature of this alkylated hematin product is tentatively proposed in species D (Fig. 3.9), following reaction of the quinone methide radical at the *meso*-position of the tetrapyrrole and release of a water molecule, as already demonstrated for artemisinin(Robert et al., 2005a). This suggested heme alkylation product has to be regarded in this experiment, as the expression of the formation of a key carbon radical generated from a redox-active agent in redox-driven bioactivation processes, and a relevant reaction occurring in the parasite *in vivo*.

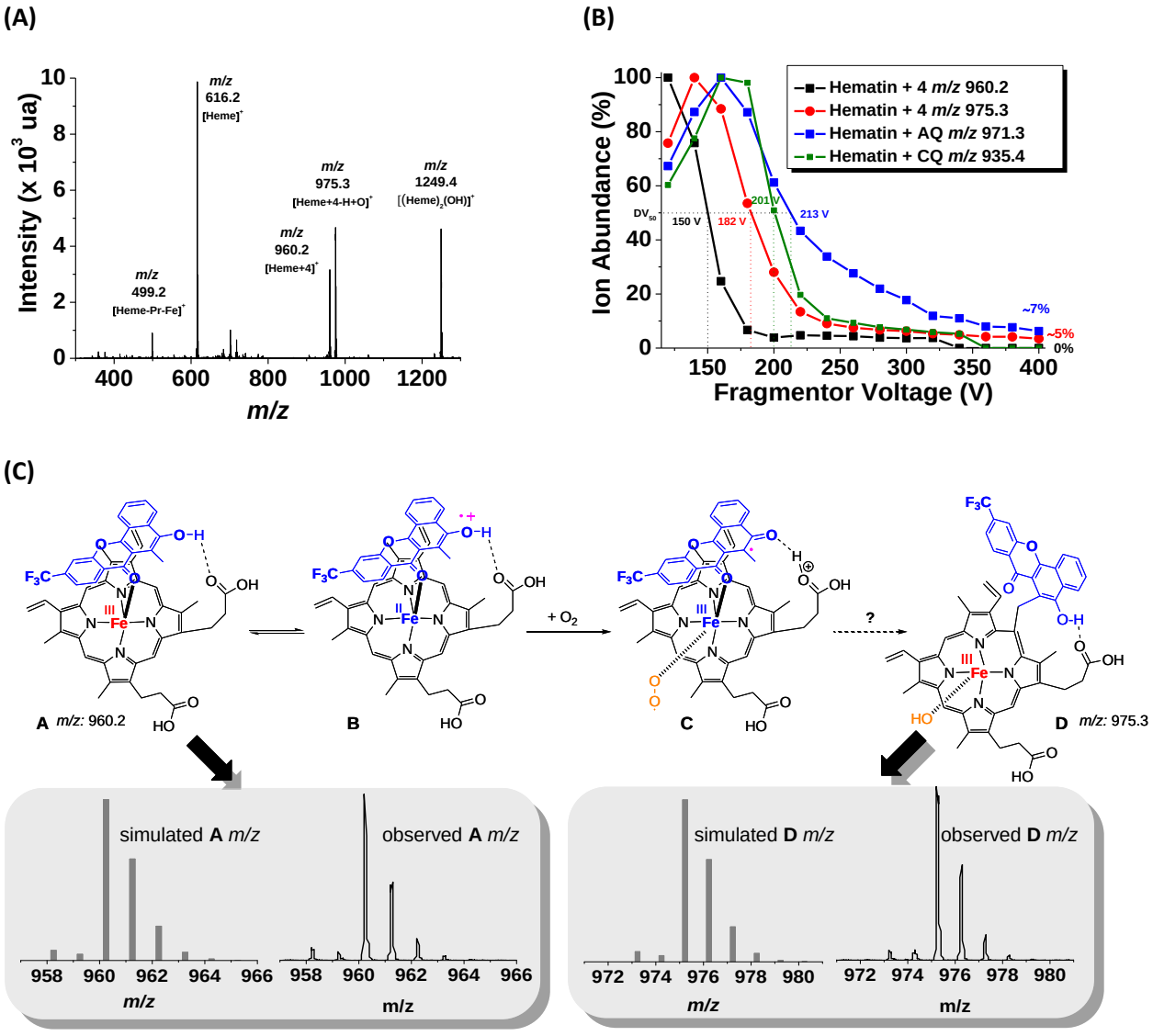

Figure 3. 9 (A) ESI mass spectrum (120 V) of a 1:1 mixture of 50 µM heme and 50 µM benzoxanthone **4** in H_2O/CH_3CN (5/95)–1% formic acid. (B) Stability responses of the **4**•heme

(at *m/z* = 960.2 and at 975.3), AQ•heme (at *m/z* = 971.3) and CQ•heme (at *m/z* = 935.4) adducts obtained by CID-MS experiments. ESI-MS^+; 120 V < fragmentor < 400 V with 20 V increments. (C) Proposed molecular structure of alkylated $iron^{III}$-hematin by the benzoxanthone and comparison between simulated and observed mass signatures of species A and D**.**

Such contribution needs more detailed investigations to understand the mechanisms of action of the redox-active lead antimalarial plasmodione. These data obtained with the benzoxanthone **4** clearly demonstrate that this species should be considered as an electroactive metabolite generated in the efficient redox cascade of bioactivation of plasmodione. Interestingly, the formation of xanthones had previously been hypothesized to explain the potentiation of antimalarial activities of polyhydroxylated benzophenone derivatives tested in the presence of Fenton catalysts upon catalysis of redox-active metals such as Fe^{III} (Winter et al., 1996; Winter et al., 1997). In the present study, upon oxidation, the benzoxanthone **4** is a powerful electrophile that can be attacked by the nucleophilic species present in the reaction, GSH or the terminal ε-amine group of K399 in hGR. As controls, we analyzed the heme interaction products under the same conditions with both antimalarial drugs, chloroquine (CQ) and amodiaquine (AQ), by CID-MS experiments. As previously reported, CQ did not show heme alkylation products, while AQ led to ca. 7% heme alkylation products in accordance with the possible Michael addition to the generated quinone methide after deamination of the side chain diethylamine group. The benzoxanthone-derived alkylation product (m/z = 975.3) was estimated to represent 6% of the bound heme species.

Evaluation of the antimalarial properties of PD-ABPP (modified IC_{50} assay, 72h drug exposure)

To validate the applicability of ABPPs in parasites, we evaluated the antimalarial activity of the four 3-benzoylmenadione-based ABPP probes (Table 3). As previously observed observed and despite being the likely key metabolites of 3-benzylmenadiones, the 3-benzoylmenadiones do not display a high antimalarial activity, with an IC_{50} of ca. 10-50 fold higher than the corresponding 3-benzylmenadiones (Müller et al., 2011; Feng et al., 2018). This can be explained by the very high absorption of 3-benz(o)ylmenadiones to serum proteins or by the very poor internalization of 3-benzoylmenadione metabolites in pRBCs when given externally. Indeed, since the 3-benzoylmenadiones (metabolite **2**, probes **6-10**, Fig. 3.1) are more polar and planar than the 3-benzylmenadiones (plasmodione **1**, probes **5** and **11**), it is likely that they are not as easily internalized in parasites as the 3-benzylmenadione probes. To act as the key active principle of the prodrug plasmodione, the metabolite must thus be generated *in situ* in the parasite to cycle with NAD(P)H-dependent reductases. On the basis of the ABPP properties studied in the click reaction and under photoirradiation we observed that probes **7** and **9** are the most efficient probes to be used in photolabeling of plasmodione targets.

This result has motivated the synthesis of a first PD-ABPP, probe **11**, in the 3-benzylmenadione series. Probe **11** (Fig. 3.1) displayed an IC_{50} value comparable to that of PD regardless of substitution of the CF_3 function at the *para*-position by an alkyne group. Thus, the work reported herein allowed us to select an optimized potential probe, probe **11,** in the 3-benzylmenadione series to be used for the ABPP approach in *Plasmodium* parasites.

Table 3. Averaged IC_{50} values for 3-benz(o)ylmenadione derivatives determined from growth inhibition assays with *Plasmodium falciparum* strain Dd2.

		IC_{50} (nM)	
Series	Copmpound	***P. falciparum* Dd2** [a,b]	**hMRC-5**
3-Benzoylmenadiones	**6**	513 ± 287	24,000
	7	1806 ± 302	20,500
	8	2993 ± 750	25,800
	9	417 ± 222	42,200
	10	> 5000	29,400
3-benzylmenadiones	**11**	49 ± 15	> 64,000
	Plasmodione	20 ± 5	> 32,000[c]

a: 3 independent experiments with the SYBR green assay; b: The *P. falciparum* Dd2 strain is sensitive to DHA (IC_{50} DHA = 0.7 ± 0.2), to methylene blue (IC_{50} MB = 7 ± 0.3), and resistant to chloroquine (IC_{50} CQ = 189 ± 12). c: value from Müller et al., 2011.

Based on our studies on the photoreactivity and clickability of 3-benzoylmenadione-based probes, probe **11** was selected for future PD interactome analysis as it is expected to become the most photoreactive upon bioactivation, the most active in killing parasites with an IC_{50} value in the same range as the value of PD.

Conclusions

Here in this work, we report the design and the synthesis of specific PD-ABPP based on the postulated MoA of PD. The photoreactive compounds in the 3-benzoylmenadione series, functionalized by an alkyne group, were produced by a recently reported innovative Friedel-Craft reaction variant (Cotos et al., 2020), without which the compounds would not have been produced easily. We also studied the influence of different electron withdrawing groups (EWG) on the photoreaction effectiveness of the newly synthesized PD-ABPP. 3-Benzoylmenadiones-ABPP probes **7** and **9** were found to be the most effective in terms of combined photoreactivity and "clickability" properties. Finally, by correlating the efficiency of PD-ABPP with the antimalarial activity, we concluded that PD-ABPP probe **11** is the most effective one to be used in parasite cultures to identify PD interactome by proteomics analysis. Identifying PD targets will be essential to further optimize the properties of this compound series, and to design more active and target specific derivatives.

Conflicts of interest

There are no conflicts to declare.

Acknowledgements

This work was supported by the French Centre National de la Recherche Scientifique (E. D.-C., S. A. B.), the Institut National de la Santé et de la Recherche Médicale (S. A. B), the University of Strasbourg (E. D.-C., C. S., J.-M. S., and S. A. B, IDEX grant for the plasmoClick project, postdoctoral salary for B. C.), the Laboratoire d'Excellence (LabEx) ParaFrap (grant LabEx ParaFrap ANR-11-LABX-0024 to E. D.-C. and S. A. B., PhD doctoral salary for V. K.), the ANR PRC2017 (grant PlasmoPrim including the salary of the PhD student M. D.), the

Fondation pour la Recherche en Chimie (grant Innovation for the FluoPlasmo project, postdoctoral salary for L. C.), and the ERC Starting Grant Nº260918 (S. A. B.). The authors are indebted to Tobias Müller for preliminary 3-benzoylmenadione photoirradiation experiments. They also thank Romain Ruppert (UMR 7177 CNRS-Strasbourg University, Laboratory of Controlled Ligand Architectures in Coordination chemistry-CLAC) and Jean-Pierre Sauvage (Institute of Supramolecular Science and Engineering-ISIS, UMR 7006 CNRS-Strasbourg University, Laboratory of Inorganic Chemistry) for the gift of the BCDA sample, Alexandre Specht (UMR 7199 CNRS-Strasbourg University, Chemical Biology group) for making available the high-intensity 1000W UV monochromator, Louis Maes (Laboratory of Microbiology, Parasitology and Hygiene-LMPH, Antwerp University, Belgium) for measuring the IC_{50} values of the probes **6-11** in cytotoxicity assays using human MRC-5 fibroblasts, and Patrick Gizzi (UMS 3286 CNRS-Strasbourg University, PCBIS, Illkirch) for the studies on absorption of the 3-benzoylmenadione **2** to serum proteins. Katja Becker (Biochemistry and Molecular Biology, Interdisciplinary Research Centre, Justus Liebig Giessen University) is acknowledged for welcoming V. K. for 2 months in the frame of the COST Action CM1307.

Chapter 3: Supplementary Information

TABLE OF FIGURES: CHAPTER 3 SUPPLEMENTARY INFORMATION

METHODS

General

Solvents and reagents: Commercially available starting materials were purchased from Sigma-Aldrich, ABCR GmbH & Co. KG, Alfa Aesar, and Apollo Scientific and were used without further purification. Solvents were obtained from Sigma-Aldrich and LPCR. All reactions were performed in standard glassware. Thin Layer Chromatography (TLC) were used to monitor reactions (vide infra). Crude mixtures were purified by flash column chromatography. The latter were performed using silica gel 60 (230-400 mesh, 0.040-0.063 mm) purchased from E. Merck. Automatic flash chromatographies were carried out in a Biotage Puriflash apparatus with UV-Vis detection at 254 nm (unless otherwise specified). Monitoring and primary characterization of products were achieved by Thin Layer Chromatography on aluminum sheets coated with silica gel 60 F254 purchased from E. Merck. Eluted TLC's were revealed under UV (325 nm and 254 nm) and with chemicals. Analytical TLC was carried out on pre-coated Sil G-25 UV_{254} plates from Macherey Nagel. Flash chromatography was performed using silica gel G60 (230–400 mesh) from E. Merck.
Nuclear Magnetic Resonance (NMR): The Nuclear Magnetic Resonance (NMR) spectra were recorded by a *Bruker avance 400* apparatus (^{1}H NMR 400 MHz, ^{13}C NMR 100 MHz, ^{19}F NMR 376 MHz) and *Bruker avance 500* apparatus (^{1}H NMR 500 MHz, ^{13}C NMR 126 MHz, ^{19}F NMR 376 MHz) at the ECPM. All chemical shifts (δ) are quoted in parts per million (ppm). The chemical shifts are referred to the used partial deuterated NMR solvent (for $CDCl_3$: ^{1}H NMR, 7.26 ppm and ^{13}C NMR, 77.00 ppm and for DMSO: ^{1}H NMR, 2.50 ppm and ^{13}C NMR 39.52 ppm. The coupling constants (J) and the non-equivalence ($\Delta\nu$) are given in Hertz (Hz). Resonance patterns are reported with the following notations: br (broad), s (singlet), d (doublet), t (triplet), q (quartet), m (multiplet), dd (doublet of doublets), AB (AB system), (ABX) (AB system of an ABX) and A_2B_2 (A_2B_2 aromatic system). In addition, the following acronyms will be used: C=O carbonyl group; C_q: quaternary carbon; CH_2: secondary carbon; CH_3: methyl group.

Microanalyses: Microanalyses were obtained at *"Service de Microanalyses" at the Institut de Chimie de Strasbourg.*
Mass spectrometry: Mass spectra (ESI-MS) were obtained on a microTOF LC spectrometer (Bruker Daltonics, Bremen). High Resolution Mass (HRMS) spectra were measured and fitted with calculated data.
Melting point: Melting points were determined on a Büchi melting point apparatus and were not corrected.

The synthesis of the 3-benzylmenadione **5** (P_TM37) and 3-benzoylmenadione **6** (P_TM40) (Fig. 1b) was described in Müller et al, 2011. Detailed experimental procedures and spectral data for starting materials, 1H and 13C NMR spectra of all new compounds are given in the Supporting Information.

Synthesis of PD-ABPP

General procedure of reduction and protection of Menadione and 3-benzyl-menadione derivatives[1]: All the experiments were carried out under argon atmosphere. Menadione or 3-benzyl-menadione derivatives (1 equiv., 7.47 mmol) was suspended in ethanol (29.1 mL). Then, stannous chloride (3 equiv.) was dissolved in HCl (8 equiv.), added dropwise to the previous solution at room temperature and the mixture was stirred for 2 h, during the reduction process a white solid is observed. The solvent was removed in vacuum and the solid was

[1] T. Meller, L. Johann, B. Jannack, M. Bruckner,D.A.Lanfranchi,H.Bauer, C. Sanchez, V. Yardley,C.Deregnaucourt, J. Schrevel, M. Lanzer,R.H. Schirmer,E.Davioud-Charvet, J. Am. Chem. Soc. 2011, 133,11557 –11571.

washed with distilled water and filtrated, quickly to avoid the re-oxidation upon the O_2 atmosphere. Subsequently, the resulting crude product was dissolved in acetone (36.4 mL), generating Ar atmosphere. At that point, Dimethyl-sulphate (3 equiv.) was added, the system was heated up to 60°C. KOH (5 equiv.) dissolved in methanol (16.6 mL) was added dropwise to the previous solution at the same temperature for 4h. Once the time described for the reaction finished, was added KOH (7.94 equiv.) in 30 mL H_2O to quench the reaction. The crude of the reaction was obtained, after several extractions with DCM (5x35 mL), dried over $MgSO_4$ and finally concentrated. The pure compound was isolated after a purification by chromatography (DCM/ Cyclohexane, 1:1 to 7:3).

2-(4-iodobenzyl)-1,4-dimethoxy-3-methylnaphthalene (**11b**) **(EDC-AZ.1.17.)**: Starting with **11a** Yield 56 %; **^{1}H NMR (CDCl3, 400 MHz):** δ 8.12–8.06 (m, 2H), 7.54 (d, *J*=8.3 Hz, 2H), 7.52–7.47 (m, 2H), 6.87 (d, *J*=8.5 Hz, 2H), 4.21 (s, 2H), 3.86 (s, 3H), 3.83 (s, 3H), 2.24 (s, 3H) ppm.**^{13}C NMR ($CDCl_3$, 100 MHz):** 150.57, 150.44, 140.22, 137.39, 130.20, 128.42, 128.05, 127.16, 126.81, 125.87, 125.53, 122.46, 122.24, 90.89, 62.31, 61.41, 32.30, 12.65. **HRMS (ESI):** 418.041278 m/z (cal. $C_{20}H_{19}O_2I$ 418.042429)**; Done but not good analysis.**

General procedure for the Friedel-Craft acylation based on TfOH-TFAA mixture of reagent[2]**:** 1,4-Dimethoxy-2-methylnaphthalene (1.5 mmol) and benzoic acid (1 mmol) were dissolved in dichloromethane (0.2 m). At 0 °C, TFAA (2 mmol) was added. After stirring for 10 min, TfOH (0.5 mmol) was added cautiously and the reaction mixture was allowed to warm up slowly to room temperature and stirred for 16 h. Then, the reaction was quenched with an aqueous saturated NaHCO3 solution and the aqueous phase was extracted three times with dichloromethane. The combined organic phases were dried over MgSO4 and the solvent was removed under reduced pressure. The reaction crude was purified by silica gel chromatography by using a mixture of cyclohexane and toluene as eluent to afford analytically pure Friedel–Crafts products.

(1,4-dimethoxy-3-methylnaphthalen-2-yl)(4-iodophenyl)methanone (7b) (LCM.1.303) : 47 % Yield, white solid. m.p : 133 °C. **^{1}H NMR (400 MHz, Chloroform-d) δ :** 8.14 (d, *J* = 8.24 Hz, 1H), 8.07 (d, *J* = 7.92 Hz, 1H), 7.82 (d, *J* = 8.5 Hz, 2H), 7.61 – 7.52 (m, 4H), 3.91 (s, 3H), 3.80 (s, 3H), 2.22 (s, 3H).**^{13}C NMR (100 MHz, Chloroform-*d*) δ :** 196.75, 150.49, 149.26, 138.09 (2C), 136.59, 130.83 (2C), 130.34, 129.43, 127.21, 127.09, 126.09, 123.45, 122.60, 122.43, 102.18, 63.59, 61.54, 12.74. **HRMS (ESI)** calcd. for $C_{20}H_{18}IO_3$: 433.029519. Found: 433.027541 (MH^+).

(1,4-dimethoxy-3-methylnaphthalen-2-yl)(3-iodo-4-(trifluoromethyl)phenyl)methanone (**8b**) **(MD401)**: 66% Yield, **^{1}H NMR (400 MHz, Chloroform-d) δ** 8.54 (s, 1H), 8.17-8.15 (m, 1H), 8.08-8.06 (m, 1H), 7.80 – 7.77 (m, 1H), 7.70 (d, J = 8.16 Hz, 1H), 7.64-7.60 (m, 1H), 7.58-7.54 (m, 1H), 3.93 (s, 3H), 3.80 (s, 3H), 2.23 (s, 3H).**^{19}F NMR (376 MHz, Chloroform-*d*)** δ -63.22. **^{13}C NMR (100 MHz, Chloroform-*d*)** δ 195.19, 150.72, 149.65, 142.05, 140.52, 137.5 (q, *J* = 31.0 Hz), 129.75, 129.47, 129.09, 127.99 (q, *J* = 6.0 Hz), 127.55, 127.04, 126.29, 123.30, 122.65, 122.53, 122.36 (q, *J* = 272 Hz), 91.37(q, *J* = 1.81 Hz), 63.69, 61.60, 12.79. **No HRMS are relationated with this compound.**

(1,4-dimethoxy-3-methylnaphthalen-2-yl)(3-fluoro-4-nitrophenyl)methanone (**9b**) **(MD121):** Yield 82%, orange solid. **m.p :** 120 °C. **^{1}H NMR (400 MHz, Chloroform-*d*) δ :** 8.15-8.17 (m, 1H), 8.05 – 8.10 (m, 2H), 7.78 (dd, *J* = 10.84, 1.68 Hz, 1H), 7.70-7.72 (m, 1H), 7.61-7.65 (m, 1H), 7.55-7.59 (m, 1H), 3.93 (s, 3H), 3.80 (s, 3H), 2.24 (s, 3H).**^{13}C NMR (100 MHz, Chloroform-*d*) δ :** 194.76 (d, *J* = 1.06 Hz), 155.44 (d, *J* = 264.9 Hz), 150.84, 149.82, 142.84 (d, *J* = 6.2 Hz), 140.08 (d, *J* = 8.4 Hz), 129.87, 128.95, 127.74, 126.95, 126.55(d, *J* = 2.6 Hz),

[2] L. Cotos, M. Donzel, M. Elhabiri, E. Davioud-Charvet, Chem. - A Eur.J. (2020), 26(15), 3314-3325.

126.42, 125.20 (d, *J* = 4.3 Hz), 123.20, 122.57(d, *J* = 0.9 Hz), 119.00, 18.79, 63.69, 61.60, 12.72.**^{19}F NMR (376 MHz, Chloroform-*d*) δ :** -116.05 (dd, *J* = 10.9, 6.9 Hz). **HRMS (ESI)** calcd. for $C_{20}H_{17}FNO_5$: 370.1085. Found: 370.1072 (MH^+). **Elemental analysis** calcd. : 3.79%N. 65.04%C. 4.37%H. Found : 3.79%N. 65.54%C. 4.57%H.

(1,4-dimethoxy-3-methylnaphthalen-2-yl)(3-fluoro-4-(trifluoromethyl)phenyl)methanone (**10b**) **(MD501) :** Yield 67%, **^{1}H NMR (500 MHz, Chloroform-*d*) δ** 8.16 (d, J = 8.3 Hz, 1H), 8.07 – 8.06 (m, 1H), 7.71-7.65 (m, 3H), 7.64-7.61 (m, 1H), 7.58-7.54 (m, 1H), 3.93 (s, 3H), 3.81 (s, 3H), 2.23 (s, 3H).**^{19}F NMR (376 MHz, Chloroform-*d*)** δ -61.85 (d, J = 12.7 Hz), -112.51 – -112.74 (m). **^{13}C NMR (126 MHz, Chloroform-*d*) δ** 195.29 (d, J = 1.3 Hz), 160.04 (dq, J = 259.11, 2.0 Hz), 150.74, 149.63 , 142.37 (d, J = 6.4 Hz), 129.74 , 129.52 , 127.87 (q, J = 4.4 Hz), 127.60 , 127.06 , 126.36 , 125.03 (d, J = 3.6 Hz), 123.31 , 122.79 (dq, J = 12.8, 33.2 Hz), 122.60 (d, J = 7.2 Hz), 122.11 (q, J = 273.5 Hz), 117.34 , 117.17 , 63.73 , 61.64 , 12.77. **No HRMS are relationated with this compound.**

General procedure to achieve the Sonogashira cross coupling reaction: The experiments were performed under Argon and dry conditions. Triethylamine (14 mL) was added to benzoyldimethoxy-iodine derivative (1 equiv., 1 mmol) at room temperature. Subsequently, were added in the following order Dichlorobis(triphenylphosphine)palladium(ii) (0.06 eq, 0.06 mmol), Copper iodide (0.01 eq, 0.01 mmol) and Ethynyl(trimethyl)silane (3 equiv., 3.0 mmol). The solution darkens to brown, stirring at room temperature overnight. The reaction was quenched with a 1:1 brine: H_2O mixture and the crude of the reaction was extracted three times with Et_2O. The combined organic extracts were dried over Na_2SO_4, filtered through celite, and concentrated in vacuo to obtain the pure product by flash chromatography using as a mixture of eluents, Cyclohexane: EtOAc.

(1,4-dimethoxy-3-methylnaphthalen-2-yl)(4-((trimethylsilyl)ethynyl)phenyl) methanone trimethyl-silane (**7c**) (**AZ.1.36**)**:** Yield: 100% **^{1}H NMR (400 MHz, $CDCl_3$)** δ 8.14 (d, 1H, *J* = 8.17 Hz), 8.07 (d, 1H, *J* = 8.3 Hz), 7.78 (d, 2H, *J* = 8.50 Hz), 7.61-7.57 (m, 1H), 7.55-7.50 (m, 3H), 7.510 (d, 2H, *J* = 8.55 Hz), 3.91 (s, 3H), 3.80 (s, 3H), 2.20 (s, 3H), 0.250 (s, 9H). **^{13}C NMR (100 MHz, $CDCl_3$)**: δ 195.67, 149.42, 148.25, 135.59, 131.21, 129.67, 128.40, 128.32, 127.59, 126.14 ($CH+C_q$), 125.03, 122.53, 121.64, 121.41, 103.08, 97.56, 62.54, 60.53, 11.75 (CH_3), -1.21. **HRMS (ESI)** calcd. For $C_{25}H_{27}O_3Si$: 403.172398. Found: 403.171498 (MH^+).

(1,4-dimethoxy-3-methylnaphthalen-2-yl)(4-(trifluoromethyl)-3 ((trimethylsilyl)ethynyl)phenyl) methanone (**8c**) **(MD406) :** 85% yield.**^{1}H NMR (400 MHz, Chloroform-d)** δ 8.17 (d, J = 8.2 Hz, 1H), 8.08 (d, J = 8.2 Hz, 1H), 8.05 (s, 1H), 7.81 (d, J = 8.2 Hz, 1H), 7.71 (d, J = 8.2 Hz, 1H), 7.64-7.60 (m, 1H), 7.58-7.54 (m, 1H), 3.93 (s, 3H), 3.80 (s, 3H), 2.23 (s, 3H), 0.24 (s, 9H).**^{19}F NMR (376 MHz, Chloroform-d)** δ -62.88. **^{13}C NMR (100 MHz, Chloroform-*d*)** δ 195.91, 150.65, 149.60, 139.57, 136.00 (q, *J* = 30.6 Hz), 134.49, 129.83, 129.67, 128.79, 127.45, 127.09, 126.47 (q, *J* = 5.1 Hz), 126.23, 123.41, 122.91 (q, *J* = 272.2 Hz), 122.67, 122.51, 122.37 (q, *J* = 1.9 Hz), 102.72, 99.46, 63.61, 61.58, 12.77, -0.55. **No HRMS Spectrum found in the report and from another source.**

((4-((1,4-dimethoxy-3-methylnaphthalen-2-yl)methyl)phenyl)ethynyl)trimethylsilane (**11c**) (**JG31.PUR**) Yield 90%; **^{1}H NMR ($CDCl_3$, 400 MHz):** δ 8.13–8.08 (m, 2H), 7.54–7.49 (m, 2H), 7.35 (d, *J*=8.3 Hz, 2H), 7.05 (d, *J*=8.1 Hz, 2H), 4.27 (s, 2H), 3.86 (s, 3H), 3.82 (s, 3H), 2.22 (s, 3H), 0.24 (s, 9H) ppm.^{13}C **NMR ($CDCl_3$, 100 MHz):** δ150.58, 150.40, 141.23, 132.03, 128.58, 128.02, 128.00, 127.16, 126.94, 125.82, 125.49, 122.46, 122.22, 120.52, 105.15, 93.55, 62.30, 61.37, 32.33, 13.02, -0.03. **No HRMS Spectrum found in the report and from another source.**

General procedure of alkyne Trimethylsilyl (TMS) deprotection: The TMS-protected alkyne derivate (1 equiv., 1.0 mmol) was dissolved in THF (6mL). Then a solution of TBAF (2.3 equiv, 2.3 mmol) in THF (3 mL) was added drop by drop to the original solution, and the

reaction was stirred during 1.5h at room temperature. The reaction was quenched with NH_4Cl (20mL) and extracted with ether (3 x 10 mL). The organic layers were combined, dried on $MgSO_4$ and concentrated in vacuum without heating. Flash-chromatography on silica gel (Cyclohexane: AcOEt).

(1,4-dimethoxy-3-methylnaphthalen-2-yl)(4-ethynylphenyl)methanone (**7d**) (**AZ.1.45**)**:** Yield: 100% ^{1}H NMR **(400 MHz, $CDCl_3$) δ** 8.14 (d, *J* = 8.28 Hz, 1H), 8.07 (d, *J* = 8.18 Hz, 1H), 7.81 (d, *J* = 8.36 Hz, 2H), 7.61-7.52 (m, 4H), 3.91 (s, 3H), 3.81 (s, 3H), 3.25 (s, 1H), 2.22 (s, 3H). **^{13}C NMR (100 MHz, $CDCl_3$) δ** 196.66, 150.47, 149.26, 136.99, 132.45, 130.58, 129.43, 129.36, 127.54, 127.18, 127.12, 126.07, 123.50, 122.62, 122.43, 82.83, 80.64, 63.58, 61.54, 12.75. **HRMS (ESI) calcd. For $C_{22}H_{18}NaO_3$**: 353.114005. Found: 1 353.114815 (MNa).

(1,4-dimethoxy-3-methylnaphthalen-2-yl)(3-ethynyl-4-(trifluoromethyl)phenyl)methanone (**8d**) **(MD434)** (88% yield). **^{1}H NMR (400 MHz, Chloroform-*d*) δ** 8.15-8.17 (m, 1H), 8. 09 (s, 1H), 8.08 – 8.06 (m, 1H), 7.87 (dd, *J* = 8.2, 0.9 Hz, 1H), 7.75 (d, *J* = 8.2 Hz, 1H), 7.64-7.60 (m, 1H), 7.58-7.54 (m, 1H), 3.93 (s, 3H), 3.80 (s, 3H), 3.39 (s, 1H), 2.23 (s, 3H). **^{19}F NMR (377 MHz, Chloroform-*d*) δ** -62.71. **^{13}C NMR (100 MHz, Chloroform-*d*) δ** 195.73, 150.70, 149.62, 139.68, 136.00 (q, *J* = 31.1 Hz), 135.26, 129.71, 129.67, 129.26, 127.50, 127.06, 126.56 (q, *J* = 4.9 Hz), 126.27, 123.35, 122.82 (q, *J* = 272.0 Hz), 122.65, 122.53, 121.32 (q, *J* = 2.1 Hz), 84.21, 78.56, 63.65, 61.59, 12.76. **No HRMS are relationated with this compound.**

2-(4-ethynylbenzyl)-1,4-dimethoxy-3-methylnaphthalene (**11d**)**:** brown liquid. JG0038 (JM0038) (Yield 97%); ^{1}H NMR ($CDCl_3$, 400 MHz): δ7.82–7.94 (m, 2H), 7.23–7.32 (m, 2H), 7.13 (d, *J*=8.1 Hz, 4H), 6.84 (d, *J*=8.1 Hz, 2H), 4.03 (s, 2H), 3.62(s, 3H), 3.58 (s, 3H), 2.78 (s, 1H), 2.00 (s, 3H) ppm;^{13}C NMR ($CDCl_3$, 400 MHz): δ **No good NMR were found (^{1}H and ^{13}C). Have to be Checked in Hard disk.**

General procedure to achieve the Propargylic alcohol Nucleophilic aromatic substitution[3]:

All the experiments were carried out under Argon atmosphere. **1,4-Dimethoxy2-methylnaphtalene-Benzoyl alkyne derivate** (1 equiv., 1.00 mmol) was dissolved in DMF (5 mL). Propargyl alcohol (4 equiv., 4 mmol) and K_2CO_3 (6 equiv., 6 mmol) were added, in the described order. The system was heat up to 60°C and the stirred for 24 hours at the same temperature. Once the time described for the reaction finished, the system was cold down at room temperature (without external agent). Then Et_2O was added and the organic phase was washed with water. Aqueous phase was extracted 3 times with Et_2O. The organic layers were combined, washed with brine, dried over $MgSO_4$ and the solvent was removed under vacuum. Purification was performed by silica gel chromatography CHX/AcOEt 5% up to 20%.

(1,4-dimethoxy-3-methylnaphthalen-2-yl)(4-nitro-3-(prop-2-yn-1-yloxy)phenyl)methanone (**9c**) **(MD396) :**(65% yield). **^{1}H NMR (400 MHz, Chloroform-*d*) δ** 8.16 – 8.15 (m, 1H), 8.07-8.05 (m, 1H), , 7.83 (d, *J* = 1.60 Hz, 1H), 7.81 (d, *J* = 8.3 Hz, 1H), 7.63-7.60 (m, 1H), 7.58-7.53 (m, 1H), 7.44 (dd, *J* = 8.3, 1.6 Hz, 1H), 4.84 (d, *J* = 2.4 Hz, 2H), 3.92 (s, 3H), 3.81 (s, 3H), 2.49 (t, *J* = 2.4 Hz, 1H) 2.24 (s, 3H). **^{13}C NMR (100 MHz, Chloroform-*d*) δ** 195.61, 150.67, 150.61, 149.65, 143.25, 141.11, 129.71, 129.63, 129.02, 128.21, 127.54, 127.07, 126.31, 125.76, 123.28, 122.77, 122.58, 122.54, 115.54, 77.54, 76.47, 63.70, 61.59, 57.43, 12.78. Note: Toluene signals: 137.83, 129.09 (2C), 128.28(2C), 125.38, 21.41. $ClCD_3$. In the ^{1}HNMR of this compound is observed toluene. This compound incorporates 23 Carbons, by the structure should bring 23 signals of Carbon in the ^{13}C-NMR.

[3] S. Raeppel, F. Raeppel, J. Suffert, Synlett (1998), (7), 794-796.

25 signals of C were noted from the 13CNMR. The signals 129.02 and 128.21 belongs to Toluene. **No HRMS are relationated with this compound.**

(1,4-dimethoxy-3-methylnaphthalen-2-yl)(3-(prop-2-yn-1-yloxy)-4 (trifluoromethyl)phenyl)methanone (**10c**) **(MD533) :** (75% yield).**^{1}H NMR (400 MHz, Chloroform-*d*) δ** 8.16-8.14 (m, 1H), 8.08 – 8.05 (m, 1H), 7.76 (s, 1H), 7.66 (d, J= 7.68 Hz, 1H), 7.61-7.53 (m, 2H), 7.39 (d, J = 7.9 Hz, 1H), 7.39 (d, J = 8.0 Hz, 1H), 4.81 (d, J = 2.4 Hz, 2H), 3.92 (s, 3H), 3.82 (s, 3H), 2.47 (t, J = 2.4 Hz, 1H), 2.24 (s, 3H).**^{19}F NMR (376 MHz, Chloroform-*d*) δ** -62.73. **^{13}C NMR (100 MHz, Chloroform-*d*) δ** 196.29, 155.78 (q, J = 1.5 Hz), 150.56, 149.49, 141.36, 130.15, 129.58, 127.84 (q, J = 5.1 Hz), 127.36, 127.10, 126.19, 123.96 (q, J = 48.23 Hz), 123.38, 122.76 (q, J = 251.06 Hz), 122.60, 122.58, 122.50, 113.21, 77.07, 63.66, 61.57, 56.66, 12.77. **Signal due to one carbon obscured or overlapping. Note: 24 Carbons integrate this structure. Due the lack of any element of symmetry, 24 signals are expected. Only 23 signals are noted. All the aromatic C_q (9) noted (without taking account CF_3 and C=O), from 7 CH, 7CH signals are noted, there is a carbon signal of the alkyne is overlapped in the CDCl3 peaks. No HRMS are relationated with this compound.**

Synthesis of 2-(4-iodobenzyl)-3-methylnaphthalene-1,4-dione (**11a**) **(JG08) through Kochi-Anderson Reaction**[4]**:** Menadione (1 equiv., 5.81 mmol) and 4-Iodophenylacetic acid (2 equiv., 12.2 mmol) were dissolved in a mixture 3:1 acetonitrile (173 mL) and water (58 mL). The mixture was heated to 85°C and silver nitrate (0.35 equiv., 2.03 mmol) was added. Then, ammonium persulfate (1.3 equiv., 7.55 mmol) was dissolved in a mixture MeCN: water (3:1) and added dropwise. The reaction was stirred for 4.5h at 85°C. MeCN was removed by reduced pressure, Ethyl acetate was added, and the organic phase was washed with water several times. The organic phase was dried over Mg_2SO_4 and the solid was discard by filtration. The excess of the liquid was removed by reduced pressure, and the crude of the reaction was purified by flash chromatography (eluent: toluene). Yellow crystals were obtained and recrystallized in pure *n*-hexane to obtain the pure product (bright yellow crystals).Yield 81 %; m.p. (*n*-hexane) = 130-131 °C; **^{1}H NMR ($CDCl_3$, 400 MHz):** δ 8.11–8.06 (m, 2H), 7.73–7.68 (m, 2H), 7.58 (d, *J*=78.36 Hz, 2H), 6.98 (d, *J*=8.44 Hz, 2H), 3.97 (s, 2H), 2.23 (s, 3H) ppm; **^{13}C NMR ($CDCl_3$, 100 MHz)**: δ185.2, 184.53, 144.7, 144.59, 137.75, 137.68, 133.58, 132.07, 131.92, 130.62, 126.49, 126.34, 91.65, 32.01, 13.3 ppm; **IR (neat, cm^{-1})**: 1659.5 (s, C=O), 1616.9 (s, C=O), 1590.1(s, C=C), 487.0 (s, C-I); **HRMS (ESI):** 426.9577 m/z (cal. $C_{18}H_{13}IKO_2$ 426.9592 m/z); **Elemental analysis**: C 55.54%, H 3.38% (cal. C 55.69%,H 3.38%).

General procedure of deprotection and oxidation of 3-benzyl-menadione derivatives: the 1,4-dimethoxy-2-methylnaphthaleneBenzoyl/Benzyl derivative (1 equiv., 1 mmol) was dissolved in acetonitrile (24 mL) water (8 mL), cerium ammonium nitrate (2.5 equiv., 2.5 mmol) was added portion wise at room temperature to give a yellow-orange solution. The reaction mixture was stirred for 3h. Acetonitrile was removed under reduced pressure and the residue was extracted with DCM (2x), the organic layers were washed with brine (1x) and dried over Na_2SO_4. A flash chromatography was performed (cyclohexane: EtOAc 99.8:0.2 to 90:10).

2-(4-ethynylbenzoyl)-3-methylnaphthalene-1,4-dione (**7**) (**AZ.1.39**)**:** Yield: 66%. **^{1}H NMR (400 MHz, $CDCl_3$) δ** 8.18-8.16 (m, 1H), 8.08-8.06 (m, 1H), 7.87 (d, *J* = 8.64 Hz, 2H), 7.82-7.75 (m, 2H), 7.60 (d, *J* = 8.68 Hz, 2H), 3.29 (s, 1H), 2.06 (s, 3H). **^{13}C NMR (100 MHz, $CDCl_3$) δ** 192.91, 184.68, 183.34, 144.23, 143.99, 135.29, 134.26, 134.17, 132.73, 131.87, 131.50, 128.97, 128.40, 126.76, 126.44, 82.54, 81.33, 8.85. **HRMS (ESI) calcd. for $C_{20}H_{12}NaO_3$** 323.067865. Found : 323.067180.

[4] J.M. Anderson andJ.K. Kochi, J.Am.Chem.Soc.,92,1651(1970).(I don't find from 1965 as is remarked in synthetic scheme 2)

2-(3-ethynyl-4-(trifluoromethyl)benzoyl)-3-methylnaphthalene-1,4-dione (**8**) **(MD65):** (96% yield), pale yellow solid.**^{1}H NMR (400 MHz, Chloroform-*d*)** δ 8.20 – 8.18 (m, 1H), 8.09 (s, 1H), 8.08 – 8.06 (m, 1H), 7.95 (d, *J* = 8.18 Hz, 1H), 7.84 – 7.77 (m, 3H), 3.44 (s, 1H), 2.09 (s, 3H). **^{19}F NMR (376 MHz, Chloroform-*d*)** δ -62.86.**^{13}C NMR (100 MHz, Chloroform-*d*)** δ 192.26, 184.39, 183.29, 144.99, 143.17, 138.06, 136.71 (q, *J*= 31.27 Hz), 134.87, 134.48, 134.32, 131.84, 131.36, 128.65, 126.90 (q, *J* = 4.8 Hz), 126.90, 126.48, 122.63 (q, *J* = 273.1 Hz), 121.79 (q, J=2.12 Hz) 84.77, 78.23, 13.62. **No HRMS are relationated with this compound.**

2-methyl-3-(4-nitro-3-(prop-2-yn-1-yloxy)benzoyl)naphthalene-1,4-dione (**9**) **(MD43):**yellow crystals (65% yield).**^{1}H NMR (400 MHz, Chloroform-*d*) δ** 8.20 – 8.18 (m, 1H), 8.08 – 8.06 (m, 1H), 7.89 (d, *J* = 1.6 Hz, 1H), 7.86 (d, *J* = 8.3 Hz, 1H), 7.85 – 7.78 (m, 2H), 7.51 (dd, *J* = 8.32, 1.6 Hz, 1H) 4.91 (d, *J* = 2.4 Hz, 2H), 2.57 (t, *J* = 2.4 Hz, 1H), 2.10 (s, 3H). **^{13}C NMR (100 MHz, Chloroform-*d*) δ** 192.12, 184.34, 183.24, 150.84, 144.97, 143.68, 143.17, 139.23, 134.53, 134.36, 131.81, 131.35, 126.94, 126.44, 126.04, 122.32, 115.03, 77.89, 76.39, 57.51, 13.66. **HRMS (ESI) calcd. for $C_{21}H_{14}NO_6$:** 376.081564. Found: 376.082321 (MH^+). **Elemental analysis** C 67.01%, H 3.62%, N 3.75 %. (cal. C 67.20%, H 3.73%, N 3.73%).

2-methyl-3-(3-(prop-2-yn-1-yloxy)-4-(trifluoromethyl)benzoyl)naphthalene-1,4-dione (**10**) **(MD134) :** Yield 64%. **^{1}H NMR (400 MHz, Chloroform-*d*) δ** 8.20 – 8.17 (m, 1H), 8.08 – 8.06 (m, 1H), 7.84 – 7.77 (m, 3H), 7.69 (d, *J* = 8.08, 1H), 7.47 (d, *J* = 8.00, 1H) 4.87 (d, *J* = 2.4 Hz, 2H), 2.53 (t, *J* = 2.4 Hz, 2H), 2.09 (s, 3H). **^{13}C NMR (100 MHz, Chloroform-*d*) δ** 192.72, 184.50, 183.28, 156.05 (q, J 1.49 Hz), 144.61, 143.57, 139.56, 134.41, 134.28, 131.84, 131.43, 128.15 (q, J = 5.1 Hz), 126.87, 126.43, **124.62 (q, J= 31.67 Hz), 122.65(q, J= 271.4 Hz),** 122.10, 112.70, 77.05, 56.74, 13.63. Not NMR data description was done before about this product. In Enovalys from Maxime, experiments describing this compound as a product are MD134 and MD126. No ^{19}F are done. No HRMS. NMR was done very diluited and is difficult to make the assignation of the two quartets between 124 and 122 ppm. One signal of the alkyne is overlapped in the ClCD3 peaks.

2-(4-ethynylbenzyl)-3-methylnaphthalene-1,4-dione (**11**)**(JG-43)** Yield 72 % m.p. (n-hexane) = 146°C -147°C; **^{1}H NMR (CDCl3, 400 MHz):** δ 8.10–8.07 (m, 2H), 7.73–7.69 (m, 2H), 7.39 (d, *J*=8.16 Hz, 2H), 7.18 (d, *J*=8.24 Hz, 2H), 4.03 (s, 2H), 3.03 (s, 1H), 2.23 (s, 3H) ppm; **^{13}C NMR ($CDCl_3$, 100 MHz):** δ 185.21, 184.53, 144.74, 144.65, 138.96, 133.55, 132.39, 132.07, 131.93, 128.56, 126.49, 126.32, 120.22, 83.40, 77.05, 32.35, 13.30. **IR (neat, cm-1)**: 3278.4 (s, Csp-H), 2105.7 (s, C≡C), 1659.5 (s, C=O), 1616.9 (s, C=O), 1590.1 (s, C=C). **HRMS:** 325.0618 m/z (cal. $C_{20}H_{14}KO_2$ = 325.0625 m/z); **Elemental analysis:** C 83.86%, H 4.92% (cal. C 83.90%, H 4.93%).

Irradiation experiments for model photoreaction:

The photochemical reaction of P_TM52 with Benzophenone and Enone derivatives was carried out in a pyrex tube (filter for hν < 300 nm) at a final concentration of 0.1 M acetonitrile. The reaction was irradiated to 350nm 8 RPR-3500A lamps of 200W Rayonet photochemical reactor at a distance of 7cm from the light source at 5°C for 24 hours. Finally, the reaction was analysed by field-desorption mass spectrometry (FD-MS).

Standardization of UV crosslinking parameters using nMet:

We first analysed the extinction coefficient εmax and ʎmax of all the PD-ABPP by UV-Vis absorption spectrophotometry (Fig. supplementary information). Since the maximum of absorption ʎmax is about 340 nm for probes 3, 4, 6, 7 and 320 nm for probe 2 and 8, and 350

nm for benzophenone; we selected a closest optimal wavelength of 365 nm as the light excitation source for studying the corresponding photoreaction as it is likely in the proximity of max of the probe and doesn't damage the protein as the light excitation source for studying the corresponding photoreaction. The photoreaction of nMet and probes was performed using 2 different light sources: 1. photoreactors with 350 nm UV lamp of Rayonet photochemical reactor with 224W of intensity; 2. a UV monochromator with 350 nm and 1000W high intensity. Various factors such as photoirradiation wavelength, solvent, and t distance of sample from light source, the exposure time to photoirradiation of the sample and the presence or the absence of oxygen were varied and analysed. The covalently crosslinked product was confirmed by TLC and NMR analysis. Following are the reaction conditions: 1 equiv. of PD-ABPP + 5 equiv. of P_TM52 i.e. (100µl of 20mM PD-ABPP in ACN)+ (100µl of 1000mM PD-ABPP in ACN), total 200µl in oxygen free condition. (JG43 and P_TM40 takes more time to solubilize, vortex and ultrasonication helps)

Inhibition potency of naphthoquinones towards human GR and Plasmodium falciparum GR

The inhibition assays for hGR and PfGR by naphthoquinones was a standard GR assay (T Müller et al., 2011) with 100 µM NADPH and 1mM GSSG in in GR buffer (100 mM potassium phosphate buffer, 200 mM KCl, 1 mM EDTA, pH 6.9) at 25 °C in a 1 ml-cuvette using the inhibitor concentrations within range of 0 to 100 µM. The final concertation of DMSO in assay was 1%. Initial rates of NADPH oxidation by hGR (8 mU or 0.85 pmol) or PfGR (6.5 mU or 0.97 pmol) was monitored at 340 nm with a Cary 50 spectrophotometer.

Glutathione reductase-catalyzed naphthoquinone reductase activity

In comparison to the standard GR assay (T Müller et al., 2011) where GSSG is used as a substrate for the glutathione disulfide reductase the1,4-Naphthoquinone was used as a substrate instead of GSSG albeit with a 1000-fold increased enzyme concentration. The 1, 4-naphthoquinone reductase activity was evaluated by recording the initial velocities of NADPH oxidation in the presence of increasing naphthoquinone concentrations (0 – 300 µM) in GR buffer (100 mM potassium phosphate buffer pH 6.9, 200 mM KCl, 1 mM EDTA) with 100 µM NADPH and 0.5 µM PfGR (3.9 U) with final 1 % DMSO concentration in a total volume of 1 ml. For the determination of Km and Vmax values, the steady-state rates were fitted by using nonlinear regression analysis software (Kaleidagraph) to the Michaelis-Menten equation. From these values, the turnover number kcat and the catalytic efficiency kcat/KM were calculated.

Photoreaction of peptides and proteins

Peptides and protein were photoirradiated for with 365 nm light with a UV monochromator of 1000 W high intensity. For peptide crosslinking a stock solution of GSH was prepared in 20 mM PBS pH=6.9 and probe 6 in 100% ACN. Next, 3 mM GSH was added to 600 µM probe 6 in a mixture of 1:1 ACN and 10 mM PBS in 200 µl volume. The reaction was deoxidized with a vacuum-argon cycler with longer argon cycles (7x15s) than vacuum cycles (7x <6s) in-between to avoid ACN evaporation. The mixture was photoirradiated for 10 min and the next day the solution was analysed by HPLC-MS.

Protein photoirradiation for crosslinking adduct formation study was performed with a mixture of 6 µM hGR (or BSA - used as negative control) with 6 µM probe 6 in 200 µl 10 mM PBS buffer pH=6.9 with 2% ACN. For reactions in which hGR redox cycled the probe 52.5 µM of NADPH was added additionally to induce redoxcycling. The reaction was deoxidized with a vacuum-argon cycler with 7x argon and vacuum cycles (10s each). Subsequently, the mixture

was photoirradiated for 8 min and afterwards 100 µl of 3x Laemmli buffer was added. The next day the samples were separated on 10% SDS-Page gels, stained with Coomassie solution and de-stained according to published protocol (Simpson, 2007). Protein bands were cut out and subjected to trypsin digestion and HPLC-MS analysis.

Biotin pulldown

Biotin-protein adducts we pulled down by binding to Streptavidin agarose beads (Pierece). Prior to use the beads were washed 5x with 1.5 ml washing buffer (47 mM sodium based PBS, pH=6.9) (5000 g, 1 min, RT). Unspecific sites on the Streptavidin agarose beads were blocked by incubating the beads for 1.5 hour at 4°C with 0.05% Tween20. Overnight click reactions were diluted with 47 mM PBS to 1 ml volume and incubated for 2h with beads at RT. The suspension was washed 3x with washing buffer, 1x with washing buffer + 0.05% Tween20 and 1x washing buffer + 0.25 % SDS (4500 g, 1 min, RT). Bound proteins were eluted at 96°C for 10 min with 40 µl Laemmli buffer. Subsequently, eluted proteins were separated on 10% SDS-PAGE gel, cut and subjected to HPLC-MS analysis.

HPLC-MS and nanoLC-MS/MS analysis

Protein preparation for in gel digestion

The gel pieces were successively washed with 50 µL of 25 mM NH4HCO3 and 50 µL of acetonitrile (three times), and dehydrated with 100 µL of acetonitrile before reduction in the presence of 10 mM DTT in 25 mM NH4HCO3 (1h at 57°C) and alkylation in the presence of 55 mM iodoacetamide in 25 mM NH4HCO3. For tryptic digestion, the gel pieces were resuspended in 2 volumes of trypsin (12.5 ng/µL; Promega V5111) freshly diluted in 25 mM NH4HCO3 and incubated overnight at 37°C. The digested peptides were then extracted from the gel in a buffer containing 34.9% H2O, 65% acetonitrile, and 0.1% HCOOH, the acetonitrile was removed by evaporation and peptides analyzed by nanoLC-MS/MS.

NanoLC-MS/MS analysis.Peptide digests analysis was performed on a nanoACQUITY Ultra-Performance-LC (Waters, Milford, MA, USA) coupled to a TripleTOF 5600+ mass spectrometer (Sciex, Framingham, USA).

The samples were trapped on a 20 x 0.18 mm, 5 µm Symmetry C18 precolumn (Waters Corp.), and the peptides were separated on a nanoEase M/Z Peptide BEH C18 Column, 130Å, 1.7 µm, 75 µm X 150 mm. The solvent system consisted of 0.1% formic acid in water (solvent A) and 0.1% formic acid in acetonitrile (solvent B). Trapping was performed during 3 min at 5 µL/min with 99% of solvent A and 1% of solvent B. Elution was performed at a flow rate of 300 nL/min, using 1-40% gradient (solvent B) over 35 min at 60°C followed by 65% (solvent B) over 5 min.

The mass spectrometer was operated in positive mode, with the following settings: ion spray voltage floating (ISVF) 2300 V, curtain gas (CUR) 25 psi, interface heater temperature (IHT) 75°C, ion source gas 1 (GS1) 2 psi, declustering potential (DP) 100 V. Information-dependent acquisition (IDA) mode was used with top 5 MS/MS scans. The MS scan had an accumulation time of 250 ms on m/z [400-1250] range and the MS/MS scans 100 ms m/z [150-1600] range in high sensitivity mode. Switching criteria were set to ions with charge state of 2-4 and an abundance threshold of more than 150 counts, exclusion time was set at 12 s. IDA rolling

collision energy script was used for automatically adapting the CE. Mass calibration of the analyser was achieved using peptides from digested BSA. The complete system was fully controlled by AnalystTF 1.6 (AB Sciex).

Proteins identification

Mass data collected during nanoLC-MS/MS were searched using a local Mascot server (Matrix Science, London, UK) against an in-house-generated protein database composed of protein sequences of hGR and BSA using an in-house database generation toolbox (https://msda.unistra.fr). Searches were performed with selected modification (On each 20 encoded proteinogenic aminoacids either +375.07 Da, +374.07 Da, +357.07 Da, 356.07 Da or 358.07 Da), trypsin was selected as the enzyme, carbamidomethylation of cysteine (+57 Da) and oxidation of methionine (+16 Da) were set as variable modifications, three miscleavages were tolerated and mass tolerances on precursor and fragment ions of 20 ppm and 0.07Da were used, respectively. Modified peptides were manually validated.

LC-MS analysis

LC/MS analyses were performed using an Agilent 1100 series LC coupled to a MicrOTOF-Q (Bruker Daltonics, Bremen, Germany) or to a maXis II Q-TOF mass spectrometer (Bruker)

The mass spectrometer was operated in positive mode with a capillary voltage of 4,500 V. Acquisitions were performed on the mass range 200-1850 m/z. Calibration was performed using the singly charged ions produced by a solution of Tune mix (G1969-85000, Agilent, U.S.A.). Data analysis was performed by using Compass DataAnalysis 4.3 (Bruker Daltonics).

GSH and probe6 crosslinking reaction was directly injected onto a HPLC connected to Micro-QTOF (Bruker). Compounds were separated on a XBridge Peptide BEH C18 Column (300Å, 3.5 µm, 2.1 mm X 250 mm) column. The gradient was generated at a flow rate of 250 µL/min using 0.1% trifluoroacetic acid (TFA) in water for mobile phase A and acetonitrile containing 0.08% TFA for mobile phase B at 60°C. B was raised from 5 to 85% in 45 min.

Click reaction products were analysed by Micro-QTOF or maXis II QTOF mass spectrometer (Bruker Daltonics, Bremen, Germany) coupled to HPLC. Samples were injected on a XBridge Peptide BEH C18 Column, 300 Å, 3.5 µm, 2.1 mm X 250 mm column. The gradient was generated at a flow rate of 250 µL/min using 0.1% trifluoroacetic acid (TFA) in water for mobile phase A and acetonitrile containing 0.08% TFA for mobile phase B at 60°C. B was raised from 20 to 80% in 45 min. UV and MS chromatograms were analysed by Hystar Bruker Data Compass program.

Characterization of clickability property of PD probes using azide models

Characterization of clickability property of PD probes using rhodamine azide in aqueous conditions:

The click reaction between probes and rhodamine azide was performed in a specialized dark quartz cuvette under strict inert conditions. First, in a separate glass tube, CuI complex was

formed by preincubating 36µM of each $CuSO_4$, THPTA and TCEP reductant (TCEP stock of 1500 µM prepared in 75%:25% H_2O: DMF solution) followed by argon and vacuum cycles and incubation for 35-45 minutes. In a special black quartz cuvette, alkyne and azide were premixed in H_2O followed by argon vacuum cycles. Finally, the click reaction was initiated by addition of CuI complex to the premix of alkyne and azide followed by argon vacuum cycles to maintain strict oxygen free conditions. At T_0 the absorbance spectra of the reaction was recorded on UV-vis spectrophotometer Cary 50. Further at T_{30}, T_{60} and T_{90} one dose of 20 minutes preincubated Cu(I) complex was administered in the cuvette using syringe, followed by quick argon vaccum cycles and recording of the absorbance spectra. At T_{120} the fluorometric analysis of the 20 times diluted reaction was recorded and the HPLC-MS analysis was performed on C18 column of MicroTof-Q. The sapmles were run for 60 minutes cycle in a gradient of ACN/TFA 0.08% and H_2O with 0.250 mL/min flow rate and at 60°C in such a way that it was 20% ACN upto 5 minutes, further increasing the concentration of ACN up to 60% until 40 minutes and 85% until 50 minutes followed by storage of sample at 45°C as indicated in (fig S3.16). The mass of probes and click products are in (Fig. S3.17 to S3.25)

Following table represents exact details of the click reaction conditions: * $CuSO_4$, THPTA and ligand were made freshly just before the reaction. Avoid freezing and thawing of Alkyne and Azide stocks.

Click reaction in aqueous conditions	**stock conc.**	**vol. of stock in reaction**	**final conc. in reaction**	**Solvent**
	C1 (**µM**)	V1 (**µL**)	C2 (**µM**)	
Probe 7, 8, 9, 10	1200	30	**36**	**DMF**
Rhodamine azide	1200	30	**36**	**DMF**
THPTA	1500	60 or 4x15	**90**	**H_2O**
Copper sulphate	1500	60 or 4x15	**90**	**H_2O**
TCEP	1500	60 or 4x15	**90**	**75:25 (GR buffer: DMF)**
H2O	NA	880	NA	**H_2O**

Characterization of clickability property of PD probes using azide models in PBS buffer conditions.

Copper prereduction for a reaction in PBS buffer was achieved by mixing first 132 µM to 660 µM $CuSO_4$ with 132 µM to 1.32 mM ligand (THPTA or BCDA) in H_2O. TCEP stock solution is prepared in 75%:25% H_2O:DMF solution. After addition of TCEP to a final concentration of 132 µM the mixture is deoxidized for 10 min with vacuum-argon cycling and incubated additionally for 30 min (40 min in total). For probe 2 and rhodamine or biotin azide click reaction in buffer 6 to 24 µM alkyne and azide have been mixed in 11.25 to 47 mM PBS with final 6.6% DMF (for RA) or 3.3 % ACN (for BA) concentration. The substrates were deoxidized by vacuum-argon cycling and started by addition of 40 min incubated Cu (I) complex Final organic solvent concentration in reaction was 7.2 % for DMF or 4.4 % for ACN. Reaction was held for 2h or ON in 26°C and subjected to HPLC-MS analysis.

Click reaction conditions in aqueous/phosphate buffer conditions	stock conc.	vol. of stock in reaction	final conc. in reaction	Solvent
	C1 (**µM**)	V1 (**µL**)	C2 (**µM**)	
Probe 7	720-180	3.3	24 - 6	DMF
Rhodamine/Biotin azide	720-180	3.3	24 - 6	DMF
THPTA/BCDA	16500 - 330	8	1320 - 66	H_2O
Copper sulphate	8250-1650	8	660 - 132	H_2O
TCEP	1650	8	132	75:25 (H_2O: DMF)
PBS or H_2O	NA	89.4	NA	H_2O

Antimalarial activity

Antimalarial activity is represented by IC_{50} the concertation of biomolecule at which the half of the parasites survive. The antimalarial activity of PD-ABPP on asexual stages of parasites was evaluated on Dd2 a chloroquine-resistant strain of P. falciparum by IC_{50} analysis of 72 h PD-ABPP treated 3 h old ring stage of parasite. The IC_{50} protocol was a combination of ring survival assay (Ariey et al., 2014; B Witkowski et al., 2013) and fluorescent staining based IC_{50} assay that stains parasite DNA as reported earlier (Beez et al., 2011; Smilkstein et al., 2004). For this, the mature schizont stage of parasites of highly synchronous parasite cultures was separated using 60% percoll gradient and the mature segmented schizonts were incubated for 3 hours for reinvasion. The ring stage parasites produced during these 3 hours were then synchronized with 5% sorbitol to kill mature stages. These 3h old rings were exposed to the PD-ABPPs for 72h drug with 1/3rd decreasing concentrations in microtiter plates (0.5% parasitemia, 1.5% haematocrit for SYBR green assay). Each inhibitor was analysed in a three-fold serial dilution in duplicates in three independent experiments. Parasite replication was assessed by fluorescent SYBR® green staining of parasitic DNA (Smilkstein et al., 2004) as previously described (Beez et al., 2011). PD was used as a control. After 72 hours, the parasites were frozen at -80°C overnight, followed by thawing and the fluorescent SYBR green assay for determining the percentage survival of parasites via fluorescence analysis on Promega plate reader at 591nm wavelength. The parasitemia at T0 and T72 was determined by microscopic blood smear analysis after Giemsa staining to follow the pattern of growth and multiplication factor of parasites over time and IC_{50} values were calculated using Prism (GraphPad, log(inhibitor) vs. normalized response – Variable slope).

Supplementary information:

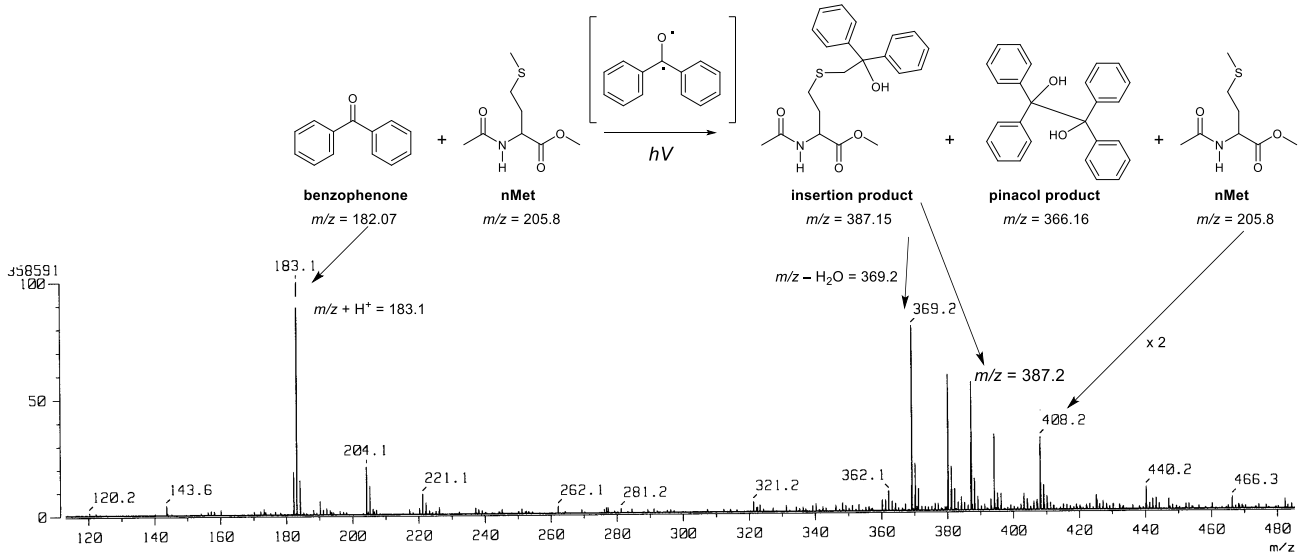

Figure S.3. 1. FD-MS analyses of the reaction mixtures of benzopheneone in the presence of the diprotected methionine P_TM52 (panel A) in the absence of UV-irradiation, (panel B) upon photoirradiation.

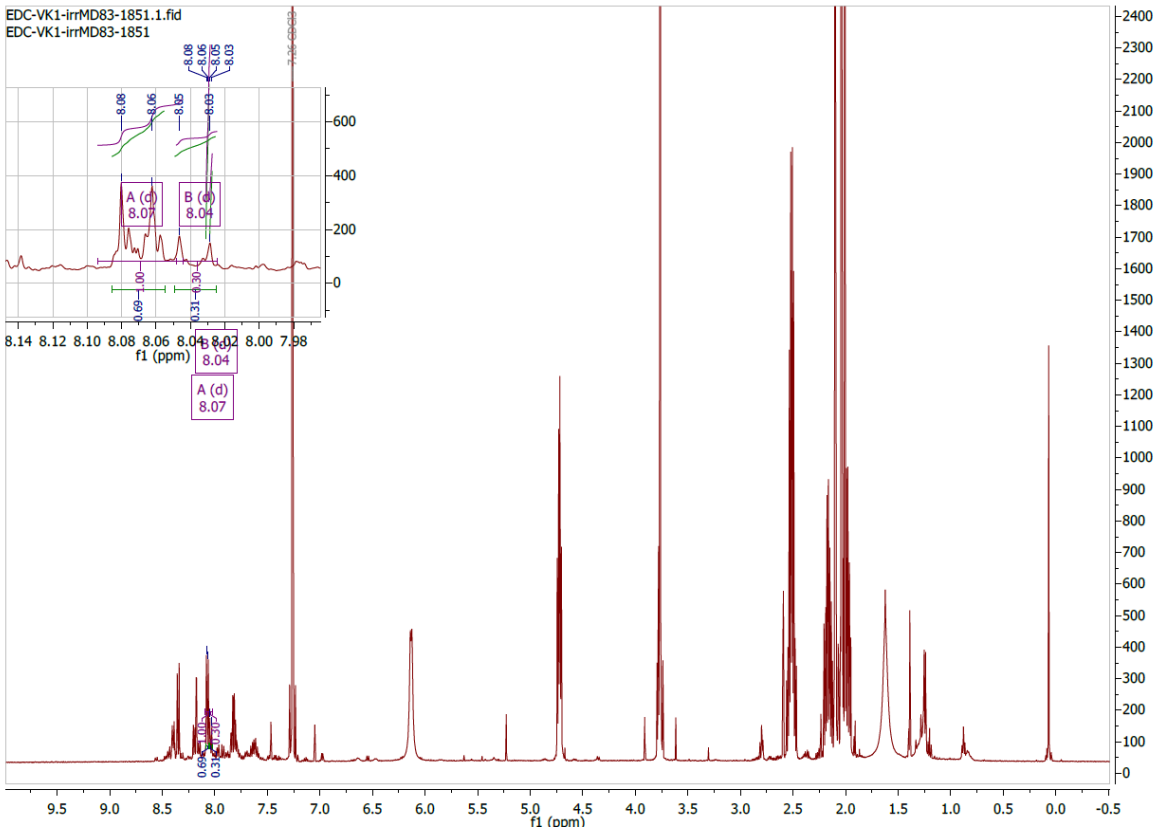

Figure S.3. 2. NMR spectras, Photoreaction between probe 6 and nMet

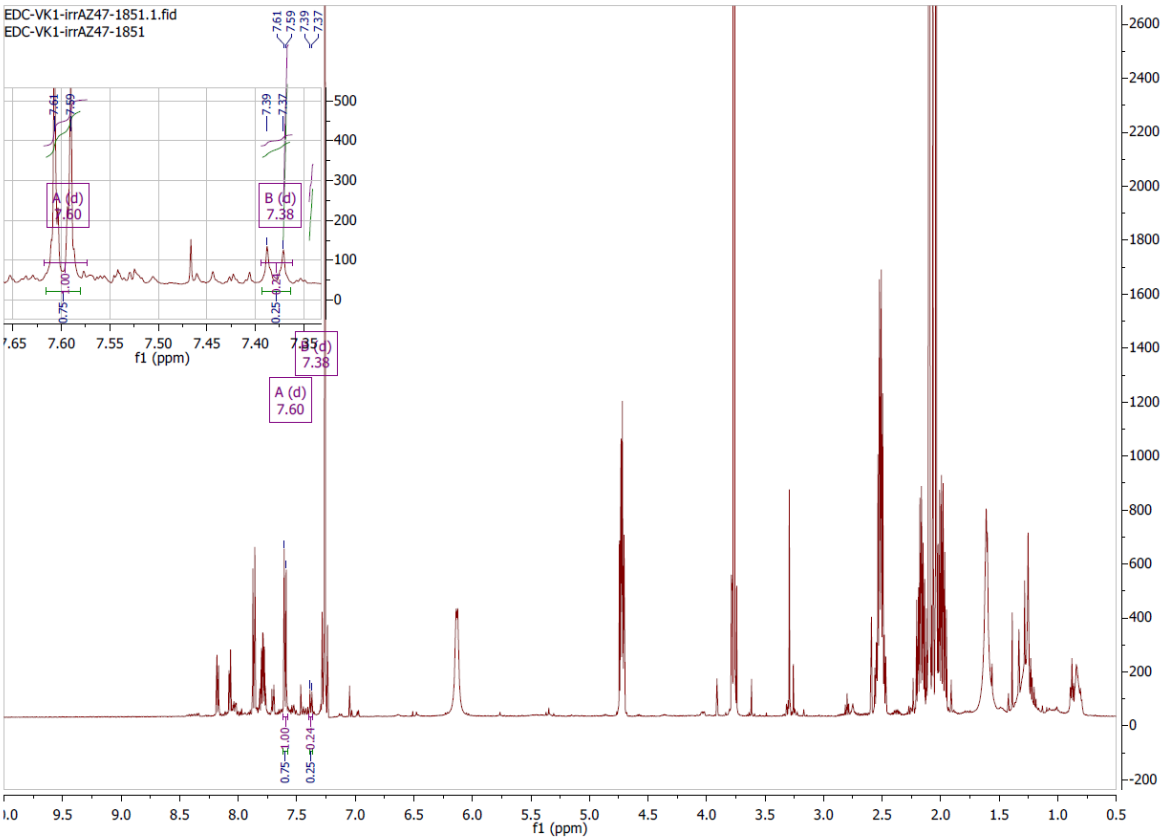

Figure S.3. 3. NMR spectra for photoreaction between nMet and probe 7

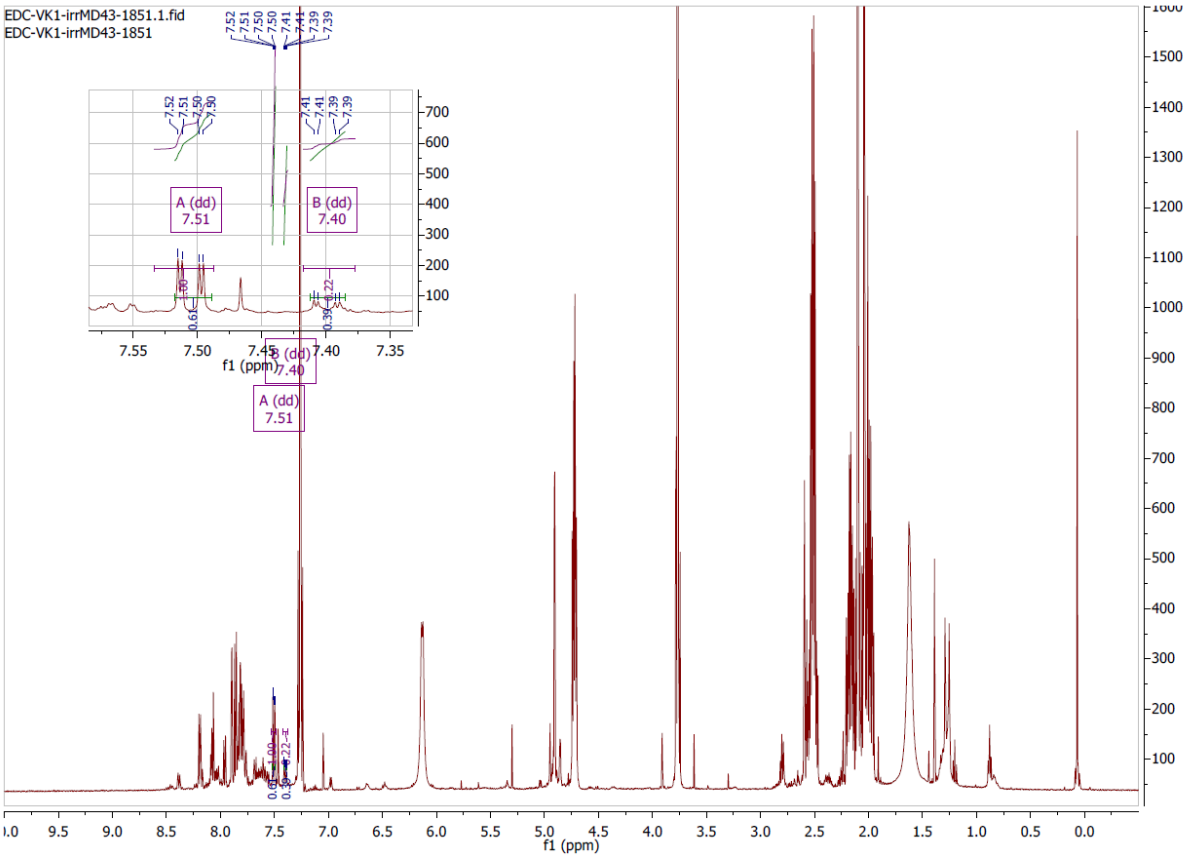

Figure S.3. 4. NMR spectra for photoreaction between nMet and probe 9

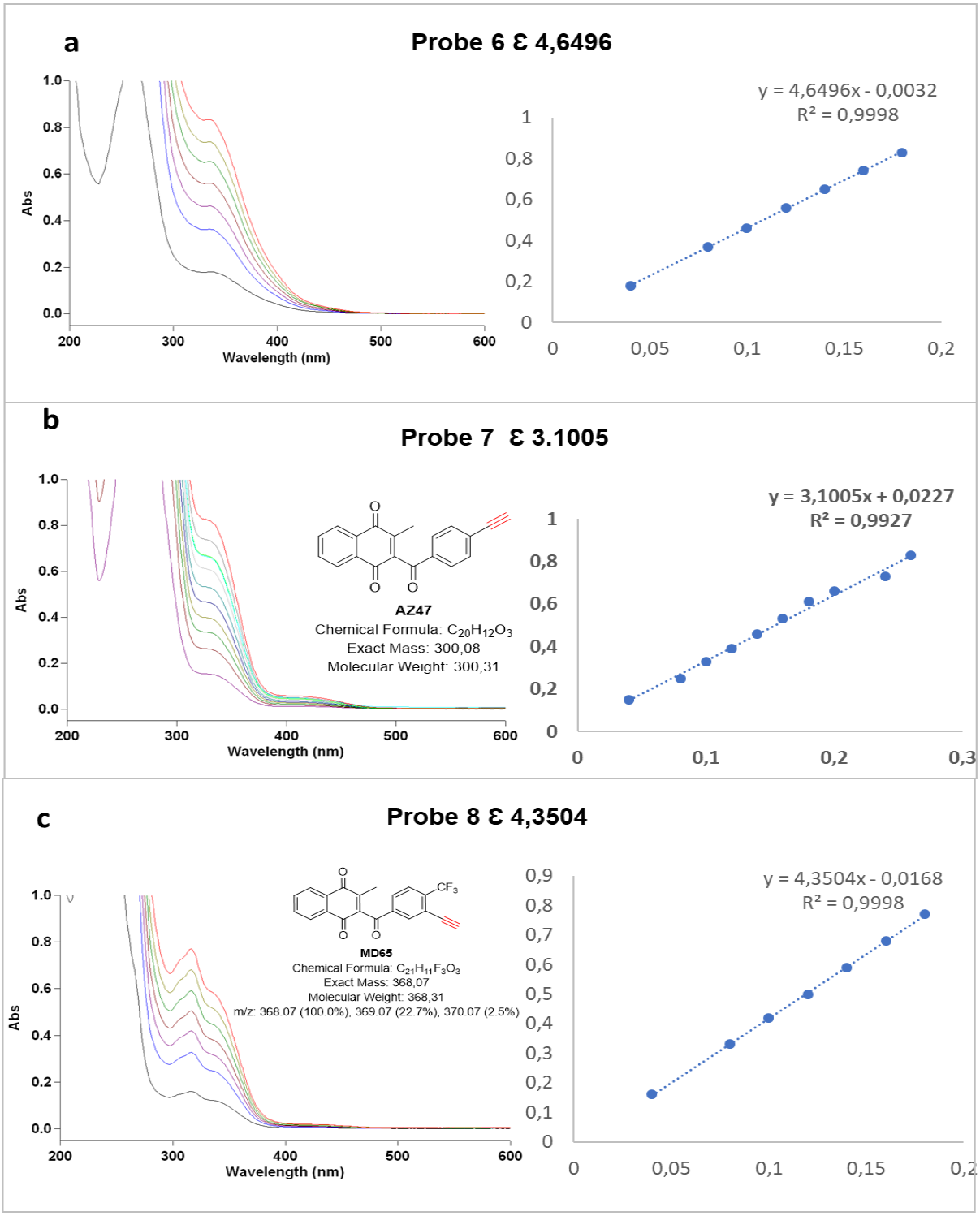

Figure S.3. 5. US-Vis spectrometry indicating εmax and λmax of probe 6 (a), probe 7 (b) and probe 8 (c) in 20% ACN

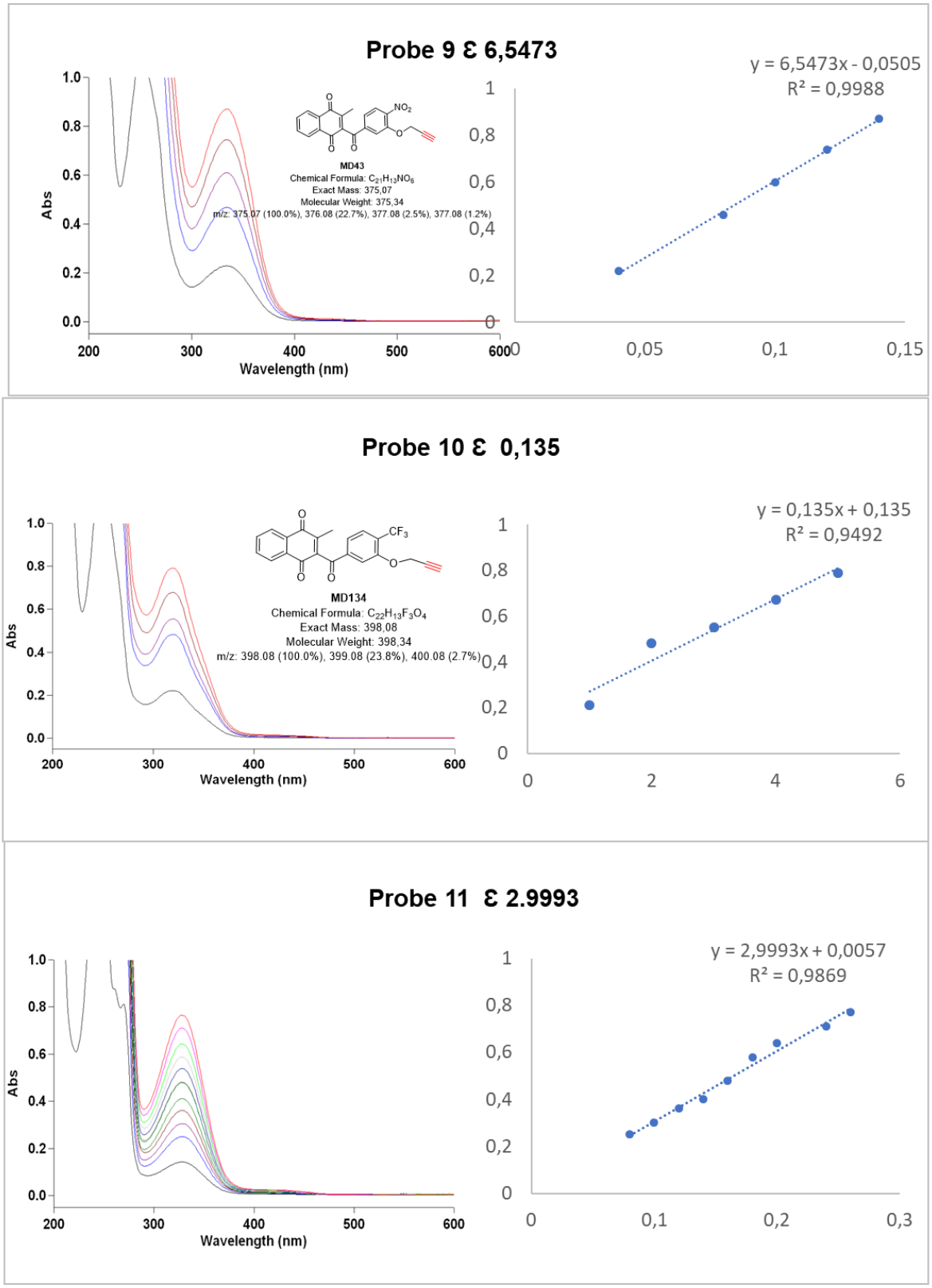

Figure S.3. 6. US-Vis spectrometry indicating εmax and λmax of probe 9 (a), probe 10 (b) and probe 11 (c) in 20% ACN

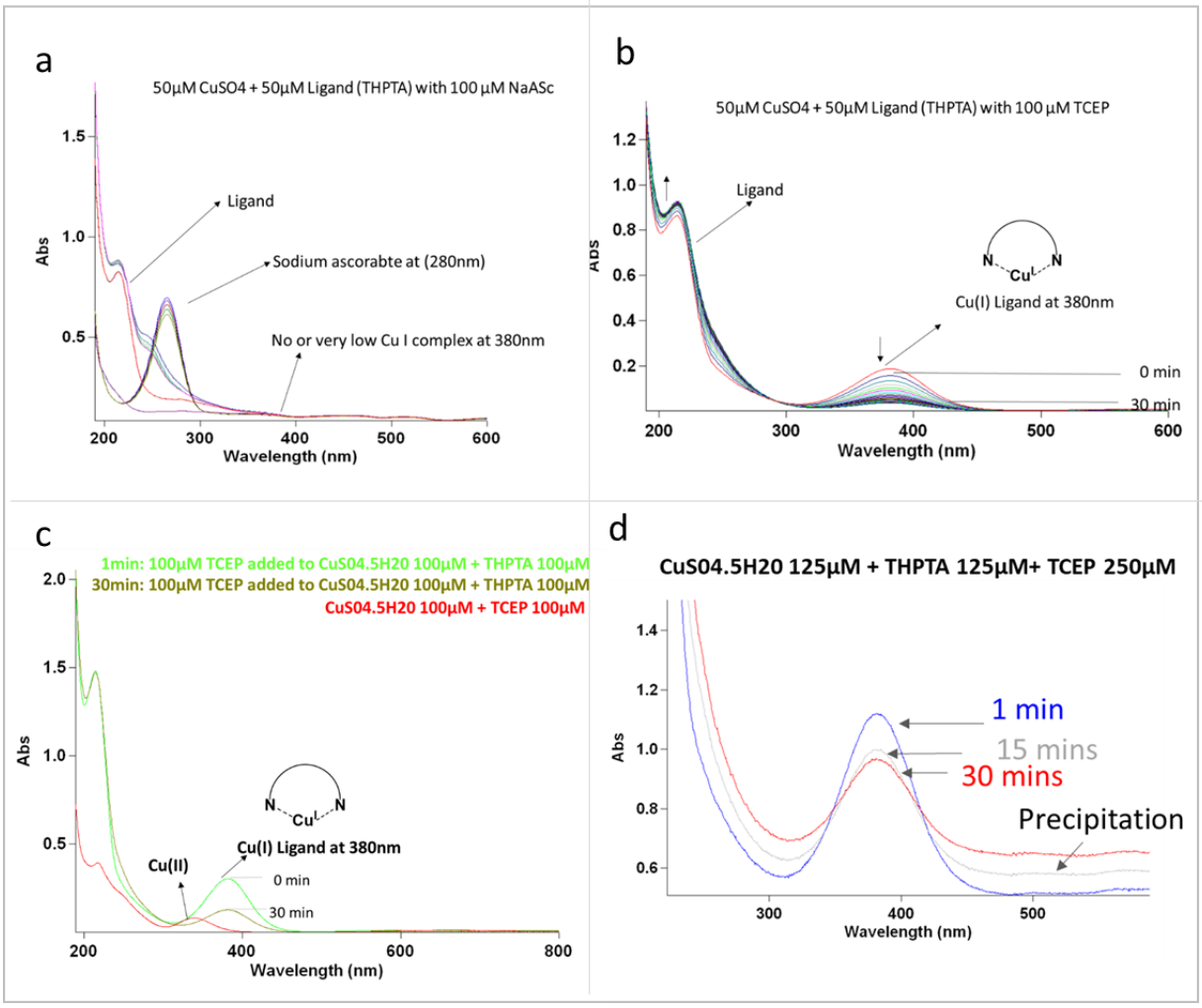

Figure S.3. 7. CuI complex formation with NaASc (a) and TCEP (b) as per UV-vis spectrometry. (c) Comparision between Cu(I) species at 380nm and Cu (II) species at ~350nm. (d) Precipitation of CuI complex takes place above especially with excess TCEP (~250µM)

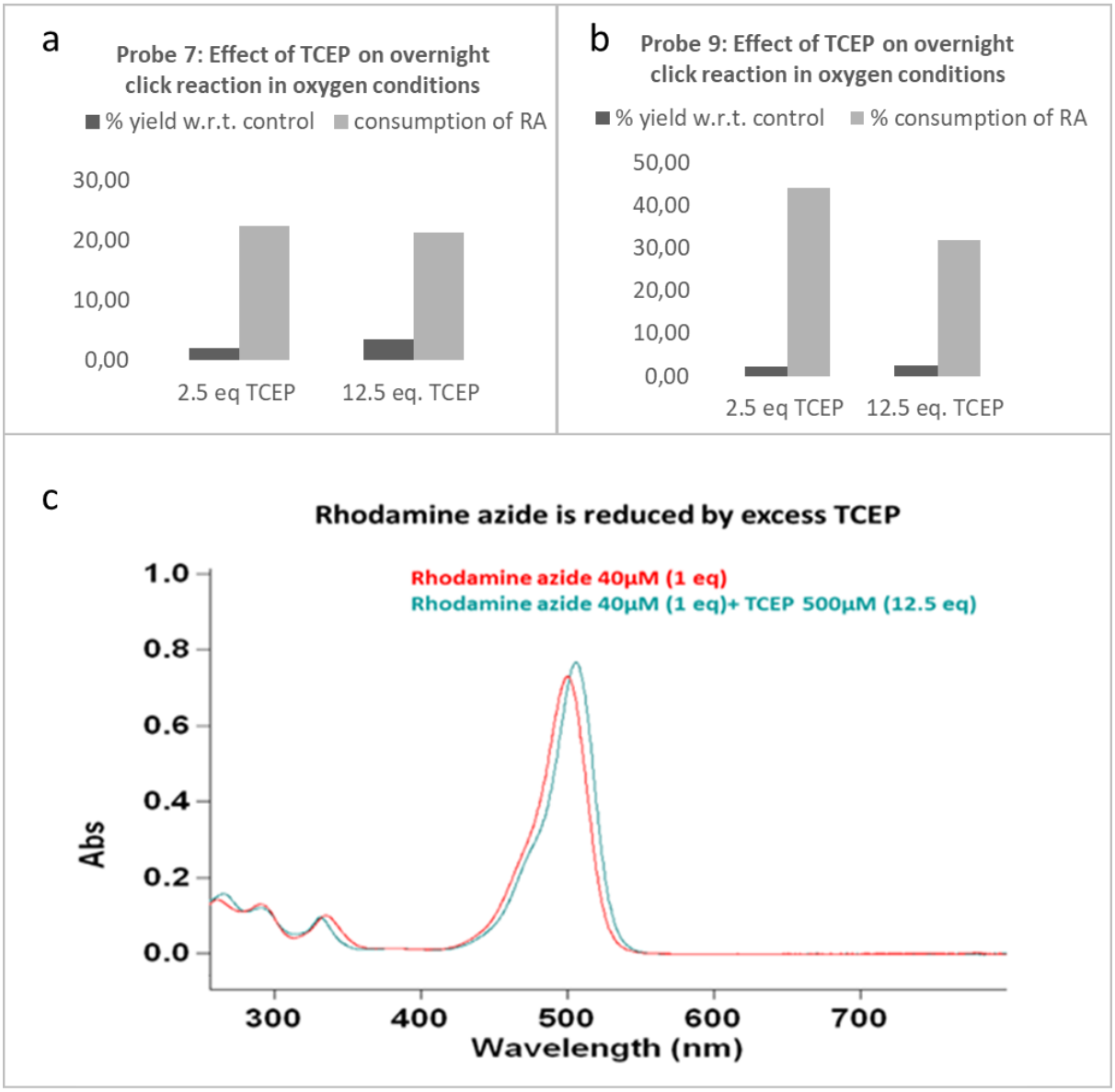

Figure S.3. 8. Reduction of azide takes place in excess TCEP.

a) The yield of overnight CuAAC reaction in oxygen conditions between 1 equiv. of probe 4 (AZ47) with 1 equiv. of rhodamine azide, with either 1 dose of CuSO4.5H2O 2.5 equiv. + THPTA 2.5 equiv. or with CuSO4.5H2O 2.5 equiv. + THPTA 12.5 equiv. Above CuAAC reaction is between 1 equiv. of probe 4 and probe 6 individually with 1 equiv. of rhodamine azide, with either 1 dose of CuSO4.5H2O 2.5 equiv. + THPTA 2.5 equiv. + TCEP 2.5 equiv. overnight or CuSO4.5H2O 2.5 equiv. + THPTA 2.5 equiv. + TCEP 12.5 equiv. Increase in TCEP did not significantly increase the yield of reaction but lead to a side reaction that can be seen with the drop in RA consumption overnight. The consumption of rhodamine azide in presence of 2.5 equiv. of TCEP is 44% while for 12.5 equiv. of TCEP is 32%. The extra consumption of rhodamine azide in excess TCEP can be explained by the fact that TCEP brings about a side reaction of reducing the azide via Staudinger ligation (Saxon & Bertozzi, 2000).

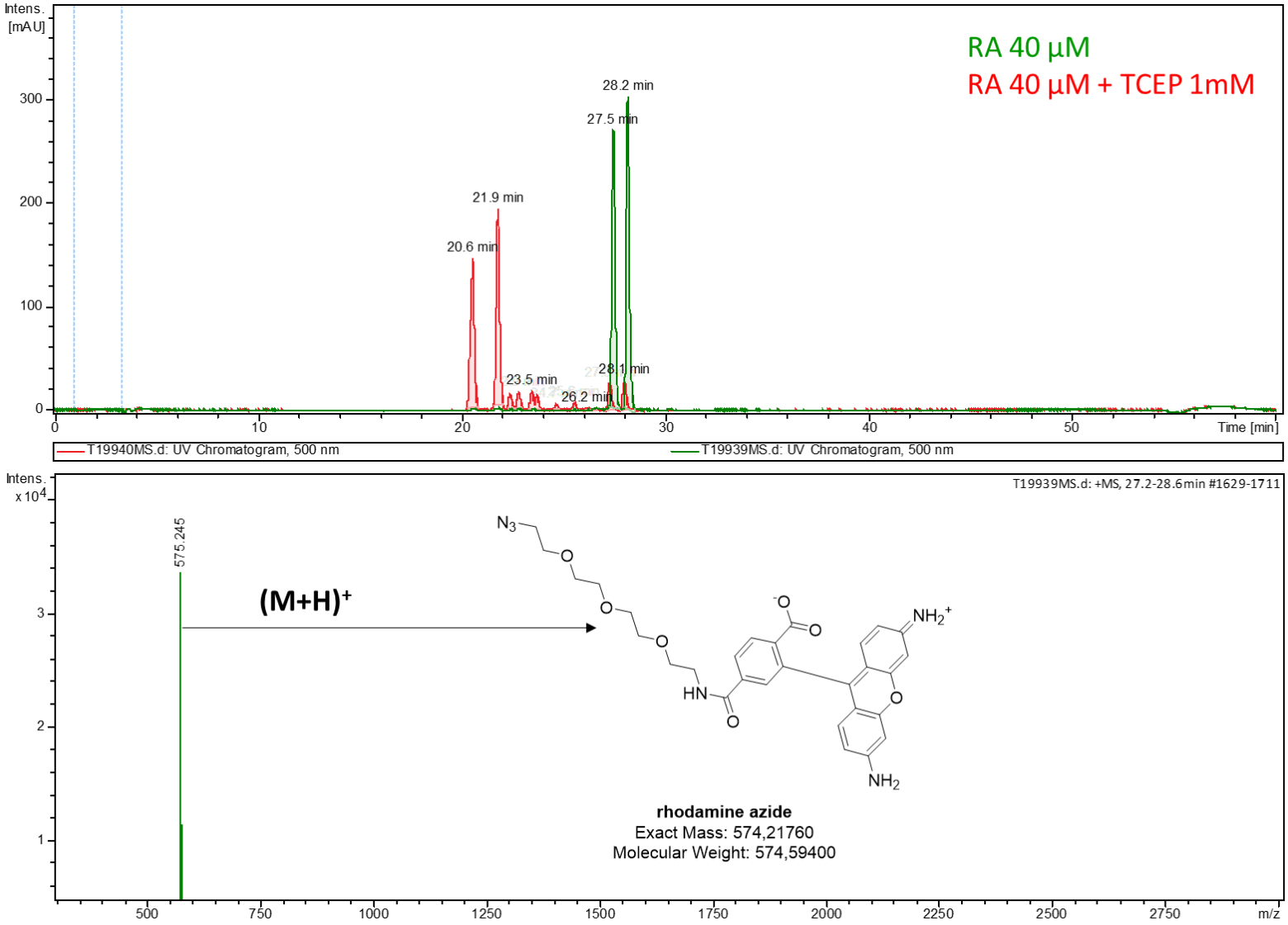

Figure S.3. 9. HPLC-MS data indicating mass of 575.24 for rhodamine azide

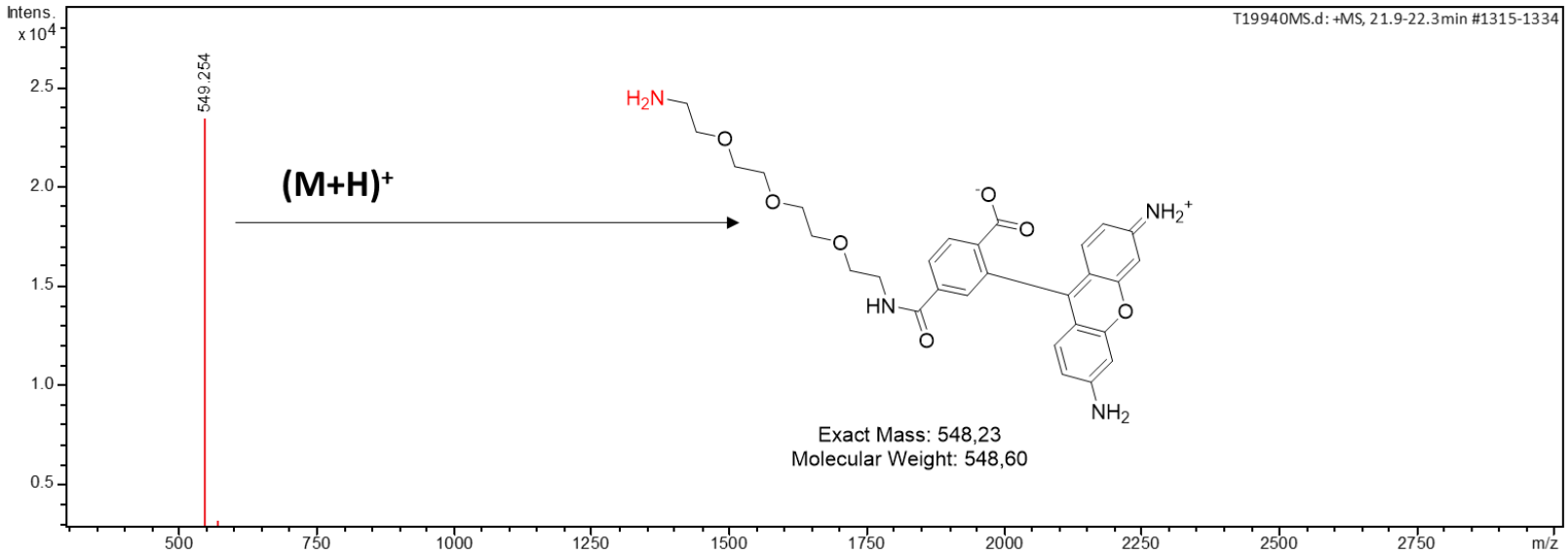

Figure S.3. 10. HPLC-MS data indicating mass of 548.23 for reduced rhodamine azide.

The extra consumption of rhodamine azide in excess TCEP can be explained by the fact that TCEP brings about a side reaction of reducing the azide via Staudinger ligation (Saxon & Bertozzi, 2000). Previously it's also reported that even though TCEP is a reductant, phosphine of TCEP inhibits click reaction by competing for binding to Cu and reducing the azide (Wang et al., 2003). Therefore, for standardizing the click reaction further in our case we did not use more than 2.5 equiv. of TCEP for the click reaction.

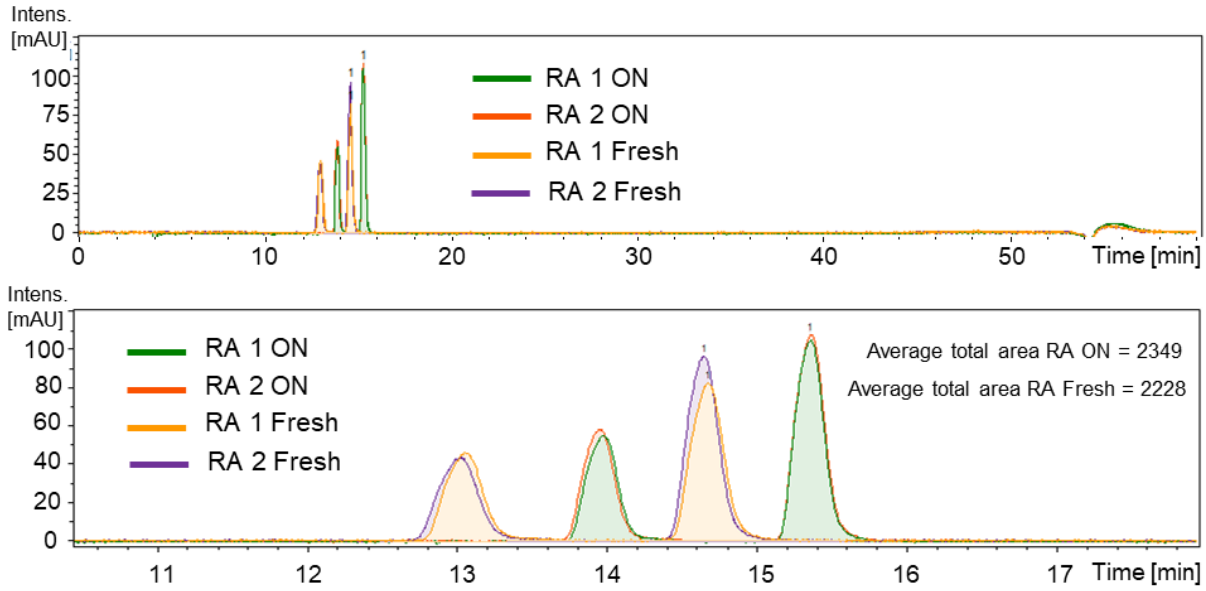

Figure S.3. 11. Overnight stability of Rhodamine azide. 24 µM of RA in PBS with 7.2% DMF was analyzed by HPLC freshly or after overnight incubation in room temperature. Total RA peak absorbance in the 507 nm chromatogram was counted.

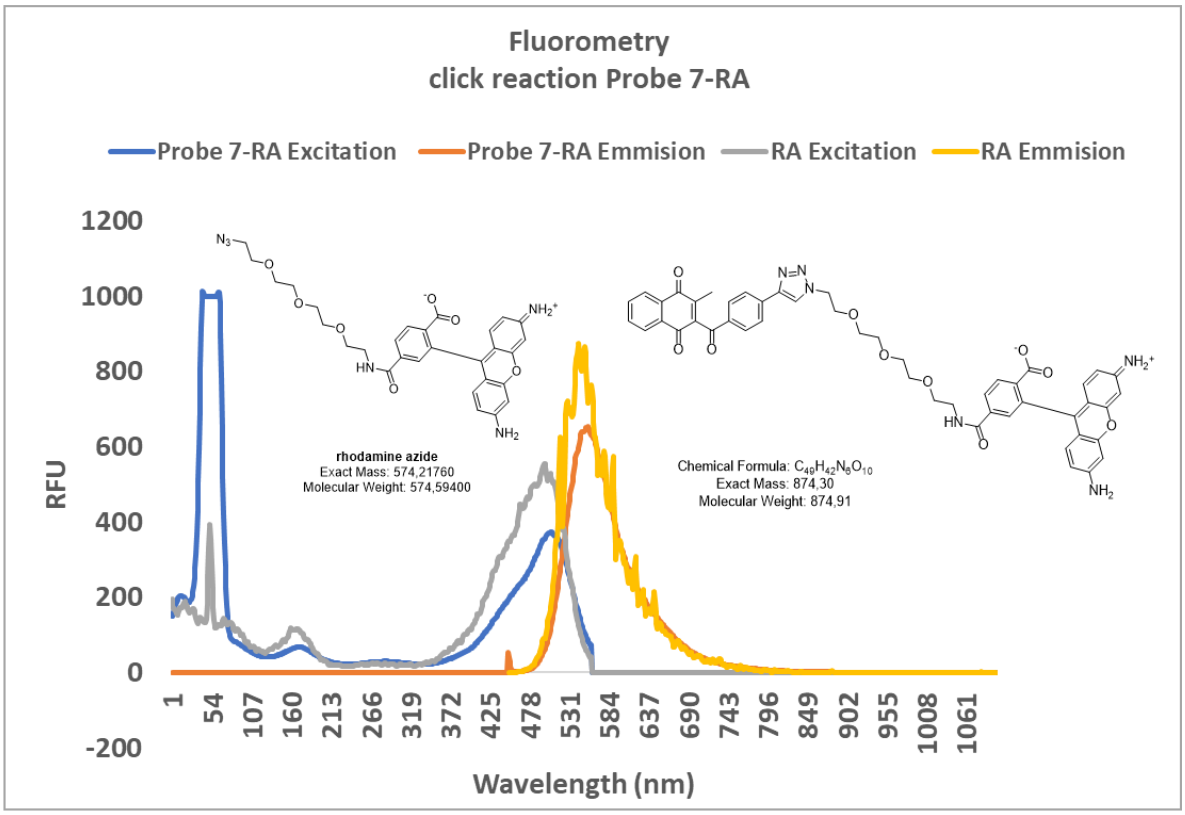

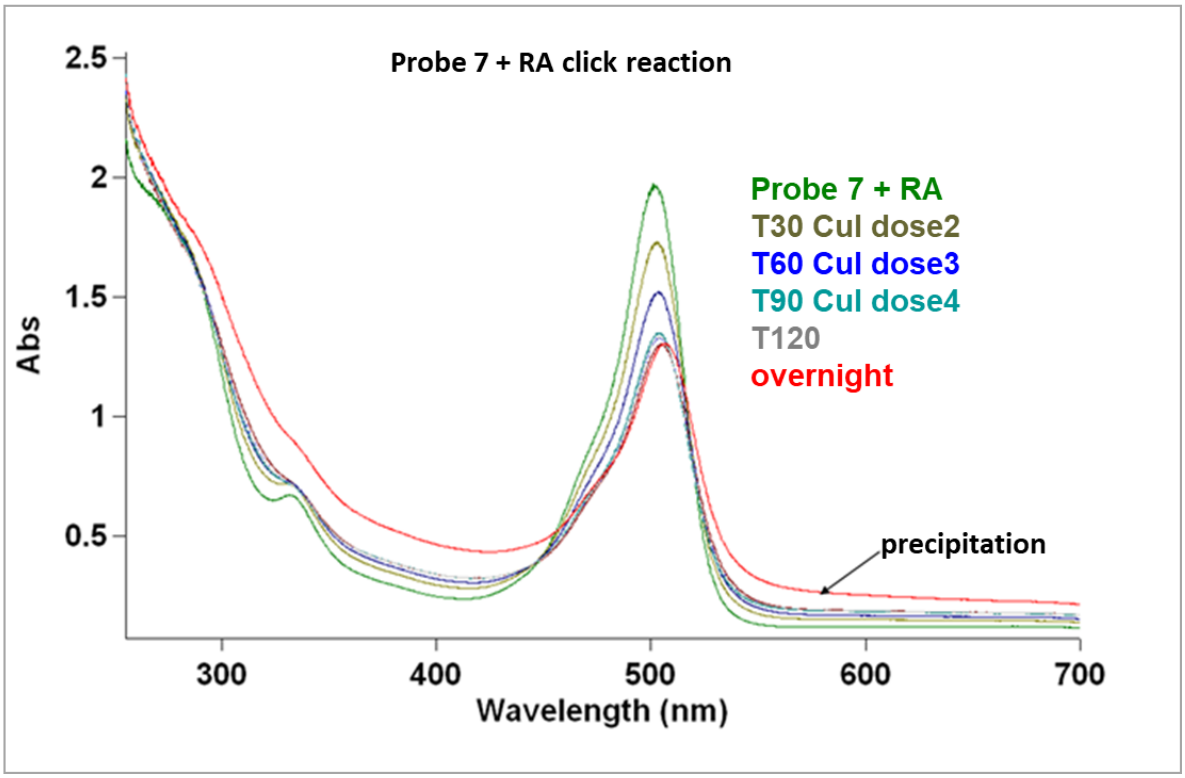

Figure S.3. 12. Probe 7 + RA click reaction UV-vis spectrometry over time and fluorometry post 2h

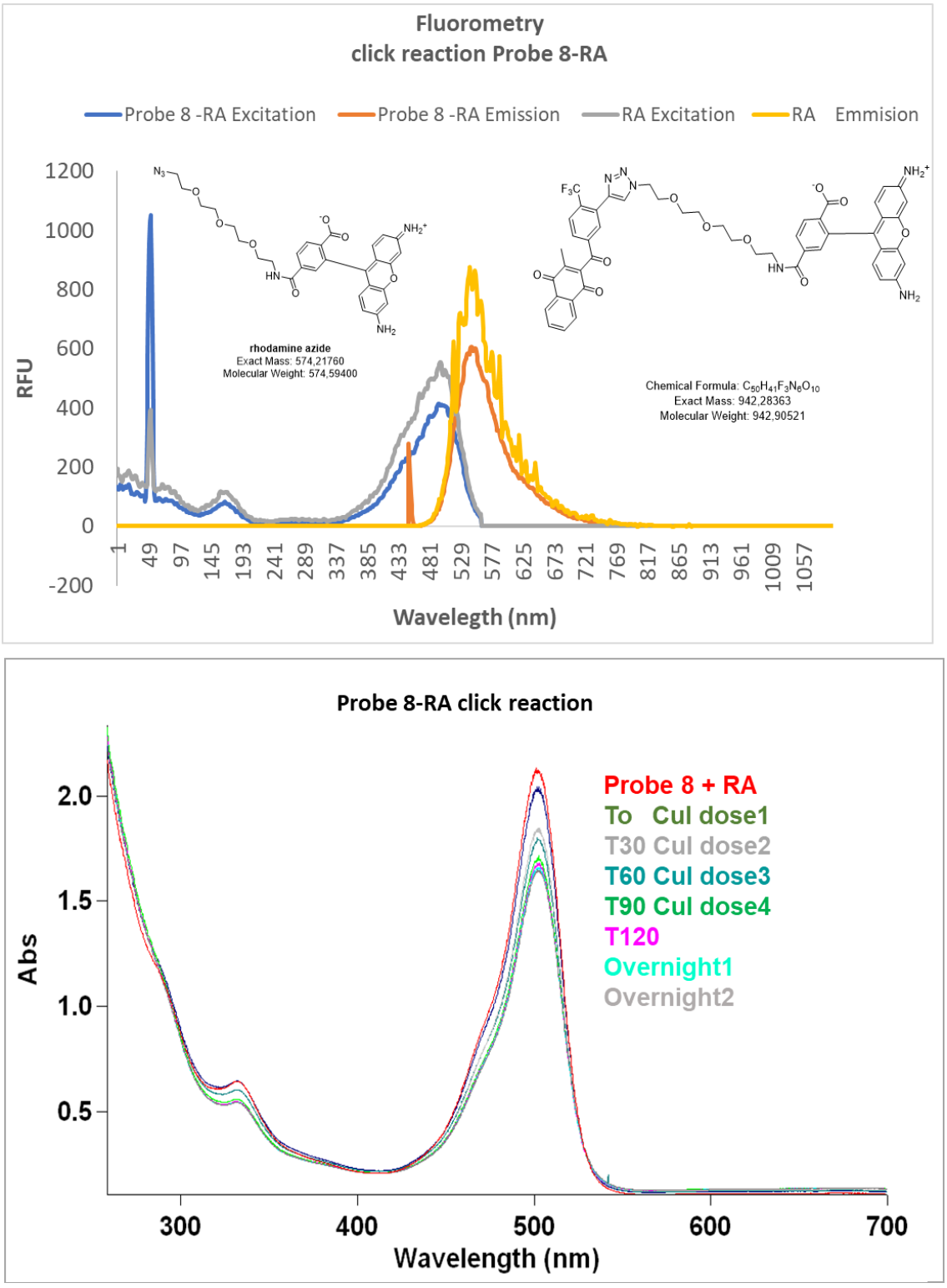

Figure S.3. 13. Probe 8 + RA click reaction UV-vis spectrometry over time and fluorometry post 2h

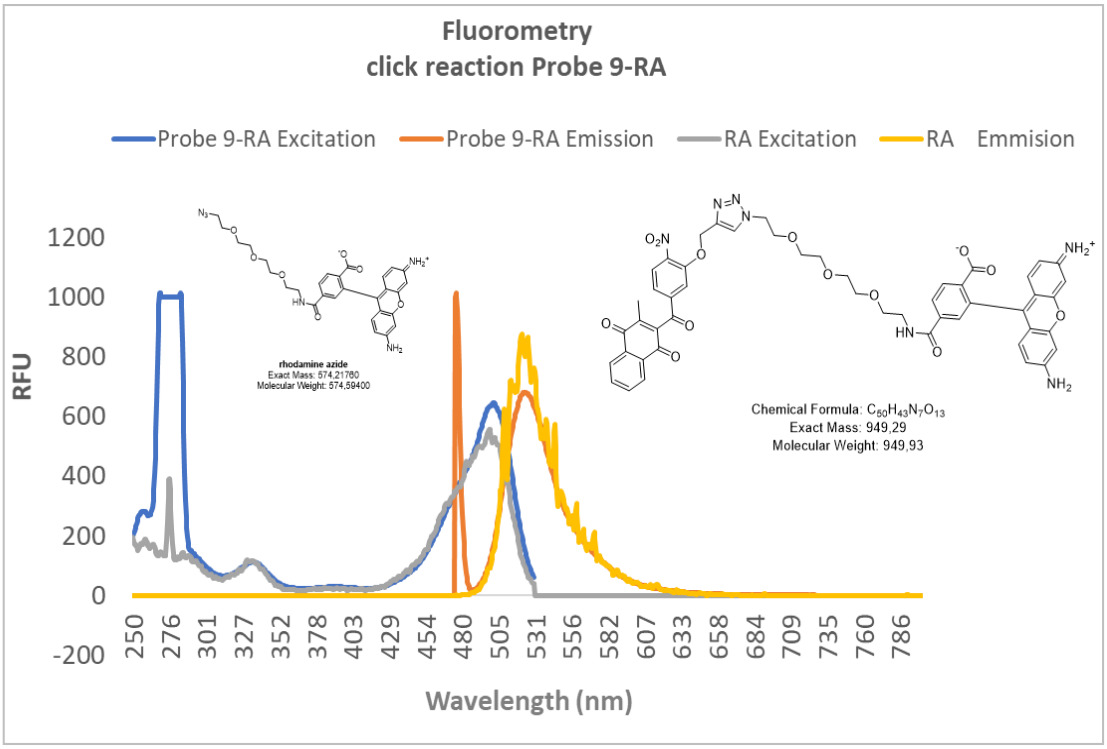

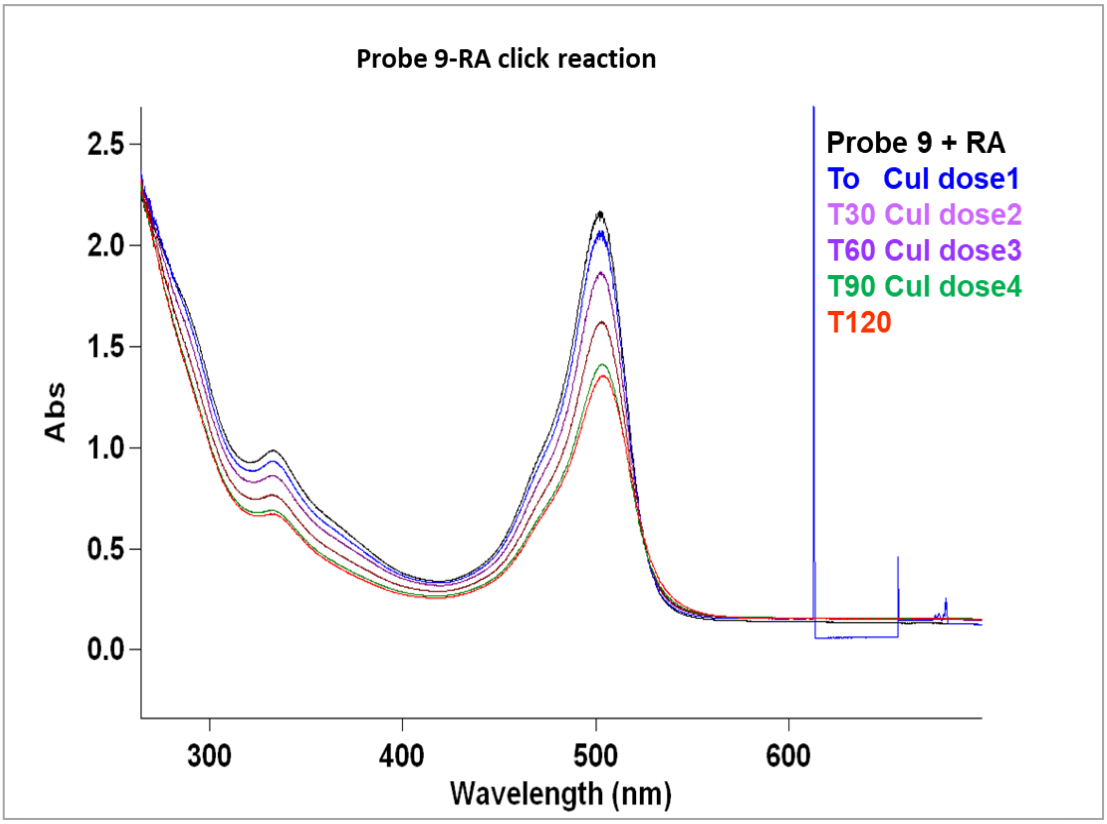

Figure S.3. 14. Probe 9 + RA click reaction UV-vis spectrometry over time and fluorometry post 2h

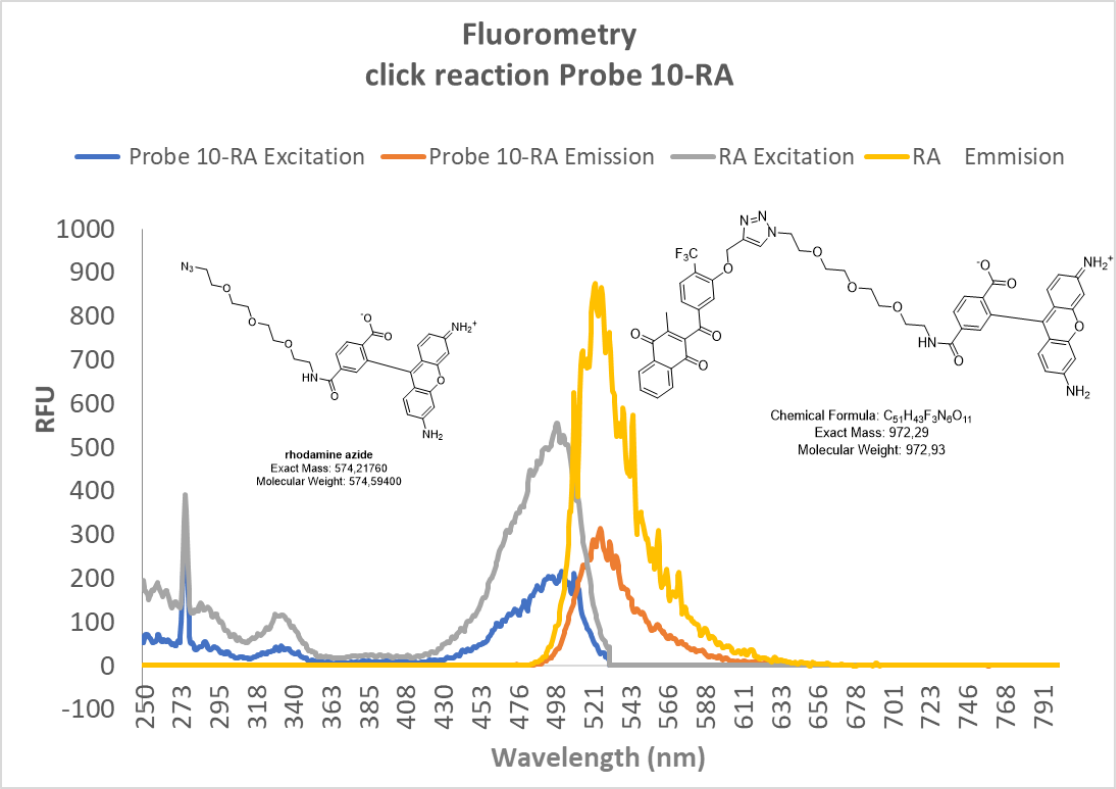

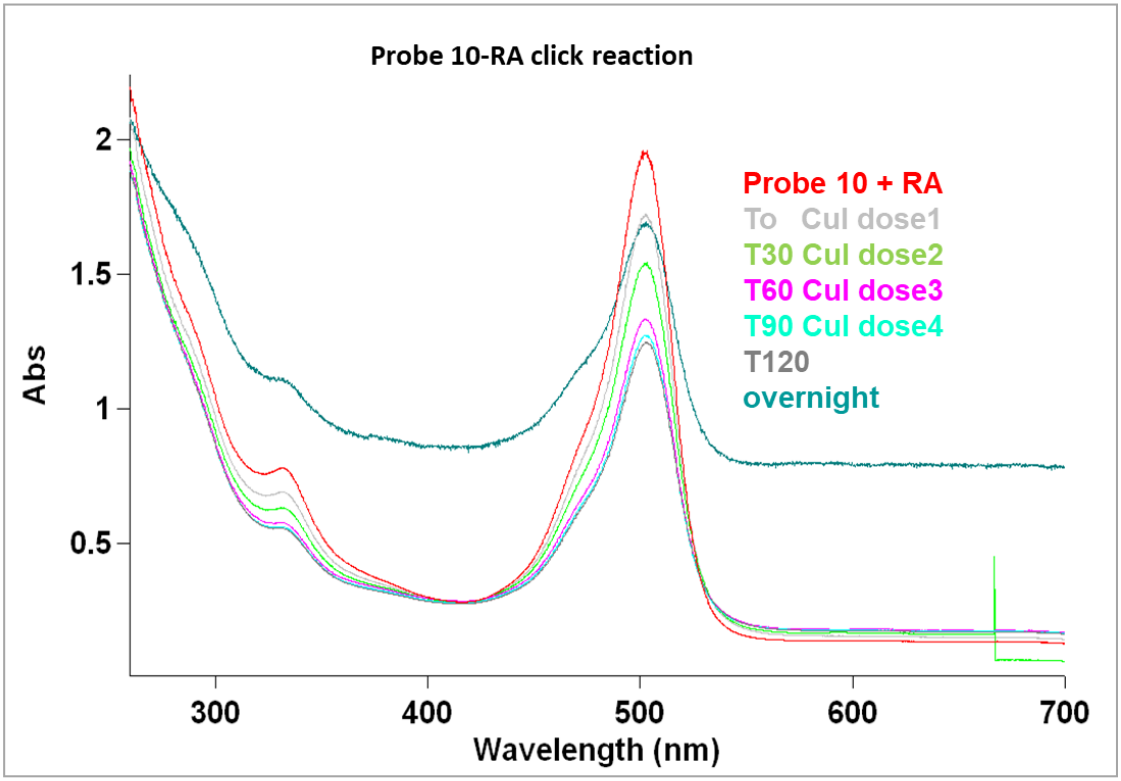

Figure S.3. 15. Probe 10 + RA click reaction UV-vis spectrometry over time and fluorometry post 2h

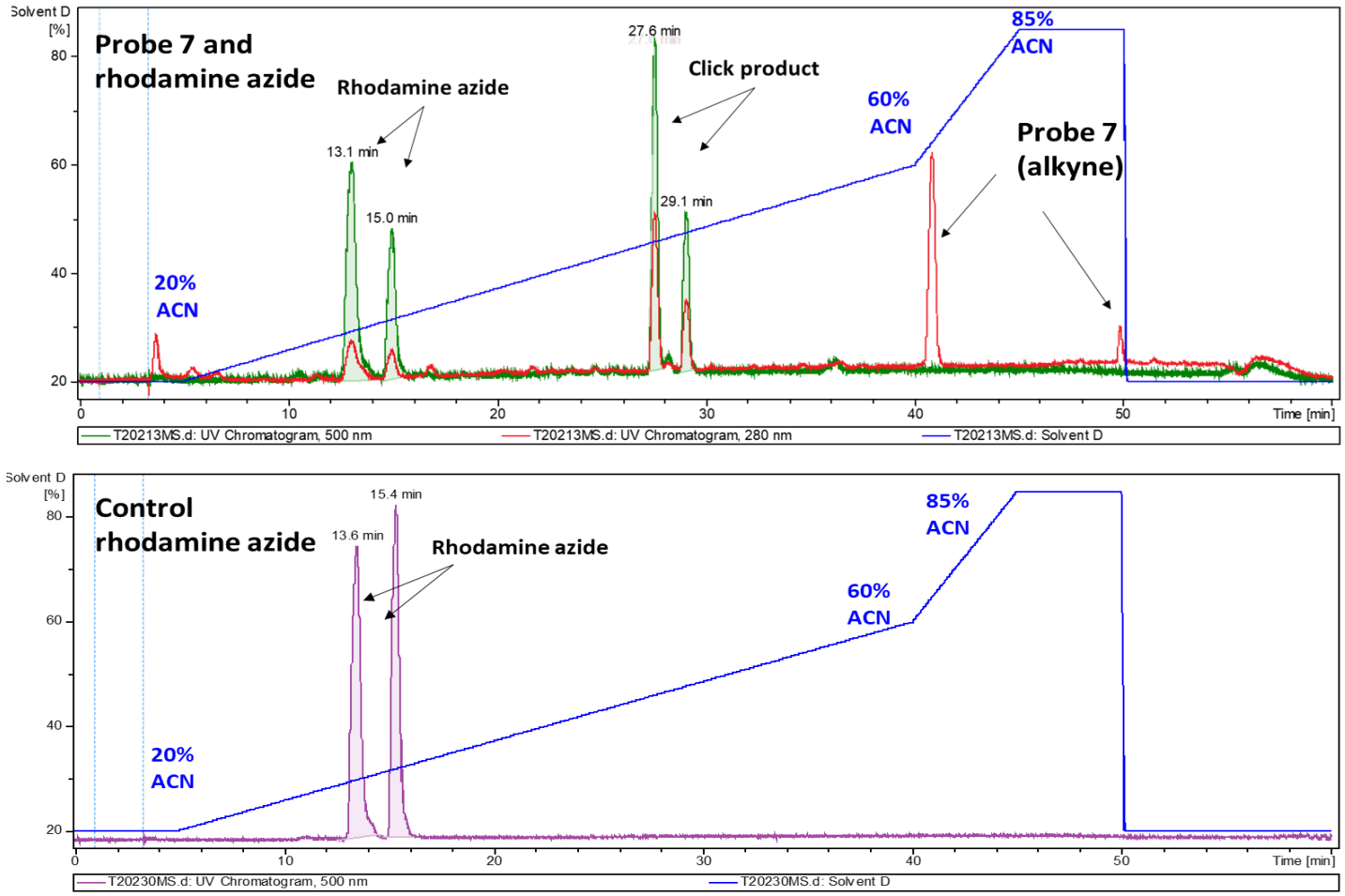

Figure S.3. 16. HPLC-MS analysis conditions for evaluation of click reaction: For all the click reaction the yield of the product was calculated based on the HPLC-MS analysis. The rhodamine azide (RA) was detected at 500nm wavelength and probe was detected at 280nm wavelength. Depending on the hydrophobicity and molecule the retention time (RT) was shifted while separation in HPLC. The azide being hydrophilic retention time 13.1 and 15 min, the click product was observed at 27.6 and 29.1min probe is the most hydrophobic with retention time closer to 40 minutes. %yield = (Area of product at RT 27.6 min +29.1min)/(Area of control azide at RT 13.6 min+ RT 15.4 min) and % RA consumption = 100-(area of leftover RA from reaction at 13.1min + 15.0 min/area of control RA at 13.6 min + 15.4 min)

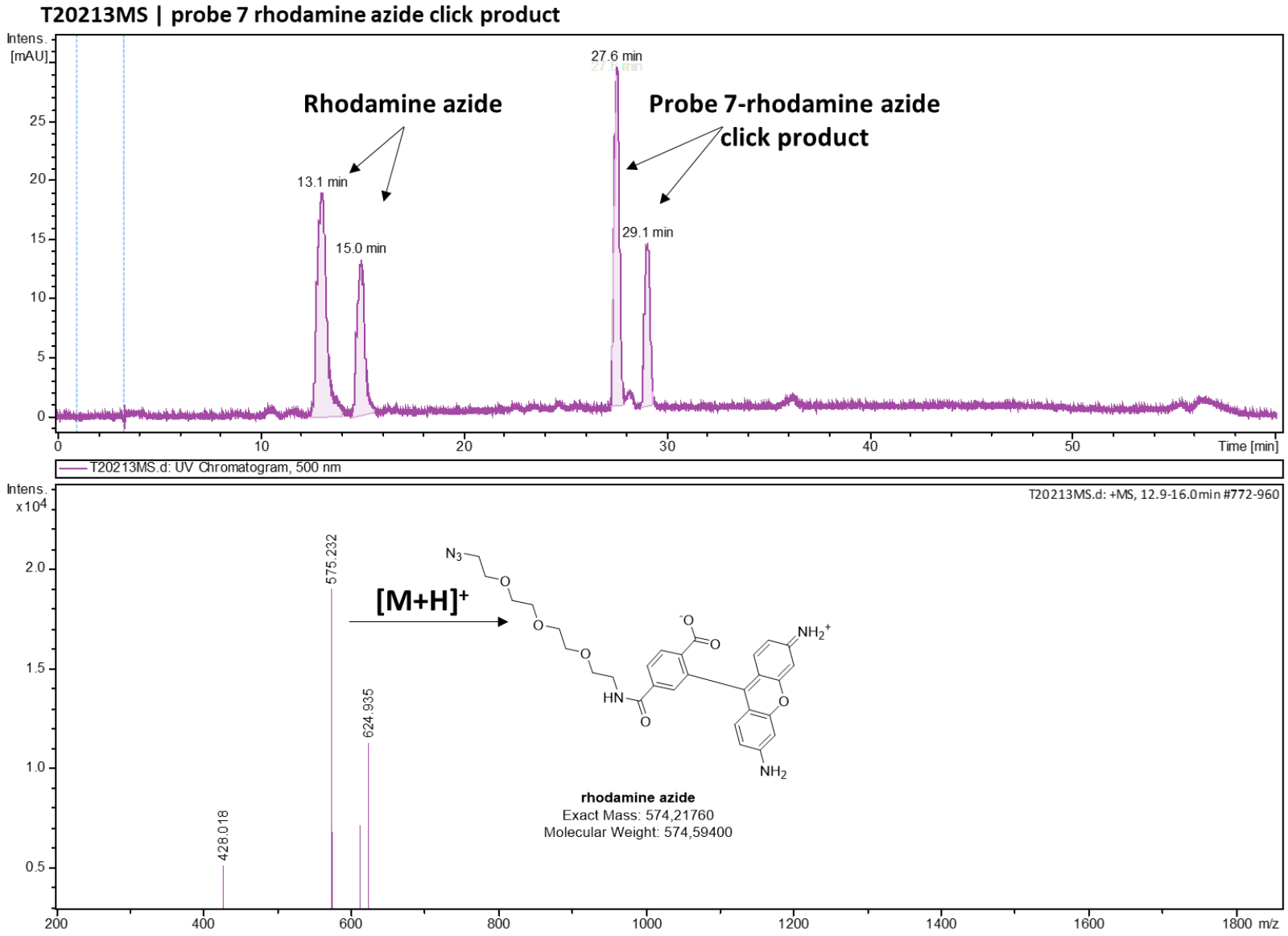

Figure S.3. 17. HPLC-MS analysis of rhodamine azide in probe 7-RA click reactions

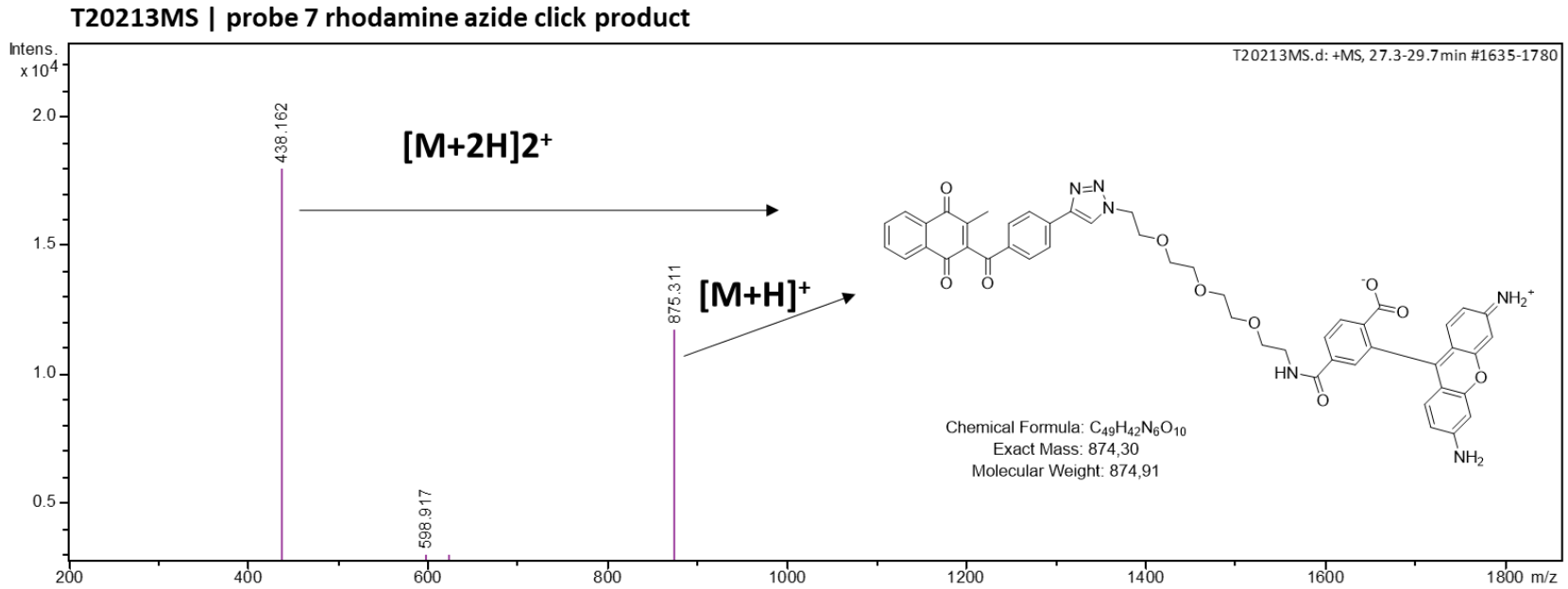

Figure S.3. 18. HPLC-MS analysis of probe 7-RA click product. For probe 7 click reaction, calculated mass of click product is 874.30 and we observed it's hydrated form with mass 875.311 and m/z= 1/2 with mass 438.162 at Rt 27.6 and 29.1 minutes for 2 isomers. RA with 575.22 was observed at Rt.27.6 and 29.1 for two isomers.

T20279MS | Probe 8 rhodamine azide click product

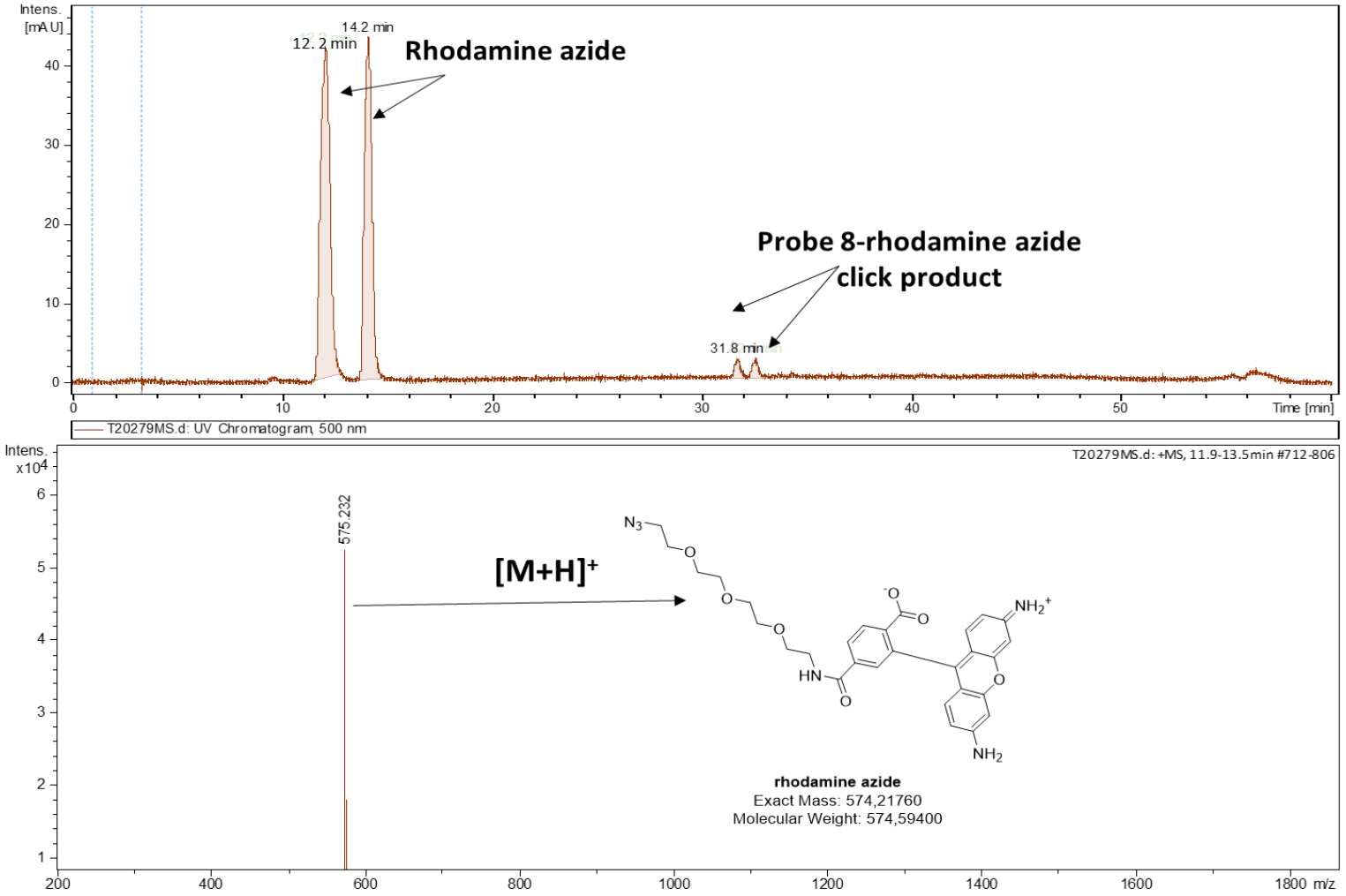

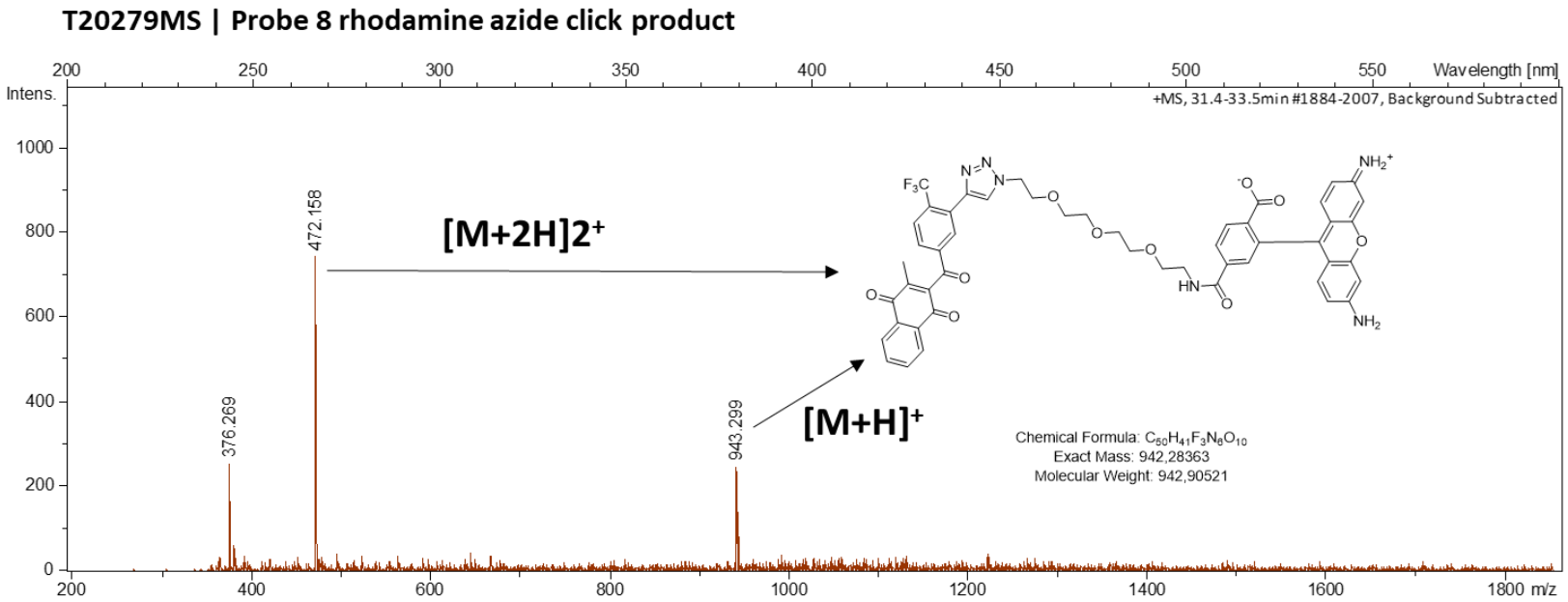

Figure S.3. 19. HPLC-MS analysis of probe 8-RA click reactions.

For probe 8 click reaction, calculated mass of click product is 948.283 and we observed it's hydrated form with mass 943.299 and m/z= 1/2 with mass 472.158 at retention time (Rt) 31.8 minutes. RA with 575.22 was observed at Rt.12.2 and 14.2 for two isomers.

(a)

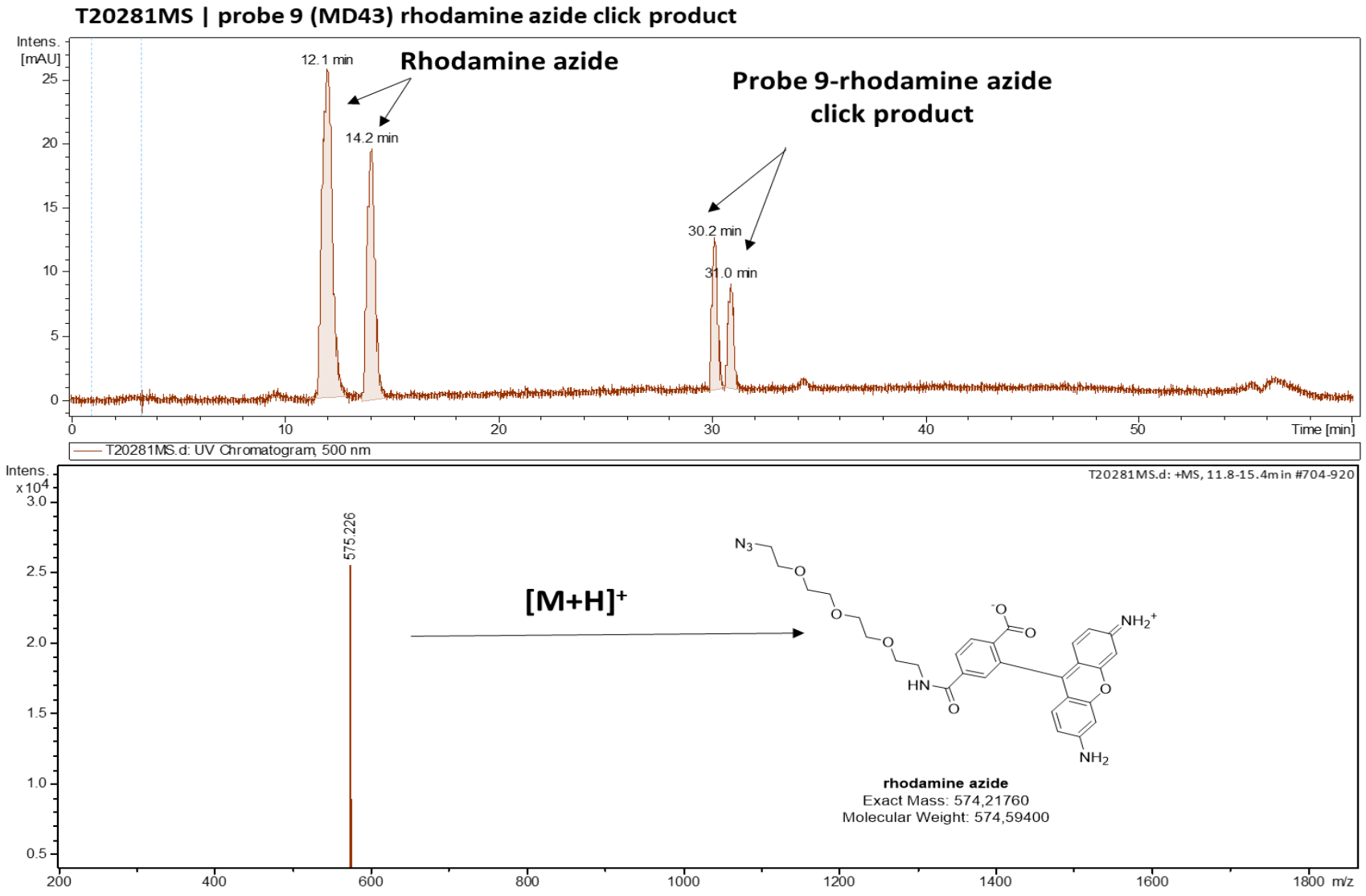
T20281MS | probe 9 (MD43) rhodamine azide click product
Intens. [mAU]
12.1 min
Rhodamine azide
14.2 min
Probe 9-rhodamine azide click product
30.2 min
31.0 min
Time [min]
T20281MS.d: UV Chromatogram, 500 nm
Intens. x10^4
T20281MS.d: +MS, 11.8-15.4min #704-920
575.226
[M+H]+
rhodamine azide
Exact Mass: 574,21760
Molecular Weight: 574,59400
m/z

(b)

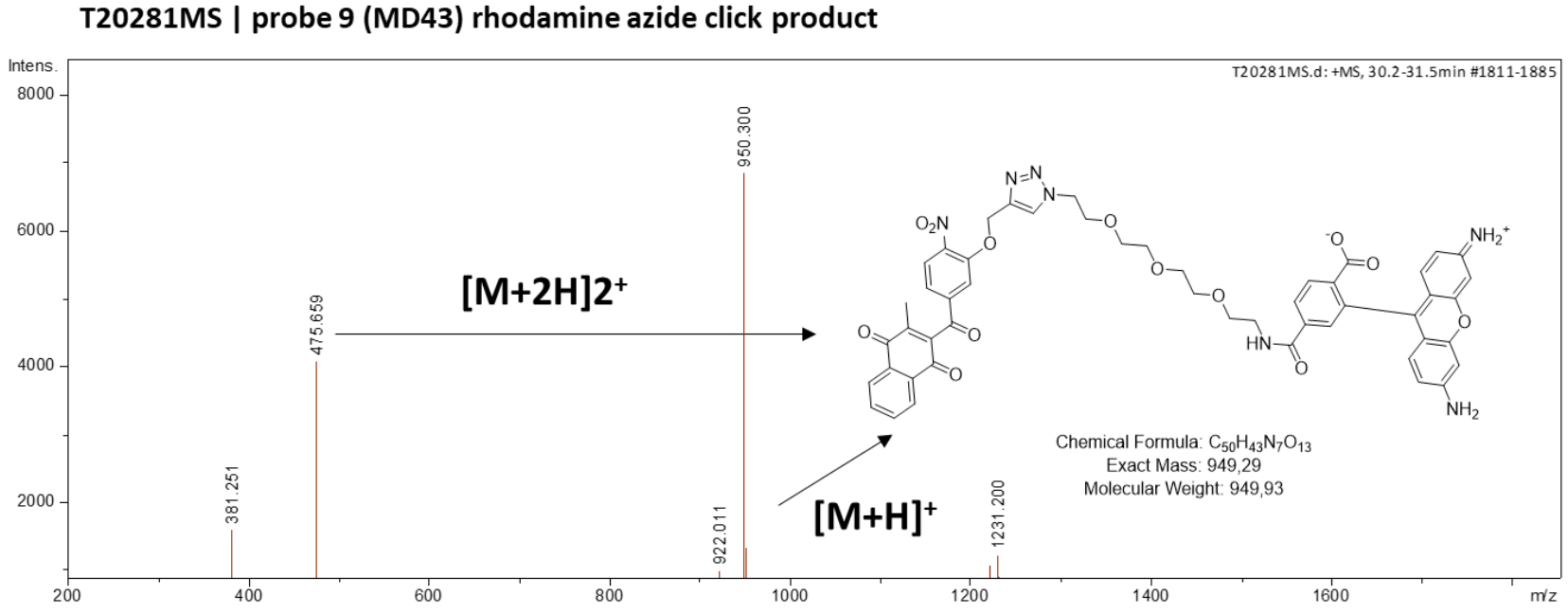

Figure S.3. 20. HPLC-MS analysis of probe 9-RA click reactions.

For probe 9 click reaction, calculated mass of click product 949.29 and we observed 950.30 and m/z=1/2 with mass 475.66 at Rt 30.2 and 31.0 minutes for 2 isomers. RA with 575.22 was observed at Rt. 12.1 and 14.2 for two isomers.

T20259MS | probe 10 (MD134) rhodamine azide click product

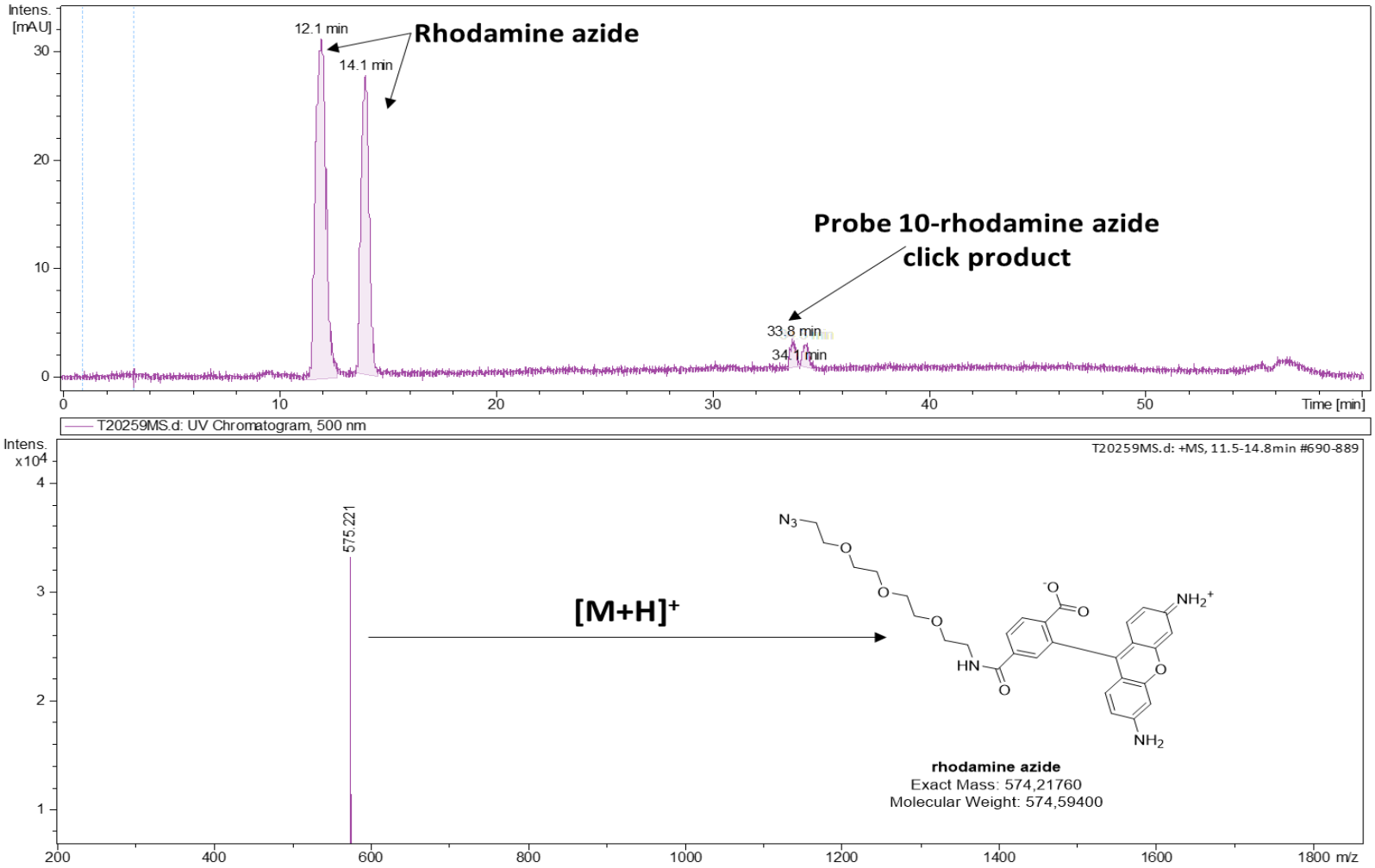

(b)

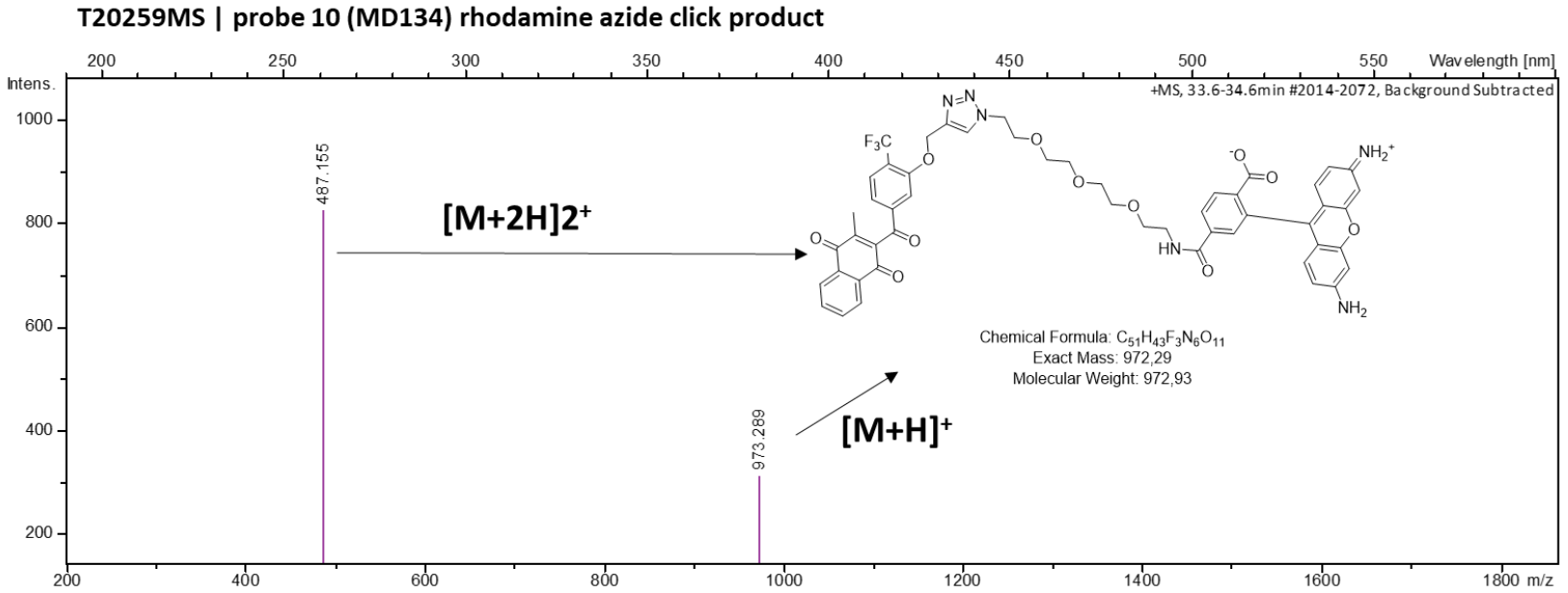

Figure S.3. 21. HPLC-MS analysis of probe 10-RA click reactions

For probe 10 click reaction, calculated mass of click product 972.29 and we observed 973.28 and m/z=$[M+H]^{2+}$ with mass 487.155 at Rt 30.2 and 31.0 minutes for 2 isomers. RA with 575.22 was observed at Rt. 12.1 and 14.1 for two isomers.

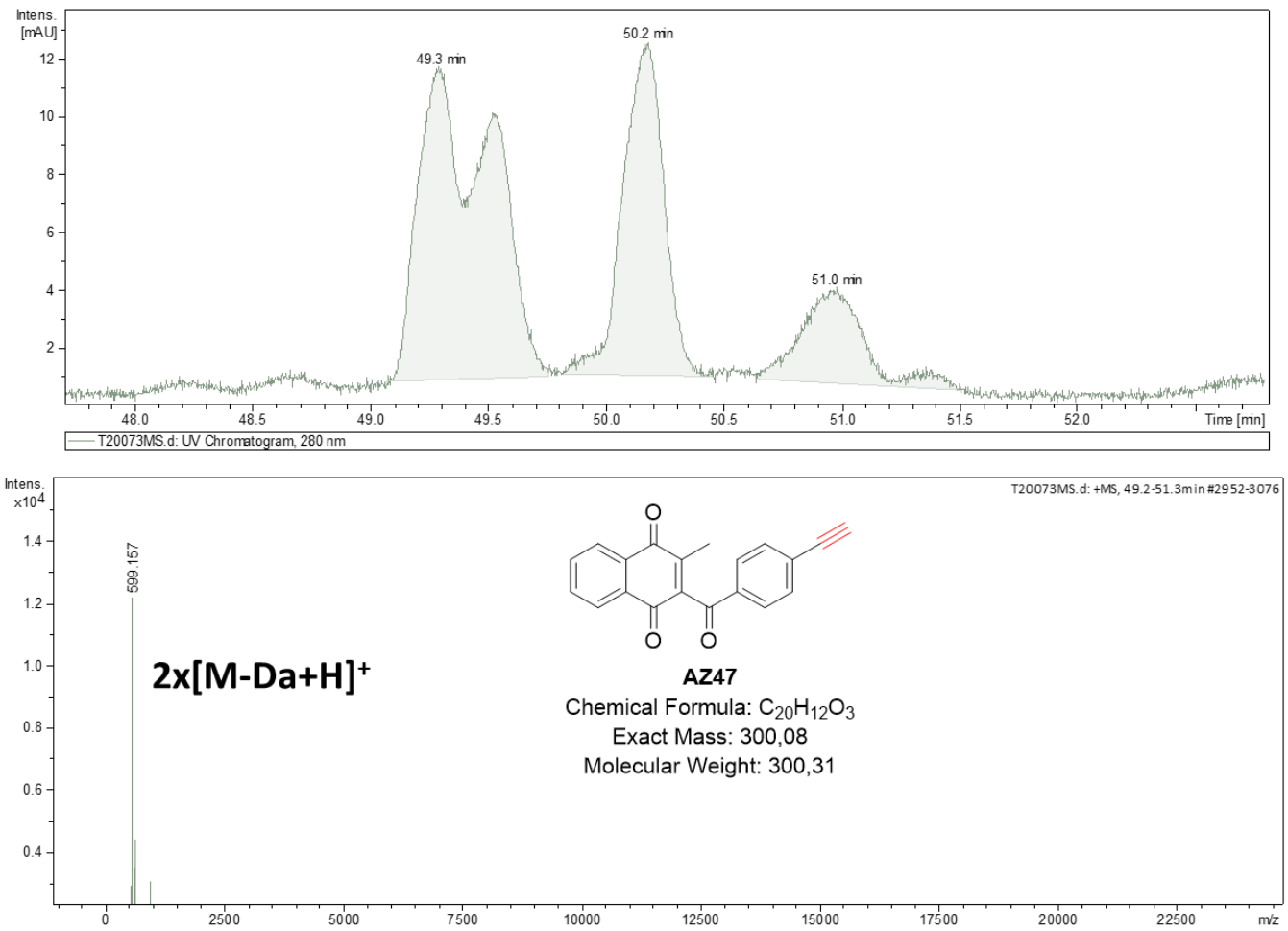

Figure S.3. 22. HPLC-MS analysis of probe 7

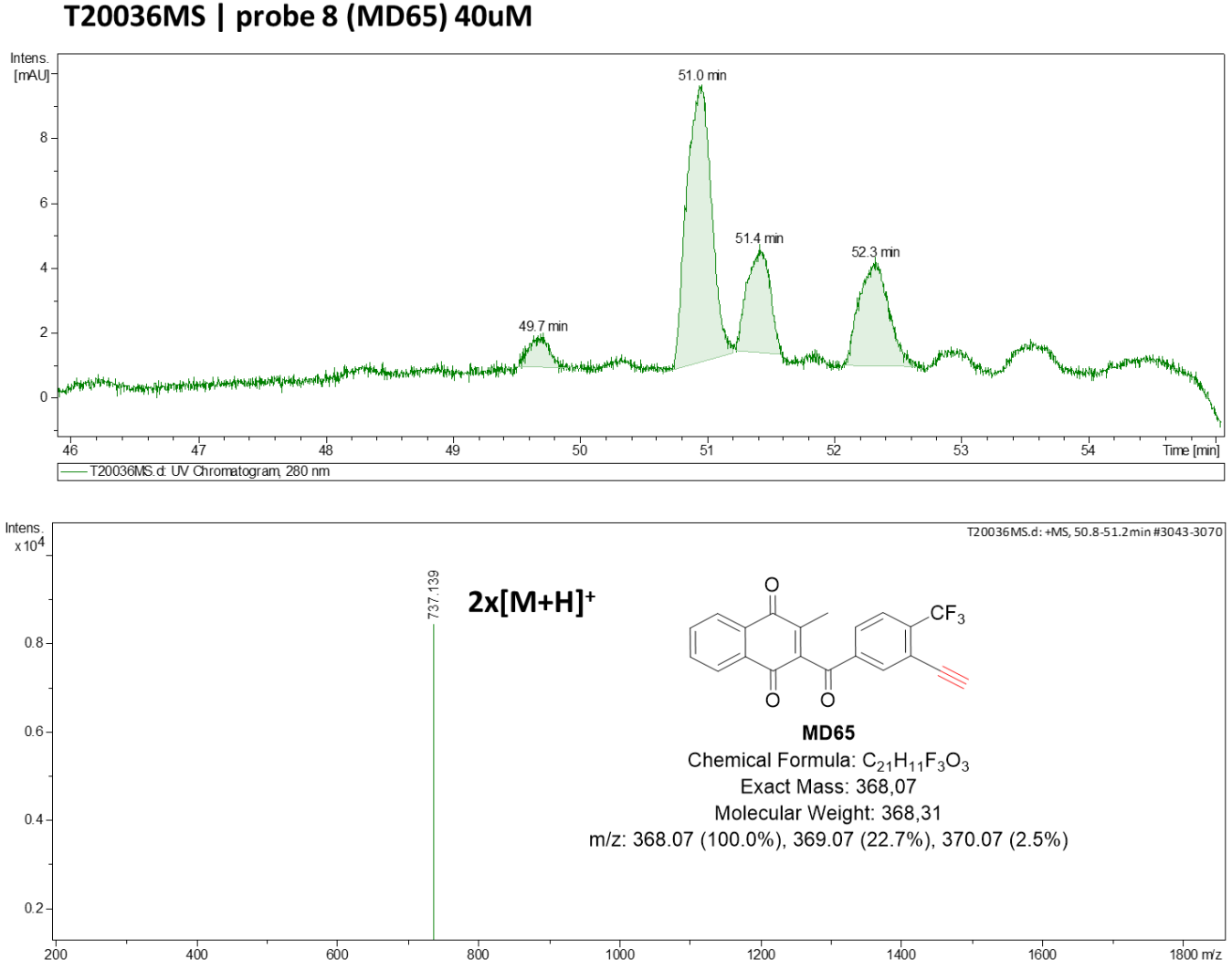

Figure S.3. 23. HPLC-MS analysis of probe 8

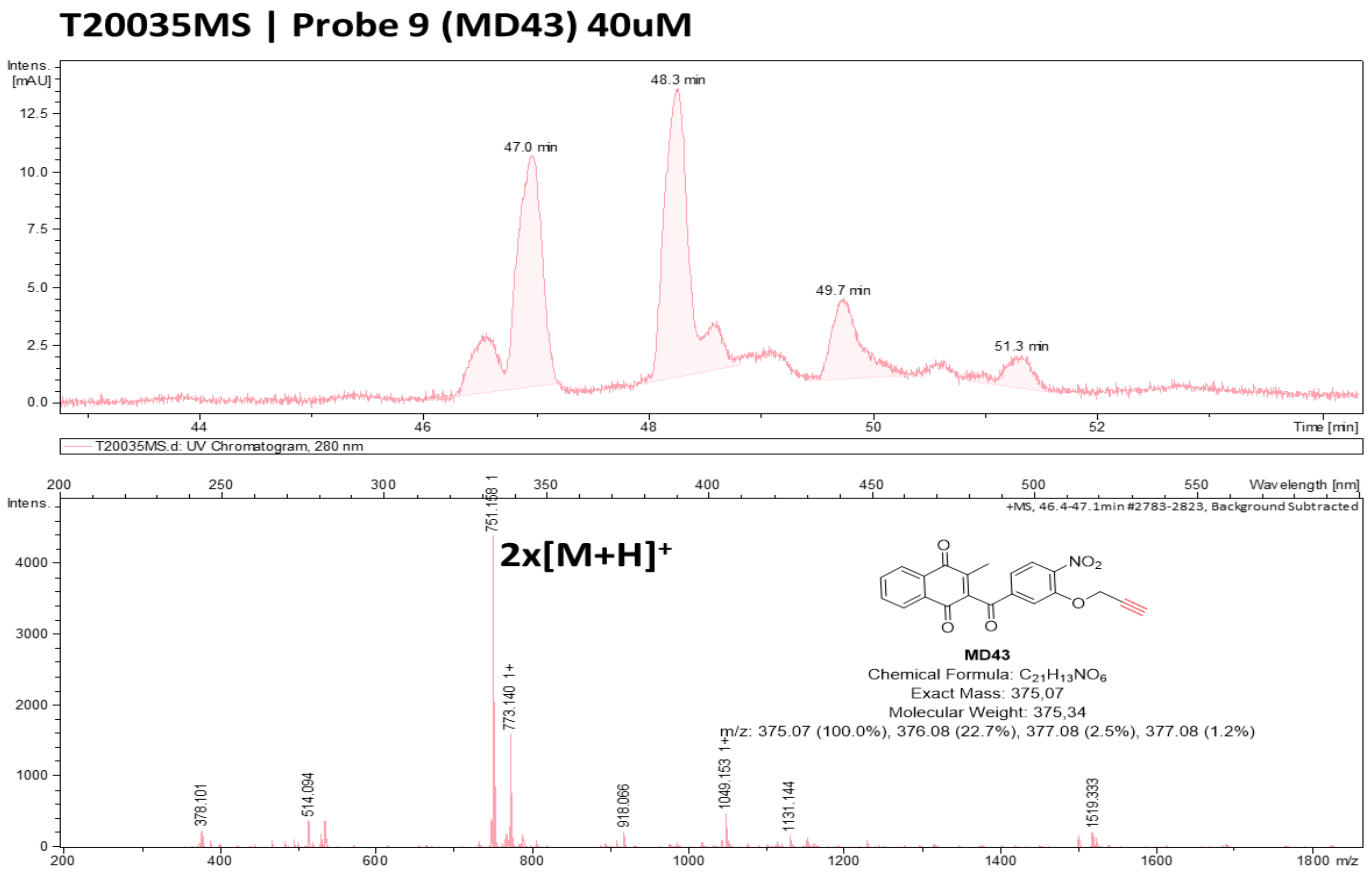

Figure S.3. 24.HPLC-MS analysis of probe 9

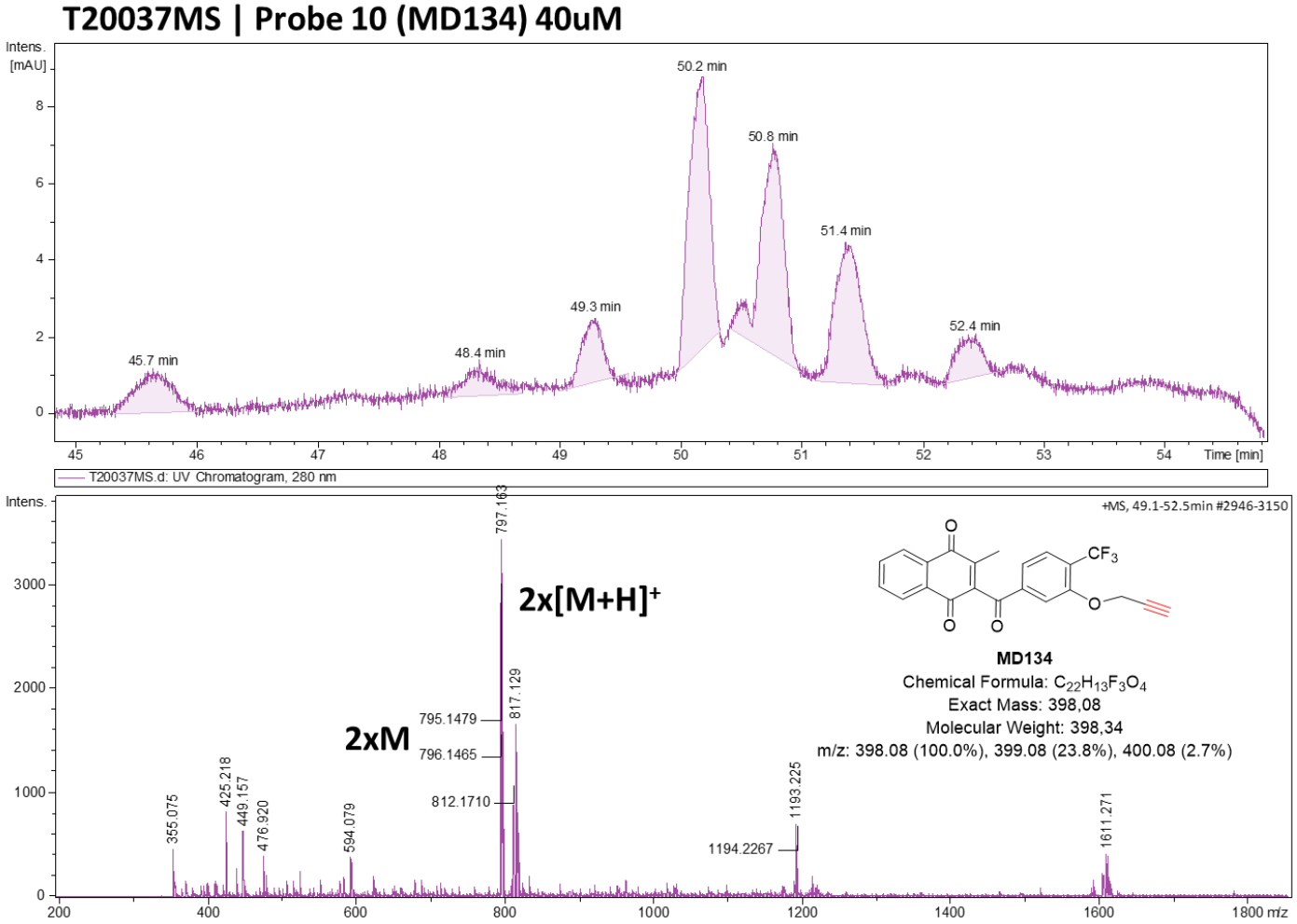

Figure S.3. 25. HPLC-MS analysis of probe 10

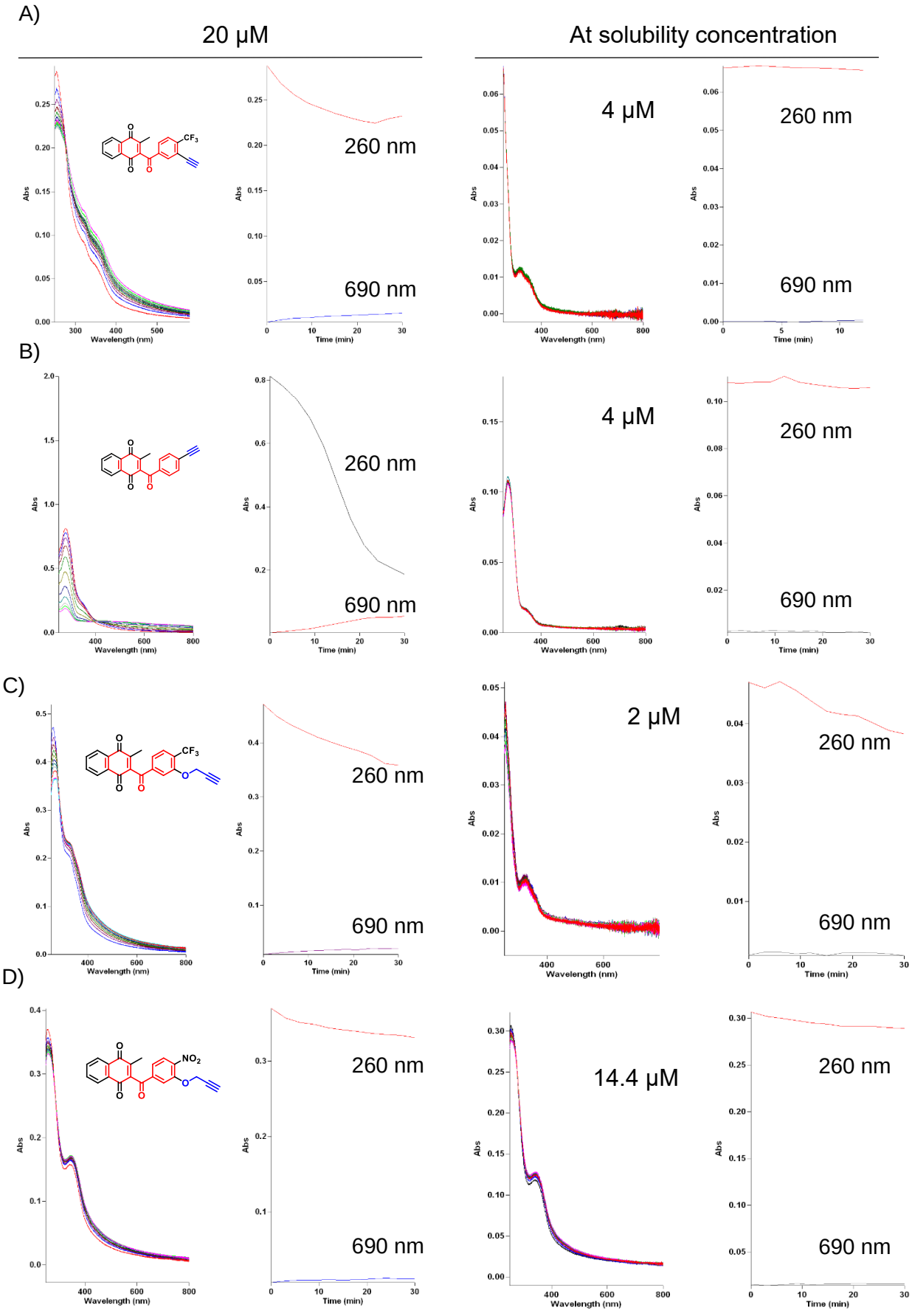
A)
20 µM
At solubility concentration
260 nm
690 nm
4 µM
260 nm
690 nm
B)
4 µM
260 nm
690 nm
260 nm
690 nm
C)
2 µM
260 nm
690 nm
260 nm
690 nm
D)
14.4 µM
260 nm
690 nm
260 nm
690 nm
Abs
Wavelength (nm)
Time (min)

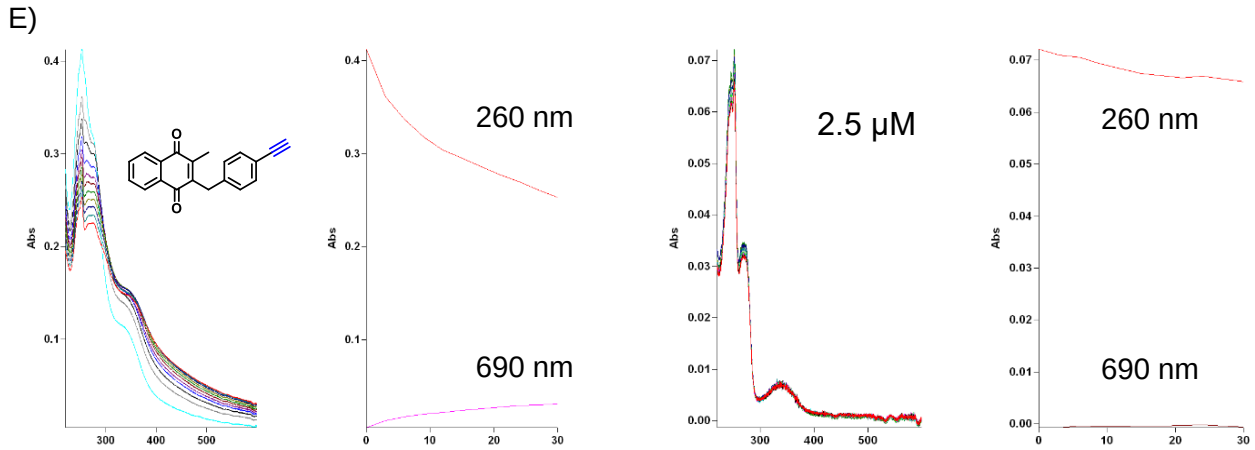

Figure S.3. 26. Solubility concentrations of ABPs in 2% ACN.

Probe solubility has been determined by spectroscopic measurement of ABP absorbance kinetics during 30 minutes after addition to solvent (H_2O with 2% ACN) (Left panel). Changes have been monitored at 290 nm -characteristic absorbance for ABPS; and 790 nm absorbance – to determine increase of absorbance of precipitant (Right panel). A) Probe 8 B) Probe 7 C) Probe 10 D) Probe 9 E) Probe 11. For probe 8 and 11 at the maximum measurable concentration the absorbance at 290nm was still dropping indicating that the real solubility concentration value is lower than tested.

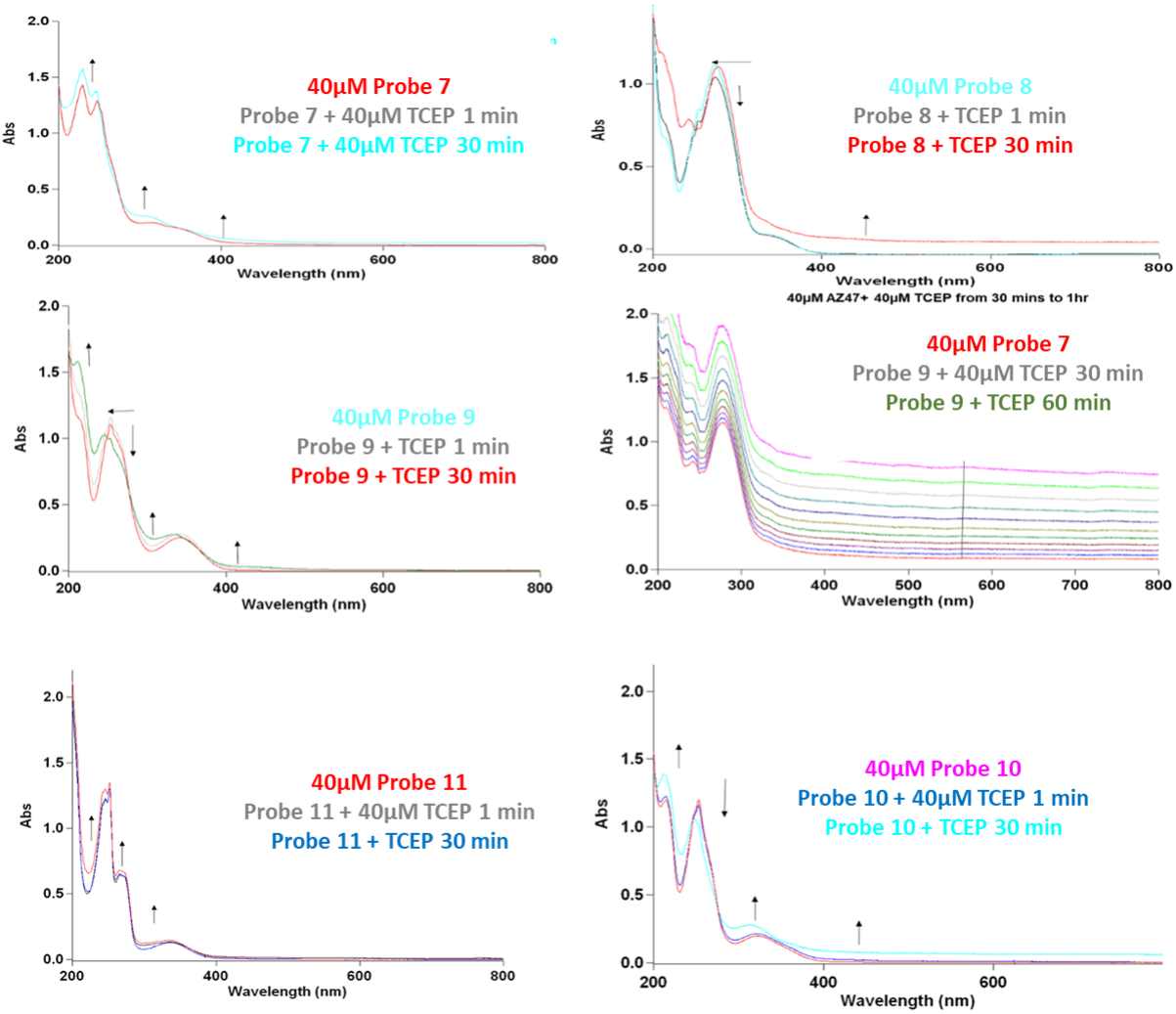

Figure S.3. 27. Solubility concentrations of ABPs in 20% ACN**.**

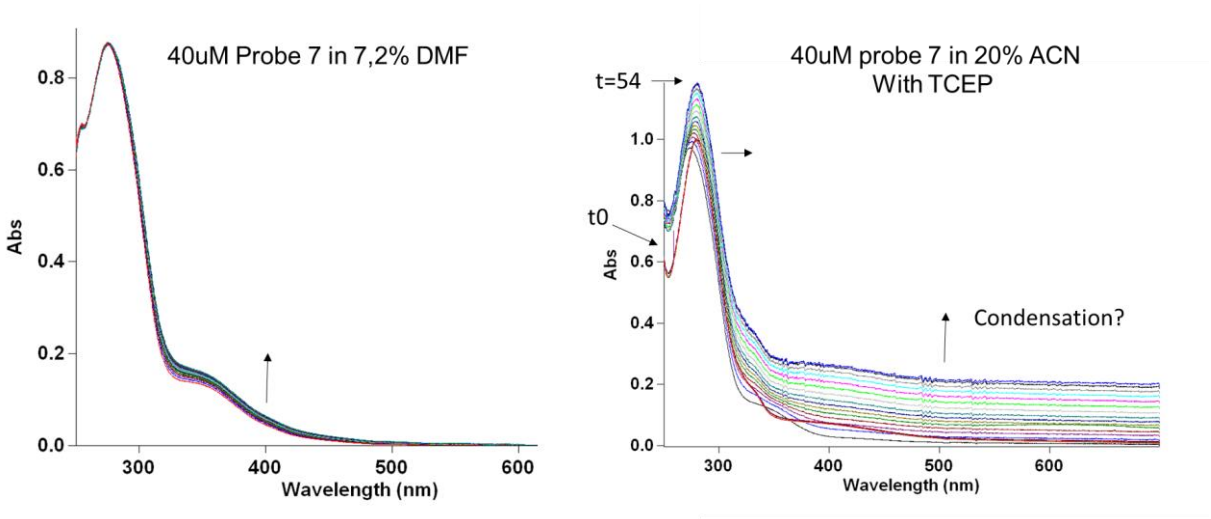

Figure S.3. 28. The tendency of probe precipitation is in 20% ACN and not in 7.2% DMF, which is closer to click reaction conditions.

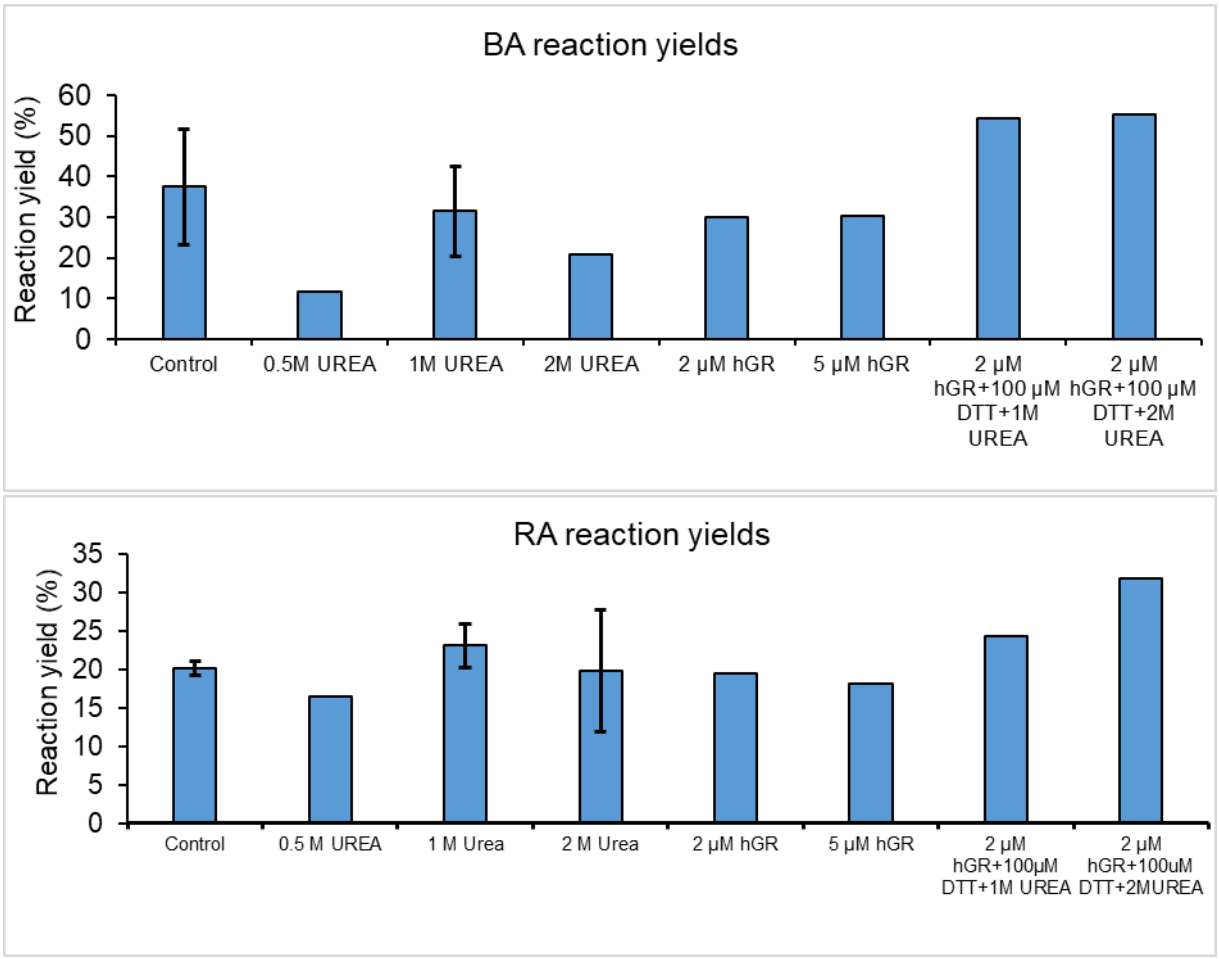

Figure S.3. 29. Click reaction efficencies have a similar pattern for biotin azide like for rhodamine azide.

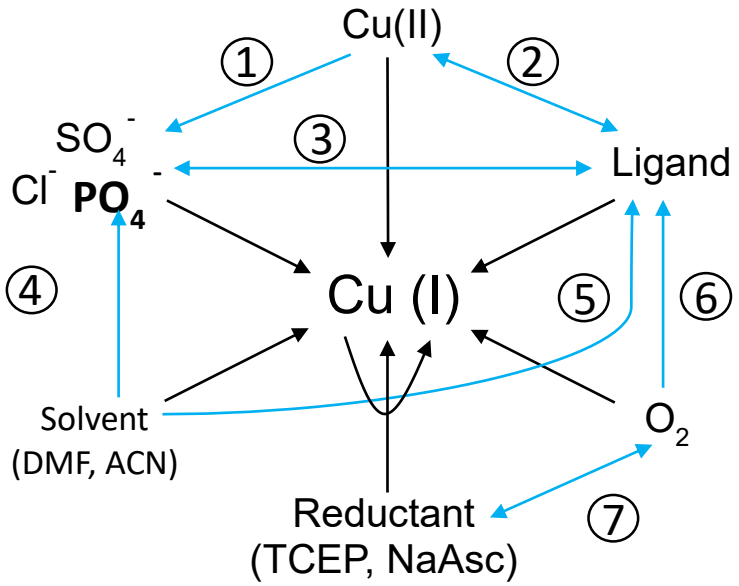

Scheme S1. Hypothetical interplay of factors in Cu(I) catalyst formation. Many of the factors involved in Cu(I) formation can have a direct (black) on indirect (blue) effect on the availability of the catalyst. (1) Inhibitory effect of anions is prevented by salt formation with Cu(II) cations. (2) Coordinating ligands like THPTA interact with Cu(I) as well as Cu(II). (3) Ligand prevents Copper anions interaction. PBS bufferisation increases the effectiveness of ligands (BCDA, THPTA). (4) Copper salts and (5) Ligand-Copper complexes have a higher dissociation constant in organic solvent than aqueous solution. Organic solvent is competitive for copper ions. (6) Some ligands like BCDA are suspectible to oxidation in air condition (7) Oxygen and reductant have an has adverse effects on Cu(I) generation. Oxygen presence with reductant leads to generation of reactive oxygen species, damage of reductant and potentially unspecific product formation.

CHAPTER 4: Click Chemistry of bioinspied/fluorogenic flavylium azide

This chapter includes the proof of concept for using fluorogenic chemical tools with the property of emitting bright fluorescence upon click reaction for in vivo imaging as an alternative to commercially available traditional and expensive rhodamine azide. These newly designed derivatives did not show distinguishable emission properties prior and after the triazole formation in click reaction, however the yield of probe 9-FA1 triazole product of FA1 was better than rhodamine azide. The fluorogenic flavylium azides (FA1 and FA2) were designed by Mourad Elhabiri and synthesized by Mustapha Khelladi with the assistance of the master student Lea Vella. My role was to validate the physicochemical properties of two azides together with Valérie Mazan and Bogdan Cichocki. Further, I standardized the clickability properties of FA1 and FA2 with PD ABPP alkyne partners. This involved extensive UV-Vis spectrophotometry to understand the stability of azides, followed by HPLC-MS, and fluorometric analysis of the click reactions with probe 7 and probe 9. This study paved the way to develop novel, affordable, water-soluble, and photostable fluorogenic chemical tools for in vivo imaging. Our study has shown that the substitution pattern of FA1 is important for its reactivity and fluorescence emission properties. FA1 is an affordable, water-soluble and (photo)stable chemical tool, whose reactivity in cycloaddition reactions has been found to be improved with respect to that of rhodamine azide. However, the fluorescence of the constrained flavylium chromophore was not reinstated on reaction with alkyne-based probes (i.e., FA1 did not act as a fluorogenic system). On the other hand, we also clearly demonstrated that the reactivity in CuAAC-type reactions also closely depends on the physico-chemical properties of the alkyne partner."

TABLE OF FIGURES: CHAPTER 4

Introduction and Results

During its intra-erythrocytic development in humans, the parasite ensures its need of nutrients through the digestion of hemoglobin in its acidic food vacuole (FV) (pH ~ 5). The hemoglobin is converted into methemoglobin by a redox reaction (Gitta, B. *et al.,* 2020). This methemoglobin digestion in the parasite's FV generates peptides, reduced superoxide anion ($O_2^{\bullet-}$) and oxidized free heme (Egan, T. J., 2008). $O_2^{\bullet-}$ rapidly disproportionates under acidic conditions to O_2 and H_2O_2, and free heme catalyses Fenton reactions with H_2O_2, which results in the formation of deleterious hydroxyl radicals ($HO^{\bullet}$). To overcome the free heme toxicity, the parasite detoxifies it in its FV in the form of a dark biocrystal called hemozoin. On the other hand, a cytosolic redox network composed of thiols and NADPH-dependent disulfide reductases (glutathione reductases – GR – of the parasite and the host) generates high flux of glutathione, responsible for heme(Fe^{III}) reduction and, in concert with hydrogen peroxide, for destruction of the remaining released toxic heme by Fenton reaction. Because of the complexity of these interrelated processes, information on the overall redox status and pH of a healthy, parasitized or drug-induced cell could help in the diagnosis of disease and guide the therapeutic research (Krauth-Siegel, R. L. *et al.,* 2005).

One of my host research projects thus focuses on the development of red/near-infrared (NIR) ratiometric fluorescent probes for non-invasive real-time measurements in parasitized red blood cells (pRBC) to monitor and quantify local pH and redox alterations. Red/NIR fluorescent dyes are particularly suitable for *in vivo* imaging (*i.e.,* hemoglobin is the main chromophore in pRBCs) because they minimize photo-damage to the cells and avoid cell auto-fluorescence. On the other hand, ratiometric fluorophores ensure minimized interferences with external (excitation intensity, detector sensitivity, cell size) and environmental factors (photo-bleaching, inhomogeneous cellular distribution or local probe concentration). Ideal Red/NIR ratiometric fluorescent dyes have to comply with several criteria: (*i*) solubility in biological media without forming aggregates; (*ii*) (photo)stability; (*iii*) biocompatibility, (*iv*) reduced cytotoxicity, (*v*) cell permeability, (*vi*) appropriate subcellular localization, (*vii*) emission in the biological “open-window” (650-900 nm) (Ren, T. *et al.,* 2017). All these requirements are not fully reached with most of the commercial/reported dyes that still emit light in the visible region, in which absorption by biomolecules is high. In addition, most of the reported intracellular pH (Han, J *et al.,* 2010) (BCECF, SNARF, Lysosensor, Oregon green, (carboxy)fluorescein...) or redox (Amandeep, K. *et al.*, 2016; Méndez-Ardoy, A *et al.*, 2020) fluorescent indicators suffer from other drawbacks (*e.g.,* scarce ratiometric responsive dyes, low quantum yield, high costs, tedious synthesis/functionalization, λ^{em} < 600 nm, not suited for pRBCs staining, not applicable in acidic/oxidative environments, poor (photo)stability, no easy pK_a/redox fine-tuning, no vectorization to the FV) (Han, J *et al.,* 2010).

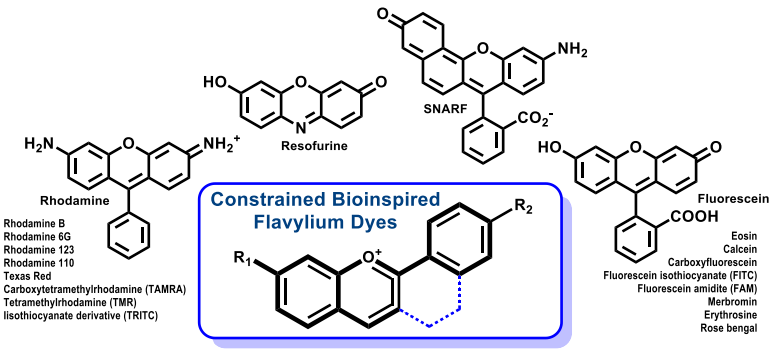

In my host team, the chosen strategy was to develop functional molecular tools bioinspired from a family of ubiquitous natural pigments called anthocyanins. Anthocyanins are pigments

based on a flavylium skeleton (*i.e.,* 2-aryl-substituted benzopyrylium, Figure 4.1) that are of biological importance. They are responsible for most of the wide variety of yellow to blue colours in the flowers, fruits and leaves of many plants. The diversity and complexity of substitution of these photo-stable anthocyanic pigments allows for a wide spectrum of colours. However, no example of naturally occurring brightly fluorescent anthocyanin has been described so far (Duval, R. *et al.*, 2017) due to its instability in weakly acidic to neutral aqueous media (nucleophilic reaction on the 2 or 4-position of ring C, Figure 1) and poor quantum yield. Free rotation through the single bond between rings B and C indeed dissipates away the excitation energy (Figure 4.1). A water molecule can indeed readily react at position 2 of the flavylium core leading to the formation of a reservoir of colourless forms (hemiacetal and chalcones) according to a reversible process called the hydration reaction. *In vivo*, these pigments can be linked to metal ions (metal complexes), interact with other flavonoids (non-covalent π-stacking complexes) or polysaccharide macromolecular carriers so that the corresponding anthocyanins are stabilized. For example, cyanin chloride has a hydration constant $pK_{h'}$ of 2.07 ± 0.02 (*i.e.,* overall hydration equilibrium connecting the flavylium ion to the mixture of colorless forms, hemiacetal and chalcone forms; the flavylium ion is stable up to pH 1-2) and a deprotonation constant $pK_a = 4.03 \pm 0.02$ (proton-transfer equilibrium between the flavylium ion and the coloured quinonoidal base). Interestingly, introduction of a structural constraint in B ring by modifications at position 3 and 2' (*i.e.,* bridging prevents free rotation) resulted in stable and brightly emissive flavyliums with good aqueous solubility and (photo)stability. The nucleophilic attack of a water molecule at the C2 atom of pyrylium ion causes a change in its hybridization from sp2 to sp3. The rigidity and coplanarity induced by $(CH_2)_2$-bridging significantly modify this change in hybridization, make the formation of the constrained 2-hydroxylflavene more difficult, and consequently increases the dye stability in aqueous solutions (Figure 4.1). On the other hand, the free rotation through the single bond between rings B and C dissipates away the excitation energy by a Twisted Intramolecular Charge Transfer (TICT) state. Bridging by an ethylene group prevents this TICT process and thus leads to fluorescent dyes.

Several water-soluble flavylium-based pigments for pH detection (1st generation) with a constrained structure (Figure 4.1). have been accordingly synthesized with good yields (50-70%, unpublished data). The measured pK_a values of these flavylium ions range from 4.3 to 7 and fall in the range of interest for the study of pRBCs. This series of constrained flavylium ions allows detection over a wide spectral range (510-640 nm) with good to excellent quantum yields. The covalent bridging prevents nucleophilic attack of H_2O in position 2 or 4 and induces a significant aqueous stabilization from acidic pH to pH 9-10. Once functionalized with an ionizable site, many compounds demonstrated an emission and excitation ratiometric pH-response. Preliminary imaging experiments with pRBCs showed that MM1-031 (non-pH-sensitive probe) and MM1-063 (pH-sensitive probe) were effective in staining the cytosol of pRBCs (Figure 4.2). MM1-063 and

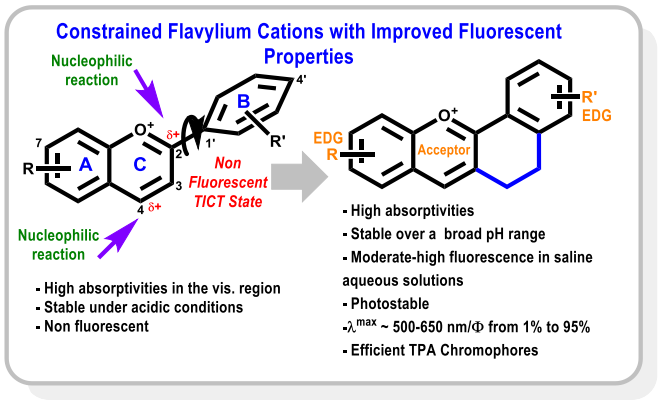

Figure 4. 1. Chemical structure of constrained flavylium ions studied by my host team (unpublished data).

MM1-031 give an easily detectable signal at 5 µM in the red spectral domain and stain parasites exclusively without affecting healthy erythrocytes. All fluorophores stain parasites exclusively without labelling healthy erythrocytes. The different parasite stages were equally stained and the bright field transmission images confirmed cell-permeability and viability of cells after exposure to the dyes.

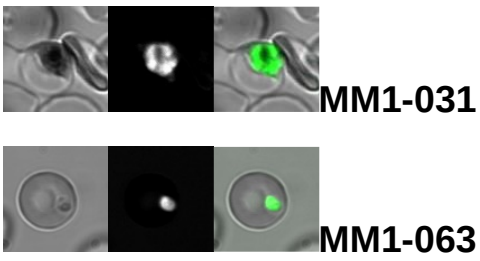

Figure 4. 2. pRBCs imaging with MM1-031 and MM1-063 at 5 µM.Ex 561 nm. Em 570-780 nm. The images have been colorized in green**.**

Auxochromic effects are known to influence the absorption of these dyes but the effects on emission are hardly predictable. In an exploratory approach, my host team used a combinatorial approach (*i.e.,* acidic condensation between tetralones/indanones and substituted salicylaldehydes) to generate about 250 probes, which were then screened in an absorption/emission microplate-reader (Thermofischer Varioskan Flash). A series of potent pH-sensitive fluorescent probes (2nd generation) were accordingly selected, synthesized and investigated with respect to their bright emission. The pK_a values of the ionisable site(s) can be further fine-tuned from 3.3 to 7.3. Several probe candidates display ratiometric responses in two (Figure 4.3) or even three channels (unpublished results) with bright emission.

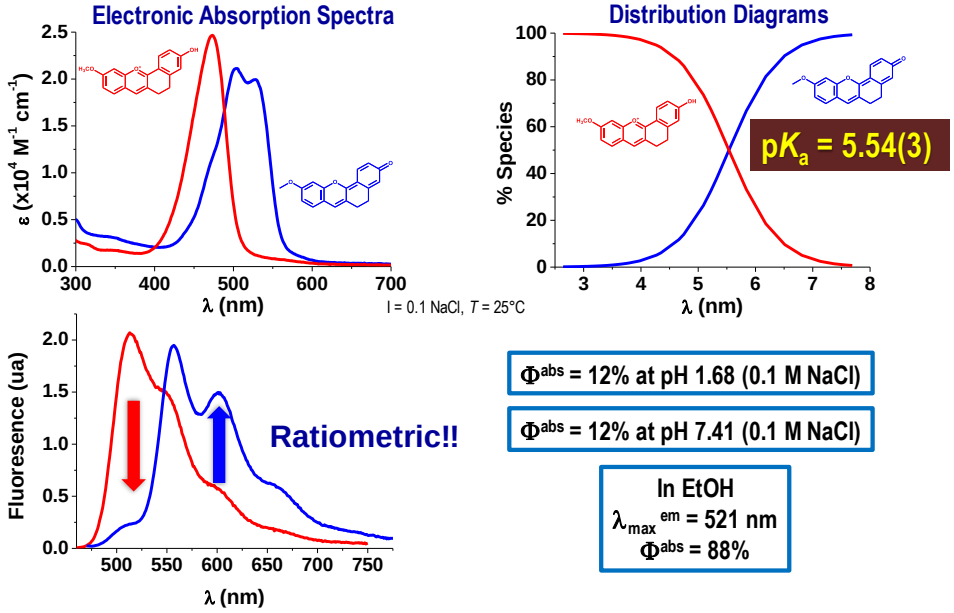

Figure 4. 3. Physico-chemical data obtained for MM1-171. Solvent: water; I = 0.1 M (NaCl); T = 25.0°C.

From this 2nd generation of dyes, a compound allowed determining the vacuole pH of BY2 tobacco plants by confocal fluorescence microscopy (unpublished data) and demonstrated the

proof of concept of this approach. Interestingly, depending on the nature of the probe, specific cell compartments were specifically stained (membrane, mitochondria, vacuole, cytosol, Figure 4.4).

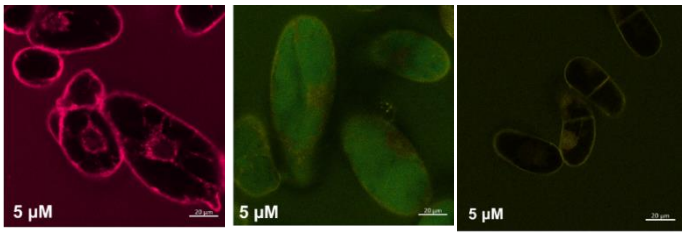

Figure 4. 4. In vivo imaging via fluorescent dyes**:** Specific staining of (A) the membranes and mitochondria, (B) the vacuole, nucleus and cytosol and (C) the membranes of BY2 tobacco cells by confocal microscopy with three related fluorescent dyes.

Synthesis and physico-chemical investig Continued cytoadherence of P*lasmodium falciparum* infected red blood cells after antimalarial treatmentations of azide constrained flavylium-based fluorophores

Finally, other functional fluorescent probes have been also engineered for biological purposes. Azide-derived constrained flavyliums have been prepared (designated LV05N3 or "fluorogenic" azide 1 FA1 and MK34N3 or FA2,Scheme1). Flavylium LV05 was first synthesized by condensation in an acidic medium with gaseous hydrochloric acid in ethyl acetate for 24 hours. The product precipitated in the reaction medium and was obtained with a yield of 60% (after purification on silica gel). LV05 was measured to be a bright red-emitting compound (λ_{em} = 628 nm/Φ^{abs} = 14% at pH 7.41 and λ_{em} = 626 nm/Φ^{abs} = 73% in ethanol). The azide LV05N3 was then synthesized by a Sandmeyer reaction ($NaNO_2$, NaN_3) in ethanol for 3 hours. The resulting product was not pure enough because sodium azide was added in excess to ensure that all of the starting material reacted. The residue was purified by silica gel chromatography (CH_2Cl_2/ethanol = 90:10, v/v) to afford LV05N3 with a yield of 55%.

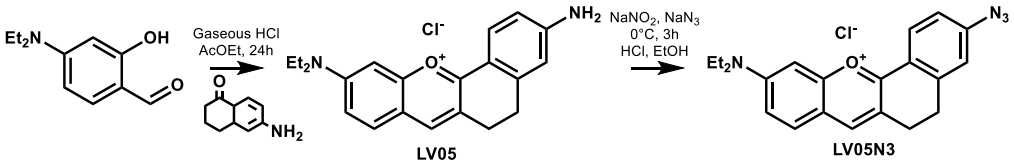

Scheme 1. Synthetic route to the azide derived constrained flavylium LV05N3.

Interestingly, the fluorescence emission of LV05 was almost completely vanished upon conversion of the amino into the azide function. This likely originates from the azide lone pair electrons that participate in fluorescence quenching either through internal charge transfer (ICT) or by photoinduced electron transfer (PET) processes. Furthermore, the absorption spectrophotometric properties of LV05 were found to be markedly altered upon this amino-to-azide conversion (Figure 4.5 in ethanol and at pH 7.41). Therefore, it was expected that the fluorescence emission seen for the amino derivative LV05 could be recovered upon the formation of a triazole ring (“Huisgen-clik” conditions) as already observed in some reported systems (Noda, H. *et al.,* 2019; Shieh, P. *et al.,* 2015; Decuypère, E. *et al.*, 2018). This azide dye would therefore act as a "fluorogenic" system that turns on brightly fluorescent upon functionalization with an alkyne function. If successful, this functional tool could be of great use

with the potent antimalarial plasmodione (*click&fish*" approach for identification of the plasmodione biological targets).

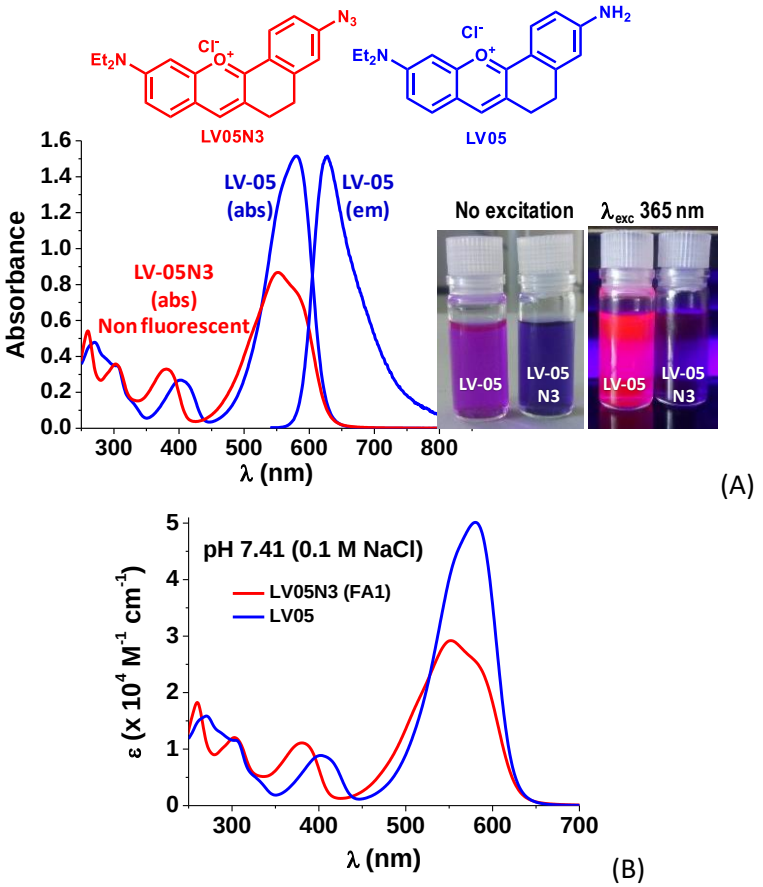

Figure 4. 5. Physiochemical parameters of the LV05N3: (A) Absorption and emission spectrophotometric data recorded for LV05 and LV05N3 (FA1) in ethanol demonstrating the quenching process that occurs for the azido derivative. (B) Absorption spectrophotometric data recorded for LV05 and LV05N3 (FA1) in aqueous buffered solution (pH 7.41 with 0.1 M NaCl).

Scheme 2 depicts the synthetic approach use to prepare MK34N3 (FA2) that displays an ionizable site. 2,4-dihdroxy-5-methoxybenzaldehyde was first synthesized by performing a selective deprotection using $AlCl_3$ in dichloromethane for 23 hours (Cananzi, S. *et al.*, 2011). The product was obtained pure with a yield of 40% (after recrystallization). This reaction required 8 equivalents of $AlCl_3$ to ensure the deprotection of the two methoxy into the corresponding hydroxy groups. MK34 was then prepared by acidic condensation (gaseous HCl in ethyl acetate) between 2,4-dihdroxy-5-methoxybenzaldehyde with 6-amino-tetralone (isolated after precipitation in ethyl acetate, yield 48%).

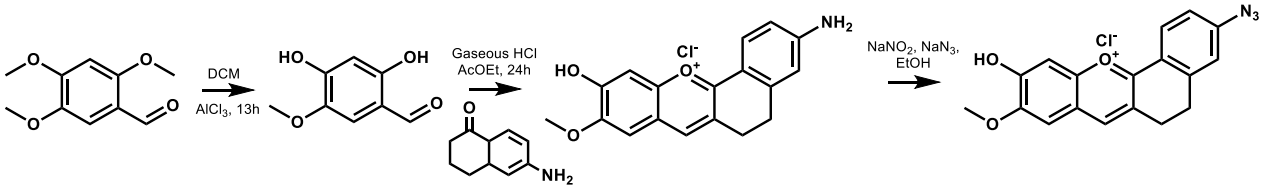

Scheme 2. Synthetic route to the azide derived constrained flavylium MK34N3 (FA2).

The physico-chemical investigation on MK34 provided interesting results. MK34 is associated to protonation equilibrium with a pK_a value of 4.89(3) thus indicating that the quinonoidal base (Figure 4.6) will be the predominant species under physiological conditions (pH 7.4). This is in contrast with

LV05 which does not display any ionizable site and remains the predominant species over a broad range of pH. The flavylium species is characterized by an intense emission centred at 574 nm (Φ^{abs} = 22%; λ^{em} = 583 nm, Φ^{abs} = 50 % in ethanol) while its related quinonoidal analogue was found to display a bathochromically shifted emission (λ^{em} = 595 nm, Φ^{abs} = 31 %). MK34 was then converted into its azide analogue by using the same experimental conditions than those used for LV05N3. MK34N3 was purified by using semi-preparative silica chromatography.

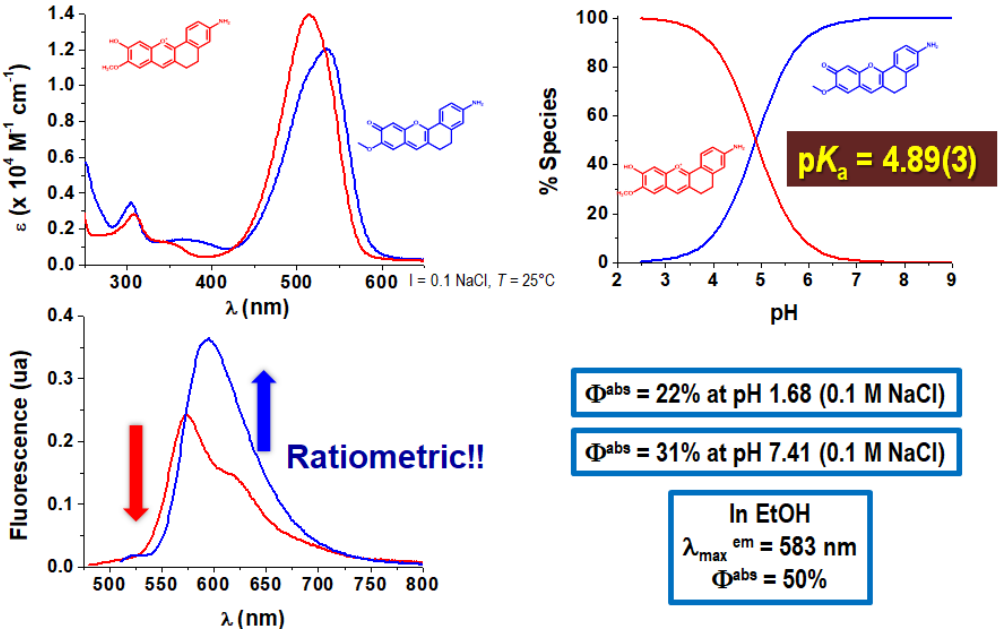

Figure 4. 6. Physico-chemical data obtained for MK34. Solvent: water; *I* = 0.1 M (NaCl); *T* = 25.0°C.

Clickability properties

To select the best probe for identifying the PD interactome, we first evaluated the clickability of different PD-ABPs using characteristically distinct azides such as the commercially available fluorescent rhodamine azide (RA) and the two "fluorogenic" azides (LV05N3 - "fluorogenic" azide 1 - FA1 - and MK34N3 "fluorogenic" azide 2 - FA2,Figure 4.7). The "fluorogenic" azides are not fluorescent as such on their azide form and are anticipated to brightly emit fluorescence emission after their conversion into their triazole form following a click reaction (Shieh et al., 2015; X. Zhu et al., 2016).

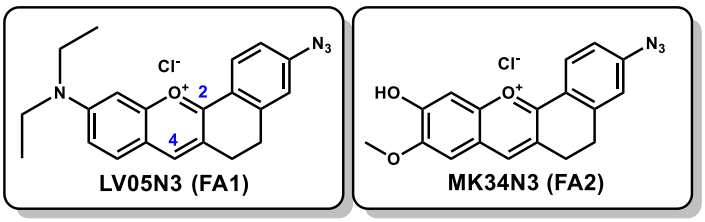

Figure 4. 7. Chemical structures of LV05N3 (FA1) and MK34N3 (FA2)

As stated previously, FA1 and FA2 were built on a constrained bioinspired flavylium core and were specifically synthesized to discriminate the fluorescence of the reactants (azide form: fluorescence OFF) with respect to that of the click product (triazole form: fluorescence ON) that was not possible with the commercially available fluorescent rhodamine azide (RA). Probe 7

and 9 being abundantly available and found to be the better soluble PD-ABPP probes, we then used these two compounds to set the flavylium azide click reaction conditions.

The stability and reactivity of the two major partners of the “Huisgen-click” reaction (alkyne and azide) are important factors to control since they contribute to the successful formation of triazole product. Since triazole formation is mediated by the copper(I) catalyst in the click reaction, we first tried to define the optimal conditions and combination of copper(II) source, ligand and reductant. Prior using LV05N3 (FA1) for the click reactions, we first studied its stability with respect to the reductants classically used in the “Huisgen-clik” reaction such as sodium ascorbate (NaASc) and tris(2-carboxyethyl)phosphine (TCEP,Figure 4.8).

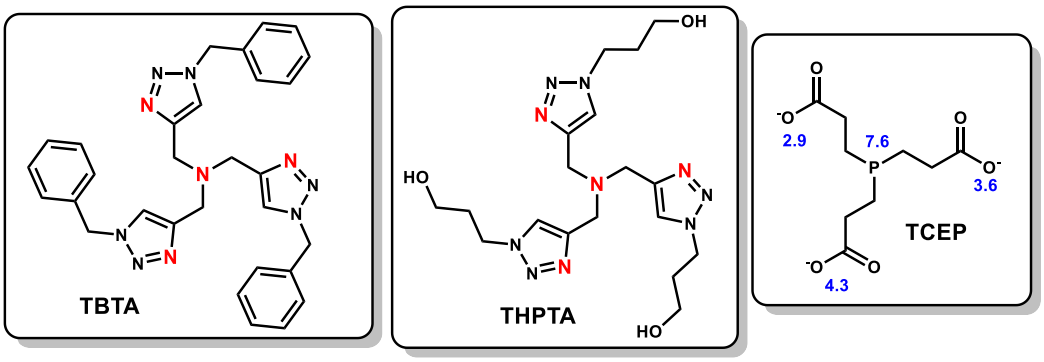

Figure 4. 8. Chemical structures of TBTA/THPTA (the red colour indicates the Cu(I) binding units) and of TCEP (pK_a values are given in blue).

As compared to free FA1, excess of tris((1-benzyl-4-triazolyl)methyl)amine ligand (TBTA,Figure 4.8) and sodium ascorbate (NaASc) reductant (> 1 mM) leads to precipitation as well as the degradation of the FA1 as seen by the apparent fading in its violet colour. Precipitation was noticeably evident by increasing NaASc and TBTA (Figure 4.9) A). It has been reported that the degradation of anthocyanins in the presence of ascorbic acid can result from a condensation of ascorbic acid on the C4 position of the pyrylium moiety (Figure 4.7) leading to bleaching of the dye (De Rosso, V. V. *et al.*, 2007). It has also been proposed that this bleaching process results from oxidative cleavage of the pyrylium ring. In this radical mechanism (Iacobucci, G.A. *et al.*, 1983), ascorbic acid acts as a molecular oxygen activator thereby producing free radicals that markedly alter the dye chromophore. This therefore prompted us to opt for the water-soluble tris(3-hydroxypropyltriazolylmethyl)amine ligand (THPTA, Figure 4.8) and the reductant TCEP for optimizing the click reaction conditions at physiological pH (pH 7.2) (Stanislas, I., *et al.* 2011; Hong, V., *et al.* 2009) However, the phosphine-based TCEP reagent has to be used in controlled conditions. TCEP potentially binds copper ions (carboxylate based chelator) and induces inhibitory effects on the click reaction (Krezel, A. *et al.*, 2003). TCEP can also contribute to consumption of azide compounds in Staudinger reactions (Staudinger, H. *et al.*, 1919; Gololobov, Y. G.; *et al.*; 1981) leading to the corresponding amines and tris(2-carboxyethyl)phosphine oxide as byproducts (Chen, Y. *et al.*, 2011; Sletten, E. M. *et al.*, 2009).

As shown in Figure 4.9B, FA1 also showed susceptibility to reduction by TCEP. Using absorption spectrophotometry and TCEP as the reductant, it was found that the main absorption band centred at 550 nm for FA1 underwent significant bathochromic and hyperchromic shifts. These spectral properties were found to be similar to those of LV05 (*i.e.,* amino-derived analogue of LV05N3, see above). This behaviour contrasts with the feature observed with the NaASc reductant with which a significant bleaching of the flavylium-based dye and its subsequent precipitation was observed (see above).

With NaASc at 1 mM, reduction (and subsequent degradation) of the flavylium backbone can thus be proposed to rationalize the corresponding observations (see above). In the presence of TCEP, the increase in fluorescence observed at the end of reaction is thus proposed to be related to the reduction of the azide function of FA1 into the amine one rather than the click product (Figure 4.9c). This azide reduction is related to the Staudinger reaction (very mild azide reduction discussed above, Figure 4.9D) (Leffler, J. E. *et al.*, 1967; Gololobov, Y. G. *et al.*, 1992). We indeed do not observe any additional absorption bands that could account for the formation of the triazole moiety. In addition, even though the fluorescence emission was reinstated upon reaction with TCEP, this latter was similar to that of LV05.

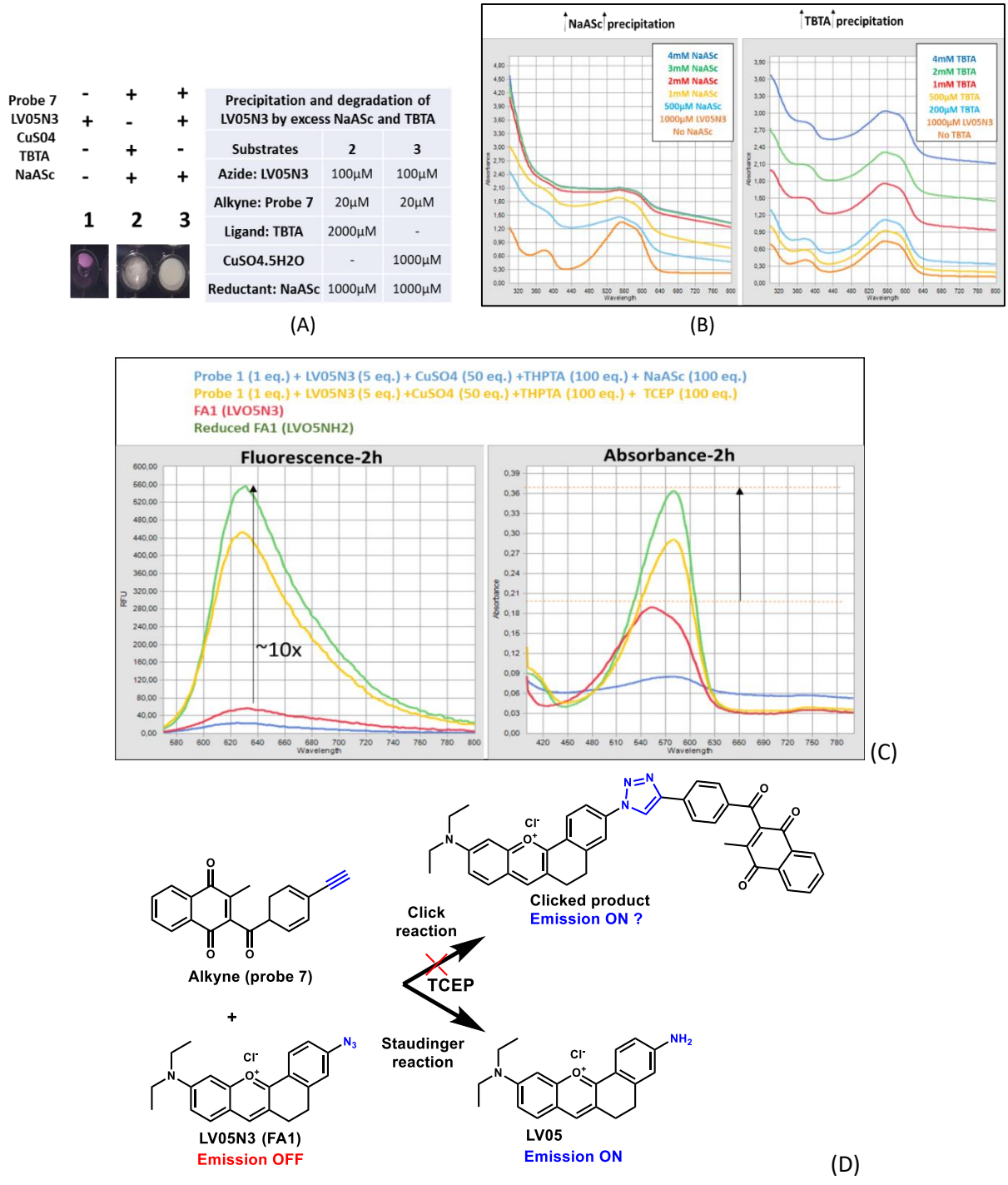

Figure 4. 9. Feasibility of ligand TBTA and reductant NaASc for flavilium azide click reaction. (A) Effect of ligand TBTA and NaASc reductant used in excess on FA1 in aqueous conditions with ~ 3% DMF. 1.

FA1 alone (100 µM), 2. Excess of NaASc, 3. Excess of TBTA. (B) Effect of increased concentrations of NaASc (left) and TBTA (right) on FA1 absorption properties. (C) Influence of the reductants NaASc and TCEP on the click reaction. Conditions: Probe 7 (1 equiv.) + FA1 (5 equiv.) + $CuSO_4$ (50 equiv.) +THPTA (100 equiv.) + NaASc (100 equiv.) or TCEP (100 equiv.). FA1 (LV05N3) and its reduced form (LV05) were used as controls to monitor the absorbance and fluorescence variations. (D) Schematic representation of the click reaction and Staudinger reaction.

Following these first results, we tried to define appropriate experimental conditions that could help to avoid the reduction of FA1 by TCEP. We indeed decided to rule out the use of NaASc since this reductant was shown to lead to the degradation of the flavylium backbone. As indicated above, the introduction of a structural constrain (*i.e,* bridging with an ethyl group between position 3 and 2') significantly increased the aqueous stability of LV05 and LV05N3 (FA1). However, under basic conditions, FA1 can undergo a reversible and slow attack of a hydroxyl anion on the electro-deficient positions of the pyrylium moiety (C2, Figure 4.7) and subsequently lead to ring opening to provide the neutral or ionized chalcones (Figure 4.7) (Pessêgo, M. *et al.*, 2017). Decreasing the pH value reinstates the pyrylium ion. The formation of the chalcones is characterized by the appearance of a new absorption band at 435 nm (associated to a yellowish to orange colour,Figure 4.10). This ring opening and isomerization to chalcones most likely increase the hydrophobicity of the compound and lead to the slow precipitation over time under basic to neutral conditions.

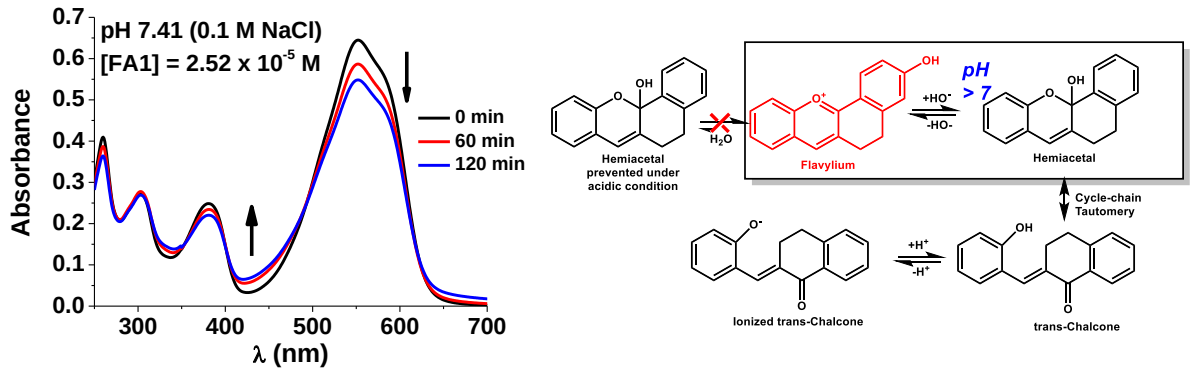

Figure 4. 10. Slow conversion of the flavylium LV05N3 into its corresponding chalcone as evidenced by the absorbance increase at 435 nm.

Reduction of FA1 by TCEP was closely related to the acidity of the medium (Figure 4.11). Under acidic conditions, the azide reduction of FA1 is indeed significantly prevented. It is worth mentioning that TCEP is characterized by four protonation constants (pK_a of TCEP: 2.9, 3.6, 4.3 and 7.6) (Krezel, A. *et al.*, 2003). The highest pK_a value (pK_a = 7.6) is associated to the protonation of the phosphine function thus explaining the inability of TCEP to significantly contribute to the azide reduction (Staudinger reaction) when decreasing the acidity of the medium. As a consequence, no reduction of FA1 could be observed at pH 4.8 and 3.0 (Figure 4.11B and C).

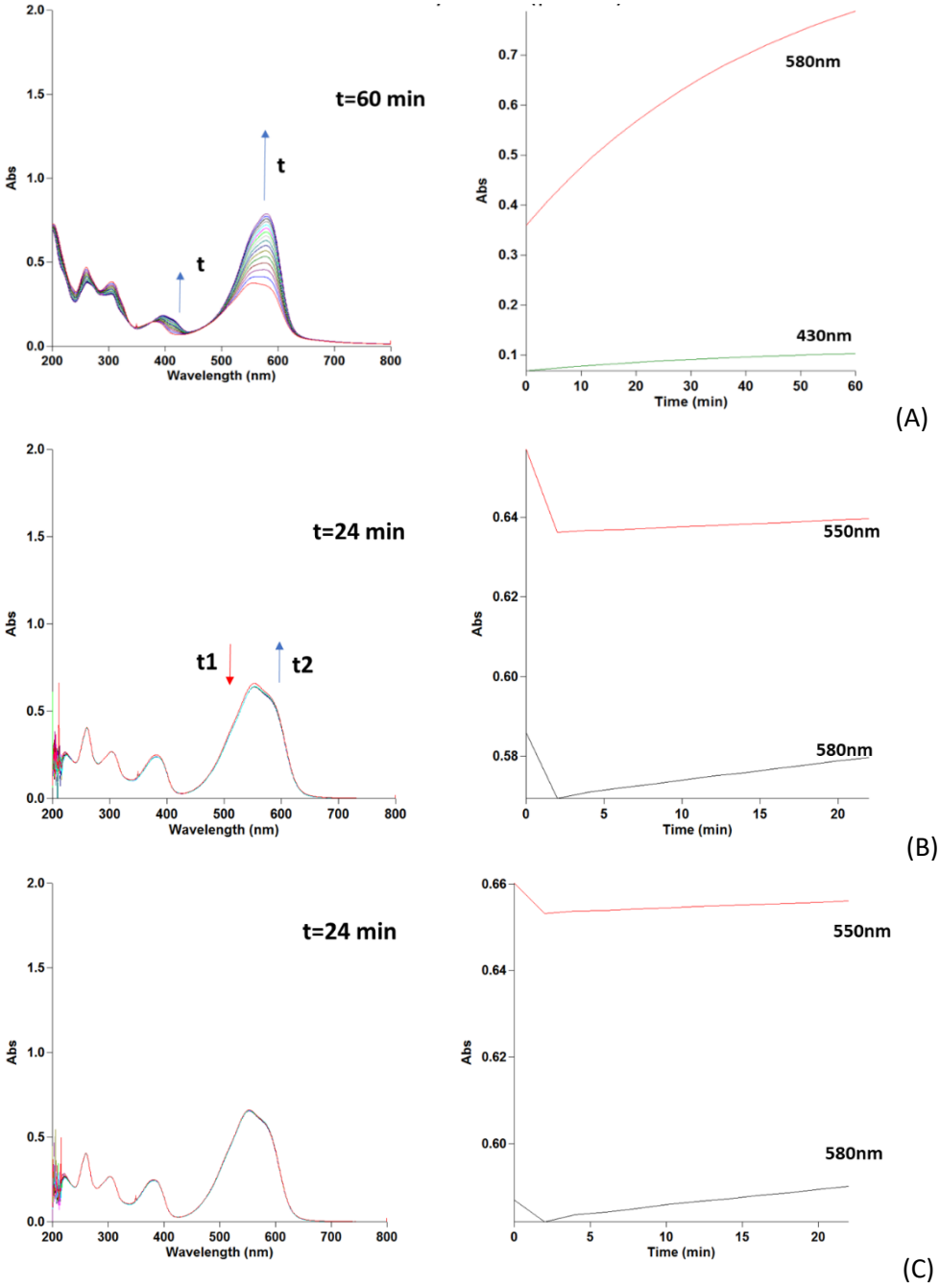

Figure 4. 11. Absorption spectrophotometric spectra of LV05N3 (FA1) in the presence of TCEP at different pH values. (A) pH 7.2; (B) pH 4.8; (C) pH 3.0. Azide reduction by TCEP can be observed by the bathochromic and hyperchromic shifts of the main absorption band at 550 nm.

However, lowering the pH value would most likely prevent Cu(II) reduction as TCEP was used for this purpose. Indeed, the phosphine unit is the central element to enable this redox reaction. We thus examined the order of addition of the different partners in the click reaction. It is indeed anticipated that the reduction of FA1 by TCEP could be minimized if this addition sequence is well controlled. As demonstrated in Figure 4.12A the order of the addition of the different partners (pre-reduction of the Cu(II) complex) is extremely important in click reaction with FA1 and PD-ABPP. Reacting the alkyne and the azide with pre-incubated copper(II), THPTA ligand and TCEP reductant led to formation of cuprous catalyst and pre-oxidation of TCEP. This allowed protecting FA1 from undesired Staudinger reaction and, thus participation of the azide with the alkyne in the triazole formation. In spite of FA1 being water-soluble, the

percentage of acetonitrile solvent was further increased up to 50% to protect from the precipitation over the click reaction with PD-ABPP(Figure 4.12). This likely arose from the simultaneous precipitation of probe and of the click product in aqueous conditions. With the objective of using the "fluorogenic" azides FA1 or FA2 for *in vivo* imaging, we continued to use below 10% of solvent concentration for the reaction unless mentioned otherwise.

Solvent	TCEP	$CuSO_4$	THPTA	Azide	Alkyne (probe 7 or AZ47)
2% ACN	25 µM	20 µM	20 µM	20 µM	20 µM

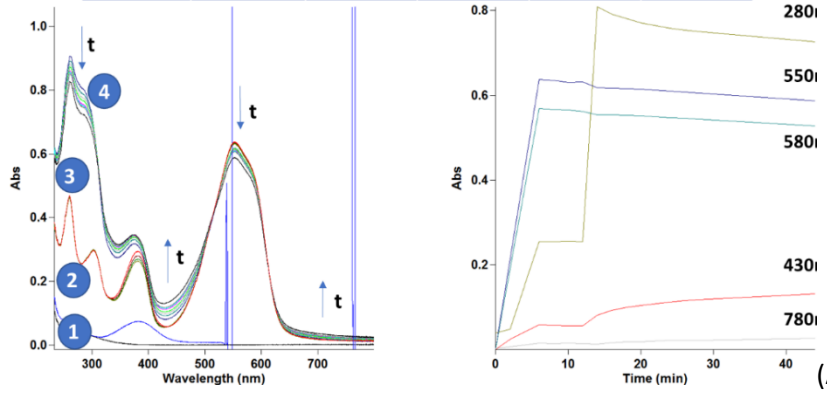

(A)

Solvent	TCEP	$CuSO_4$	THPTA	Azide	Alkyne (AZ47)
50% ACN	25 µM	20 µM	20 µM	20 µM	20 µM

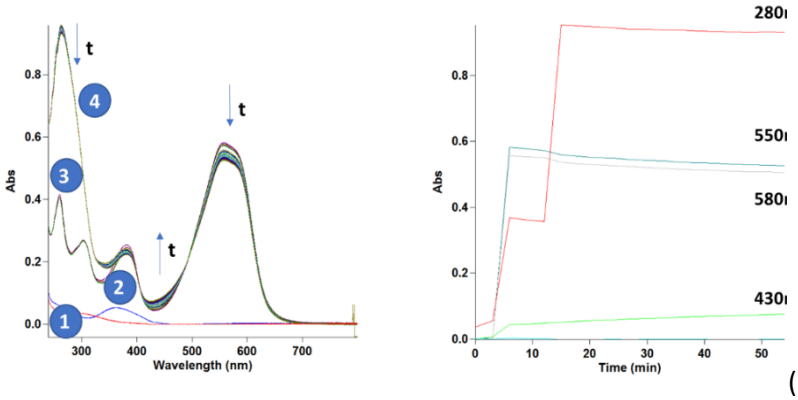

(B)

Solvent	TCEP	$CuSO_4$	THPTA	Azide	Alkyne (MD43)
50% ACN	25 µM	20 µM	20 µM	20 µM	20 µM

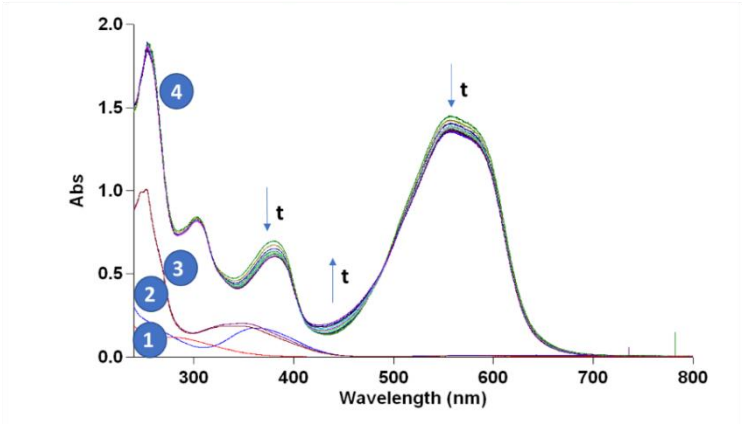

(C)

Figure 4. 12. Absorption spectra indicating the order of addition of the reactants as well as percentage of the acetonitrile ACN solvent used in the click reaction with either probe 7 (AZ47) or probe 9 (MD43).Sequence of addition: **1.** $CuSO_4$+THPTA: weak absorption band at about 260 nm. **2.** TCEP (reductant): bathochromic shift of the absorption band (~ 360 nm) indicative of Cu(II) to Cu(I) reduction. **3.** Alkyne (Probe 7/AZ47 for A and B or probe 9 for C) absorption corresponding to the sum of the cuprous complex and the alkyne. **4.** Azide (FA1) to initiate the click reaction. ACN solvent %: (A) 2% for FA1-probe 7 click reaction (B) 50% for FA1-probe 7 click reaction and (C) 50% for FA1-probe 9 click reaction.

Based on these initial results and the modified conditions set with rhodamine azide (RA) for which addition of stepwise doses of pre-incubated Cu(I) complex was carried out, we performed the click reactions of FA1 with probes 7 and 9. As shown in (Figure 4.14). A, the yield of the click reaction of probe 7 with FA1 carried over 2 hours or overnight was approximately 20% while about 80% of the FA1 dye was consumed in both situations, indicating that no more than 80% of FA1 was consumed in 2 hours to produce the triazole-based product (Figure 4.14A and B). On the other hand, after the addition of Cu(I) complex, the colour of the FA1 solution was slightly altered and faded away completely after the click reaction proceeded regardless of the probe involved in this process. This was clearly evident with the significant decrease of the absorbance of the main absorption band over time (Figure 4.14C).

To assess these properties, LC-MS measurements were performed on the 7/FA1 and 9/FA1 reaction mixtures. For 7/FA1, using absorption detection at 540 nm, the LC chromatograms clearly showed the presence of three distinct and major peaks with retention time of 27.2, 31.9 and 42.9 minutes, respectively (Figure 4.14E). Interestingly, the peaks at retention times of 27.2 and 31.9 minutes were already present for solutions containing only FA1 (Figure 4.14E). FA1 was easily assigned to the retention peak measured at 31.9 minutes as evidenced by the experimental *m/z* of 345.178 (Figure 4.14E) that perfectly matches the theoretical pseudomolecular peak expected for FA1 ($[FA1]^+$ *m/z* = 345.171 for $C_{21}H_{21}N_4O^+$). The retention peak at 27.2 minutes was associated to a species with a *m/z* value of 523.334 that could not be characterized (Figure 4.14E). To get a better understanding, the UV-visible absorption spectrum of the FA1 species related to the retention peak at 31.7 minutes (Figure 4.15D) was recorded using a diode array detector (DAD, λ^{max} = 552 nm) and perfectly matched that measured in aqueous solution (Figure 4.5, λ^{max} = 552 nm), while that measured for the retention peak at 27.1 minutes showed a significant bathochromic shift of the absorption lying

at high energies (DAD, λ^{max} = 586 nm) in agreement with LV05 and QP4 taken as references (Figure 4.13).

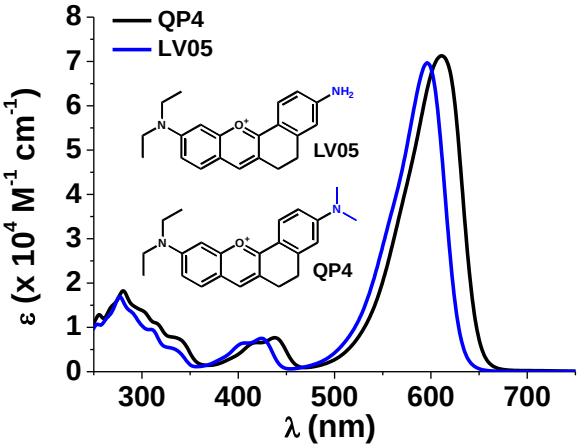

Figure 4. 13. Electronic absorption spectra of fluorophores LV05 and QP4 closely related to LV05N3 and the expected absorption of the click products.

The addition of Cu(I) catalyst (Figure 4.14F) does not significantly alter the LC profile observed for FA1 alone. The two retention peaks at 27.2 and 31.9 minutes were still observed and corresponded to the same *m/z* values described in the absence of Cu(I).

Importantly, the click product derived from the reaction of FA1 with probe 7 was clearly evidenced with the retention peak at 42.9 minutes (Figure 4.14F). The theoretical pseudomolecular peak expected for the 7/FA1 click product ($[7\text{-FA1}]^+$, *m/z* = 645.2501 for $C_{41}H_{33}N_4O_4^+$) perfectly matches that determined experimentally (*m/z* = 645.254). This substantiated the ability of FA1 to efficiently participate to CuAAC reaction with PD-ABPs such as probe 7.

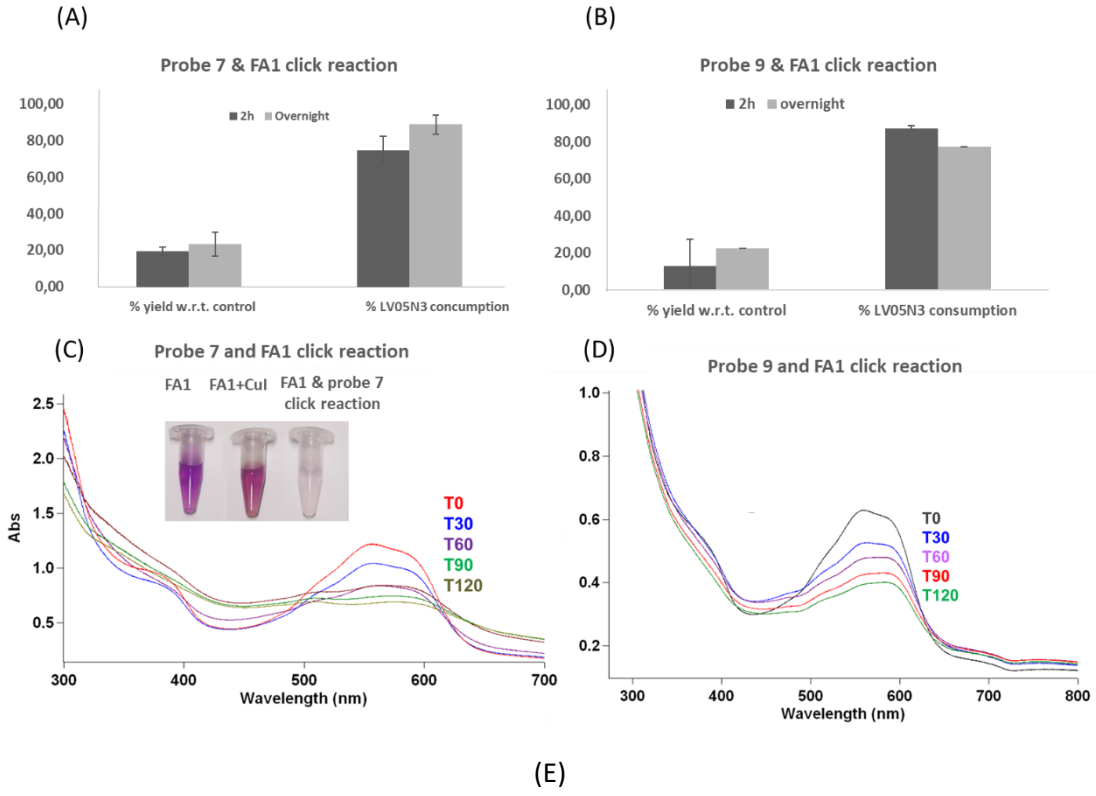

(E)

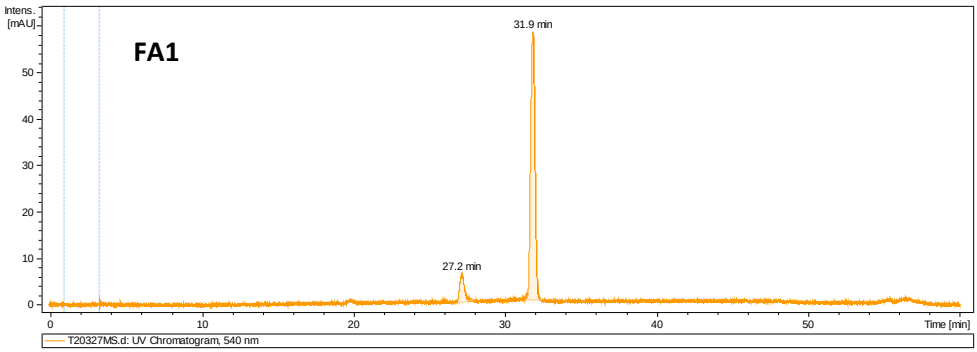
FA1
31.9 min
27.2 min
Intens. [mAU]
Time [min]
T20327MS.d: UV Chromatogram, 540 nm

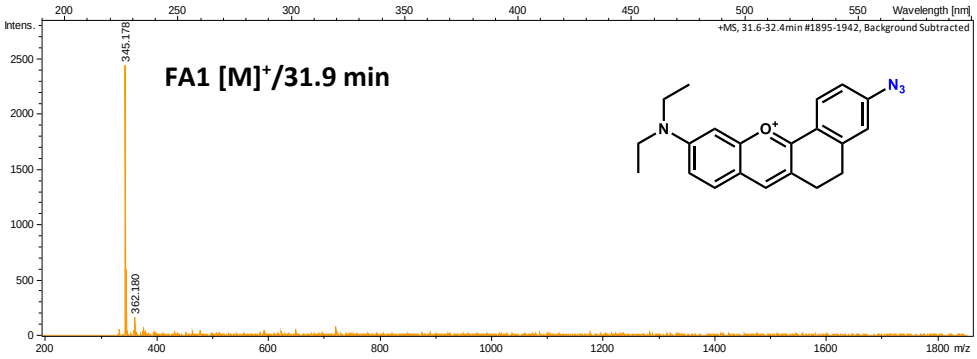
Wavelength [nm]
+MS, 31.6-32.4min #1895-1942, Background Subtracted
FA1 [M]+/31.9 min
345.178
362.180
m/z

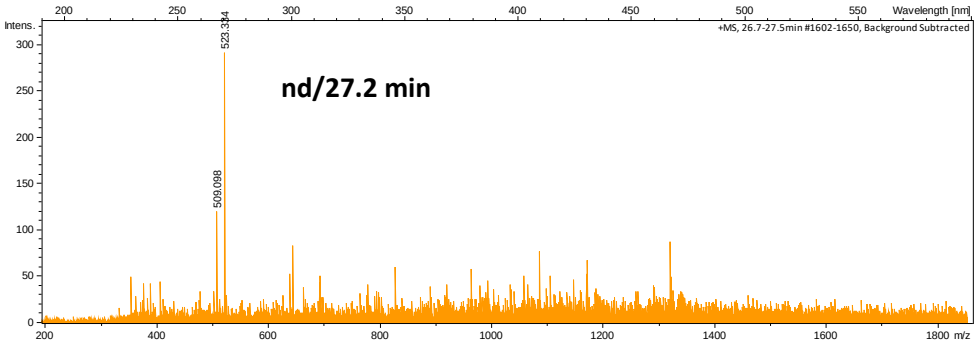
Wavelength [nm]
+MS, 26.7-27.5min #1602-1650, Background Subtracted
nd/27.2 min
523.354
509.098
m/z

(F)

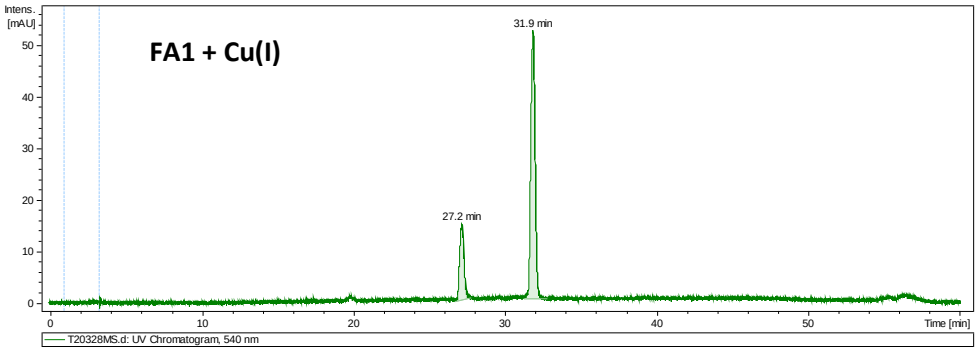
FA1 + Cu(I)
31.9 min
27.2 min
Intens. [mAU]
Time [min]
T20328MS.d: UV Chromatogram, 540 nm

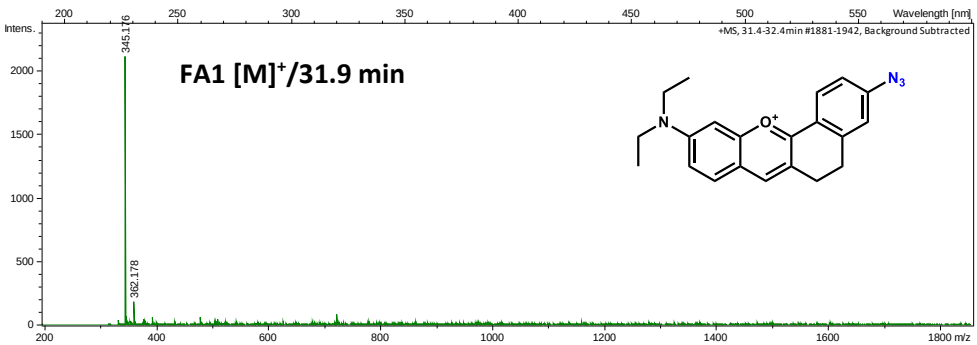
Wavelength [nm]
+MS, 31.4-32.4min #1881-1942, Background Subtracted
FA1 [M]+/31.9 min
345.176
362.178
m/z

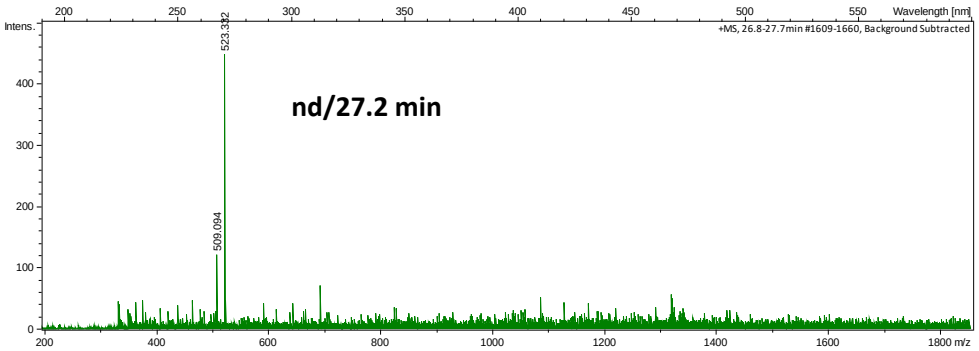
nd/27.2 min
523.342
509.094
+MS, 26.8-27.7min #1609-1660, Background Subtracted
Wavelength [nm]
Intens.
m/z

(G)

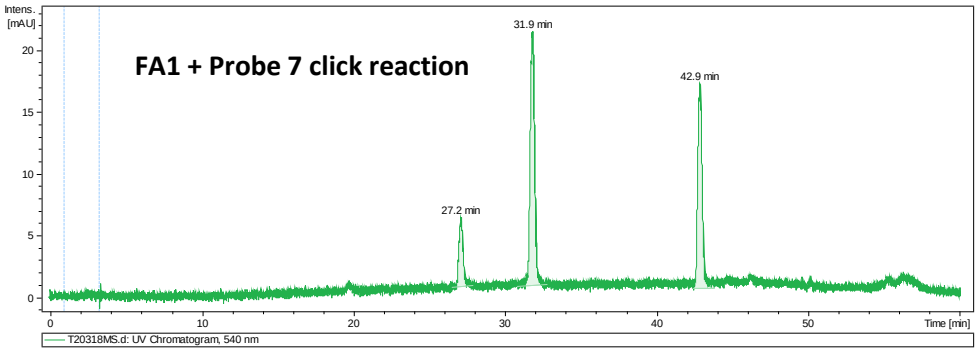
FA1 + Probe 7 click reaction
31.9 min
42.9 min
27.2 min
Intens. [mAU]
Time [min]
T20318MS.d: UV Chromatogram, 540 nm

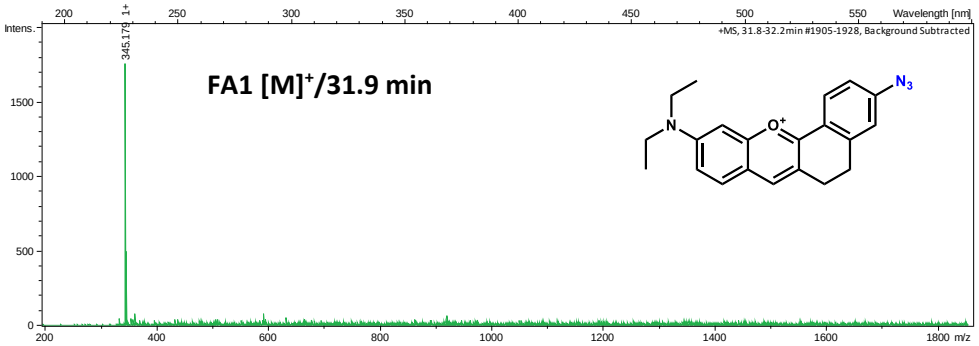
FA1 [M]+/31.9 min
345.179 1+
+MS, 31.8-32.2min #1905-1928, Background Subtracted
Wavelength [nm]
Intens.
m/z

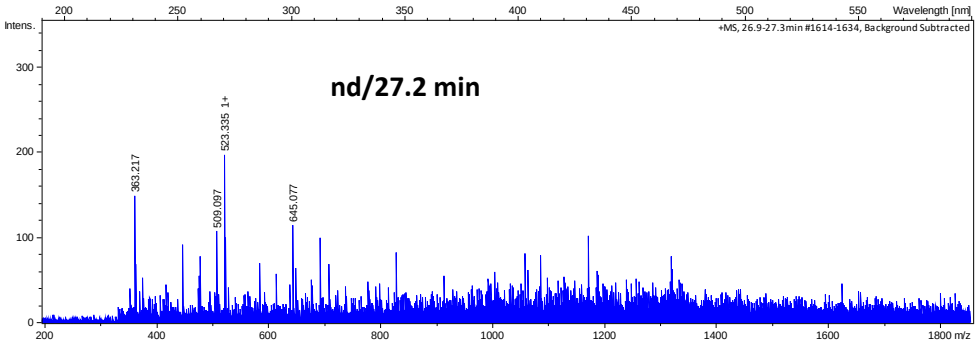
nd/27.2 min
523.335 1+
363.217
509.097
645.077
+MS, 26.9-27.3min #1614-1634, Background Subtracted
Wavelength [nm]
Intens.
m/z

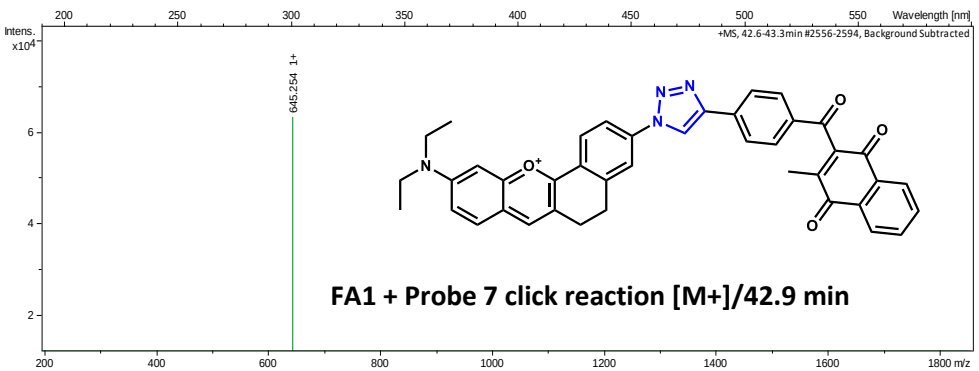
FA1 + Probe 7 click reaction [M+]/42.9 min
645.254 1+
+MS, 42.6-43.3min #2556-2594, Background Subtracted
Wavelength [nm]
Intens.
x10^4
m/z

Figure 4. 14. Click reaction of FA1 with probe 7 (AZ47) and probe 9 (MD43)in aqueous conditions with 6.8% DMF under strict oxygen-free conditions with 4 stepwise additions of doses of pre-formed Cu(I) complex freshly prepared from $CuSO_4.5H_2O$ (1 equiv.) + THPTA (1 equiv.) + TCEP (1 equiv.) in the following manner: at T_0 a pre-incubated Cu(I) complex during 45 minutes was added, while at T_{30}, T_{60} and T_{90} a pre-incubated Cu(I) complex during 20 minutes was added. Reaction time: 2h. By the end of reaction (*i.e.,* at 2h or overnight reaction), the CuAAC products with probe 7 (C) or probe 9 (D) was analysed by absorption spectrophotometry and ESI-MS (E, F and G for probe 7, Figure 4.14. for probe 9). For 2h and 24h reaction N=3 for probe 7 (A) and probe 9 (B).

Using the same analytical tools, we then investigated the click reaction between FA1 and probe 9 (Figure 4.15A). As seen previously, FA1 was related to a retention peak at about 31.9 minutes. MS analysis of this retention peak (Figure 4.15B) confirmed the presence of the flavylium azide as shown by the experimental *m/z* at 345.178 that agrees with the theoretical pseudomolecular peak expected for FA1 ($[FA1]^+$ *m/z* = 345.171 for $C_{21}H_{21}N_4O^+$). The LC profile of FA1 alone or in the presence of Cu(I) also showed the presence of a retention peak of weak intensity at 27.2 minutes. As seen previously, this retention peak is mainly associated to a species with a *m/z* value of 523.334 that could not be characterized (Figure 4.15C) . As observed with probe 7, addition of Cu(I) catalyst (Figure 4.14A) does not influence the LC profile measured for FA1 alone. The two retention peaks at 27.2 and 31.9 minutes were still observed and corresponded to the same *m/z* values described in the absence of Cu(I). Interestingly, addition of probe 7 to FA1/Cu(I) resulted in the formation of an intense retention peak at about 42.6 minutes (Figure 4.15D). Detailed analysis of the MS spectrum associated to this retention peak clearly revealed the presence of the click product between FA1 and probe 7 as evidenced by the experimental *m/z* value at 720.248. This experimental value perfectly matches that calculated for the theoretical pseudomolecular mass ($[9\text{-}FA1]^+$, *m/z* = 720.2458 for $C_{42}H_{34}N_5O_7^+$). The data obtained for FA1 with the PD-ABPs 7 and 9 thus demonstrate unambiguously the ability of azido-flavylium to participate effectively in CuAAC cycloaddition reactions.

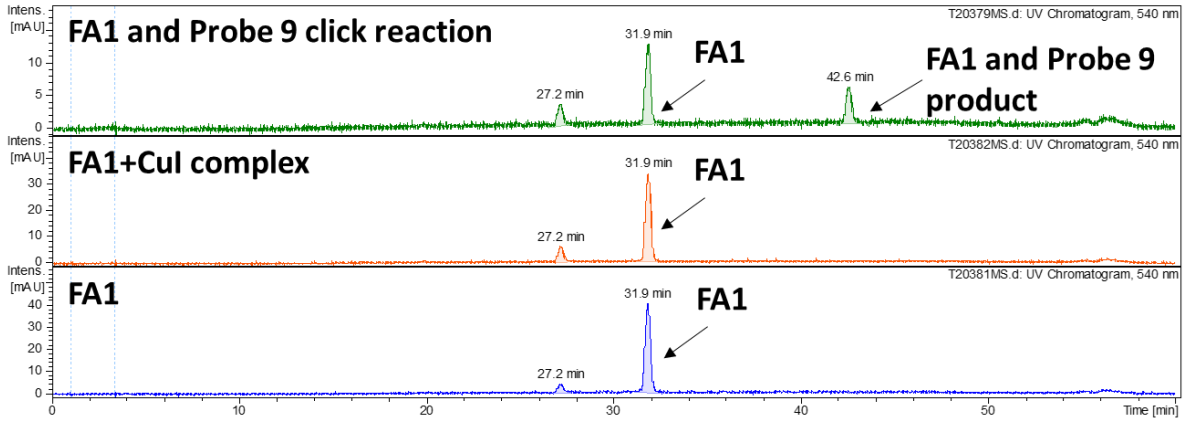

(A)

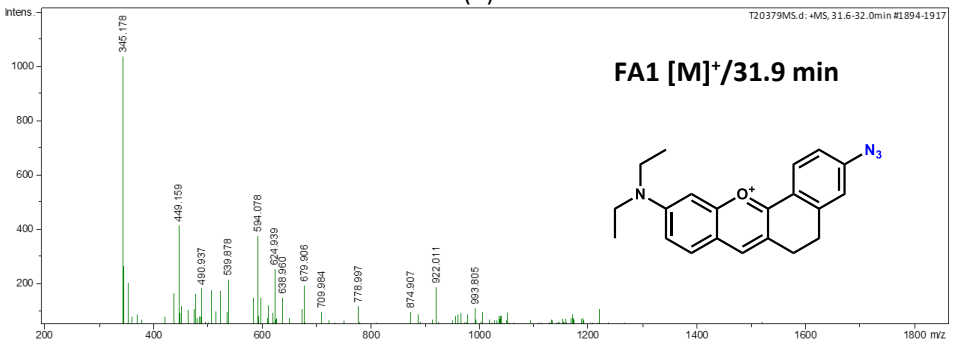

(B)

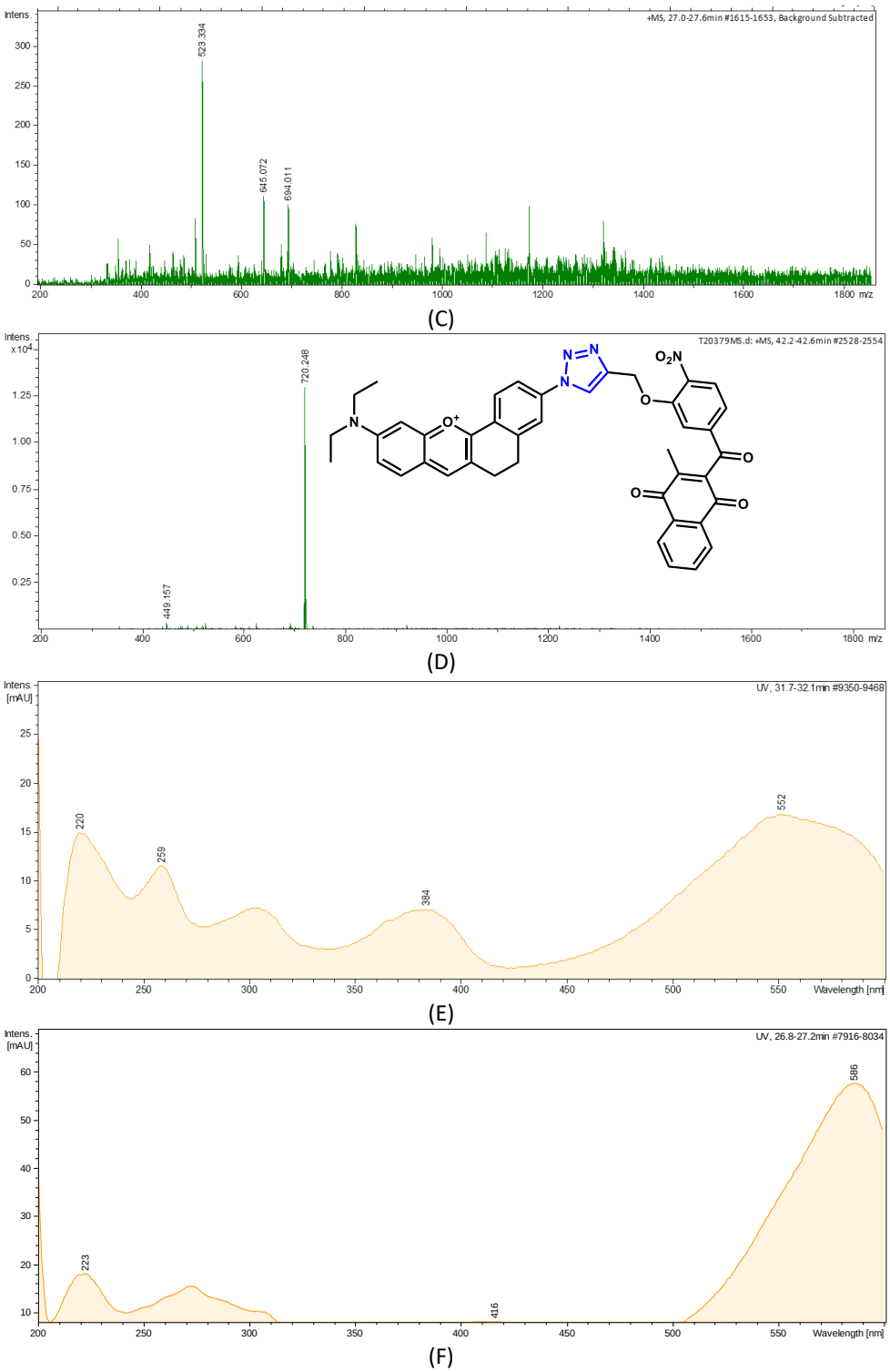

Figure 4. 15. Click reaction of FA1 with probe 9 (MD43) (A) in aqueous conditions with 6.8% DMF under strict oxygen-free conditions with 4 stepwise addition of doses of pre-formed Cu(I) complex, freshly prepared from $CuSO_4.5H_2O$ (1 equiv.) + THPTA (1 equiv.) + TCEP (1 equiv.) in the following manner – at T_0 a pre-incubated Cu(I) complex during 45 minutes was added, while at T_{30}, T_{60} and T_{90} a pre-incubated Cu(I) complex during 20 minutes was added. Reaction time: 2h. By the end of reaction (*i.e.,* at 2h or

overnight reaction), the CuAAC product with probe 9 was analysed by ESI-MS (B, C and D). Absorption spectra recorded with DAD for the retention peaks at 27.2 and 31.9 minutes (E and F)

We then compared FA1 with another flavylium-based azide FA2 (MK34N3) (Figure 7). It is worth mentioning that FA2 displays an ionizable site on cycle A so deprotonation occurs at physiological pH affording the neutral quinonoidal base (Figure 4.16). Even though the protonation constant was not determined for FA2, the physico-chemical data obtained on its precursor MK34 (Figure 4.6) allowed estimating a pKa value at about 5-6.

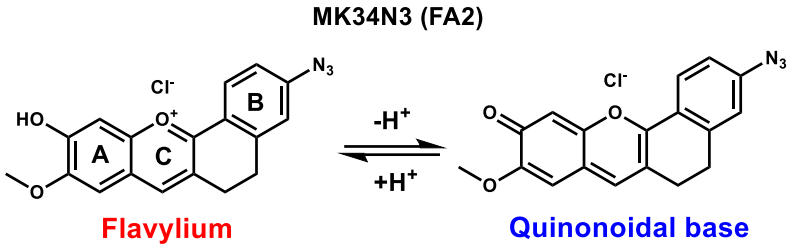

Figure 4. 16. Protonation equilibrium for the flavylium azide FA2 leading the predominant quinonoidal base under physiological conditions**.**

It is interesting to note that of the two flavylium azides examined in this work, FA2 was found to be more stable than FA1 in solution at pH 7.2, as well as with respect to reduction by TCEP (Staudinger azide reduction). FA1 was reduced even at 50 µM of TCEP while FA2 gets reduced at 500 µM of TCEP (Figure 4.17C). Upon its quinonoidal state (neutral species, no electrophilic positions), FA2 is thus seemingly more stable with respect to reduction with TCEP. However, this also has a consequence on the reactivity of the FA2 with regard to the CuAAC reaction since no cycloaddition product could be detected with probe 7. The same experimental conditions than those employed for probe 7 and FA1 were applied with FA2. The LC profile of the FA2 showed two retention peaks at 13.0 (major peak) and 20.4 (minor peak), respectively. Regardless of the conditions used, no additional retention peak could be observed when probe 7 was combined with FA2, suggesting little or no reactivity of this azide and lack of efficacy in a CuAAC reaction. Nevertheless, the experimental conditions still need to be optimized with this new azide compound in order to confirm these preliminary results (*i.e.,* only one experiment has been conducted with FA2).

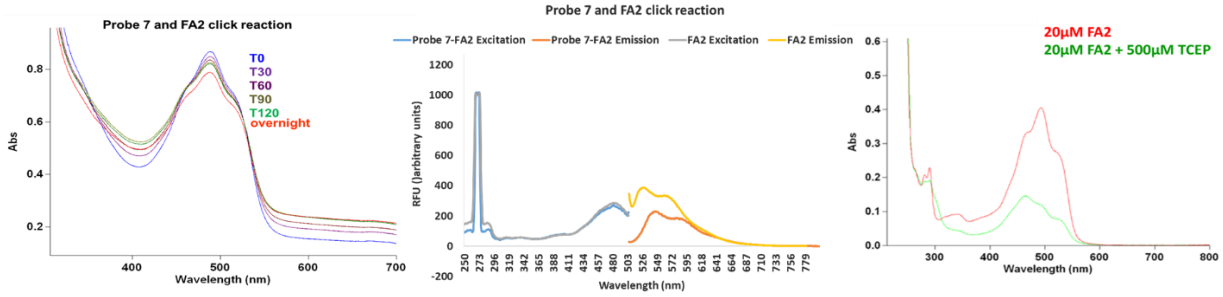

(A) (B) (C)

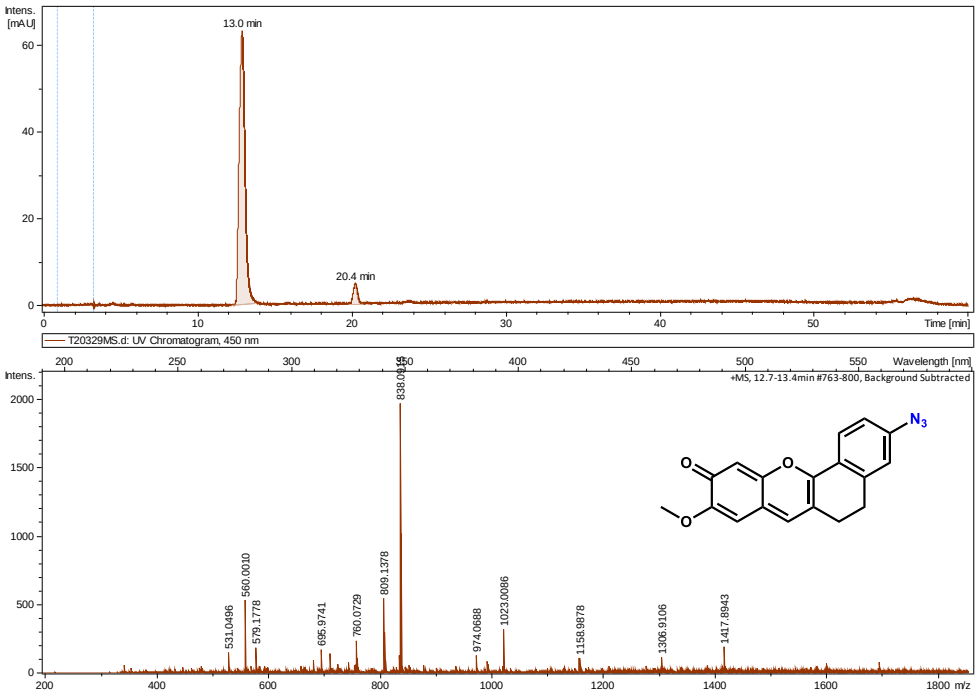
Intens.
[mAU]
13.0 min
20.4 min
Time [min]
T20329MS.d: UV Chromatogram, 450 nm
Wavelength [nm]
+MS, 12.7-13.4min #763-800, Background Subtracted
838.0950
809.1378
560.0010
531.0496
579.1778
695.9741
760.0729
974.0688
1023.0086
1158.9878
1306.9106
1417.8943
m/z
N3
O
O
O

(D)

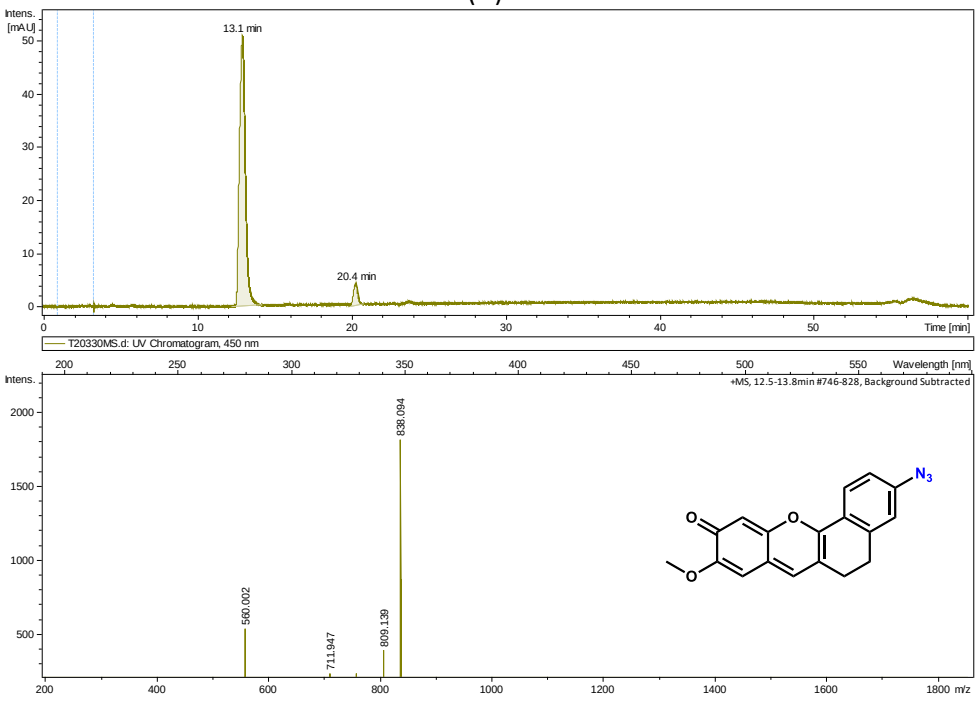
Intens.
[mAU]
13.1 min
20.4 min
Time [min]
T20330MS.d: UV Chromatogram, 450 nm
Wavelength [nm]
+MS, 12.5-13.8min #746-828, Background Subtracted
838.094
560.002
711.947
809.139
m/z
N3
O
O
O

(E)

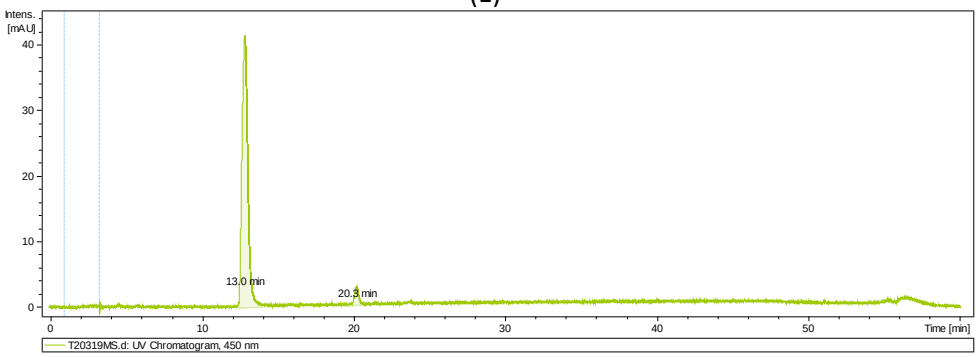
Intens.
[mAU]
13.0 min
20.3 min
Time [min]
T20319MS.d: UV Chromatogram, 450 nm

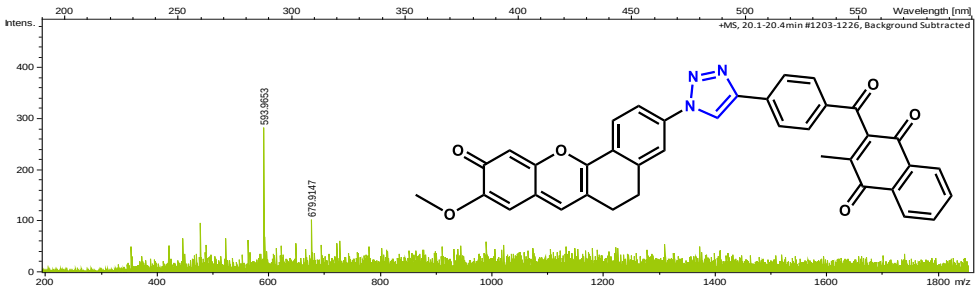

(F)

Figure 4. 17. Click reaction of FA2 with probe 7 (AZ47) (A) in aqueous conditions with 6.8% DMF under strict oxygen-free conditions with 4 stepwise addition of doses of pre-formed Cu(I) complex, freshly prepared from $CuSO_4.5H_2O$ (1 equiv.) + THPTA (1 equiv.) + TCEP (1 equiv.) in the following manner – at T_0 a pre-incubated Cu(I) complex during 45 minutes was added, while at T_{30}, T_{60} and T_{90} a pre-incubated Cu(I) complex during 20 minutes was added. Reaction time: overnight. By the end of reaction, the CuAAC product with probe 7 was analysed by absorption spectrophotometry (A), fluorimetry (B), HPLC-ESI-MS (D, E and F). n=1 for probe 7. (C) Reduction of FA2 by TCEP.

After demonstrating that FA1 was able to achieve cycloaddition reactions in the presence of a pre-catalyst (THPTA + Cu(II)) in combination with a reducing agent (TCEP), we wanted to evaluate the efficacy of this new azide derivative compared to a commercial compound, rhodamine azide (RA). Indeed, we sought to verify whether flavylium azide could be an alternative to rhodamine azide although the latter does not operate as a fluorogenic probe (*i.e.,* fluorescence ON for the cycloaddition product and fluorescence OFF for FA1). The easiness of synthesis and the low cost of FA1 are indeed interesting features for FA1. We therefore compared the yield of the cycloaddition reactions of FA1 and RA with probes 7 and 9 under strictly identical experimental conditions.

We observed that after 2 hours of reaction (Figure 4.18), FA1 has a slightly better reactivity than rhodamine azide. Indeed, the cycloaddition reaction yield determined by LC-MS for RA and probe 7 led to a 17% yield while a yield of 20% was reached with FA1 with the same probe under identical experimental conditions. However, after overnight reaction, the efficiency increases to almost 60% with RA while for FA1 the yield was only doubled to nearly 40%. After overnight reaction, FA1 and RA were found to be fully consumed as evidenced by the absence of retention peaks at 31.8 minutes for FA1 and at 12.3 and 14.3 minutes for RA, respectively. When compared to the CuAAC yields, this indicates that, in addition to the cycloaddition reaction, FA1 undergoes degradation, conversion or precipitation reactions (probe 7 has a solubility limit of 4 µM and the cycloaddition product is likely poorly soluble and can precipitate under the experimental conditions used).

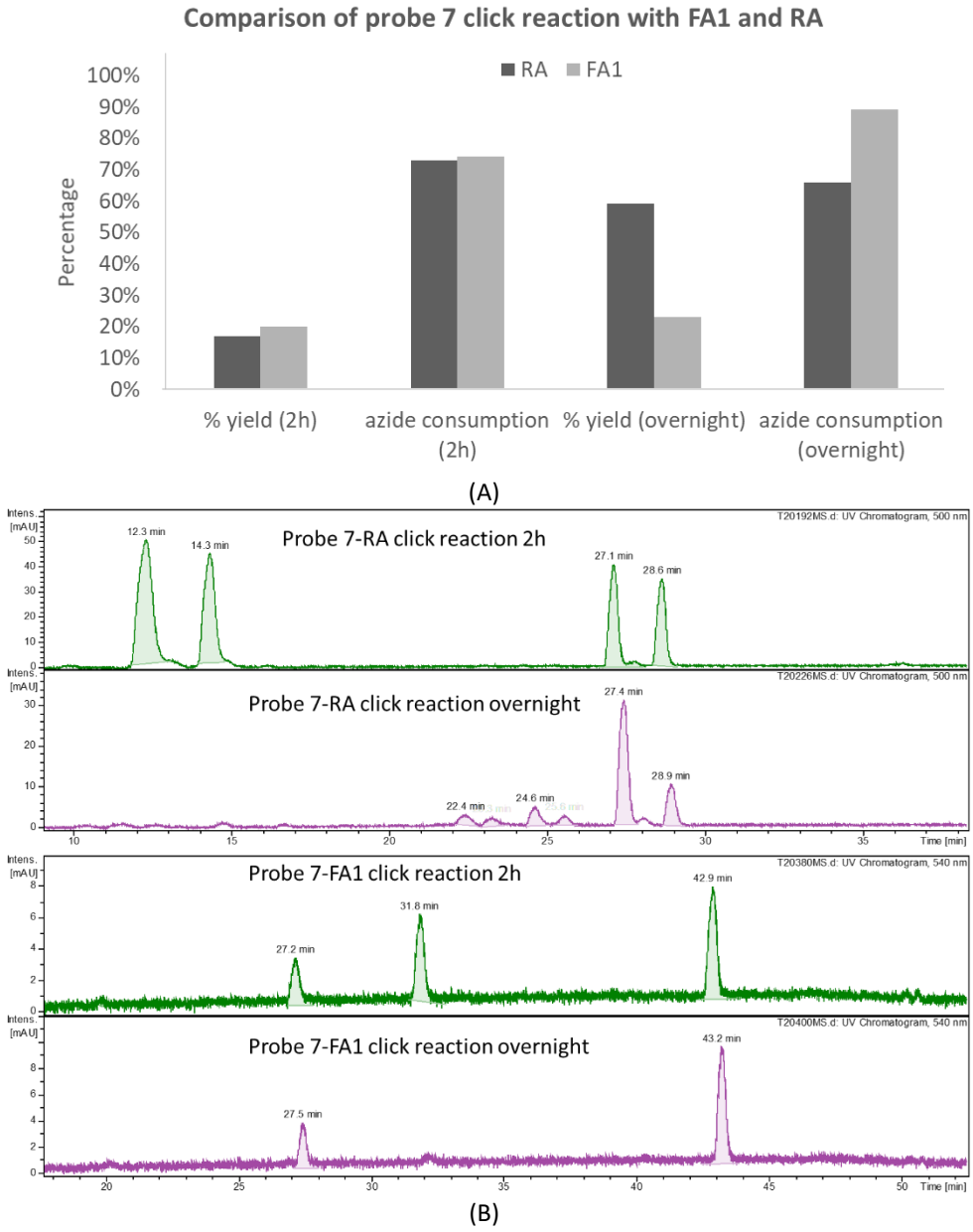

Figure 4. 18. Comparison of the overnight click reaction yields of RA and FA1 with probe 7. Yields (A) and LC chromatograms (B).

With respect to probe 9, FA1 has demonstrated better efficiency than RA (Figure 4.19). Indeed, after 2 hours of reaction, a yield of 9% was determined with RA while it was found to be 15% for FA1. FA1 thus showed a better reactivity whatever the probe used after a reaction time of 2h. After one night of reaction, the reaction yield was only 15% with RA while it increased up to 23% for FA1. This indicates that, although essential to promote coupling reactions by photoirradiation, the presence of a nitro group displays several drawbacks for the CuAAC reaction (electronic or steric effect). Note that MD43 has a better solubility (solubility of 14.4 µM). These results showed that the efficacy of the CuAAC reaction does not depend only on the azide partner, but also on the physico-chemical properties of the alkyne one. Based on these data, we can conclude that FA1 is comparable or even slightly more reactive than AR in cycloaddition reactions.

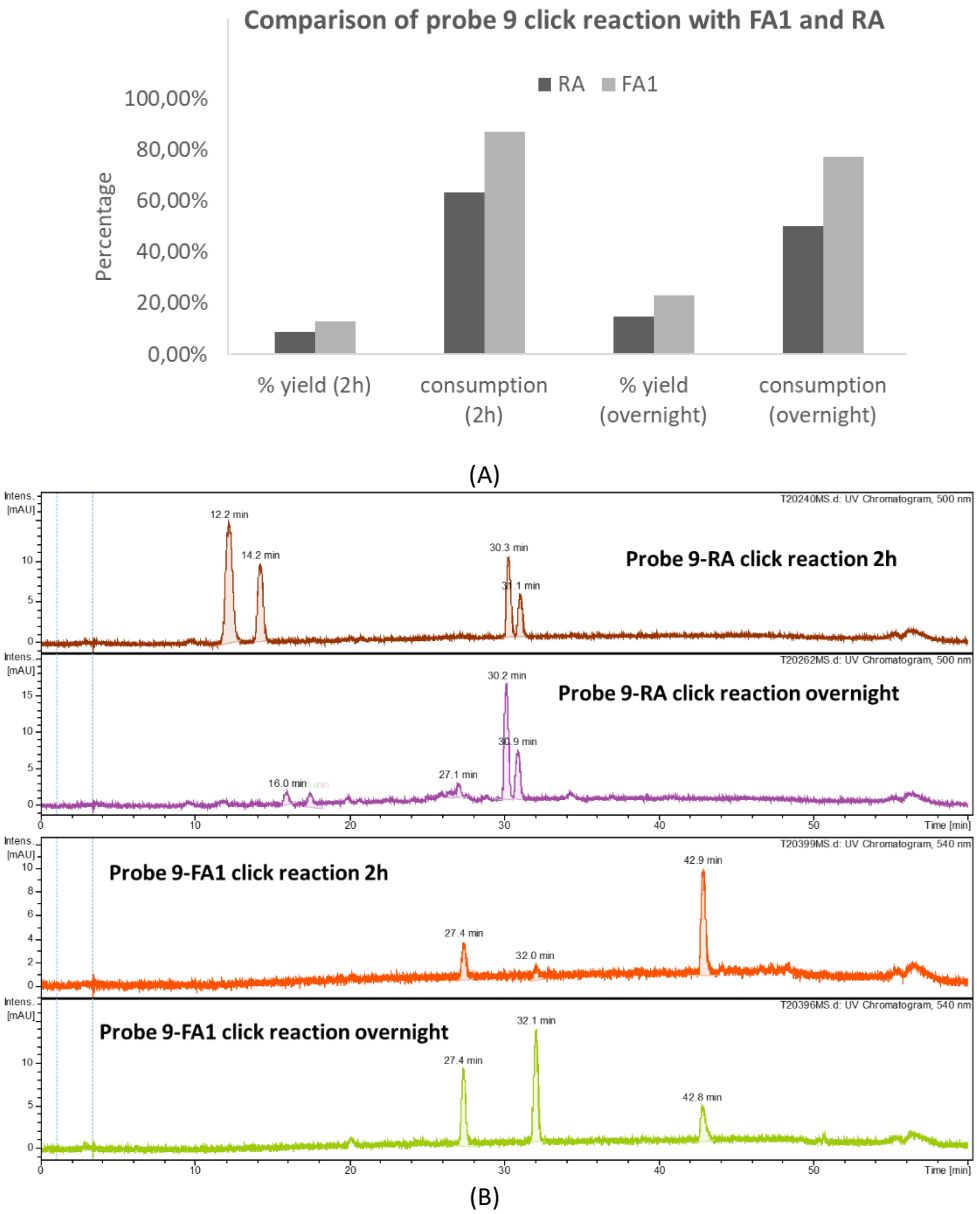

Figure 4. 19. Comparison of the overnight click reaction yields of RA and FA1 with probe 9. Yields (A) and LC chromatograms (B).

Conclusion

In this study, we considered two bioinspired bright fluorophores LV05 and MK34 synthesized within my host team. These compounds are based on a constrained flavylium structure and have very interesting emission properties (high brightness, red emission, water solubility and straightforward synthesis). For the "click and fish" approach investigated in this PhD thesis, it appeared interesting to have fluorogenic compounds capable of emitting light after a cycloaddition reaction on an alkyne derivative of the plasmodione type. Indeed, RA is a fluorophore of choice but which is emissive whatever its state (in free form or as a cyclo-adduct). In their azide form (LV05N3 or FA1 and MK34N3 or FA2), fluorescence quenching was observed. It was therefore expected that after a CuAAC cycloaddition, this emission would be restored to allow easy identification of the labelled biological targets. However, after reaction with several probes (7 and 9), no fluorescence exhalation could be observed, which limit the interest for these derivatives. However, the chosen strategy is worth pursuing, as FA1 in

particular has demonstrated strong reactivity in cycloaddition reactions. With probe 9, FA1 is more reactive than RA after 2 hours or after an overnight reaction. With Probe 7, FA1 is more reactive than RA after 2 hours of reaction but slightly less effective after an overnight reaction. Therefore, our approach has several advantages: (i) FA1 is easily synthesized with a much lower synthesis cost than RA; (ii) this ease of synthesis allows easily introducing structural diversity that will allow us to meet our initial objectives; (iii) FA1 is water soluble and photostable; (iv) FA1 is reactive in cycloaddition reactions; (iv) the study of FA1 and FA2 has led to a better understanding of the reactivity of these compounds; and (v) this work constitutes the first proof of concept of this type of compound in CuAAC-type cycloaddition reactions.

Experimental section/Methods

LC-MS analysis

LC/MS analyses were performed using an Agilent 1100 series LC coupled to a MicrOTOF-Q (Bruker Daltonics, Bremen, Germany) or to a maXis II Q-TOF mass spectrometer (Bruker). The mass spectrometer was operated in positive mode with a capillary voltage of 4,500 V. Acquisitions were performed on the mass range 200-1850 m/z. Calibration was performed using the singly charged ions produced by a solution of Tune mix (G1969-85000, Agilent, U.S.A.). Data analysis was performed by using Compass DataAnalysis 4.3 (Bruker Daltonics).

Click reaction products were analysed by Micro-QTOF or maXis II QTOF mass spectrometer (Bruker Daltonics, Bremen, Germany) coupled to HPLC. Samples were injected on a XBridge Peptide BEH C18 Column, 300 Å, 3.5 µm, 2.1 mm X 250 mm column. The gradient was generated at a flow rate of 250 µL/min using 0.1% trifluoroacetic acid (TFA) in water for mobile phase A and acetonitrile containing 0.08% TFA for mobile phase B at 60°C. B was raised from 20 to 80% in 45 min. UV and MS chromatograms were analysed by Hystar Bruker Data Compass program.

Physico-Chemistry

Starting Materials and Solvents. Distilled water was purified by passing it through a mixed bed of ion-exchanger (BIOBLOCK Scientific R3-83002, M3-83006) and activated carbon (BIOBLOCK Scientific ORC-83005) and was de-oxygenated by CO_2- and O_2-free argon (SIGMA Oxiclear cartridge) just before use. Spectroscopic grade methanol (E. Merck Uvasol, for spectroscopy) was used to prepare the stock solutions of the fluorescent dyes. The stock solutions were prepared by weighing solids using an AG 245 METTLER TOLEDO analytical balance (accuracy 0.01 mg). The ionic strength was maintained at 0.1 M with sodium chloride (NaCl, CARLO-ERBA-SDS PHAR. EUR. 99-100.5%), and all measurements were carried out at 25.0(2) °C.

Spectrophotometric Titrations *vs.* pH. The spectrophotometric titrations of MM1-171 will not be detailed in this chapter, while LV05 does not display any ionisable site. Therefore, only the spectrophotometric titration of **MK34** was carried out to investigate its protonation and photophysical properties. An aliquot of 40 mL of solutions containing **MK34** (8.80×10^{-5} M) was introduced in a jacketed cell (METROHM) maintained at 25.0(2) °C (LAUDA E200). The free hydrogen ion concentration was measured with a combined glass electrode (METROHM 6.0234.500, Long Life) and an automatic titrator system 794 Basic Titrino (METROHM). The Ag/AgCl reference glass electrode was filled with NaCl (0.1 M, CARLO-ERBA-SDS PHAR. EUR. 99-100.5%) and was calibrated as a hydrogen concentration probe by titrating known amounts of hydrochloric acid (~0.1 M from HCl, SIGMA-ALDRICH, puriss pa, >37 %) with CO_2-free sodium hydroxide solution (~ 0.1 M from NaOH, BDH, AnalaR, 98%) (Gans, P. *et al.,* 2000). The HCl and NaOH solutions were freshly prepared just before use and titrated with sodium tetraborate decahydrate ($B_4Na_2O_7.10H_2O$, FLUKA, puriss, p.a., > 99.5%) and potassium hydrogen phthalate ($C_8H_5KO_3$, FLUKA, puriss, p.a., > 99.5%), respectively, with methyl orange (RAL) and phenolphthalein (PROLABO, purum) used as colorimetric indicators. The temperature of the titration cell was maintained at 25.0 ± 0.2 °C with the help of a LAUDA E200 thermostat. The GLEE program was applied for the glass electrode calibration (standard electrode potential E_0/mV and slope of the electrode/mV pH^{-1}) and to check carbonate levels of the NaOH solutions used (< 5 %). The initial pH was adjusted to ~ 2.5 with HCl (SIGMA-ALDRICH, puriss pa, >37%) and the titration of MK34 (2.48 < pH < 11.04) was then carried out by automatic addition of known volumes of NaOH solutions (BDH, AnalaR). After each addition (*i.e.,* volume

of base/pH automatically adjusted according to the potentiometric signal drift of the solution with the Dynamic Potential Titration - DET - of the Tiamo program with a measuring point density of 3; duration between two additions of 210 s), an absorption spectrum was recorded using a Varian CARY 50 spectrophotometer fitted with Hellma optical fibres (Hellma, 041.002-UV) and an immersion probe made of quartz suprasil (Hellma, 661.500-QX) and interfaced (Cetrib) with the automatic titrator system 794 Basic Titrino.

Analysis and Processing of the Spectroscopic Data. The spectrophotometric data were analysed with SPECFIT (Gampp, H. *et al.,* 1985; Gampp, H. *et al.*, 1985; Gans, P., 1992) program which adjusts the absorptivities and the stability constants of the species formed at equilibrium. SPECFIT uses factor analysis to reduce the absorbance matrix and to extract the eigenvalues prior to the multiwavelength fit of the reduced data set according to the Marquardt algorithm (Marquardt, D.W., 1963; Maeder, M. *et al.*, 1990).

Spectroscopic and photophysical properties.

The fluorescence quantum yield of a molecule reflects the effectiveness of the radiative fluorescence deactivation with respect to the other non-radiative deactivation processes. The absorption spectrophotometric spectra of the fluorophores (250 nm to 750 nm) have been first recorded on a UV-Vis-PIR Cary 5000 absorption spectrophotometer (Agilent Technologies) in several media (NIST buffered solutions at pH 1.68 and 7.41 and in EtOH with 2µL of TFA). The pH values were selected on the basis of the pK_a values (when applicable) to correspond to the almost quantitative formation of a protonated species. In a suprasil quartz optical cell (Hellma), an aliquot of the pigment stock solution was added to 2 ml of a buffered solution with 0.1 M NaCl or to 2 ml ethanol with 2 µl TFA. The dilution factor in the optical cell was calculated to ensure that the absorbance at the maximum of absorption was close to 1. For the solutions used for the spectrofluorimetric determinations, the solutions were further diluted by 10 to obtain absorption values below 0.1 at wavelength > λ_{ex} in order to avoid any errors due to the inner filter effect. Emission and excitation spectra were then recorded on a Jobin Yvon Horiba Fluoromax 4 fluorimeter. The fluorescence quantum yields were determined relative to two references depending on the spectroscopic properties of the dye, the fluorescent standards cresyl violet (510-635 nm) or rhodamine (470-555 nm), with the possibility of correcting for differences between the refractive index of the reference n_r, and the sample solutions n_s (n_S^{20} = 1.36 for ethanol, n_S^{20} = 1.33 for the aqueous buffered solutions) using the following expression:

$$Q_f(s) = Q_f(r)\frac{\int I_s(\lambda) \times A_r \times n_s^2}{\int I_r(\lambda) \times A_s \times n_r^2}$$

The indices s and r denote sample and reference, respectively. The integrals over *I* represent areas of the corrected emission spectra (calculated with Origin 7.0 software), and A is the optical density at the excitation wavelength. The quantum efficiency measurements are performed several times per sample, by varying the values of excitation wavelength and the excitation and/or emission bandwidths.

Synthesis of LV05N3 (FA1) and MK34N3 (FA2).

5-methoxy-2,4-dihydroxybenzaldehyde. To a suspension of $AlCl_3$ (4 equiv., 6.8 g, 50.97 mmol) in dry dichloromethane (51 mL), a solution of 2,4,5-trimethoxybenzaldehyde (1 equiv., 2.5 g, 12.74 mmol) in dry dichloromethane (13 mL) was added dropwise. After 2 hours of mixing at room temperature, another portion of $AlCl_3$ (4 equiv., 6.8 g, 50.97 mmol) was added. The reaction mixture was vigorously stirred for 13 h. The reaction suspension was then poured in 160 g of ice in which 5 mL of concentrated hydrochloric acid was previously added. The organic phase was separated and the aqueous phase was further extracted with dichloromethane (3 x 30 mL). The organic phases were collected, filtered over silica, dried with Na_2SO_4 and evaporated under vacuum. Cold crystallization in dichloromethane and ethyl acetate was performed to afford 5-methoxy-2,4-dihydroxybenzaldehyde (457 mg; 21 %). ^{1}H RMN (CD_3OD, 300 MHz) δ (ppm)**:** 3.84 (s, 3H, OCH_3), 6.33 (s, 1H, H_3), 7.11 (s, 1H, H_6), 9.72 ppm (s, 1H, CHO). ^{13}C NMR (101 MHz, CD_3OD) δ (ppm)**:** 194.74, 160.37, 157.42, 143.41, 114.73, 114.60, 104.02, 56.87.

3-amino-10-(diethylamino)-5,6-dihydrobenzo[c]xanthen-12-ium chloride (LV05). 6-Amino-3,4-dihydro-1(2H)-naphthalenone (1 equiv., 435 mg, 2.7 mmol) and 4-amino-2-hydroxybenzaldehyde (1 equiv., 521 mg, 2.7 mmol) were dissolved in ethyl acetate (22 mL). Gaseous hydrochloric acid HCl was then bubbled for 20 minutes in the solution. The reaction mixture was then stirred at room temperature for 48 hours. The solution was filtered and the solid was copiously washed with cold ethyl acetate. The residue was then purified on silica gel chromatography (CH_2Cl_2/ethanol = 90:10, v/v) to afford LV05 with a yield of 61% (582 mg). ^{1}H RMN (CD_3OD-d4, 400 MHz) δ (ppm): 1.30 (t, 6H, J=7.1 Hz, NCH_2CH_3), 2.97 (m, 4H, H_5 et H_6), 3.64 (q, 4H, J=7.2 Hz, NCH_2CH_3), 6.58 (d, 1H, J=2.2 Hz, H_4), 6.72 (dd, 1H, J=8.8 Hz and J=2.2 Hz, H_9), 7.02 (d, 1H, J=2.0 Hz, H_{11}), 7.17 (dd, 1H, J=2.5 Hz and J=9.2 Hz, H_2), 7.69 (d, 1H, J=9.2 Hz, H_1), 8.03 (d, 1H, J=8.8 Hz, H_8), 8.15 (s, 1H, H_7). ^{13}C NMR (CD_3OD-d4, 101 MHz) δ (ppm)**:** 167.07, 158.87, 158.62, 155.41, 148.48, 145.90, 131.94, 131.12, 121.75, 116.55, 116.28, 115.41, 114.90, 113.74, 96.98, 46.44, 28.58, 26.82, 12.72.

3-azido-10-(diethylamino)-5,6-dihydrobenzo[c]xanthen-12-ium chloride (LV05N3/FA1). HCl (4.8 mL) and LV05 (1 equiv., 125 mg, 0.35 mmol) were dissolved in EtOH (12 mL). After the solution was cooled to 0 °C, sodium nitrite $NaNO_2$ (3 equiv., 73.32 mg, 1.06 mmol) was added and the mixture was stirred for 30 min at 0 °C. Sodium azide NaN_3 (3 equiv., 69.09 mg, 0.037 mL, 1.06 mmol) was added slowly and the mixture was stirred for 2 hours at room temperature. The suspension was then extracted with CH_2Cl_2 (3 x 40 mL) and the combined organic layers were dried by $MgSO_4$. After drying, the organic layers were concentrated under reduced pressure. The residue was purified by silica gel chromatography (CH_2Cl_2/ethanol = 90:10, *v/v*) to afford LV05N3/FA1 (73 mg, yield 55%). ^{1}H RMN (CD_3OD-d4, 400 MHz) δ (ppm): 1.36 (t, 6H, J=7.1 Hz, NCH_2CH_3), 3.12 (br s, 4H, H_5 et H_6), 3.76 (q, 4H, J=7.2 Hz, NCH_2CH_3), 7.15 (d, 1H, J=2.1 Hz, H_4), 7.20 (dd, 1H, J=8.5 Hz and J=2.2 Hz, H_9), 7.23 (d, 1H, J=2.1 Hz, H_{11}), 7.46 (dd, 1H,

J=2.3 Hz and J=9.5 Hz, H_2), 7.90 (d, 1H, J=9.5 Hz, H_1), 8.26 (d, 1H, J=8.5 Hz, H_8), 8.53 (s, 1H, H_7). ^{13}C NMR (CD_3OD-d4, 101 MHz) δ (ppm)**:** 163.78, 160.36, 157.66, 149.55, 147.99, 145.71, 133.28, 128.89, 124.36, 122.45, 120.66, 120.28, 119.93, 119.52, 96.84, 47.17, 27.88, 26.03, 12.76.

3-amino-9-methoxy-10-hydroxy-5,6-dihydrobenzo[c]xanthen-12-ium chloride (MK34). 6-Amino-3,4-dihydro-1(2H)-naphthalenone (1 equiv., 288 mg, 1.79 mmol) and 5-methoxy-2,4-dihydroxybenzaldehyde (1 equiv., 300 mg, 1.79 mmol) were dissolved in ethyl acetate (30 mL). Gaseous HCl gas was then bubbled for 20 minutes in the solution. The reaction mixture was then stirred for 48 hours at room temperature. The solution was filtered and the solid was copiously washed with cold ethyl acetate. The residue was purified on silica gel chromatography (CH_2Cl_2/ethanol = 90:10, v/v) to afford MK34 with a yield of 48% (280 mg). ^{1}H RMN (CD_3OD-d4, 300 MHz) δ (ppm): 2.92 (m, 4H, H_5 et H_6), 4.00 (s, 3H, O*CH₃*), 6.51 (br s, 1H, H_4), 6.65 (d, 1H, J=9.2 Hz, H_2), 7.09 (d, 1H, H_8), 7.20 (s, 1H, H_{11}), 7.92 (d, 1H, J=8.5 Hz, H_1), 8.18 (s, 1H, H_7).

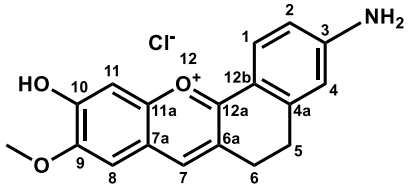

3-azido-9-methoxy-10-hydroxy-5,6-dihydrobenzo[c]xanthen-12-ium chloride (MK34N3/FA2). HCl (3.5 mL) and MK34 (1 equiv., 70 mg, 0.21 mmol) were dissolved in EtOH (20 mL). After the solution was cooled to 0°C, sodium nitrite $NaNO_2$ (6 equiv., 87.34 mg, 1.27 mmol) was added and the mixture was stirred for 30 min. Sodium azide NaN_3 (6 equiv., 82.29 mg, 0.044 mL, 1.27 mmol) was added slowly and the mixture was stirred for 2 hours at room temperature. The suspension was then extracted with CH_2Cl_2 (3 x 40 mL) and the combined organic layers were dried by $MgSO_4$. After drying, the organic layers were concentrated under reduced pressure. The residue was purified by silica gel chromatography (CH_2Cl_2/ethanol = 90:10, *v/v*) to afford MK34N3/FA2 (12 mg, yield 16%). ^{1}H RMN (CD_3OD-d4, 300 MHz) δ (ppm): 2.95 (m, 4H, H_5 et H_6), 3.87 (s, 3H, O*CH₃*), 6.60 (s, 1H, H_{11}), 6.89 (d, 1H, H_8), 7.32 (d, 1H, J= 10 Hz, H_1), 7.39 (dd, 1H, J=9.2 Hz and J=1.8 Hz, H_2), 7.89 (d, 1H, J=1.5 Hz, H_4), 7.96 (s, 1H, H_7). ^{13}C NMR (CD_3OD-d4, 101 MHz) δ (ppm)**:** 177.42, 159.42, 156.70, 156.43, 142.03, 140.68, 133.11, 129.58, 128.67, 128.19, 124.63, 122.53, 119.26, 105.13, 103.63, 56.48, 27.94, 26.01.

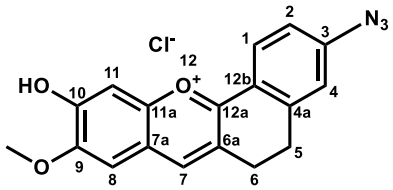

GENERAL CONCLUSION OF THE THESIS

Fundamentals of drug discovery are vast. Despite high throughput molecule screening methodology and vast investment of money by pharmaceutical industries, the life span of a drug from its discovery, comprising of the pre-clinical experiments to clinical trials, i.e. for bringing the molecule from lab to launching it in the market takes between 12-15 years (J. P. Hughes et al., 2011; Munos, 2009)(J. P. Hughes et al., 2011). Revisiting old drugs, drug target- or phenotypic-based approaches are most commonly used for drug discovery at present (Swinney & Anthony, 2011). The new drug is acceptable only if it could fulfill the medical unmet need for a particular disease in the given time. Among a few thousands of antimalarial compounds that passed through such critical hurdles MB, CQ, PQ and Art have been sustainable drugs in the era with the urgent need of combatting the parasitic disease first, and then drug resistance thereby bringing in the ACT for chemotherapeutic approach ("Advances in Parasitology, Volume 36," 2013; Yadav et al., 2019). In my Ph.D. research, I observed and reported that bMD40 displayed cross-resistance with Art. However, it's improved pharmacokinetic properties makes this PD analog superior and efficient in killing both the early ring stages and late gametocyte stages that are crucial for causing the drug resistance and parasite transmission from human to mosquito(*Goetz et al* in preparation). Since, PD was proven to be as fast as and synergistic with the most efficient antimalarial agent artemisinin(Katharina Ehrhardt et al., 2016) and it is anticipated that further improvement of PD or bMD40 derivatives seems to be promising. In the future, we would like to test a new analogue combining bMD30 and bMD40 modifications on the 3-bMD scaffold to assess whether we could further improve the antimalarial properties of this series. To be one-step ahead in the list of all other lead antimalarial compounds it will be essential to identify strategic drug combinations of an improved PD or bMD40 derivative to bypass the cross-resistance with Art. Therefore, it would strengthen its chances of landing at a good position for translational medicine in the malaria box. The literature review summarizing the activity of redox-cyclers and ROS-inducers on critical and fittest parasite stages. The latter involve various biological processes giving a broader perspective about understanding the drug metabolism, mode of action, and potential targets and reason for the possible failure of drug activity, and strategies for novel drug combinations.

Diverse genomic and proteomic approaches are commonly used for deciphering the drug targets. Ignoring the validation of probes before applying to the parasites in activity-based protein profiling approaches for drug target identification has earlier led to acquiring unspecific protein targets in parasite models but also in bacterial models (Duckworth et al., 2012; Ismail et al., 2016; Lubin et al., 2018; Penarete-Vargas et al., 2014; Sun et al., 2016; Wright et al., 2014). Therefore, we extensively screened and validated the functionality of the ABPP probes derived from the antimalarial drug PD before applying them to parasites, in order to hunt for specific drug targets, rule out the unspecific targets and be able to catch even the less abundantly expressed protein targets. By the end of strategical inspection of every aspect of photoreaction and click reaction using chemical models, we identified probes 7 and 9 as both clickable and photoreactive probes. The EWG -4'-alkyne group for probe 7 and 4'-NO_2 for probe 9 contribute to the reactivity of the probes for triazole formation in CuAAC reaction. In contrast to published protocols, we are likely the first ones to use the strict oxygen-free conditions and intermittent doses of CuI complex for successful click reaction by maintaining the stability and availability of the catalyst CuI complex in aqueous conditions. We clearly demonstrated that the click reaction is a biorthogonal reaction highly sensitive to the compatibility of alkyne and azide partners and various factors such as oxygen, solvent, ligand, copper source, reductant, and pH, which means a lot of troubleshooting. Click reaction is solely

dependent on the formation of CuI complex; it is noteworthy that TCEP is a preferred reductant, while THPTA is a preferred ligand for CuI complex formation from $CuSO_4.5H_2O$ under oxygen-free conditions. Four doses of 1 equiv: 1 equiv: 1 equiv of $CuSO_4.5H_2O$:THPTA:TCEP with a span of 30 minutes, are required enough to achieve highest yield in aqueous conditions, while it takes just one dose of 5:5:1 conditions in phosphate buffer. It is very important to stick with the ratio of reactant to avoid the side reactions such as the Staudinger reaction between the azide and TCEP-reductant. Relying only on colour change to understand if the click reaction is successful or not is like finding a needle in the hays stack. The BCDA ligand is compatible for click reaction in phosphate buffer and can preferentially be used over THPTA. We prefer to use biotin azide with pull down tag instead of rhodamine azide for enrichment of crosslinked protein after the click reaction. Biotin azide seemed to have similar reactivity to rhodamine azide. Powerful, accurate, and sensitive tools such as HPLC-MS analysis give proof by mass to support the UV-vis and fluorimeter analysis. This analysis data was highly important in our case especially because click product of ABPP and rhodamine azide did not change the emission pattern after the click reaction.

We have found that the 3-benzoylmenadione-derived ABPP probes are photoreactive and can form covalent adducts with the GSH peptide as well as with the drug-protein interactor – hGR upon photoirradiation. Two pathways might co-exist and two adducts were revealed and analysed. In the presence of peptide and protein models, the nature of the crosslinking implies i) the photoreduction of the naphthoquinone core, ii) an oxidative phenolic coupling reaction releasing a benzoxanthone, and iii) the formation of adducts between the benzoxanthone-derived enone and the H-donor partner (GSH, or protein) through a nucleophilic attack. Future work will clarify which conditions promote one binding pathway (benzophenone adduct) over the other (benzoxanthone adduct). Both mechanisms of crosslinking could potentially be of use in the parasite for *in vivo* ABPP, especially if the benzoxanthone represents the next metabolite in PDs MoA cascade. Additionally, learning the behavior of the probe will allow us to study in-depth the relation of metabolites to different identified binding sites on PDs targets – like in case of hGR.

Conclusively, the clickability and photoreactivity of the probes have been validated individually using chemical models and the proof of concept of both photoreaction followed by click reaction will be continued by B. Cichocki – the postdoctoral researcher. The best optimal conditions would be used for identifying the drug targets in the future with the antimalarial activity of probe 4 (benzylMD) a prodrug of probe 7 (benzoylMD). The chemogenomics approach and bioinformatics approach would help in unravelling the targets and understanding structure-activity based relationships between drug and targets. Even though our putative model evidences the metabolite 1 formation, it would be essential to confirm PD drug metabolism in parasites by using ^{13}C-enriched PD (Feng et al., 2018). There are diverse chemogenomics, genomic, proteomic, and metabolomics strategies for drug target identifications. One very well developed techniques to identify the drug targets such as CETSA technique (Jerzy M. Dziekan et al., 2019; Jerzy Michal Dziekan et al., 2020) which depends on the melting temperature of the proteins, or still maturing technique Proteolysis-targeting chimeras (PROTACs), which focus on inducing targeted protein degradation by the ubiquitin-proteasome system (Schapira et al., 2019). Nevertheless, every approach has its share of specific demands and troubleshooting that needs well-established cross-functional expertise in medicinal, analytical chemistry, parasitology, mass spectrometry, and proteomics. Having considered continuing with the PD-ABPP approach to identify PD targets has enriched my knowledge and understanding of this highly specific reaction known in the medicinal chemistry for the past >20 years.

In addition to this, I explored the proof of concept for using fluorogenic chemical tools with the property of emitting bright fluorescence upon click reaction for in vivo imaging as an alternative

to commercially available traditional and expensive rhodamine azide. These newly designed derivatives LV05N3 (or FA1) and MK34N3 (or FA2) did not show distinguishable emission properties prior and after the triazole formation in click reaction, however, FA1 showed better reactivity than RA for the CuAAC reaction with probe 9 within 2 hours and the overnight reaction. For probe 7 as well the yield of reaction with FA1 was better than RA within 2 hours and slightly less in overnight reaction. Therefore, in the future, the development with the substitution pattern of these bioinspired bright fluorophores would be of utmost interest to find a cheaper alternative to rhodamine azide as a chemical tool for in vivo imaging.

My multidisciplinary Ph.D. research in biological and therapeutical chemical sciences involved thorough study, problem-solving and troubleshooting for the click reaction, photoreaction for developing chemical tools derived from 20 years rich platform of PD- the antimalarial drug and its derivatives with enzyme kinetics and parasitology approaches. The diverse techniques and linking complex biochemical concepts have eventually contributed to setting up the ground for broader development and improvements of chemical tools for identifying drug targets.

REFERENCES

Adjalley, S H, Johnston, G. L., Li, T., Eastman, R. T., Ekland, E. H., Eappen, A. G., Richman, A., Sim, B. K., Lee, M. C., Hoffman, S. L., & Fidock, D. A. (2011). Quantitative assessment of Plasmodium falciparum sexual development reveals potent transmission-blocking activity by methylene blue. *Proc Natl Acad Sci U S A*, *108*(47), E1214-23. https://doi.org/10.1073/pnas.1112037108

Adjalley, Sophie H., Johnston, G. L., Li, T., Eastman, R. T., Ekland, E. H., Eappen, A. G., Richman, A., Sim, B. K. L., Lee, M. C. S., Hoffman, S. L., & Fidock, D. A. (2011a). Quantitative assessment of Plasmodium falciparum sexual development reveals potent transmissionblocking activity by methylene blue. *Proceedings of the National Academy of Sciences of the United States of America*. https://doi.org/10.1073/pnas.1112037108

Adjalley, Sophie H., Johnston, G. L., Li, T., Eastman, R. T., Ekland, E. H., Eappen, A. G., Richman, A., Sim, B. K. L., Lee, M. C. S., Hoffman, S. L., & Fidock, D. A. (2011b). Quantitative assessment of Plasmodium falciparum sexual development reveals potent transmissionblocking activity by methylene blue. *Proceedings of the National Academy of Sciences of the United States of America*, *108*(47). https://doi.org/10.1073/pnas.1112037108

Advances in Parasitology, Volume 36. (2013). *Advances in Quantum Chemistry*. https://doi.org/10.1016/B978-0-12-411544-6.00030-3

Akoachere, M., Buchholz, K., Fischer, E., Burhenne, J., Haefeli, W. E., Schirmer, R. H., & Becker, K. (2005). In vitro assessment of methylene blue on chloroquine-sensitive and -resistant Plasmodium falciparum strains reveals synergistic action with artemisinins. *Antimicrobial Agents and Chemotherapy*. https://doi.org/10.1128/AAC.49.11.4592-4597.2005

Amaratunga, C, Neal, A. T., & Fairhurst, R. M. (2014). Flow cytometry-based analysis of artemisinin-resistant Plasmodium falciparum in the ring-stage survival assay. *Antimicrob Agents Chemother*, *58*(8), 4938–4940. https://doi.org/10.1128/AAC.02902-14

Amaratunga, Chanaki, Neal, A. T., & Fairhurst, R. M. (2014). Flow cytometry-based analysis of artemisinin-resistant Plasmodium falciparum in the ring-stage survival assay. *Antimicrobial Agents and Chemotherapy*, *58*(8), 4938–4940. https://doi.org/10.1128/AAC.02902-14

Amaratunga, Chanaki, Sreng, S., Suon, S., Phelps, E. S., Stepniewska, K., Lim, P., Zhou, C., Mao, S., Anderson, J. M., Lindegardh, N., Jiang, H., Song, J., Su, X. zhuan, White, N. J., Dondorp, A. M., Anderson, T. J. C., Fay, M. P., Mu, J., Duong, S., & Fairhurst, R. M. (2012). Artemisinin-resistant Plasmodium falciparum in Pursat province, western Cambodia: A parasite clearance rate study. *The Lancet Infectious Diseases*. https://doi.org/10.1016/S1473-3099(12)70181-0

Ando, Y., & Suzuki, K. (2018). Frontispiece: Photoredox Reactions of Quinones. *Chemistry - A European Journal*. https://doi.org/10.1002/chem.201886062

Ariey, F., Witkowski, B., Amaratunga, C., Beghain, J., Langlois, A. C., Khim, N., Kim, S., Duru, V., Bouchier, C., Ma, L., Lim, P., Leang, R., Duong, S., Sreng, S., Suon, S., Chuor, C. M., Bout, D. M., Ménard, S., Rogers, W. O., … Ménard, D. (2014). A molecular marker of artemisinin-resistant Plasmodium falciparum malaria. *Nature*, *505*(7481), 50–55. https://doi.org/10.1038/nature12876

Ashley, E. A., Dhorda, M., Fairhurst, R. M., Amaratunga, C., Lim, P., Suon, S., Sreng, S., Anderson, J. M., Mao, S., Sam, B., Sopha, C., Chuor, C. M., Nguon, C., Sovannaroth,

S., Pukrittayakamee, S., Jittamala, P., Chotivanich, K., Chutasmit, K., Suchatsoonthorn, C., … White, N. J. (2014). Spread of artemisinin resistance in Plasmodium falciparum malaria. *New England Journal of Medicine*. https://doi.org/10.1056/NEJMoa1314981

Ashley, Elizabeth A., Recht, J., & White, N. J. (2014). Primaquine: The risks and the benefits. In *Malaria Journal*. https://doi.org/10.1186/1475-2875-13-418

Atamna, H., Krugliak, M., Shalmiev, G., Deharo, E., Pescarmona, G., & Ginsburg, H. (1996). Mode of antimalarial effect of methylene blue and some of its analogues on Plasmodium falciparum in culture and their inhibition of P. vinckei petteri and P. yoelii nigeriensis in vivo. *Biochemical Pharmacology*. https://doi.org/10.1016/S0006-2952(95)02258-9

Aweeka, F. T., & German, P. I. (2008). Clinical pharmacology of artemisinin-based combination therapies. In *Clinical Pharmacokinetics*. https://doi.org/10.2165/00003088-200847020-00002

Ayi, K., Turrini, F., Piga, A., & Arese, P. (2004). Enhanced phagocytosis of ring-parasitized mutant erythrocytes: A common mechanism that may explain protection against falciparum malaria in sickle trait and beta-thalassemia trait. *Blood*. https://doi.org/10.1182/blood-2003-11-3820

Bancone, G., Gornsawun, G., Chu, C. S., Porn, P., Pal, S., Bansil, P., Domingo, G. J., & Nosten, F. (2018). Validation of the quantitative point-of-care CareStart biosensor for assessment of G6PD activity in venous blood. *PLoS ONE*. https://doi.org/10.1371/journal.pone.0196716

Barnes, K. I., Watkins, W. M., & White, N. J. (2008). Antimalarial dosing regimens and drug resistance. In *Trends in Parasitology*. https://doi.org/10.1016/j.pt.2007.11.008

Bates, M. D., Meshnick, S. R., Sigler, C. I., Leland, P., & Hollingdale, M. R. (1990). In vitro effects of primaquine and primaquine metabolites on exoerythrocytic stages of Plasmodium berghei. *American Journal of Tropical Medicine and Hygiene*. https://doi.org/10.4269/ajtmh.1990.42.532

Bauer, H., Fritz-Wolf, K., Winzer, A., Kühner, S., Little, S., Yardley, V., Vezin, H., Palfey, B., Schirmer, R. H., & Davioud-Charvet, E. (2006). A fluoro analogue of the menadione derivative 6-[2′-(3′-methyl) -1′,4′-naphthoquinolyl]hexanoic acid is a suicide substrate of glutathione reductase. Crystal structure of the alkylated human enzyme. *Journal of the American Chemical Society*, *128*(33), 10784–10794. https://doi.org/10.1021/ja061155v

Beez, D., Sanchez, C. P., Stein, W. D., & Lanzer, M. (2011). Genetic predisposition favors the acquisition of stable artemisinin resistance in malaria parasites. *Antimicrobial Agents and Chemotherapy*. https://doi.org/10.1128/AAC.00916-10

Bellanca, S., Summers, R. L., Meyrath, M., Dave, A., Nash, M. N., Dittmer, M., Sanchez, C. P., Stein, W. D., Martin, R. E., & Lanzer, M. (2014). Multiple drugs compete for transport via the Plasmodium falciparum chloroquine resistance transporter at distinct but interdependent sites. *Journal of Biological Chemistry*. https://doi.org/10.1074/jbc.M114.614206

Belorgey, D., Antoine Lanfranchi, D., & Davioud-Charvet, E. (2013). 1,4-Naphthoquinones and Other NADPH-Dependent Glutathione Reductase- Catalyzed Redox Cyclers as Antimalarial Agents. *Current Pharmaceutical Design*, *19*(14), 2512–2528. https://doi.org/10.2174/1381612811319140003

Bennett, A., Kazembe, L., Mathanga, D. P., Kinyoki, D., Ali, D., Snow, R. W., & Noor, A. M. (2013). Mapping malaria transmission intensity in Malawi, 2000-2010. *American Journal of Tropical Medicine and Hygiene*. https://doi.org/10.4269/ajtmh.13-0028

Bennett, J. W., Pybus, B. S., Yadava, A., Tosh, D., Sousa, J. C., McCarthy, W. F., Deye, G.,

Melendez, V., & Ockenhouse, C. F. (2013). Primaquine failure and cytochrome P-450 2D6 in Plasmodium vivax malaria. In *New England Journal of Medicine*. https://doi.org/10.1056/NEJMc1301936

Berg, R., & Straub, B. F. (2013). Advancements in the mechanistic understanding of the copper-catalyzed azide-alkyne cycloaddition. *Beilstein Journal of Organic Chemistry*, *9*(December 2013), 2715–2750. https://doi.org/10.3762/bjoc.9.308

Bielitza, M, Belorgey, D., Ehrhardt, K., Johann, L., Lanfranchi, D. A., Gallo, V., Schwarzer, E., Mohring, F., Jortzik, E., Williams, D. L., Becker, K., Arese, P., Elhabiri, M., & Davioud-Charvet, E. (2015). Antimalarial NADPH-Consuming Redox-Cyclers As Superior Glucose-6-Phosphate Dehydrogenase Deficiency Copycats. *Antioxid Redox Signal*, *22*(15), 1337–1351. https://doi.org/10.1089/ars.2014.6047

Bielitza, Max, Belorgey, D., Ehrhardt, K., Johann, L., Lanfranchi, D. A. D. A., Gallo, V., Schwarzer, E., Mohring, F., Jortzik, E., Williams, D. L. D. L., Becker, K., Arese, P., Elhabiri, M., & Davioud-Charvet, E. (2015). Antimalarial NADPH-consuming redox-cyclers as superior glucose-6-phosphate dehydrogenase deficiency copycats. *Antioxidants and Redox Signaling*, *22*(15), 1337–1351. https://doi.org/10.1089/ars.2014.6047

Biot, C., Chavain, N., Dubar, F., Pradines, B., Trivelli, X., Brocard, J., Forfar, I., & Dive, D. (2009). Structure-activity relationships of 4-N-substituted ferroquine analogues: Time to re-evaluate the mechanism of action of ferroquine. *Journal of Organometallic Chemistry*. https://doi.org/10.1016/j.jorganchem.2008.09.033

Biot, C., Glorian, G., Maciejewski, L. A., Brocard, J. S., Domarle, O., Blampain, G., Millet, P., Georges, A. J., & Lebibi, J. (1997). Synthesis and antimalarial activity in vitro and in vivo of a new ferrocene-chloroquine analogue. *Journal of Medicinal Chemistry*. https://doi.org/10.1021/jm970401y

Birnbaum, J., Scharf, S., Schmidt, S., Jonscher, E., Maria Hoeijmakers, W. A., Flemming, S., Toenhake, C. G., Schmitt, M., Sabitzki, R., Bergmann, B., Fröhlke, U., Mesén-Ramírez, P., Soares, A. B., Herrmann, H., Bártfai, R., & Spielmann, T. (2020). A Kelch13-defined endocytosis pathway mediates artemisinin resistance in malaria parasites. *Science*, *367*(6473), 51–59. https://doi.org/10.1126/science.aax4735

Blank, O., Davioud-Charvet, E., & Elhabiri, M. (2012). Interactions of the antimalarial drug methylene blue with methemoglobin and heme targets in Plasmodium falciparum: A physico-biochemical study. *Antioxidants and Redox Signaling*. https://doi.org/10.1089/ars.2011.4239

Bosson-Vanga, H., Franetich, J. F., Soulard, V., Sossau, D., Tefit, M., Kane, B., Vaillant, J. C., Borrmann, S., Müller, O., Dereuddre-Bosquet, N., Le Grand, R., Silvie, O., & Mazier, D. (2018). Differential activity of methylene blue against erythrocytic and hepatic stages of Plasmodium. *Malaria Journal*. https://doi.org/10.1186/s12936-018-2300-y

Brewer, T. G. (1998). Factors relating to neurotoxicity of artemisinin antimalarial drugs «listening to arteether». *Medecine Tropicale*.

Bridgford, J. L., Xie, S. C., Cobbold, S. A., Pasaje, C. F. A., Herrmann, S., Yang, T., Gillett, D. L., Dick, L. R., Ralph, S. A., Dogovski, C., Spillman, N. J., & Tilley, L. (2018). Artemisinin kills malaria parasites by damaging proteins and inhibiting the proteasome. *Nature Communications*, *9*(1), 1–9. https://doi.org/10.1038/s41467-018-06221-1

Buchholz, K., Burke, T. A., Williamson, K. C., Wiegand, R. C., Wirth, D. F., & Marti, M. (2011). A high-throughput screen targeting malaria transmission stages opens new avenues for drug development. *Journal of Infectious Diseases*. https://doi.org/10.1093/infdis/jir037

Buchholz, K., Comini, M. A., Wissenbach, D., Schirmer, R. H., Krauth-Siegel, R. L., & Gromer, S. (2008). Cytotoxic interactions of methylene blue with trypanosomatid-specific disulfide reductases and their dithiol products. *Molecular and Biochemical Parasitology*. https://doi.org/10.1016/j.molbiopara.2008.03.006

Buchholz, K., Schirmer, R. H., Eubel, J. K., Akoachere, M. B., Dandekar, T., Becker, K., & Gromer, S. (2008). Interactions of methylene blue with human disulfide reductases and their orthologues from Plasmodium falciparum. *Antimicrobial Agents and Chemotherapy*. https://doi.org/10.1128/AAC.00773-07

Burrows, J. N., Hooft Van Huijsduijnen, R., Möhrle, J. J., Oeuvray, C., & Wells, T. N. (2013). Designing the next generation of medicines for malaria control and eradication. In *Malaria Journal*. https://doi.org/10.1186/1475-2875-12-187

Butler, A. R., & Wu, Y. L. (1992). Artemisinin (qinghaosu): A new type of antimalarial drug. In *Chemical Society Reviews*. https://doi.org/10.1039/CS9922100085

Camarda, G., Jirawatcharadech, P., Priestley, R. S., Saif, A., March, S., Wong, M. H. L., Leung, S., Miller, A. B., Baker, D. A., Alano, P., Paine, M. J. I., Bhatia, S. N., O'Neill, P. M., Ward, S. A., & Biagini, G. A. (2019). Antimalarial activity of primaquine operates via a two-step biochemical relay. *Nature Communications*. https://doi.org/10.1038/s41467-019-11239-0

Cappellini, M., & Fiorelli, G. (2008). Glucose-6-phosphate dehydrogenase deficiency. In *The Lancet*. https://doi.org/10.1016/S0140-6736(08)60073-2

Cassagnes, L. E., Rakotoarivelo, N., Sirigu, S., Pério, P., Najahi, E., Chavas, L. M. G., Thompson, A., Gayon, R., Ferry, G., Boutin, J. A., Valentin, A., Reybier, K., & Nepveu, F. (2017). Role of quinone reductase 2 in the antimalarial properties of indolone-type derivatives. *Molecules*. https://doi.org/10.3390/molecules22020210

Chavain, N., Davioud-Charvet, E., Trivelli, X., Mbeki, L., Rottmann, M., Brun, R., & Biot, C. (2009). Antimalarial activities of ferroquine conjugates with either glutathione reductase inhibitors or glutathione depletors via a hydrolyzable amide linker. *Bioorganic and Medicinal Chemistry*. https://doi.org/10.1016/j.bmc.2009.10.008

Christen, E. H., Gübeli, R. J., Kaufmann, B., Merkel, L., Schoenmakers, R., Budisa, N., Fussenegger, M., Weber, W., & Wiltschi, B. (2012). Evaluation of bicinchoninic acid as a ligand for copper(i)-catalyzed azide-alkyne bioconjugations. *Organic and Biomolecular Chemistry*, *10*(33), 6629–6632. https://doi.org/10.1039/c2ob25556a

Clayman, C. B., Arnold, J., Hockwald, R. S., Yount, E. H., Edgcomb, J. H., & Alving, A. S. (1952). Toxicity of primaquine in caucasians. *Journal of the American Medical Association*. https://doi.org/10.1001/jama.1952.72930340022010b

Coertzen, D., Reader, J., Van Der Watt, M., Nondaba, S. H., Gibhard, L., Wiesner, L., Smith, P., D'Alessandro, S., Taramelli, D., Wong, H. N., Du Preez, J. L., Wu, R. W. K., Birkholtz, L. M., & Haynes, R. K. (2018). Artemisone and artemiside are potent panreactive antimalarial agents that also synergize redox imbalance in plasmodium falciparum transmissible gametocyte stages. *Antimicrobial Agents and Chemotherapy*. https://doi.org/10.1128/AAC.02214-17

Cohen, R. J., Sachs, J. R., Wicker, D. J., & Conrad, M. E. (1968). Methemoglobinemia provoked by malarial chemoprophylaxis in Vietnam. *The New England Journal of Medicine*. https://doi.org/10.1056/NEJM196811212792102

Coulibaly, B., Pritsch, M., Bountogo, M., Meissner, P. E., Nebié, E., Klose, C., Kieser, M., Berens-Riha, N., Wieser, A., Sirima, S. B., Breitkreutz, J., Schirmer, R. H., Sié, A., Mockenhaupt, F. P., Drakeley, C., Bousema, T., & Müller, O. (2015). Efficacy and safety

of triple combination therapy with artesunate-amodiaquine-methylene blue for falciparum malaria in children: A randomized controlled trial in Burkina Faso. *Journal of Infectious Diseases*. https://doi.org/10.1093/infdis/jiu540

Coulibaly, B., Zoungrana, A., Mockenhaupt, F. P., Schirmer, R. H., Klose, C., Mansmann, U., Meissner, P. E., & Müller, O. (2009). Strong Gametocytocidal Effect of Methylene Blue-Based Combination Therapy against Falciparum Malaria: A Randomised Controlled Trial. *PLoS ONE*. https://doi.org/10.1371/journal.pone.0005318

Cui, L., & Su, X. Z. (2009). Discovery, mechanisms of action and combination therapy of artemisinin. In *Expert Review of Anti-Infective Therapy*. https://doi.org/10.1586/ERI.09.68

Cyrklaff, M., Sanchez, C. P., Frischknecht, F., & Lanzer, M. (2012). Host actin remodeling and protection from malaria by hemoglobinopathies. In *Trends in Parasitology*. https://doi.org/10.1016/j.pt.2012.08.003

Cyrklaff, M., Sanchez, C. P., Kilian, N., Bisseye, C., Simpore, J., Frischknecht, F., & Lanzer, M. (2011). Hemoglobins S and C interfere with actin remodeling in Plasmodium falciparum-infected erythrocytes. *Science*. https://doi.org/10.1126/science.1213775

Davioud-Charvet, E., & Lanfranchi, D. A. (2011). Subversive Substrates of Glutathione Reductases from Plasmodium falciparum-Infected Red Blood Cells as Antimalarial Agents. In *Apicomplexan Parasites: Molecular Approaches toward Targeted Drug Development*. https://doi.org/10.1002/9783527633883.ch20

Delves, M. J., Ramakrishnan, C., Blagborough, A. M., Leroy, D., Wells, T. N. C., & Sinden, R. E. (2012). A high-throughput assay for the identification of malarial transmission-blocking drugs and vaccines. *International Journal for Parasitology*. https://doi.org/10.1016/j.ijpara.2012.08.009

Delves, M. J., Ruecker, A., Straschil, U., Lelièvre, J., Marques, S., López-Barragán, M. J., Herreros, E., & Sinden, R. E. (2013). Male and female Plasmodium falciparum mature gametocytes show different responses to antimalarial drugs. *Antimicrobial Agents and Chemotherapy*. https://doi.org/10.1128/AAC.00325-13

Delves, M., Plouffe, D., Scheurer, C., Meister, S., Wittlin, S., Winzeler, E. A., Sinden, R. E., & Leroy, D. (2012). The activities of current antimalarial drugs on the life cycle stages of plasmodium: A comparative study with human and rodent parasites. *PLoS Medicine*. https://doi.org/10.1371/journal.pmed.1001169

Demas, A. R., Sharma, A. I., Wong, W., Early, A. M., Redmond, S., Bopp, S., Neafsey, D. E., Volkman, S. K., Hartl, D. L., & Wirth, D. F. (2018). Mutations in plasmodium falciparum actin-binding protein coronin confer reduced artemisinin susceptibility. *Proceedings of the National Academy of Sciences of the United States of America*. https://doi.org/10.1073/pnas.1812317115

Dembele, L., Gego, A., Zeeman, A. M., Franetich, J. F., Silvie, O., Rametti, A., Le Grand, R., Dereuddre-Bosquet, N., Sauerwein, R., van Gemert, G. J., Vaillant, J. C., Thomas, A. W., Snounou, G., Kocken, C. H. M., & Mazier, D. (2011). Towards an in vitro model of plasmodium hypnozoites suitable for drug discovery. *PLoS ONE*. https://doi.org/10.1371/journal.pone.0018162

Deseke Yoichi Ourisson, Guy, E. (1998). Intrinsic Reactivities of Amino Acids towards Photoalkylation with Benzophenone − A Study Preliminary to Photolabelling of the Transmembrane Protein Glycophorin A. *European Journal of Organic Chemistry*, *243–251*(1434-193X NV-1998), 2. https://doi.org/10.1002/(SICI)1099-0690(199802)1998:2<243::AID-EJOC243>3.0.CO;2-I

Dicko, A., Roh, M. E., Diawara, H., Mahamar, A., Soumare, H. M., Lanke, K., Bradley, J., Sanogo, K., Kone, D. T., Diarra, K., Keita, S., Issiaka, D., Traore, S. F., McCulloch, C., Stone, W. J. R., Hwang, J., Müller, O., Brown, J. M., Srinivasan, V., … Bousema, T. (2018). Efficacy and safety of primaquine and methylene blue for prevention of Plasmodium falciparum transmission in Mali: a phase 2, single-blind, randomised controlled trial. *The Lancet Infectious Diseases*. https://doi.org/10.1016/S1473-3099(18)30044-6

Ding, Y., Chen, M., Liu, Z., Ding, D., Ye, Y., Zhang, M., Kelly, R., Guo, L., Su, Z., Harris, S. C., Qian, F., Ge, W., Fang, H., Xu, X., & Tong, W. (2012). atBioNet- an integrated network analysis tool for genomics and biomarker discovery. *BMC Genomics*. https://doi.org/10.1186/1471-2164-13-325

Djimde, A. A., Maiga, A. W., Ouologuem, D., Fofana, B., Sagara, I., Dembele, D., Toure, S., Sanogo, K., Dama, S., Sidibe, B., & Doumbo, O. K. (2016). Gametocyte clearance dynamics following oral artesunate treatment of uncomplicated falciparum malaria in Malian children. *Parasite*. https://doi.org/10.1051/parasite/2016003

Dogovski, C., Xie, S. C., Burgio, G., Bridgford, J., Mok, S., McCaw, J. M., Chotivanich, K., Kenny, S., Gnädig, N., Straimer, J., Bozdech, Z., Fidock, D. A., Simpson, J. A., Dondorp, A. M., Foote, S., Klonis, N., & Tilley, L. (2015). Targeting the Cell Stress Response of Plasmodium falciparum to Overcome Artemisinin Resistance. *PLoS Biology*. https://doi.org/10.1371/journal.pbio.1002132

Dondorp, A M, Nosten, F., Yi, P., Das, D., Phyo, A. P., Tarning, J., Lwin, K. M., Ariey, F., Hanpithakpong, W., Lee, S. J., Ringwald, P., Silamut, K., Imwong, M., Chotivanich, K., Lim, P., Herdman, T., An, S. S., Yeung, S., Singhasivanon, P., … White, N. J. (2009). Artemisinin resistance in Plasmodium falciparum malaria. *N Engl J Med*, *361*(5), 455–467. https://doi.org/10.1056/NEJMoa0808859

Dondorp, Arjen M., Yeung, S., White, L., Nguon, C., Day, N. P. J., Socheat, D., & Von Seidlein, L. (2010). Artemisinin resistance: Current status and scenarios for containment. In *Nature Reviews Microbiology*. https://doi.org/10.1038/nrmicro2331

Dubar, F., Bohic, S., Dive, D., Guérardel, Y., Cloetens, P., Khalife, J., & Biot, C. (2012). Deciphering the resistance-counteracting functions of ferroquine in plasmodium falciparum -infected erythrocytes. *ACS Medicinal Chemistry Letters*. https://doi.org/10.1021/ml300062q

Dubar, F., Egan, T. J., Pradines, B., Kuter, D., Ncokazi, K. K., Forge, D., Paul, J. F., Pierrot, C., Kalamou, H., Khalife, J., Buisine, E., Rogier, C., Vezin, H., Forfar, I., Slomianny, C., Trivelli, X., Kapishnikov, S., Leiserowitz, L., Dive, D., & Biot, C. (2011). The antimalarial ferroquine: Role of the metal and intramolecular hydrogen bond in activity and resistance. *ACS Chemical Biology*. https://doi.org/10.1021/cb100322v

Duckworth, B. P., Wilson, D. J., Nelson, K. M., Boshoff, H. I., Barry, C. E., & Aldrich, C. C. (2012). Development of a selective activity-based probe for adenylating enzymes: profiling MbtA Involved in siderophore biosynthesis from Mycobacterium tuberculosis. *ACS Chem Biol*, *7*(10), 1653–1658. https://doi.org/10.1021/cb300112x

Duvalsaint, M., & Kyle, D. E. (2018). Phytohormones, isoprenoids, and role of the apicoplast in recovery from dihydroartemisinin-induced dormancy of plasmodium falciparum. *Antimicrobial Agents and Chemotherapy*. https://doi.org/10.1128/AAC.01771-17

Dziekan, Jerzy M., Yu, H., Chen, D., Dai, L., Wirjanata, G., Larsson, A., Prabhu, N., Sobota, R. M., Bozdech, Z., & Nordlund, P. (2019). Identifying purine nucleoside phosphorylase as the target of quinine using cellular thermal shift assay. *Science Translational Medicine*. https://doi.org/10.1126/scitranslmed.aau3174

Dziekan, Jerzy Michal, Wirjanata, G., Dai, L., Go, K. D., Yu, H., Lim, Y. T., Chen, L., Wang, L. C., Puspita, B., Prabhu, N., Sobota, R. M., Nordlund, P., & Bozdech, Z. (2020). Cellular thermal shift assay for the identification of drug–target interactions in the Plasmodium falciparum proteome. *Nature Protocols*. https://doi.org/10.1038/s41596-020-0310-z

Ebstie, Y. A., Abay, S. M., Tadesse, W. T., & Ejigu, D. A. (2016). Tafenoquine and its potential in the treatment and relapse prevention of Plasmodium vivax malaria: The evidence to date. In *Drug Design, Development and Therapy*. https://doi.org/10.2147/DDDT.S61443

Ehrhardt, K, Davioud-Charvet, E., Ke, H., Vaidya, A. B., Lanzer, M., & Deponte, M. (2013). The antimalarial activities of methylene blue and the 1,4-naphthoquinone 3-[4-(trifluoromethyl)benzyl]-menadione are not due to inhibition of the mitochondrial electron transport chain. *Antimicrob Agents Chemother*, *57*(5), 2114–2120. https://doi.org/10.1128/AAC.02248-12

Ehrhardt, Katharina, Davioud-Charvet, E., Ke, H., Vaidya, A. B. A. B., Lanzer, M., & Deponte, M. (2013). The Antimalarial activities of methylene blue and the 1,4-naphthoquinone 3-[4-(Trifluoromethyl)Benzyl]-menadione are not due to inhibition of the mitochondrial electron transport chain. *Antimicrobial Agents and Chemotherapy*, *57*(5), 2114–2120. https://doi.org/10.1128/AAC.02248-12

Ehrhardt, Katharina, Deregnaucourt, C., Goetz, A. A., Tzanova, T., Gallo, V., Arese, P., Pradines, B., Adjalley, S. H., Bagrel, D., Blandin, S., Lanzer, M., & Davioud-Charvet, E. (2016). The redox cycler plasmodione is a fast-acting antimalarial lead compound with pronounced activity against sexual and early asexual blood-stage parasites. *Antimicrobial Agents and Chemotherapy*, *60*(9), 5146–5158. https://doi.org/10.1128/AAC.02975-15

Elhabiri, M., Sidorov, P., Cesar-Rodo, E., Marcou, G., Lanfranchi, D. A., Davioud-Charvet, E., Horvath, D., & Varnek, A. (2015). Electrochemical properties of substituted 2-methyl-1,4-naphthoquinones: Redox behavior predictions. *Chemistry - A European Journal*. https://doi.org/10.1002/chem.201403703

Elliott, P. I. P. (2014). Organometallic complexes with 1,2,3-triazole-derived ligands. In *Organometallic Chemistry*. https://doi.org/10.1039/9781849737692-00001

Färber, P. M., Arscott, L. D., Williams, C. H., Becker, K., & Schirmer, R. H. (1998). Recombinant Plasmodium falciparum glutathione reductase is inhibited by the antimalarial dye methylene blue. *FEBS Letters*. https://doi.org/10.1016/S0014-5793(98)00031-3

Feng, L., Lanfranchi, D. A., Cotos, L., Cesar-Rodo, E., Ehrhardt, K., Goetz, A. A., Zimmermann, H., Fenaille, F., Blandin, S. A., & Davioud-Charvet, E. (2018). Synthesis of plasmodione metabolites and 13C-enriched plasmodione as chemical tools for drug metabolism investigation. *Organic and Biomolecular Chemistry*, *16*(15), 2647–2665. https://doi.org/10.1039/c8ob00227d

Ferru, E., Giger, K., Pantaleo, A., Campanella, E., Grey, J., Ritchie, K., Vono, R., Turrini, F., & Low, P. S. (2011). Regulation of membrane-cytoskeletal interactions by tyrosine phosphorylation of erythrocyte band 3. *Blood*. https://doi.org/10.1182/blood-2010-11-317024

Francis, R. O., Jhang, J. S., Pham, H. P., Hod, E. A., Zimring, J. C., & Spitalnik, S. L. (2013). Glucose-6-phosphate dehydrogenase deficiency in transfusion medicine: The unknown risks. In *Vox Sanguinis*. https://doi.org/10.1111/vox.12068

Fukuda, M. M., Krudsood, S., Mohamed, K., Green, J. A., Warrasak, S., Noedl, H., Euswas,

A., Ittiverakul, M., Buathong, N., Sriwichai, S., Miller, R. S., & Ohrt, C. (2017). A randomized, double-blind, active-control trial to evaluate the efficacy and safety of a three day course of tafenoquine monotherapy for the treatment of Plasmodium vivax malaria. *PLoS ONE*. https://doi.org/10.1371/journal.pone.0187376

Gallo, V., Skorokhod, O. A., Simula, L. F., Marrocco, T., Tambini, E., Schwarzer, E., Marget, P., Duc, G., & Arese, P. (2018). No red blood cell damage and no hemolysis in G6PD-deficient subjects after ingestion of low vicine/convicine Vicia faba seeds. In *Blood*. https://doi.org/10.1182/blood-2017-09-806364

Galmozzi, A., Dominguez, E., Cravatt, B. F., & Saez, E. (2014). Application of activity-based protein profiling to study enzyme function in adipocytes. In *Methods in Enzymology*. https://doi.org/10.1016/B978-0-12-800280-3.00009-8

Ganesan, S., Chaurasiya, N. D., Sahu, R., Walker, L. A., & Tekwani, B. L. (2012). Understanding the mechanisms for metabolism-linked hemolytic toxicity of primaquine against glucose 6-phosphate dehydrogenase deficient human erythrocytes: Evaluation of eryptotic pathway. *Toxicology*. https://doi.org/10.1016/j.tox.2012.01.015

Ghatak, T., Poddar, B., & Baronia, A. K. (2013). Dapsone induced methemoglobinemia and hemolysis in a G6PD deficient girl, possibly aggravated by aggressive methylene blue therapy. In *Indian Journal of Dermatology*. https://doi.org/10.4103/0019-5154.117360

Graves, P. M., Gelband, H., & Garner, P. (2015). Primaquine or other 8-aminoquinoline for reducing Plasmodium falciparum transmission. In *Cochrane Database of Systematic Reviews*. https://doi.org/10.1002/14651858.CD008152.pub4

Henrici, R. C., Edwards, R. L., Zoltner, M., van Schalkwyk, D. A., Hart, M. N., Mohring, F., Moon, R. W., Nofal, S. D., Patel, A., Flueck, C., Baker, D. A., John, A. R. O., Field, M. C., & Sutherland, C. J. (2020). The plasmodium falciparum artemisinin susceptibility-associated ap-2 adaptin μ subunit is clathrin independent and essential for schizont maturation. *MBio*. https://doi.org/10.1128/mBio.02918-19

Henrici, R. C., van Schalkwyk, D. A., & Sutherland, C. J. (2020). Modification of pfap2μ and pfubp1 Markedly Reduces Ring-Stage Susceptibility of Plasmodium falciparum to Artemisinin in Vitro. *Antimicrobial Agents and Chemotherapy*. https://doi.org/10.1128/AAC.01542-19

Henriques, G., Hallett, R. L., Beshir, K. B., Gadalla, N. B., Johnson, R. E., Burrow, R., Van Schalkwyk, D. A., Sawa, P., Omar, S. A., Clark, T. G., Bousema, T., & Sutherland, C. J. (2014). Directional selection at the pfmdr1, pfcrt, pfubp1, and pfap2mu loci of Plasmodium falciparum in Kenyan children treated with ACT. *Journal of Infectious Diseases*. https://doi.org/10.1093/infdis/jiu358

Henriques, G., Martinelli, A., Rodrigues, L., Modrzynska, K., Fawcett, R., Houston, D. R., Borges, S. T., D'Alessandro, U., Tinto, H., Karema, C., Hunt, P., & Cravo, P. (2013). Artemisinin resistance in rodent malaria - Mutation in the AP2 adaptor μ-chain suggests involvement of endocytosis and membrane protein trafficking. *Malaria Journal*. https://doi.org/10.1186/1475-2875-12-118

Henriques, G., Van Schalkwyk, D. A., Burrow, R., Warhurst, D. C., Thompson, E., Baker, D. A., Fidock, D. A., Hallett, R., Flueck, C., & Sutherland, C. J. (2015). The Mu subunit of Plasmodium falciparum clathrin-associated adaptor protein 2 modulates in vitro parasite response to artemisinin and quinine. *Antimicrobial Agents and Chemotherapy*. https://doi.org/10.1128/AAC.04067-14

Hockwald, R. S., Arnold, M. J., Clayman, C. B., & Alving, A. S. (1952). Toxicity of primaquine in negroes. *Journal of the American Medical Association*. https://doi.org/10.1001/jama.1952.72930340027010c

Hong, V., Presolski, S. I., Ma, C., & Finn, M. G. (2009). Analysis and optimization of copper-catalyzed azide-alkyne cycloaddition for bioconjugation. *Angewandte Chemie - International Edition*. https://doi.org/10.1002/anie.200905087

Hong, V., Udit, A. K., Evans, R. A., & Finn, M. G. (2008). Electrochemically protected copper(I)-catalyzed azide-alkyne cycloaddition. *ChemBioChem*, *9*(9), 1481–1486. https://doi.org/10.1002/cbic.200700768

HOOPER, M., PATTERSON, D. A., & WIBBERLEY, D. G. (1965). Preparation and antibacterial activity of isatogens and related compounds. *Journal of Pharmacy and Pharmacology*. https://doi.org/10.1111/j.2042-7158.1965.tb07596.x

Hughes, J. P., Rees, S. S., Kalindjian, S. B., & Philpott, K. L. (2011). Principles of early drug discovery. In *British Journal of Pharmacology*. https://doi.org/10.1111/j.1476-5381.2010.01127.x

Hughes, K. R., Philip, N., Lucas Starnes, G., Taylor, S., & Waters, A. P. (2010). From cradle to grave: RNA biology in malaria parasites. In *Wiley Interdisciplinary Reviews: RNA*. https://doi.org/10.1002/wrna.30

Ibrahim, H., Furiga, A., Najahi, E., Pigasse Hénocq, C., Nallet, J. P., Roques, C., Aubouy, A., Sauvain, M., Constant, P., Daffé, M., & Nepveu, F. (2012). Antibacterial, antifungal and antileishmanial activities of indolone-N-oxide derivatives. *Journal of Antibiotics*. https://doi.org/10.1038/ja.2012.60

Ibrahim, H., Pantaleo, A., Turrini, F., Arese, P., Nallet, J. P., & Nepveu, F. (2011). Pharmacological properties of indolone-N-oxides controlled by a bioreductive transformation in red blood cells? *MedChemComm*. https://doi.org/10.1039/c1md00127b

Ismail, H. M., Barton, V. E., Panchana, M., Charoensutthivarakul, S., Biagini, G. A., Ward, S. A., & O'Neill, P. M. (2016). Corrigendum: A Click Chemistry-Based Proteomic Approach Reveals that 1,2,4-Trioxolane and Artemisinin Antimalarials Share a Common Protein Alkylation Profile. *Angew Chem Int Ed Engl*, *55*(36), 10548. https://doi.org/10.1002/anie.201607032

Johann, L. (2012). A Physico-Biochemical Study on Potential Redox-Cyclers as Antimalarial and Antischistosomal Drugs. *Current Pharmaceutical Design*. https://doi.org/10.2174/138161212801327284

Jortzik, E., & Becker, K. (2012). Thioredoxin and glutathione systems in Plasmodium falciparum. In *International Journal of Medical Microbiology*. https://doi.org/10.1016/j.ijmm.2012.07.007

Josling, G. A., & Llinás, M. (2015). Sexual development in Plasmodium parasites: Knowing when it's time to commit. *Nature Reviews Microbiology*, *13*(9), 573–587. https://doi.org/10.1038/nrmicro3519

Karbwang, J., & Na-Bangchang, K. (2020). The Role of Clinical Pharmacology in Chemotherapy of Multidrug-Resistant Plasmodium falciparum. In *Journal of Clinical Pharmacology*. https://doi.org/10.1002/jcph.1589

Kehr, S., Sturm, N., Rahlfs, S., Przyborski, J. M., & Becker, K. (2010). Compartmentation of redox metabolism in malaria parasites. *PLoS Pathogens*. https://doi.org/10.1371/journal.ppat.1001242

Kessl, J. J., Meshnick, S. R., & Trumpower, B. L. (2007). Modeling the molecular basis of atovaquone resistance in parasites and pathogenic fungi. In *Trends in Parasitology*. https://doi.org/10.1016/j.pt.2007.08.004

Kim, Y. R., Kuh, H. J., Kim, M. Y., Kim, Y. S., Chung, W. C., Kim, S. I., & Kang, M. W. (2004). Pharmacokinetics of primaquine and carboxyprimaquine in Korean patients with vivax malaria. *Archives of Pharmacal Research*. https://doi.org/10.1007/BF02980134

Klayman, D. L. (1985). Qinghaosu (artemisinin): An antimalarial drug from China. *Science*. https://doi.org/10.1126/science.3887571

Klonis, N., Crespo-Ortiz, M. P., Bottova, I., Abu-Bakar, N., Kenny, S., Rosenthal, P. J., & Tilley, L. (2011). Artemisinin activity against Plasmodium falciparum requires hemoglobin uptake and digestion. *Proceedings of the National Academy of Sciences of the United States of America*. https://doi.org/10.1073/pnas.1104063108

Kondratskyi, A., Kondratska, K., Vanden Abeele, F., Gordienko, D., Dubois, C., Toillon, R. A., Slomianny, C., Lemière, S., Delcourt, P., Dewailly, E., Skryma, R., Biot, C., & Prevarskaya, N. (2017). Ferroquine, the next generation antimalarial drug, has antitumor activity. *Scientific Reports*. https://doi.org/10.1038/s41598-017-16154-2

Krauth-Siegel, R. L., Bauer, H., & Schirmer, R. H. (2005). Dithiol proteins as guardians of the intracellular redox milieu in parasites: Old and new drug targets in trypanosomes and malaria-causing plasmodia. In *Angewandte Chemie - International Edition*. https://doi.org/10.1002/anie.200300639

Krotoski, W. A., Krotoski, D. M., Garnham, P. C. C., Bray, R. S., Killick-Kendrick, R., Draper, C. C., Targett, G. A. T., & Guy, M. W. (1980). Relapses in primate malaria: Discovery of two populations of exoerythrocytic stages. Preliminary note. *British Medical Journal*. https://doi.org/10.1136/bmj.280.6208.153-a

Krungkrai, J., Burat, D., Kudan, S., Krungkrai, S., & Prapunwattana, P. (1999). Mitochondrial oxygen consumption in asexual and sexual blood stages of the human malarial parasite, Plasmodium falciparum. *Southeast Asian Journal of Tropical Medicine and Public Health*.

Krungkrai, S. R., & Yuthavong, Y. (1987). The antimalarial action on Plasmodium falciparum of qinghaosu and artesunate in combination with agents which modulate oxidant stress. *Transactions of the Royal Society of Tropical Medicine and Hygiene*. https://doi.org/10.1016/0035-9203(87)90003-4

Kumar, N., & Zheng, H. (1990). Stage-specific gametocytocidal effect in vitro of the antimalaria drug qinghaosu on Plasmodium falciparum. *Parasitology Research*. https://doi.org/10.1007/BF00930817

Kupferschmid, M., Aquino-Gil, M. O., Shams-Eldin, H., Schmidt, J., Yamakawa, N., Krzewinski, F., Schwarz, R. T., & Lefebvre, T. (2017). Identification of O-GlcNAcylated proteins in Plasmodium falciparum. *Malaria Journal*. https://doi.org/10.1186/s12936-017-2131-2

Lalève, A., Vallières, C., Golinelli-Cohen, M. P., Bouton, C., Song, Z., Pawlik, G., Tindall, S. M., Avery, S. V., Clain, J., & Meunier, B. (2016). The antimalarial drug primaquine targets Fe-S cluster proteins and yeast respiratory growth. *Redox Biology*. https://doi.org/10.1016/j.redox.2015.10.008

Landier, J., Parker, D. M., Thu, A. M., Lwin, K. M., Delmas, G., Nosten, F. H., Andolina, C., Aguas, R., Ang, S. M., Aung, E. P., Baw, N. B., Be, S. A., B'Let, S., Bluh, H., Bonnington, C. A., Chaumeau, V., Chirakiratinant, M., Cho, W. C., Christensen, P., … Yuwapan, D. (2018). Effect of generalised access to early diagnosis and treatment and targeted mass drug administration on Plasmodium falciparum malaria in Eastern Myanmar: an observational study of a regional elimination programme. *The Lancet*. https://doi.org/10.1016/S0140-6736(18)30792-X

Lanfranchi, D. A., Cesar-Rodo, E., Bertrand, B., Huang, H. H., Day, L., Johann, L., Elhabiri, M., Becker, K., Williams, D. L., & Davioud-Charvet, E. (2012). Synthesis and biological evaluation of 1,4-naphthoquinones and quinoline-5,8-diones as antimalarial and schistosomicidal agents. *Organic and Biomolecular Chemistry*. https://doi.org/10.1039/c2ob25812a

Lewis, W. G., Magallon, F. G., Fokin, V. V., & Finn, M. G. (2004). Discovery and characterization of catalysts for azide-alkyne cycloaddition by fluorescence quenching. *Journal of the American Chemical Society*. https://doi.org/10.1021/ja048425z

Li, H., Aneja, R., & Chaiken, I. (2013). Click chemistry in peptide-based drug design. *Molecules*, *18*(8), 9797–9817. https://doi.org/10.3390/molecules18089797

Li, Q., O'Neil, M., Xie, L., Caridha, D., Zeng, Q., Zhang, J., Pybus, B., Hickman, M., & Melendez, V. (2014). Assessment of the prophylactic activity and pharmacokinetic profile of oral tafenoquine compared to primaquine for inhibition of liver stage malaria infections. *Malaria Journal*. https://doi.org/10.1186/1475-2875-13-141

Li, S., Wang, L., Yu, F., Zhu, Z., Shobaki, D., Chen, H., Wang, M., Wang, J., Qin, G., Erasquin, U. J., Ren, L., Wang, Y., & Cai, C. (2017). Copper-catalyzed click reaction on/in live cells. *Chemical Science*, *8*(3), 2107–2114. https://doi.org/10.1039/c6sc02297a

Li, W., Mo, W., Shen, D., Sun, L., Wang, J., Lu, S., Gitschier, J. M., & Zhou, B. (2005). Yeast model uncovers dual of mitochondria in the action of artemisinin. *PLoS Genetics*. https://doi.org/10.1371/journal.pgen.0010036

Lu, G., Nagbanshi, M., Goldau, N., Mendes Jorge, M., Meissner, P., Jahn, A., Mockenhaupt, F. P., & Müller, O. (2018). Efficacy and safety of methylene blue in the treatment of malaria: A systematic review. *BMC Medicine*. https://doi.org/10.1186/s12916-018-1045-3

Lubin, A. S., Rueda-Zubiaurre, A., Matthews, H., Baumann, H., Fisher, F. R., Morales-Sanfrutos, J., Hadavizadeh, K. S., Nardella, F., Tate, E. W., Baum, J., Scherf, A., & Fuchter, M. J. (2018). Development of a Photo-Cross-Linkable Diaminoquinazoline Inhibitor for Target Identification in Plasmodium falciparum. *ACS Infect Dis*, *4*(4), 523–530. https://doi.org/10.1021/acsinfecdis.7b00228

Luzzatto, L., & Arese, P. (2018a). Favism and glucose-6-phosphate dehydrogenase deficiency. *New England Journal of Medicine*, *378*(1), 60–71. https://doi.org/10.1056/NEJMra1708111

Luzzatto, L., & Arese, P. (2018b). Favism and glucose-6-phosphate dehydrogenase deficiency. In *New England Journal of Medicine*. https://doi.org/10.1056/NEJMra1708111

Magwere, T., Naik, Y. S., & Hasler, J. A. (1997). Primaquine alters antioxidant enzyme profiles in rat liver and kidney. *Free Radical Research*. https://doi.org/10.3109/10715769709097849

Marcsisin, S. R., Reichard, G., & Pybus, B. S. (2016). Primaquine pharmacology in the context of CYP 2D6 pharmacogenomics: Current state of the art. In *Pharmacology and Therapeutics*. https://doi.org/10.1016/j.pharmthera.2016.03.011

Mbengue, A., Bhattacharjee, S., Pandharkar, T., Liu, H., Estiu, G., Stahelin, R. V., Rizk, S. S., Njimoh, D. L., Ryan, Y., Chotivanich, K., Nguon, C., Ghorbal, M., Lopez-Rubio, J. J., Pfrender, M., Emrich, S., Mohandas, N., Dondorp, A. M., Wiest, O., & Haldar, K. (2015). A molecular mechanism of artemisinin resistance in Plasmodium falciparum malaria. *Nature*. https://doi.org/10.1038/nature14412

Meissner, P. E., Mandi, G., Coulibaly, B., Witte, S., Tapsoba, T., Mansmann, U.,

Rengelshausen, J., Schiek, W., Jahn, A., Walter-Sack, I., Mikus, G., Burhenne, J., Riedel, K. D., Schirmer, R. H., Kouyaté, B., & Müller, O. (2006). Methylene blue for malaria in Africa: Results from a dose-finding study in combination with chloroquine. *Malaria Journal*. https://doi.org/10.1186/1475-2875-5-84

Meissner, P. E., Mandi, G., Witte, S., Coulibaly, B., Mansmann, U., Rengelshausen, J., Schiek, W., Jahn, A., Sanon, M., Tapsoba, T., Walter-Sack, I., Mikus, G., Burhenne, J., Riedel, K. D., Schirmer, H., Kouyaté, B., & Müller, O. (2005). Safety of the methylene blue plus chloroquine combination in the treatment of uncomplicated falciparum malaria in young children of Burkina Faso [ISRCTN27290841]. *Malaria Journal*. https://doi.org/10.1186/1475-2875-4-45

Ménard, S., Haddou, T. Ben, Ramadani, A. P., Ariey, F., Iriart, X., Beghain, J., Bouchier, C., Witkowski, B., Berry, A., Mercereau-Puijalon, O., & Benoit-Vical, F. (2015). Induction of multidrug tolerance in Plasmodium falciparum by extended artemisinin pressure. *Emerging Infectious Diseases*. https://doi.org/10.3201/eid2110.150682

Meshnick, S. R., Taylor, T. E., & Kamchonwongpaisan, S. (1996). Artemisinin and the antimalarial endoperoxides: From herbal remedy to targeted chemotherapy. In *Microbiological Reviews*. https://doi.org/10.1128/mmbr.60.2.301-315.1996

Meshnick, Steven R. (2002). Artemisinin: Mechanisms of action, resistance and toxicity. *International Journal for Parasitology*. https://doi.org/10.1016/S0020-7519(02)00194-7

Meunier, B., & Robert, A. (2010). Heme as trigger and target for trioxane-containing antimalarial drugs. *Accounts of Chemical Research*. https://doi.org/10.1021/ar100070k

Miguel-Ávila, J., Tomás-Gamasa, M., Olmos, A., Pérez, P. J., & Mascareñas, J. L. (2018). Discrete Cu(i) complexes for azide-alkyne annulations of small molecules inside mammalian cells. *Chemical Science*, *9*(7), 1947–1952. https://doi.org/10.1039/c7sc04643j

Milner, E. E., Berman, J., Caridha, D., Dickson, S. P., Hickman, M., Lee, P. J., Marcsisin, S. R., Read, L. T., Roncal, N., Vesely, B. A., Xie, L. H., Zhang, J., Zhang, P., & Li, Q. (2016). Cytochrome P450 2D-mediated metabolism is not necessary for tafenoquine and primaquine to eradicate the erythrocytic stages of Plasmodium berghei. *Malaria Journal*. https://doi.org/10.1186/s12936-016-1632-8

Mohring, F., Jortzik, E., & Becker, K. (2016). Comparison of methods probing the intracellular redox milieu in Plasmodium falciparum. *Molecular and Biochemical Parasitology*. https://doi.org/10.1016/j.molbiopara.2015.11.002

Mok, S., Ashley, E. A., Ferreira, P. E., Zhu, L., Lin, Z., Yeo, T., Chotivanich, K., Imwong, M., Pukrittayakamee, S., Dhorda, M., Nguon, C., Lim, P., Amaratunga, C., Suon, S., Hien, T. T., Htut, Y., Faiz, M. A., Onyamboko, M. A., Mayxay, M., … Bozdech, Z. (2015). Population transcriptomics of human malaria parasites reveals the mechanism of artemisinin resistance. *Science*. https://doi.org/10.1126/science.1260403

Mounkoro, P., Michel, T., Blandin, S., Golinelli-Cohen, M. P., Davioud-Charvet, E., & Meunier, B. (2019). Investigating the mode of action of the redox-active antimalarial drug plasmodione using the yeast model. *Free Radical Biology and Medicine*, *141*(March), 269–278. https://doi.org/10.1016/j.freeradbiomed.2019.06.026

Müller, O., Mockenhaupt, F. P., Marks, B., Meissner, P., Coulibaly, B., Kuhnert, R., Buchner, H., Schirmer, R. H., Walter-Sack, I., Sié, A., & Mansmann, U. (2013). Haemolysis risk in methylene blue treatment of G6PD-sufficient and G6PD-deficient West-African children with uncomplicated falciparum malaria: A synopsis of four RCTs. *Pharmacoepidemiology and Drug Safety*. https://doi.org/10.1002/pds.3370

Müller, T, Johann, L., Jannack, B., Brückner, M., Lanfranchi, D. A., Bauer, H., Sanchez, C., Yardley, V., Deregnaucourt, C., Schrével, J., Lanzer, M., Schirmer, R. H., & Davioud-Charvet, E. (2011). Glutathione reductase-catalyzed cascade of redox reactions to bioactivate potent antimalarial 1,4-naphthoquinones--a new strategy to combat malarial parasites. *J Am Chem Soc*, *133*(30), 11557–11571. https://doi.org/10.1021/ja201729z

Müller, Tobias, Johann, L., Jannack, B., Brückner, M., Lanfranchi, D. A., Bauer, H., Sanchez, C., Yardley, V., Deregnaucourt, C., Schrével, J., Lanzer, M., Schirmer, R. H., & Davioud-Charvet, E. (2011). Glutathione reductase-catalyzed cascade of redox reactions to bioactivate potent antimalarial 1,4-naphthoquinones - A new strategy to combat malarial parasites. *Journal of the American Chemical Society*, *133*(30), 11557–11571. https://doi.org/10.1021/ja201729z

Munos, B. (2009). Munos, B. Lessons from 60 years of pharmaceutical innovation. Nat. Rev. Drug Discov. 8, 959-968. *Nature Reviews. Drug Discovery*. https://doi.org/10.1038/nrd2961

Murphy, M. P. (2009). How mitochondria produce reactive oxygen species. In *Biochemical Journal*. https://doi.org/10.1042/BJ20081386

Nardella, F., Halby, L., Hammam, E., Erdmann, D., Cadet-Daniel, V., Peronet, R., Ménard, D., Witkowski, B., Mecheri, S., Scherf, A., & Arimondo, P. B. (2020). DNA Methylation Bisubstrate Inhibitors Are Fast-Acting Drugs Active against Artemisinin-Resistant Plasmodium falciparum Parasites. *ACS Central Science*. https://doi.org/10.1021/acscentsci.9b00874

Nepveu, F., Kim, S., Boyer, J., Chatriant, O., Ibrahim, H., Reybier, K., Monje, M. C., Chevalley, S., Perio, P., Lajoie, B. H., Bouajila, J., Deharo, E., Sauvain, M., Tahar, R., Basco, L., Pantaleo, A., Turini, F., Arese, P., Valentin, A., … Nallet, J. P. (2010). Synthesis and antiplasmodial activity of new indolone N-Oxide derivatives. *Journal of Medicinal Chemistry*. https://doi.org/10.1021/jm901300d

Nepveu, F., & Turrini, F. (2013). Targeting the redox metabolism of Plasmodium falciparum. In *Future medicinal chemistry*. https://doi.org/10.4155/fmc.13.159

Neumann, S., Biewend, M., Rana, S., & Binder, W. H. (2020). The CuAAC: Principles, Homogeneous and Heterogeneous Catalysts, and Novel Developments and Applications. In *Macromolecular Rapid Communications* (Vol. 41, Issue 1). Wiley-VCH Verlag. https://doi.org/10.1002/marc.201900359

Noedl, H., Se, Y., Schaecher, K., Smith, B. L., Socheat, D., & Fukuda, M. M. (2008). Evidence of artemisinin-resistant malaria in Western Cambodia. In *New England Journal of Medicine*. https://doi.org/10.1056/NEJMc0805011

Obaldia, N., Rossan, R. N., Cooper, R. D., Kyle, D. E., Nuzum, E. O., Rieckmann, K. H., & Shanks, G. D. (1997). WR 238605, chloroquine, and their combinations as blood schizonticides against a chloroquine-resistant strain of Plasmodium vivax in Aotus monkeys. *American Journal of Tropical Medicine and Hygiene*. https://doi.org/10.4269/ajtmh.1997.56.508

Okebe, J., Bousema, T., Affara, M., Di Tanna, G. L., Dabira, E., Gaye, A., Sanya-Isijola, F., Badji, H., Correa, S., Nwakanma, D., Van Geertruyden, J. P., Drakeley, C., & D'Alessandro, U. (2016). The Gametocytocidal Efficacy of Different Single Doses of Primaquine with Dihydroartemisinin-piperaquine in Asymptomatic Parasite Carriers in The Gambia: A Randomized Controlled Trial. *EBioMedicine*. https://doi.org/10.1016/j.ebiom.2016.10.032

Otto, T. D., Wilinski, D., Assefa, S., Keane, T. M., Sarry, L. R., Böhme, U., Lemieux, J., Barrell, B., Pain, A., Berriman, M., Newbold, C., & Llinás, M. (2010). New insights into

the blood-stage transcriptome of Plasmodium falciparum using RNA-Seq. *Molecular Microbiology*. https://doi.org/10.1111/j.1365-2958.2009.07026.x

Ouologuem, D. T., Kone, C. O., Fofana, B., Sidibe, B., Togo, A. H., Dembele, D., Toure, S., Koumare, S., Toure, O., Sagara, I., Toure, A., Dao, A., Doumbo, O. K., & Djimde, A. A. (2018). Differential infectivity of gametocytes after artemisinin-based combination therapy of uncomplicated falciparum malaria. *African Journal of Laboratory Medicine*. https://doi.org/10.4102/ajlm.v7i2.784

Pal, C., & Bandyopadhyay, U. (2012). Redox-active antiparasitic drugs. In *Antioxidants and Redox Signaling*. https://doi.org/10.1089/ars.2011.4436

Paloque, L., Ramadani, A. P., Mercereau-Puijalon, O., Augereau, J. M., & Benoit-Vical, F. (2016). Plasmodium falciparum: multifaceted resistance to artemisinins. *Malaria Journal*, *15*(1), 1–12. https://doi.org/10.1186/s12936-016-1206-9

Pantaleo, A., Ferru, E., Carta, F., Mannu, F., Simula, L. F., Khadjavi, A., Pippia, P., & Turrini, F. (2011). Irreversible AE1 tyrosine phosphorylation leads to membrane vesiculation in G6PD deficient red cells. *PLoS ONE*. https://doi.org/10.1371/journal.pone.0015847

Pantaleo, A., Ferru, E., Giribaldi, G., Mannu, F., Carta, F., Matte, A., De Franceschi, L., & Turrini, F. (2009). Oxidized and poorly glycosylated band 3 is selectively phosphorylated by Syk kinase to form large membrane clusters in normal and G6PD-deficient red blood cells. *Biochemical Journal*. https://doi.org/10.1042/BJ20081557

Pantaleo, A., Ferru, E., Vono, R., Giribaldi, G., Lobina, O., Nepveu, F., Ibrahim, H., Nallet, J. P., Carta, F., Mannu, F., Pippia, P., Campanella, E., Low, P. S., & Turrini, F. (2012). New antimalarial indolone-N-oxides, generating radical species, destabilize the host cell membrane at early stages of Plasmodium falciparum growth: Role of band 3 tyrosine phosphorylation. *Free Radical Biology and Medicine*. https://doi.org/10.1016/j.freeradbiomed.2011.11.008

Pantaleo, A., Pau, M. C., Chien, H. D., & Turrini, F. (2015). Artemisinin resistance, some facts and opinions. *Journal of Infection in Developing Countries*. https://doi.org/10.3855/jidc.7015

Parker, C. G., & Pratt, M. R. (2020). Click Chemistry in Proteomic Investigations. *Cell*, *180*(4), 605–632. https://doi.org/10.1016/j.cell.2020.01.025

Peatey, C. L., Chavchich, M., Chen, N., Gresty, K. J., Gray, K. A., Gatton, M. L., Waters, N. C., & Cheng, Q. (2015). Mitochondrial Membrane Potential in a Small Subset of Artemisinin-Induced Dormant Plasmodium falciparum Parasites in Vitro. *Journal of Infectious Diseases*. https://doi.org/10.1093/infdis/jiv048

Penarete-Vargas, D. M., Boisson, A., Urbach, S., Chantelauze, H., Peyrottes, S., Fraisse, L., & Vial, H. J. (2014). A chemical proteomics approach for the search of pharmacological targets of the antimalarial clinical candidate albitiazolium in Plasmodium falciparum using photocrosslinking and click chemistry. *PLoS One*, *9*(12), e113918. https://doi.org/10.1371/journal.pone.0113918

Peters, W., Ellis, D., Boulard, Y., & Landau, I. (1984). The chemotherapy of rodent malaria XXXVI. Causal prophylaxis. Part IV. The activity of a new 8-aminoquinoline, WR 225,448 against exo-erythrocytic schizonts of Plasmodium yoelii yoelii. *Annals of Tropical Medicine and Parasitology*. https://doi.org/10.1080/00034983.1984.11811851

Plouffe, D. M., Wree, M., Du, A. Y., Meister, S., Li, F., Patra, K., Lubar, A., Okitsu, S. L., Flannery, E. L., Kato, N., Tanaseichuk, O., Comer, E., Zhou, B., Kuhen, K., Zhou, Y., Leroy, D., Schreiber, S. L., Scherer, C. A., Vinetz, J., & Winzeler, E. A. (2016). High-Throughput Assay and Discovery of Small Molecules that Interrupt Malaria

Transmission. *Cell Host and Microbe*. https://doi.org/10.1016/j.chom.2015.12.001

Ponsa, N., Sattabongkot, J., Kittayapong, P., Eikarat, N., & Coleman, R. E. (2003). Transmission-blocking activity of tafenoquine (WR-238605) and artelinic acid against naturally circulating strains of plasmodium vivax in Thailand. *American Journal of Tropical Medicine and Hygiene*. https://doi.org/10.4269/ajtmh.2003.69.542

Portela, M. J., Moreira, R., Valente, E., Constantino, L., Iley, J., Pinto, J., Rosa, R., Cravo, P., & Do Rosario, V. E. (1999). Dipeptide derivatives of primaquine as transmission-blocking antimalarials: Effect of aliphatic side-chain acylation on the gametocytocidal activity and on the formation of carboxyprimaquine in rat liver homogenates. *Pharmaceutical Research*. https://doi.org/10.1023/A:1018922425551

Potter, B. M. J., Xie, L. H., Vuong, C., Zhang, J., Zhang, P., Duan, D., Luong, T. L. T., Herath, H. M. T. B., Nanayakkara, N. P. D., Tekwani, B. L., Walker, L. A., Nolan, C. K., Sciotti, R. J., Zottig, V. E., Smith, P. L., Paris, R. M., Read, L. T., Li, Q., Pybus, B. S., … Marcsisin, S. R. (2015). Differential CYP 2D6 metabolism alters primaquine pharmacokinetics. *Antimicrobial Agents and Chemotherapy*. https://doi.org/10.1128/AAC.00015-15

Presolski, S. I., Hong, V., Cho, S. H., & Finn, M. G. (2010). Tailored ligand acceleration of the cu-catalyzed azide-alkyne cycloaddition reaction: Practical and mechanistic implications. *Journal of the American Chemical Society*, *132*(41), 14570–14576. https://doi.org/10.1021/ja105743g

Presolski, S. I., Hong, V. P., & Finn, M. G. (2011). Copper-Catalyzed Azide–Alkyne Click Chemistry for Bioconjugation. *Current Protocols in Chemical Biology*, *3*(4), 153–162. https://doi.org/10.1002/9780470559277.ch110148

Pybus, B. S., Marcsisin, S. R., Jin, X., Deye, G., Sousa, J. C., Li, Q., Caridha, D., Zeng, Q., Reichard, G. A., Ockenhouse, C., Bennett, J., Walker, L. A., Ohrt, C., & Melendez, V. (2013). The metabolism of primaquine to its active metabolite is dependent on CYP 2D6. *Malaria Journal*. https://doi.org/10.1186/1475-2875-12-212

Pybus, B. S., Sousa, J. C., Jin, X., Ferguson, J. A., Christian, R. E., Barnhart, R., Vuong, C., Sciotti, R. J., Reichard, G. A., Kozar, M. P., Walker, L. A., Ohrt, C., & Melendez, V. (2012). CYP450 phenotyping and accurate mass identification of metabolites of the 8-aminoquinoline, anti-malarial drug primaquine. *Malaria Journal*. https://doi.org/10.1186/1475-2875-11-259

Ramharter, M., Noedl, H., Thimasarn, K., Wiedermann, G., Wernsdorfer, G., & Wernsdorfer, W. H. (2002). In vitro activity of tafenoquine alone and in combination with artemisinin against Plasmodium falciparum. *American Journal of Tropical Medicine and Hygiene*. https://doi.org/10.4269/ajtmh.2002.67.39

Ramsay, R. R., Dunford, C., & Gillman, P. K. (2007). Methylene blue and serotonin toxicity: Inhibition of monoamine oxidase A (MAO A) confirms a theoretical prediction. *British Journal of Pharmacology*. https://doi.org/10.1038/sj.bjp.0707430

Recht, J., Ashley, E. A., & White, N. J. (2018). Use of primaquine and glucose-6-phosphate dehydrogenase deficiency testing: Divergent policies and practices in malaria endemic countries. In *PLoS Neglected Tropical Diseases*. https://doi.org/10.1371/journal.pntd.0006230

Reeder, B. J. (2010). The redox activity of hemoglobins: From physiologic functions to pathologic mechanisms. In *Antioxidants and Redox Signaling*. https://doi.org/10.1089/ars.2009.2974

Reiling, S. J., & Rohrbach, P. (2015). Monitoring PfMDR1 transport in Plasmodium

falciparum. *Malaria Journal*. https://doi.org/10.1186/s12936-015-0791-3

Robert, A., Benoit-Vical, F., Claparols, C., & Meunier, B. (2005a). The antimalarial drug artemisinin alkylates heme in infected mice. *Proceedings of the National Academy of Sciences of the United States of America*. https://doi.org/10.1073/pnas.0500972102

Robert, A., Benoit-Vical, F., Claparols, C., & Meunier, B. (2005b). The antimalarial drug artemisinin alkylates heme in infected mice. *Proceedings of the National Academy of Sciences of the United States of America*. https://doi.org/10.1073/pnas.0500972102

Rocamora, F., Zhu, L., Liong, K. Y., Dondorp, A., Miotto, O., Mok, S., & Bozdech, Z. (2018). Oxidative stress and protein damage responses mediate artemisinin resistance in malaria parasites. *PLoS Pathogens*. https://doi.org/10.1371/journal.ppat.1006930

Rodo, E. C., Feng, L., Jida, M., Ehrhardt, K., Bielitza, M., Boilevin, J., Lanzer, M., Williams, D. L., Lanfranchi, D. A., & Davioud-Charvet, E. (2016). A Platform of Regioselective Methodologies to Access Polysubstituted 2-Methyl-1,4-naphthoquinone Derivatives: Scope and Limitations. *European Journal of Organic Chemistry*. https://doi.org/10.1002/ejoc.201600144

Rostovtsev, V. V, Green, L. G., Fokin, V. V, & Sharpless, K. B. (2002). A stepwise huisgen cycloaddition process: copper(I)-catalyzed regioselective “ligation” of azides and terminal alkynes. *Angew Chem Int Ed Engl*, *41*(14), 2596–2599. https://doi.org/10.1002/1521-3773(20020715)41:14<2596::AID-ANIE2596>3.0.CO;2-4

Rudrapal, M., & Chetia, D. (2016). Endoperoxide antimalarials: Development, structural diversity and pharmacodynamic aspects with reference to 1,2,4-trioxane-based structural scaffold. In *Drug Design, Development and Therapy*. https://doi.org/10.2147/DDDT.S118116

Rueangweerayut, R., Bancone, G., Harrell, E. J., Beelen, A. P., Kongpatanakul, S., Möhrle, J. J., Rousell, V., Mohamed, K., Qureshi, A., Narayan, S., Yubon, N., Miller, A., Nosten, F. H., Luzzatto, L., Duparc, S., Kleim, J. P., & Green, J. A. (2017). Hemolytic potential of tafenoquine in female volunteers heterozygous for Glucose-6-Phosphate Dehydrogenase (G6PD) Deficiency (G6PD Mahidol Variant) versus G6PD-Normal volunteers. *American Journal of Tropical Medicine and Hygiene*. https://doi.org/10.4269/ajtmh.16-0779

Ruecker, A., Mathias, D. K., Straschil, U., Churcher, T. S., Dinglasan, R. R., Leroy, D., Sinden, R. E., & Delves, M. J. (2014). A male and female gametocyte functional viability assay to identify biologically relevant malaria transmission-blocking drugs. *Antimicrobial Agents and Chemotherapy*. https://doi.org/10.1128/AAC.03666-14

Saxon, E., & Bertozzi, C. R. (2000). Cell surface engineering by a modified Staudinger reaction. *Science*, *287*(5460), 2007–2010. https://doi.org/10.1126/science.287.5460.2007

Schapira, M., Calabrese, M. F., Bullock, A. N., & Crews, C. M. (2019). Targeted protein degradation: expanding the toolbox. *Nature Reviews Drug Discovery*, *18*(12), 949–963. https://doi.org/10.1038/s41573-019-0047-y

Schirmer, R. H., Adler, H., Pickhardt, M., & Mandelkow, E. (2011). “Lest we forget you - methylene blue...” *Neurobiology of Aging*. https://doi.org/10.1016/j.neurobiolaging.2010.12.012

Schirmer, R. H., Coulibaly, B., Stich, A., Scheiwein, M., Merkle, H., Eubel, J., Becker, K., Becher, H., Müller, O., Zich, T., Schiek, W., & Kouyaté, B. (2003). Methylene blue as an antimalarial agent. *Redox Report*. https://doi.org/10.1179/135100003225002899

Shieh, P., Dien, V. T., Beahm, B. J., Castellano, J. M., Wyss-Coray, T., & Bertozzi, C. R.

(2015). CalFluors: A Universal Motif for Fluorogenic Azide Probes across the Visible Spectrum. *J Am Chem Soc*, *137*(22), 7145–7151. https://doi.org/10.1021/jacs.5b02383

Siciliano, G., Santha Kumar, T. R., Bona, R., Camarda, G., Calabretta, M. M., Cevenini, L., Davioud-Charvet, E., Becker, K., Cara, A., Fidock, D. A., & Alano, P. (2017). A high susceptibility to redox imbalance of the transmissible stages of Plasmodium falciparum revealed with a luciferase-based mature gametocyte assay. *Molecular Microbiology*. https://doi.org/10.1111/mmi.13626

Sidorov, P., Desta, I., Chessé, M., Horvath, D., Marcou, G., Varnek, A., Davioud-Charvet, E., & Elhabiri, M. (2016). Redox Polypharmacology as an Emerging Strategy to Combat Malarial Parasites. *ChemMedChem*. https://doi.org/10.1002/cmdc.201600009

Sidorov, P., Gaspar, H., Marcou, G., Varnek, A., & Horvath, D. (2015). Mappability of drug-like space: Towards a polypharmacologically competent map of drug-relevant compounds. *Journal of Computer-Aided Molecular Design*. https://doi.org/10.1007/s10822-015-9882-z

Simpson, R. J. (2007). Staining Proteins in Gels with Coomassie Blue. *Cold Spring Harbor Protocols*. https://doi.org/10.1101/pdb.prot4719

Smilkstein, M., Sriwilaijaroen, N., Kelly, J. X., Wilairat, P., & Riscoe, M. (2004). Simple and Inexpensive Fluorescence-Based Technique for High-Throughput Antimalarial Drug Screening. *Antimicrobial Agents and Chemotherapy*. https://doi.org/10.1128/AAC.48.5.1803-1806.2004

Smith, P. K., Krohn, R. I., Hermanson, G. T., Mallia, A. K., Gartner, F. H., Provenzano, M. D., Fujimoto, E. K., Goeke, N. M., Olson, B. J., & Klenk, D. C. (1985). Measurement of protein using bicinchoninic acid. *Analytical Biochemistry*. https://doi.org/10.1016/0003-2697(85)90442-7

Song, J., Socheat, D., Tan, B., Dara, P., Deng, C., Sokunthea, S., Seila, S., Ou, F., Jian, H., & Li, G. (2010). Rapid and effective malaria control in Cambodia through mass administration of artemisinin-piperaquine. *Malaria Journal*. https://doi.org/10.1186/1475-2875-9-57

Sun, J., Li, C., & Wang, S. (2016). Organism-like formation of Schistosoma hemozoin and its function suggest a mechanism for anti-malarial action of artemisinin. *Sci Rep*, *6*, 34463. https://doi.org/10.1038/srep34463

Suzuki, T., Ota, Y., Kasuya, Y., Mutsuga, M., Kawamura, Y., Tsumoto, H., Nakagawa, H., Finn, M. G., & Miyata, N. (2010). An Unexpected Example of Protein-Templated Click Chemistry. *Angewandte Chemie International Edition*, *49*(38), 6817–6820. https://doi.org/10.1002/anie.201002205

Swinney, D. C., & Anthony, J. (2011). How were new medicines discovered? *Nature Reviews Drug Discovery*, *10*(7), 507–519. https://doi.org/10.1038/nrd3480

Tahar, R., Vivas, L., Basco, L., Thompson, E., Ibrahim, H., Boyer, J., & Nepveu, F. (2011). Indolone-N-oxide derivatives: In vitro activity against fresh clinical isolates of Plasmodium falciparum, stage specificity and in vitro interactions with established antimalarial drugs. *Journal of Antimicrobial Chemotherapy*. https://doi.org/10.1093/jac/dkr320

Taylor, W. R., Widjaja, H., Basri, H., Tjitra, E., Ohrt, C., Taufik, T., Baso, S., Hoffman, S. L., & Richie, T. L. (2013). Haemoglobin dynamics in Papuan and non-Papuan adults in northeast Papua, Indonesia, with acute, uncomplicated vivax or falciparum malaria. *Malaria Journal*. https://doi.org/10.1186/1475-2875-12-209

Terkuile, F., White, N. J., Holloway, P., Pasvol, G., & Krishna, S. (1993). Plasmodium

falciparum: In vitro studies of the pharmacodynamic properties of drugs used for the treatment of severe malaria. *Experimental Parasitology*. https://doi.org/10.1006/expr.1993.1010

Teuscher, F., Gatton, M. L., Chen, N., Peters, J., Kyle, D. E., & Cheng, Q. (2010). Artemisinin-induced dormancy in Plasmodium falciparum: Duration, recovery rates, and implications in treatment failure. *Journal of Infectious Diseases*. https://doi.org/10.1086/656476

Tóth, K., Wenzel, N. I., Chavain, N., Wang, Y., Friebolin, W., Maes, L., Pradines, B., Lanzer, M., Yardley, V., Brun, R., Herold-Mende, C., Biot, C., & Davioud-Charvet, E. (2010). Antimalarial versus cytotoxic properties of dual drugs derived from 4-aminoquinolines and mannich bases: Interaction with DNA. *Journal of Medicinal Chemistry*. https://doi.org/10.1021/jm9018383

Vale, N., Prudêncio, M., Marques, C. A., Collins, M. S., Gut, J., Nogueira, F., Matos, J., Rosenthal, P. J., Cushion, M. T., Do Rosário, V. E., Mota, M. M., Moreira, R., & Gomes, P. (2009). Imidazoquines as antimalarial and antipneumocystis agents. *Journal of Medicinal Chemistry*. https://doi.org/10.1021/jm900738c

Vanaerschot, M., Lucantoni, L., Li, T., Combrinck, J. M., Ruecker, A., Kumar, T. R. S., Rubiano, K., Ferreira, P. E., Siciliano, G., Gulati, S., Henrich, P. P., Ng, C. L., Murithi, J. M., Corey, V. C., Duffy, S., Lieberman, O. J., Veiga, M. I., Sinden, R. E., Alano, P., … Fidock, D. A. (2017). Hexahydroquinolines are antimalarial candidates with potent blood-stage and transmission-blocking activity. *Nature Microbiology*. https://doi.org/10.1038/s41564-017-0007-4

Vásquez-Vivar, J., & Augusto, O. (1994). Oxidative activity of primaquine metabolites on rat erythrocytes IN vitro and in vivo. *Biochemical Pharmacology*. https://doi.org/10.1016/0006-2952(94)90022-1

Vennerstrom, J. L., Nuzum, E. O., Miller, R. E., Dorn, A., Gerena, L., Dande, P. A., Ellis, W. Y., Ridley, R. G., & Milhous, W. K. (1999). 8-Aminoquinolines active against blood stage Plasmodium falciparum in vitro inhibit hematin polymerization. *Antimicrobial Agents and Chemotherapy*. https://doi.org/10.1128/aac.43.3.598

Visser, B. J., Wieten, R. W., Kroon, D., Nagel, I. M., Bélard, S., Van Vugt, M., & Grobusch, M. P. (2014). Efficacy and safety of artemisinin combination therapy (ACT) for non-falciparum malaria: A systematic review. In *Malaria Journal*. https://doi.org/10.1186/1475-2875-13-463

Walter-Sack, I., Rengelshausen, J., Oberwittler, H., Burhenne, J., Mueller, O., Meissner, P., & Mikus, G. (2009). High absolute bioavailability of methylene blue given as an aqueous oral formulation. *European Journal of Clinical Pharmacology*. https://doi.org/10.1007/s00228-008-0563-x

Wang, Jigang, Zhang, C. J., Chia, W. N., Loh, C. C. Y., Li, Z., Lee, Y. Q. Y. M., He, Y., Yuan, L. X., Lim, T. K., Liu, M., Liew, C. X., Lee, Y. Q. Y. M., Zhang, J., Lu, N., Lim, C. T., Hua, Z. C., Liu, B., Shen, H. M., Tan, K. S. W., & Lin, Q. (2015). Haem-activated promiscuous targeting of artemisinin in Plasmodium falciparum. *Nature Communications*, *6*, 1–11. https://doi.org/10.1038/ncomms10111

Wang, Juan, Huang, L., Li, J., Fan, Q., Long, Y., Li, Y., & Zhou, B. (2010). Artemisinin directly targets malarial mitochondria through its specific mitochondrial activation. *PLoS ONE*. https://doi.org/10.1371/journal.pone.0009582

Wani, W. A., Jameel, E., Baig, U., Mumtazuddin, S., & Hun, L. T. (2015a). ChemInform Abstract: Ferroquine and Its Derivatives: New Generation of Antimalarial Agents. *ChemInform*. https://doi.org/10.1002/chin.201541255

Wani, W. A., Jameel, E., Baig, U., Mumtazuddin, S., & Hun, L. T. (2015b). Ferroquine and its derivatives: New generation of antimalarial agents. In *European Journal of Medicinal Chemistry*. https://doi.org/10.1016/j.ejmech.2015.07.009

Wellems, T. E., Sá, J. M., Su, X. zhuan, Connelly, S. V., & Ellis, A. C. (2020). 'Artemisinin Resistance': Something New or Old? Something of a Misnomer? In *Trends in Parasitology*. https://doi.org/10.1016/j.pt.2020.05.013

White, N. J. (2008). Qinghaosu (artemisinin): The price of success. In *Science*. https://doi.org/10.1126/science.1155165

White, Nicholas J. (2004). Antimalarial drug resistance. In *Journal of Clinical Investigation*. https://doi.org/10.1172/JCI21682

WHO. (2019). WHO | This year's World malaria report at a glance. *Who*.

Wilson, D. W., Langer, C., Goodman, C. D., McFadden, G. I., & Beeson, J. G. (2013). Defining the timing of action of antimalarial drugs against plasmodium falciparum. *Antimicrobial Agents and Chemotherapy*. https://doi.org/10.1128/AAC.01881-12

Witkowski, B, Amaratunga, C., Khim, N., Sreng, S., Chim, P., Kim, S., Lim, P., Mao, S., Sopha, C., Sam, B., Anderson, J. M., Duong, S., Chuor, C. M., Taylor, W. R., Suon, S., Mercereau-Puijalon, O., Fairhurst, R. M., & Menard, D. (2013). Novel phenotypic assays for the detection of artemisinin-resistant Plasmodium falciparum malaria in Cambodia: in-vitro and ex-vivo drug-response studies. *Lancet Infect Dis*, *13*(12), 1043–1049. https://doi.org/10.1016/S1473-3099(13)70252-4

Witkowski, Benoit, Amaratunga, C., Khim, N., Sreng, S., Chim, P., Kim, S., Lim, P., Mao, S., Sopha, C., Sam, B., Anderson, J. M., Duong, S., Chuor, C. M., Taylor, W. R. J., Suon, S., Mercereau-Puijalon, O., Fairhurst, R. M., & Menard, D. (2013). Novel phenotypic assays for the detection of artemisinin-resistant Plasmodium falciparum malaria in Cambodia: In-vitro and ex-vivo drug-response studies. *The Lancet Infectious Diseases*. https://doi.org/10.1016/S1473-3099(13)70252-4

Witkowski, Benoit, Lelièvre, J., Barragán, M. J. L., Laurent, V., Su, X. Z., Berry, A., & Benoit-Vical, F. (2010). Increased tolerance to artemisinin in plasmodium falciparum is mediated by a quiescence mechanism. *Antimicrobial Agents and Chemotherapy*. https://doi.org/10.1128/AAC.01636-09

Wittelsberger, A., Thomas, B. E., Mierke, D. F., & Rosenblatt, M. (2006). Methionine acts as a "magnet" in photoaffinity crosslinking experiments. *FEBS Lett*, *580*(7), 1872–1876. https://doi.org/10.1016/j.febslet.2006.02.050

Wong, W., Bai, X. C., Sleebs, B. E., Triglia, T., Brown, A., Thompson, J. K., Jackson, K. E., Hanssen, E., Marapana, D. S., Fernandez, I. S., Ralph, S. A., Cowman, A. F., Scheres, S. H. W., & Baum, J. (2017). Mefloquine targets the Plasmodium falciparum 80S ribosome to inhibit protein synthesis. *Nature Microbiology*. https://doi.org/10.1038/nmicrobiol.2017.31

Wright, M. H., Clough, B., Rackham, M. D., Rangachari, K., Brannigan, J. A., Grainger, M., Moss, D. K., Bottrill, A. R., Heal, W. P., Broncel, M., Serwa, R. A., Brady, D., Mann, D. J., Leatherbarrow, R. J., Tewari, R., Wilkinson, A. J., Holder, A. A., & Tate, E. W. (2014). Validation of N-myristoyltransferase as an antimalarial drug target using an integrated chemical biology approach. *Nat Chem*, *6*(2), 112–121. https://doi.org/10.1038/nchem.1830

Wu, Y. (2002). How might qinghaosu (artemisinin) and related compounds kill the intraerythrocytic malaria parasite? A chemist's view. In *Accounts of Chemical Research*. https://doi.org/10.1021/ar000080b

Yadav, D. K., Kumar, S., Teli, M. K., Yadav, R., & Chaudhary, S. (2019). Molecular Targets for Malarial Chemotherapy: A Review. *Current Topics in Medicinal Chemistry*, *19*(10), 861–873. https://doi.org/10.2174/1568026619666190603080000

Yang, T., Yeoh, L. M., Tutor, M. V., Dixon, M. W., McMillan, P. J., Xie, S. C., Bridgford, J. L., Gillett, D. L., Duffy, M. F., Ralph, S. A., McConville, M. J., Tilley, L., & Cobbold, S. A. (2019). Decreased K13 Abundance Reduces Hemoglobin Catabolism and Proteotoxic Stress, Underpinning Artemisinin Resistance. *Cell Reports*. https://doi.org/10.1016/j.celrep.2019.10.095

Yang, Y., Yang, X., & Verhelst, S. H. L. (2013). Comparative analysis of click chemistry mediated activity-based protein profiling in cell lysates. *Molecules*. https://doi.org/10.3390/molecules181012599

Zhu, L., Tripathi, J., Rocamora, F. M., Miotto, O., van der Pluijm, R., Voss, T. S., Mok, S., Kwiatkowski, D. P., Nosten, F., Day, N. P. J., White, N. J., Dondorp, A. M., Bozdech, Z., Phyo, A. P., Ashley, E. A., Smithuis, F., Lin, K., Tun, K. M., Faiz, M. A., … Htut, Y. (2018). The origins of malaria artemisinin resistance defined by a genetic and transcriptomic background. *Nature Communications*. https://doi.org/10.1038/s41467-018-07588-x

Zhu, X., Shieh, P., Su, M., Bertozzi, C. R., & Zhang, W. (2016). A fluorogenic screening platform enables directed evolution of an alkyne biosynthetic tool. *Chem Commun (Camb)*, *52*(75), 11239–11242. https://doi.org/10.1039/c6cc05990b

Zhu, Z., Chen, H., Li, S., Yang, X., Bittner, E., & Cai, C. (2017). Tripodal amine ligands for accelerating Cu-catalyzed azide-alkyne cycloaddition: Efficiency and stability against oxidation and dissociation. *Catalysis Science and Technology*. https://doi.org/10.1039/c7cy00587c

Zoungrana, A., Coulibaly, B., Sié, A., Walter-Sack, I., Mockenhaupt, F. P., Kouyaté, B., Schirmer, R. H., Klose, C., Mansmann, U., Meissner, P., & Müller, O. (2008). Safety and efficacy of methylene blue combined with artesunate or amodiaquine for uncomplicated falciparum malaria: A randomized controlled trial from Burkina Faso. *PLoS ONE*. https://doi.org/10.1371/journal.pone.0001630

Zuzarte-Luís, V., Mello-Vieira, J., Marreiros, I. M., Liehl, P., Chora, Â. F., Carret, C. K., Carvalho, T., & Mota, M. M. (2017). Dietary alterations modulate susceptibility to Plasmodium infection. *Nature Microbiology*. https://doi.org/10.1038/s41564-017-0025-2

Vrushali KHOBRAGADE

Développement d'outils chimiques et de sondes sélectives basées sur l'activité de la plasmodione pour identifier les cibles de ce nouvel agent antipaludique

Résumé Le paludisme cérébral est une maladie parasitaire fatale causée par *Plasmodium falciparum*. Les jeunes anneaux et les gamétocytes matures sont responsables de la multiplication chez l'homme et de sa transmission aux moustiques anophèles. Seuls quelques médicaments ciblent ces stades. L'artémisinine (Art) est le médicament antipaludique le plus efficace, mais il est menacé par l'émergence d'une résistance à l'Art en Asie du Sud-Est. Il y a donc un besoin urgent de nouveaux agents ou de combinaisons qui peuvent cibler les anneaux et les gamétocytes et contourner la résistance à l'Art. La Plasmodione (PD) est actif sur les anneaux avec une vitesse d'action aussi rapide que celle de l'Art. Elle a un faible potentiel d'induction de résistance et présente une synergie avec d'autres médicaments, dont l'Art. Des analogues optimisés de la DP ont également montré des propriétés anti-transmission. Cependant, les cibles précises de la PD chez les parasites ne sont pas encore connues. Par conséquent, la conception d'outils chimiques (PD-ABPP) pour identifier les cibles de la PD est essentielle pour identifier son interactome et pour élucider le mode d'action impliqué dans l'action toxique de la PD contre les parasites. Mon projet de thèse était axé sur une stratégie "click & fish" et visait à analyser les produits d'addition covalents générés par des sondes ABPP photoréactives et 'clickables' dérivées de la PD. Tout d'abord, mes études dans le chapitre de parasitologie ont confirmé que l'analogue supérieur de la PD, bMD40, a montré une résistance croisée avec l'Art dans les stades asexués des souches de *P. falciparum* résistantes à l'Art, ouvrant ainsi de nouvelles études pour trouver des partenaires de combinaisons de PD dans l'équipe de l'IBMC. Ensuite, mes données d'analyse ont démontré que le groupe attracteur d'électrons en para de la chaîne benzoyle des métabolites de la PD, les 3-benzoylmenadiones, est un facteur clé dans les photoréactions avec un partenaire donneur d'H. La standardisation des conditions de réaction click a été une contribution importante de mon travail axé sur les réactions des sondes ABPP et de la rhodamine azide. Enfin, en combinant la photo-irradiation des sondes ABPP dérivées de la PD et la réaction click avec différents azides - la sonde 7 avec un groupe alcyne 4' et la sonde 9 avec un 4' -nitro - se sont révélées être les sondes photoréactives et 'clickables' les plus efficaces. Troisièmement, j'ai exploré les propriétés physico-chimiques de deux nouveaux azides fluorogènes de flavylium (FA1 et FA2), conçus/synthétisés pour générer une émission de fluorescence, après la réaction clik avec les sondes ABPP dérivées de la PD. Cette étude a ouvert la voie à la mise au point de nouveaux outils chimiques fluorogènes, abordables, hydrosolubles et photostables pour l'imagerie *in vivo*.

Résumé en anglais: Cerebral malaria is a fatal disease caused by the parasite *Plasmodium falciparum.* Young rings and mature gametocytes are responsible for the multiplication of the infection in humans and its transmission to Anopheles mosquitoes. Only few drugs target these stages. Artemisinin (Art) is the most effective antimalarial drug, but it is threatened by the emergence of resistance to Art in Southeast Asia. There is therefore an urgent need for new agents or combinations that can target the rings and gametocytes and bypass Art resistance. Plasmodione (PD) is active on rings with a speed of action as fast as that of Art. It has a low potential to induce resistance and displayed synergy with other drugs including Art. Optimized analogues of PD also showed transmission-blocking properties. However, the precise PD targets in the parasites are not yet known. Therefore, the design of chemical tools (PD-ABPP) for identifying the PD targets is essential to identify the PD interactome and to elucidate the mode of action involved in the toxic action of PD against parasites. My thesis project was focused on a 'click & fish' strategy and aimed at the analysis of the covalent adducts generated from photoreactive and clickable PD-derived ABPP probes. First, my studies in the parasitology chapter confirmed that the superior PD-analogue, bMD40, showed cross-resistance with Art in asexual stages of Art-resistant *P. falciparum* strains, opening new studies to find partners for PD combinations in the IBMC team. Then, my analysis data demonstrated that the electron-withdrawing group in *para* of the benzoyl chain of PD metabolites, the 3-benzoylmenadiones, is a key factor in photoreactions with a H-donor partner. Standardization of the click reaction conditions was an important contribution of my work focused on the reactions of ABPP probes and rhodamine azide. Finally, by combining the photoirradiation of the PD-derived ABPP probes and the click reaction with different azides - probe 7 with a 4'-alkyne group and probe 9 with a 4'-nitro - proved to be the most efficient photoreactive and clickable probes. Third, I explored the physicochemical properties of two new fluorogenic flavylium azides (FA1 and FA2), designed/synthetized to generate brightly fluorescence emission, after the click reaction with PD-derived ABPP probes. This study paved the way to develop novel, affordable, water-soluble and photostable fluorogenic chemical tools for in vivo imaging.